Volume 72C
Number 1
Jan.–Mar. 1968

Engineering and Instrumentation

U.S. DEPARTMENT OF COMMERCE

SECTION C

JOURNAL OF RESEARCH

NATIONAL BUREAU OF STANDARDS

Journal of Research

of the

National Bureau of Standards

C. Engineering and Instrumentation

Jan.–Mar. • 1968

VOLUME • 72C

NUMBER • 1

Editor: Martin Greenspan

Associate Editors: G. F. Montgomery, R. V. Smith, A. F. Schmidt

Publication dates:
Feb. 15, May 15, Aug. 15, Nov. 15, 1968

JOURNAL OF RESEARCH

The National Bureau of Standards Journal of Research reports research and development in the fields of activity shown at right. Also included from time to time are survey articles on topics closely related to the Bureau's scientific and technical program.

The Journal is published in three separate sections as follows:

A. Physics and Chemistry

Contains papers of interest primarily to scientists working in these fields. Issued six times a year. Annual subscription: domestic, $5.00; foreign, $6.00. Single copy, $1.00.

B. Mathematical Sciences

Presents studies and compilations designed mainly for the mathematician and the theoretical physicist. Issued quarterly. Annual subscription: domestic, $2.25; foreign, $2.75. Single copy, 75¢.

C. Engineering and Instrumentation

Reports research and development results of interest chiefly to the engineer and the applied scientist. Issued quarterly. Annual subscription: domestic, $2.75; foreign, $3.50. Single copy, 75¢.

The National Bureau of Standards is a principal focal point in the Federal Government for assuring maximum application of the physical and engineering sciences to the advancement of technology in industry and commerce. Its responsibilities include development and maintenance of the national standards of measurement, and the provisions of means for making measurements consistent with those standards; determination of physical constants and properties of materials; development of methods for testing materials, mechanisms, and structures, and making such tests as may be necessary, particularly for government agencies; cooperation in the establishment of standard practices for incorporation in codes and specifications; advisory service to government agencies on scientific and technical problems; invention and development of devices to serve special needs of the Government; assistance to industry, business, and consumers in the development and acceptance of commercial standards and simplified trade practice recommendations; administration of programs in cooperation with United States business groups and standards organizations for the development of international standards of practice; and maintenance of a clearinghouse for the collection and dissemination of scientific, technical, and engineering information. The scope of the Bureau's activities is suggested in the following listing of its three Institutes and their organizational units.

Institute for Basic Standards. Applied Mathematics. Electricity. Metrology. Mechanics. Heat. Atomic Physics. Physical Chemistry. Radiation Physics. Laboratory Astrophysics.* Radio Standards Laboratory:* Radio Standards Physics; Radio Standards Engineering. Office of Standard Reference Data.

Institute for Materials Research. Analytical Chemistry. Metallurgy. Reactor Radiations. Polymers. Inorganic Materials. Cryogenics.* Office of Standard Reference Materials.

Institute for Applied Technology. Building Research. Electronic Instrumentation. Technical Analysis. Center for Computer Sciences and Technology. Textile and Apparel Technology Center. Office of Weights and Measures. Office of Engineering Standards Services. Office of Invention and Innovation. Office of Vehicle Systems Research. Clearinghouse for Federal Scientific and Technical Information.** NBS/GSA Testing Laboratory.

*Located at Boulder, Colo. 80302.
**Located at 5285 Port Royal Road, Springfield, Va. 22151.

U.S. DEPARTMENT OF COMMERCE
Alexander B. Trowbridge, Secretary
NATIONAL BUREAU OF STANDARDS
A. V. Astin, Director

Order all publications from the Superintendent of Documents
U.S. Government Printing Office, Washington, D.C. 20402.

Use of funds for printing this publication approved by the Director of the Bureau of the Budget (June 22, 1966).

JOURNAL OF RESEARCH of the National Bureau of Standards—C. Engineering and Instrumentation
Vol. 72C, No. 1, January–March 1968

Acceleration Due to Gravity at the National Bureau of Standards*

D. R. Tate

Institute for Basic Standards, National Bureau of Standards, Washington D.C. 20234

(September 26, 1967)

A determination of the absolute value of the acceleration due to gravity was completed in June 1965 at the National Bureau of Standards near Gaithersburg, Maryland. The determination resulted in a value of 980.1018 centimeters per second squared for a reference point on the first floor of the Engineering Mechanics Building. The result was published in The Journal of Research of the National Bureau of Standards, Vol. **70C**, No. 2, Engineering and Instrumentation, page 149, April-June 1966. The present paper describes in detail the apparatus and the techniques employed and presents the summarized data from which the value was derived.

Key Words: Absolute gravity, acceleration, free-fall, *g*, gravity, Potsdam.

1. Introduction

1.1. Absolute Gravity as the Standard of Force

Determinations of the acceleration due to the gravitational attraction of the earth have been made many times since the early observations of Galileo. Up to the end of the nineteenth century measurements were made with the primary purpose of gaining knowledge about the figure of the earth and the effects of the distribution of mass near its surface. In the years that have followed, gravity values have not only continued to be of great interest to the geodesist but also have fulfilled an additional role in supplying the base for the standard of force. Virtually every measurement which involves force, such as electrical current or pressure, depends in some manner on knowledge of the gravitational field of the earth.

It is generally agreed that the unit of force is defined by the second Newtonian law of motion and the primary standards of length, mass, and time. The determination of the acceleration due to gravity links the dynamic relationship of the Newtonian law to a permanent reference in the gravitational field of the earth. The gravitational field strength, multiplied by an accurately determined mass value, then becomes the working standard of force. From this point onward the normal process by which a measurement system is established, i.e., by the comparison of like quantities, can successfully include force as an element.

An essential part of the process, of course, is a means of extending the single point value of the field intensity to other points as needed. This extension is accomplished through the use of comparators such as geodetic pendulums and gravity meters. The results comprise a unified network which will eventually cover the habitable portions of the earth.

The relationship between the acceleration due to gravity and the concept of the gravitational field is so direct that it is frequently ignored in practical applications. However, distinction between the two concepts is essential to a logical understanding of the basic equations of mechanics.

Consider a body of mass m at rest in the gravitational field of the earth. The body experiences a force which can be expressed as

$$\mathbf{F} = -m\nabla\varphi;$$

φ is the potential, a function of position in space relative to a coordinate system at rest with respect to the earth. If now the body is free to move, it will experience an acceleration, $\mathbf{g}$, such that

$$\mathbf{F} = km\mathbf{g}.$$

Thus, with the assumption that m is the same quantity in both cases,

$$\nabla\varphi; = -k\mathbf{g}.$$

The strength of the gravitational field is, therefore, equal to the acceleration due to gravity multiplied by a numerical factor, k, which depends only upon the system of units of measurement selected. In any coherent system, k is equal to unity.

Although the validity of the assumption above, that the inertial mass is equal to the gravitational mass,

*This paper will be available as NBS Monograph 107 from the Superintendent of Documents, Government Printing Office, Washington, D.C. 20402. Price 25 cents.

has frequently been questioned, experiments such as those with the Eötvös pendulum [1][1] indicate that any effects must be less than one part in 10^{11}. This amount is several orders of magnitude less than the sensitivity of any absolute measurement now under consideration.

1.2. Previous Determinations

The history of absolute gravity experiments published within the past 70 years has been reviewed by several authorities. Cook [2], in particular, gives a very thorough treatment. Briefly summarized, an absolute determination published in Potsdam, Germany, in 1906 by Kühnen and Furtwängler [3] became the base for the world network of relative gravity observations. Two later determinations, one by Heyl and Cook [4] at Washington, D.C. and the other by Clark [5] at Teddington, England, disagreed with the Potsdam result by significant amounts. Reexamination of the Potsdam result by Dryden [6] and of Clark's and Heyl's results by Jeffreys [7] improved the agreement but did not fully resolve the questions raised.

In 1956 the results of three new determinations by Agaletskii and Egorov [8] and Martsiniak [9] tended to support the conclusion that the original Potsdam result is too high by some ten to twenty parts per million. Three other absolute determinations appeared within the next few years, Preston-Thomas et al. [10], Thulin [11], and Faller [12]; all have shown reasonably good agreement with each other and have ranged from about 12.7 to 14.5 milligals[2] (mGal) below the Potsdam result. More recently Cook [13] has reported the result of a determination at the National Physical Laboratory differing from the Potsdam result by approximately 13.7 mGal.

1.3. Accuracy and Precision

The requirements for accuracy in absolute gravity measurements are much the same for the geodesist and the metrologist. An accuracy of one part in a million is critically needed and an accuracy of one or two parts in ten million would be most desirable. It has been suggested that some form of absolute gravity apparatus which can readily be transported and set up in different sites might resolve the apparent bias between some measurements with geodetic pendulums. If such an approach is to be effective, a demonstrated stability in the portable absolute apparatus of one part in ten million is quite essential.

The results of absolute determinations in which measurements of several non-related parameters are combined to obtain an estimate of the magnitude of a presumed constant quantity, the true value of which is unknown, cannot realistically be assigned a level of accuracy. One can and does derive an index, such as the standard deviation, of the precision of individual determinations made over a short period of time. From this index an estimate may be derived of the precision which might be expected for the means of similar sized groups of measurements drawn from the same source. If such groups of measurements are actually made, separated by periods of a day or more, the standard deviations of the individual measurements may be much the same but the means of the groups will often show more scatter than would have been predicted from the internal consistency of any of the groups. The conclusion is that the composition of the population from which the samples have been drawn has changed with time. It is inferred that there must exist sources of bias which vary from day to day but which do not change appreciably over the course of a single set of measurements.

The nature and extent of variability of this bias usually remain unknown. The demonstrated presence of bias, of course, arouses the investigator to try to analyse it by looking for correlation with other parameters. In general, though, this process has already been carried out to the limits of practicality. This residuum of bias is probably a major cause of the well-known tendency of the scientist to continue his measurements indefinitely.

In a broad sense, therefore, one can consider that an estimate of the accuracy of an experimental measurement can be made only when the resultant value can be compared to a defined or assumed true norm. In the absence of such a true norm, a determination obtained from a series of measurements made with a single piece of apparatus must be regarded as only a sample from an unknown population. Estimates of the precision should be made, together with statements of the sensitivity to variations in the component measurements in relation to the precision with which those standards were established. Such statements give limits to the error only from known sources. The final appraisal of the limits of knowledge about the true value of the constant determined must come from the results of a group of completely independent experiments differing in method, location, and in the personnel conducting them.

1.4. Methods for Gravity Determinations

Taken without regard for experimental difficulty, it would appear that the most direct method for determining the absolute value of the acceleration due to gravity would be to observe the motion of some object moving without constraint under the action of the gravitational field of the earth. Up to about 1950 the use of such a method was impracticable because of the difficulty in measuring the short lengths of time involved. Virtually all gravity measurements were made with some form of pendulum.

Basically the pendulum method substitutes a system with a maximum of constraint for a system with a minimum of constraint. From a purely practical viewpoint the pendulum method offers many advantages. An uncertainty of one part in a million in the measurement of the pendulum length produces the same relative uncertainty in the determination of g. An uncertainty of one part in a million in the measurement of time results in an uncertainty of two parts in a million in g, but the length of the time interval can be

[1] Figures in brackets indicate the literature references at the end of this paper.

[2] A milligal is a geodetic unit of gravity equal to 10^{-3} cm/s^2, approximately 1 ppm of the value of g.

increased to the point where timing errors become negligible. The difficulties of the pendulum method lie in the complex theoretical corrections for pendulum flexure and the uncertainties contributed by motion of the pendulum support and by the indefinite point of rotation at the knife edge.

Experiments involving unconstrained motion under gravitational forces have, with the perfection of frequency counting electronic circuitry, developed in many diverse forms. The most elementary form of such an experiment would be one in which an object is released from rest and allowed to fall a known distance in a vacuum. If time is measured from the instant of release to the point where the object has travelled the measured distance, the acceleration may be computed from the simple relationship

$$g=\frac{2d}{t^2}.$$

Here the sensitivity in the determination of g is the same as in the case of the pendulum and the efficiency of measurement would be high. Unfortunately the experimental difficulties in the measurement of time and length and in the release of the object are so formidable that no investigator up to the present has undertaken such an experiment.

The restrictions of the elementary free-motion experiment can be eliminated by releasing the object prior to the start of the time measurement. In this case the object acquires an initial velocity of unknown magnitude which can be successfully eliminated by the addition of one or more distances over which time is measured. A parallel and equally effective approach is to measure the distance the object travels during two or more known intervals of time.

These techniques, while successfully eliminating the experimental difficulties of the elementary experiment, are introduced at the cost of an increase in sensitivity to errors in the measurement of length and time. The method offers many advantages from the experimental viewpoint and has been employed in one form or another by several investigators.

In 1947 [14], M. Charles Volet, then Director of the Bureau International des Poids et Mesures, suggested that if an object were projected upwards, passing two position sensing stations separated by a known distance and then allowed to fall back, and the time between successive passages at each level recorded, a considerable increase in measurement efficiency would be obtained. The method is indeed a most effective one since the sensitivity to length errors is the same as for the elementary experiment and the sensitivity to timing errors is very nearly equal to that in an elementary experiment with four times the height of fall. The principal disadvantage is the increased difficulty in the experimental technique required. The method is currently being employed in experiments at the National Physical Laboratory by Cook [2], and at the Bureau International des Poids et Mesures by Sakuma [15]. Sakuma's method embodies the concept of making the moving object one reflector of an interferometer system illuminated by a gas laser light source. This approach has the great advantage of making the length and time measurements occur simultaneously and avoids the limitations of an intermediate length standard. Faller's experiment [12] was the first published determination using the falling interferometer plate principle. He was limited to a very short length of drop by the necessity of using a conventional light source.

2. The NBS Determination

2.1. General Description

Following a review and appraisal of several possible approaches to absolute gravity measurements, it was decided to employ a modification of the direct free-fall method with the release of the object preceding the timing sequence. The method makes use of a concept introduced by Agaletskiĭ and Egorov [8] in which the released object falls within a chamber which is itself falling. Agaletskiĭ's technique was to determine the acceleration of the object with respect to the chamber and, separately, to determine the acceleration of the chamber with respect to the earth. The measurements were made by a multiple flash method at constant frequency.

In the experiment at the National Bureau of Standards the acceleration of the inner falling object was determined directly with respect to the earth from measurements of the time required for two intervals of length on a fused silica tube to pass an optical sensing station.

The apparatus for the experiment was first set up at the National Bureau of Standards in Washington, D.C., in 1961 in a pair of small rooms known as the sub-subbasement of the East Building. This had been the site of the absolute determination by Heyl and Cook [4]. In February of 1964 the apparatus was damaged in a flood which left the site in a nearly unusable condition. The apparatus was reconstructed in the summer of the same year and installed in room 129 of the Engineering Mechanics Building (Building 202) at the new site of the Bureau near Gaithersburg, Maryland. The measurements leading to the final value were taken during April, May, and June of 1965.

In the experiment a fused silica tube slightly more than a meter in length rested on a seat in a vacuum chamber a few centimeters longer than the tube. The vacuum chamber was mounted on a carriage and held by a latch at the top of a pair of vertical guide rods secured in a rigid frame. The arrangement was such that when the latch was released, the carriage was free to descend vertically down the guide rods under the influence of gravity. A schematic diagram of the apparatus is shown in figure 1. Friction between carriage and guide rods was reduced to a low level by antifriction bearings. In the latched position the carriage was under an additional downward force provided by an adjustable, short-travel, spring-loaded plunger. When the latch was released the carriage moved downward with an acceleration about ten per-

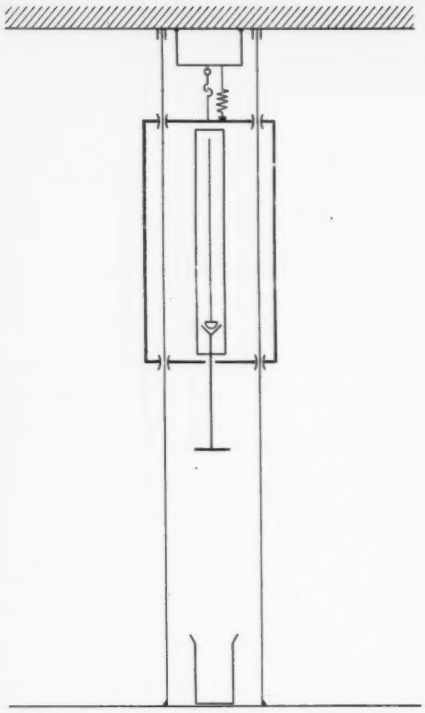

FIGURE 1. *Schematic view of gravity apparatus.*

cent greater than the acceleration due to gravity for the first 8 mm of its travel. The additional acceleration of the car effectively separated the fused silica tube from its seat inside the chamber, leaving the tube floating without contact with the chamber for the duration of the fall of the carriage. By proper adjustment of the spring plunger travel, the relative displacement between the silica tube and the chamber could be restricted to a millimeter or so after the initial separation. After a fall of about 1¼ m the carriage was brought to a smooth stop by an air dash-pot.

Only the force due to gravity acted upon the silica tube inside the chamber. The tube, which was opaque, carried three transparent slits, to be described later. The slits defined two lengths, one extending from the slit near the lower terminus of the tube to the second slit 30 cm above it, and the other extending from the lower slit to the third slit 100 cm above it. The vacuum chamber was provided with pairs of ports at locations opposite the slits. A single position-sensing station consisted of a light source, a long focus microscope, and a photomultiplier cell. As each slit passed the station, an illuminated image of it was projected on a plane containing a stationary slit within the microscope tube. Beyond this reference slit was the photomultiplier cell. The reference slit was dark until the bright image of a moving slit swept across it, causing the photomultiplier cell output to rise from nearly zero to full anode potential. A two-channel electronic timer system was triggered at some predetermined potential level near the midpoint of the linearly rising photocell output curve.

During the fall of the tube, both timer channels were started by the passage of the lower slit past the position-sensing station. One channel was stopped by the passage of the second slit and the other channel was stopped by the passage of the third slit. They thus registered the transit time for the 30-cm and 100-cm lengths, respectively.

The apparatus was arranged so that the fused silica tube fell a distance of 6.8 cm before the first slit initiated the timing sequence. Thus about 118 ms elapsed between the release of the latch and the start of the time measurements.

The lengths corresponding to the two distances on the fused silica tubes were measured, using the same apparatus employed for the free fall time measurements. The fused silica rod was secured firmly in its seat and a measurement made of the distance the carriage moved between the locations where the timers would have been triggered by the photocell signals. The technique for the length measurements is described in another part of this paper. The method has the advantage of including effects of the vacuum on the actual length of the rod as well as any optical effects from the ports in the vacuum chamber walls. More importantly, it is a direct measurement of the quantity desired.

The following summary indicates the magnitudes of the parameters measured and the sensitivity of the result in terms of the least count in the measurements.

Magnitudes of measured parameters	
Short length	30 centimeters
Long length	100 centimeters
Time for short length	156 milliseconds
Time for long length	348 milliseconds
Least count in measuring instruments	
Length	0.1 micrometer
Time	0.1 microsecond
Temperature	0.02 degree Celsius
Sensitivity of the value of g to variations equal to the least count	
Short length	0.7 milligal
Long length	0.3 milligal
Time for short length	1.8 milligal
Time for long length	1.4 milligal
Temperature of silica tube	0.01 milligal
Temperature of invar standard	0.02 milligal

2.2. The Falling Objects

Four tubes were employed in the experiment, all constructed to the same nominal dimensions from

clear, fused silica tubing having an outside diameter of 15 mm, and a wall thickness of 1 mm. Each tube had a length of 107 cm. A metal sleeve with an outside diameter of 19 mm fitted over one end of each tube and was cemented in place with epoxy cement. The external end of the sleeve was machined to a spherical radius of 12 mm. The sleeve formed the lower support tip for the silica tube.

At a point about 11 cm from the other end of the silica tube a second sleeve was attached, fitted with guide pins for alinement and rotation in the vacuum chamber. Figure 2 shows a schematic view of an assembled tube.

Each silica tube was fitted with three rectangular clear apertures formed by pairs of bevel-edge metal plates cemented to the outer surface of the tube wall. The plate edges were perpendicular to the longitudinal axis of the tube and spaced so that the aperture took the form of a transverse slit about 1 mm wide and 7 mm long. In the experiment the dimensions of the slit were of no particular consequence, as the timing sequences were generated by the transition from dark to light as the lower edges of the slits passed the optical axis of the position sensing optical system. The upper slit boundary was supplied to provide a sharp cut-off of the light beam in order to prevent spurious triggering of the timers by photo-tube noise in a slowly decaying light pattern.

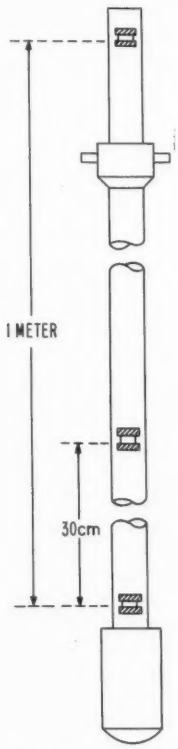

FIGURE 2. *Free-fall object showing slits and guide sleeves.*

The experiment required that the critical edges of all three slits be mutually parallel, coplanar, and perpendicular to the axis of the fused silica tube. To this end, a special jig was made to hold the silica tube and aperture edges during the operation of cementing the edges to the tube.

The jig consisted of a channel-shaped frame of steel having two vee-blocks attached on the centerline of the channel web at positions corresponding to the lower support tip and the upper guide sleeve of the silica tube. Three pairs of rectangular notches were machined into the flange-edges of the channel at locations corresponding to the 0-, 30-cm, and 1-m aperture locations on the silica tube. The parallelism of the jig notches was checked with an autocollimator and the notches hand-finished to be parallel within 7 s of arc. This amount corresponds to an error of 0.03 μm in 1 mm.

In using the jig, cut and finished aperture edges were attached to special holders. These were flat bars which could be set into the jig notches and secured in place with hold-down screws to maintain alinement during the setting of the cement. The holders were constructed with flats lapped on the leading edges at the points where they contacted the forward edges of the jig notches. The center portion of the holder edges was relieved. An aperture edge was attached to each of three such holders by metal fingers which gripped the aperture plates at the sides, the defining edges of the aperture plates being made coplanar with the lapped flats on the holders by a light lapping operation. The finished assemblies were then checked in a comparator.

A silica tube, complete with supporting tip and guide sleeve, was clamped in the vee-blocks which had been shimmed to provide a clearance of about 0.07 mm between the surface of the silica tube and the under face of the aperture plate and holder assemblies. A dot of epoxy cement was then placed on the center of each aperture plate mounted in its holder. The three holders were inverted and each carefully placed in a jig notch and secured in place with the lapped edges forced against the leading edge of each notch.

After the cement had set for 24 hr, the gripping fingers coupling the holders to the aperture edges were released and the holders removed from the jig. The bond between the silica rod and the aperture plates was then reinforced with additional cement. Three opposing aperture plates to complete the framing of the apertures were then installed by a similar technique. The bond formed between the metal aperture edge plates and the silica tube by the epoxy cement was quite strong. Even the bond formed by the initial small dot of cement had sufficient strength after 3 or 4 days to require considerable force to separate the two parts.

As a final step each silica tube was given several coats of silver conductive paint to prevent the formation of localized electrostatic charges. Preliminary experiments with silica rods or tubes in vacuum had shown that under certain conditions a substantial electrostatic charge was generated by the separation

of the supporting tip of the tube from the seat in the vacuum chamber. Even though the falling object was surrounded by the grounded metal vacuum chamber, the internal field was not necessarily zero and the silica tube tended to be drawn out of the true vertical line as it fell. In some cases the effect was so severe as to cause the timers to malfunction. The conductive paint, which reduced the surface resistance of the silica tube of less than 10 Ω, eliminated this difficulty. Only the clear apertures and corresponding areas on the opposite face of the tube were not coated.

2.3. The Vacuum Chamber

The vacuum chamber was fabricated in three sections joined by flanges with O-ring seals. It was constructed of brass tubing having an outside diameter of 4.76 cm and a wall thickness of 0.32 cm. The outside of the chamber was covered by two layers of 3-mm cork sheet and finally by a layer of heavy aluminum foil to reduce the effects of ambient temperature fluctuations. The vacuum chamber assembled on the carriage of the machine is shown in figure 3.

The lower section of the chamber contained the support cone for the silica tube, the vacuum gage, the vacuum pump connection, and the optical windows for the zero and 30 cm apertures of the silica tube. The middle section of the vacuum chamber housed the upper guide bearing for positioning the silica tube preparatory to release. In the upper section of the vacuum chamber were the optical windows for the 1-m aperture of the silica tube.

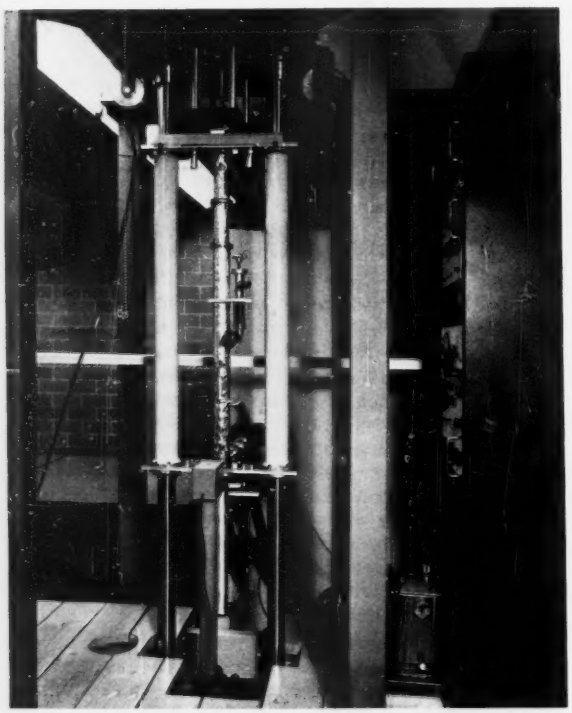

FIGURE 3. *Upper portion of gravity machine showing guide rods, carriage, and vacuum chamber.*

The vacuum chamber was so arranged that it was necessary to disassemble only the upper section in order to remove or insert a silica tube.

The support cone formed an integral part of the removable base closure for the lower section of the vacuum chamber. It was made by machining a base with a recess in the form of a 90° vertex angle cone. The major portion of the cup formed in this way was then milled out, leaving only three ribs, 120° apart and about 7 mm wide. The shape was a compromise between the desirable 3-point support and a full cone seat. It was considered that a 3-point support would tend to produce localized deformations of the silica tube support tip which would in time make the contact unstable. Earlier experiments with a support seat which more nearly approximated a full cone had likewise resulted in some undesirable characteristics.

The upper guide bearing mechanism was built as a unit into the middle section of the vacuum chamber. It consisted of two end flange plates with O-ring seals each connected by a metal bellows to a central sliding unit. A section of brass tubing of the same dimensions as the other sections of the vacuum chamber was attached between the end flange plates providing structural support and also guidance for the central sliding unit. The central sliding unit terminated in a tube having an inside diameter of 19 mm which projected above the end flange plate into the upper portion of the vacuum chamber. To this tube was attached a bushing having an inside diameter just slightly larger than the upper sleeve of the silica tube. The upper surface of the bushing was a double-vee cam surface to engage the guide pins of the silica tube sleeve as shown in figure 4.

When a silica tube is installed in the assembled vacuum chamber, the arrangement is such that when the central sliding unit is moved to the upper limit of its travel, the silica tube is picked up by the guide pins in the vee-shaped notches and rotated into the proper orientation with respect to the optical axis of the position sensing station. Then, as the central sliding unit is lowered, the silica tube is seated in the support cone at the bottom of the vacuum chamber but is precisely alined by the guide bushing surrounding the sleeve on the silica tube. When the central sliding unit reaches the lower limit of travel where it can be locked in place, the guide bushing is completely disengaged from the silica tube sleeve and the silica tube stands supported only by the support cone. It is then ready for a free-fall measurement.

During length measurements on the silica tube the central sliding unit was left in the center of its travel where the silica tube received lateral guidance from the bushing but rested on the support cone.

The six optical windows in the vacuum chamber were Pyrex glass discs, 4.5 mm thick and 19 mm in diameter. They were optically polished to be flat within one-half wave length of the green mercury line. The discs were inserted in machined wells in the cham-

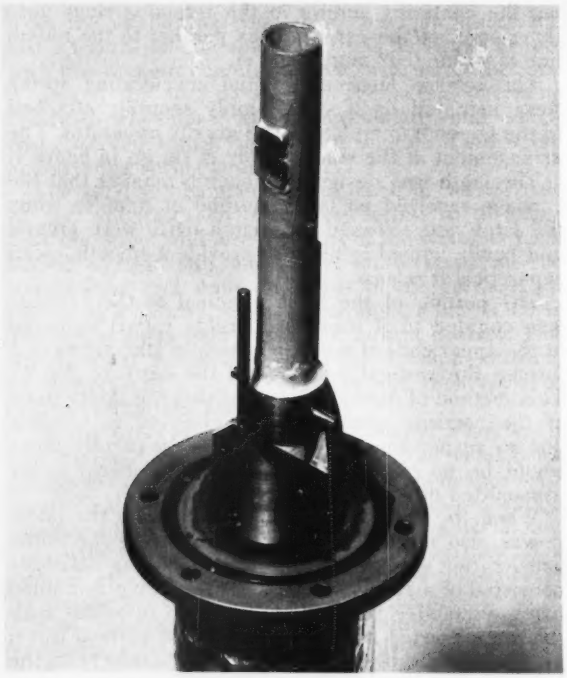

FIGURE 4. *Vacuum chamber with upper section removed, showing fused silica tube and alignment mechanism.*

ber wall on O-ring seals. The clear apertures were reduced to areas about 13 mm high by 8 mm wide by masks.

The vacuum connections to the vacuum chamber were made through a special flange and O-ring seal near the midheight of the chamber. A copper tube connected to the flange led to a 19-mm valve supported by the chamber. A detachable connection from the valve permitted coupling the system to a mechanical pump by a flexible hose. The system was designed to present a minimum throat diameter of 19 mm. The vacuum pump was a two-stage mechanical pump with a free air capacity of 140 liters per min.

The vacuum chamber was equipped with a thermocouple-type vacuum gage inserted in the chamber wall at a point about 24 cm below the connection to the vacuum pump. Once the vacuum chamber had been outgassed it was possible to attain a pressure of about 0.13 N/m^2 (1 μm of mercury). The vacuum pump was operated continuously except during the length or free-fall measurements. Generally the leakage rate for the system ranged from about 0.4 to 0.6 $N/m^2/hr$ at this pressure.

A mercury-in-glass thermometer was imbedded in the thermal insulation of the vacuum chamber near the vacuum gage. The thermometer bulb was kept in thermal contact with the brass wall of the chamber by a pad of compacted aluminum foil. The thermometer was covered by the cork insulation except for a slit exposing a portion of the engraved scale. The thermometer scale was graduated to 0.2 deg Celsius and read by estimation to 0.02 deg. This thermometer was identical to the thermometers used to measure the temperature of the length standard.

2.4. Mechanical Design

The frame of the apparatus for the determination of the acceleration due to gravity consisted of a base plate of steel 120 cm square and 3.8 cm thick, grouted to the floor of the building and held down by four 2.5-cm anchor bolts. At each corner of the plate there was a hollow square-section steel column 3.7 m high. Bridging the tops of the columns was a plate of steel 120 cm on each side and 5 cm thick, cut out along the edges to reduce the weight. Two guide rods for the carriage were supported in the frame gripped in rings bolted to the base and upper plates. The internal diameter of each ring was 7.5 cm; each ring had four centering screws. The guide rods were 6.35 cm in diam with a tolerance of 0.1 mm. They were selected to be straight to within 0.08 mm per m of length. The spacing between the guide rods was nominally 40 cm.

The carriage of the apparatus was about 117 cm long and was formed of two aluminum alloy plates separated by vertical tubes of aluminum alloy as shown in figure 3. The two guide rods passed through holes in the carriage plates and through the interior of the two aluminum alloy tubes.

At both ends of one tube two pairs of ball bearings were mounted so as to center the steel guide rod within the aluminum alloy tube. A single pair of ball bearings at the upper end of the opposite tube constrained the carriage against rotation about the opposite guide rod. The arrangement of the ball bearing guides is shown in figure 5. The five pairs of ball bearings were adjusted against the guide rod with a slight negative clearance to eliminate any possible

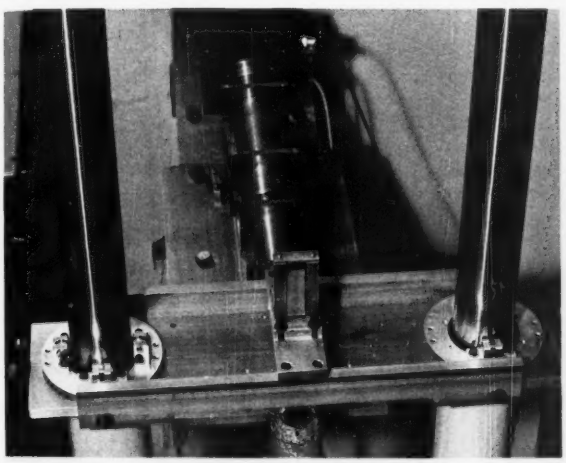

FIGURE 5. *Upper end of carriage showing guide bearings and latch connection.*

lateral freedom of motion. The motion of the carriage was found to be extremely linear and yet with only about 100 g friction in the direction of free fall.

Since it was necessary to counterbalance the weight of the carriage and vacuum chamber about 22 kg during length measurements, a pair of ball bearing pulley wheels were attached to the upper main frame plate near the vertical extension of the ends of the carriage frame. Weight hangers were connected to two spring steel ribbons 12.7 mm by 0.18 mm which passed over the pulleys and terminated in fittings that could be coupled to the frame of the carriage.

A view of the assembled frame, carriage and vacuum chamber is shown in figure 6. The wood platform for the observer was supported from the building floor and did not touch the gravity apparatus.

The main guide rods were alined parallel to the direction of gravity by the following procedure. Near each guide rod a fine wire was suspended from the upper plate of the frame. A mass of sufficient weight to stress the wire moderately was attached to the lower end of the wire. The lower end of the wire and the mass were immersed in a pot of oil to damp out oscillations. A microscope with reticule graduated to 0.01 mm was mounted on the counterbalanced carriage and focussed on the wire, first in a plane perpendicular to the face of the carriage and later in a plane parallel to the face. Microscope readings were taken on the wire at the upper and lower limits of travel of the carriage and the position of the guide rod corrected by adjusting the centering screws in the retaining rings until the motion of the carriage was parallel to the plumb line to within 0.02 mm in one m.

The release latch and initial accelerating spring were mounted on a subassembly securely attached to the upper frame plate of the gravity apparatus. The arrangement of the subassembly is shown in figure 7.

The latch was designed in such a manner that the carriage received no lateral torque or impulse when the latch was released The latch parts were ground and finally lapped in place to provide a smooth, clean separation at release.

The portion of the latch attached to the carriage was coupled to it through a bridge frame anchored at the upper ends of the two aluminum alloy tubes that formed the vertical members of the carriage (fig. 5). This method of mounting insured that the upper plate of the carriage would not be subjected to bending due to suspension at its center. Consequently there would be no sudden release of stored energy to be transmitted directly to the vacuum chamber.

When the carriage was suspended from the latch, it was also in contact with the plunger of the initial accelerating spring. The accelerating spring assembly consisted of a precompressed helical spring contained in an adjustable barrel with provision to adjust both the force exerted by the spring and the vertical travel over which the plunger remained in contact with the carriage. These parameters controlled the amount of separation between the silica tube and the vacuum chamber support cone. As adjusted in practice, the spring exerted a force equal to approximately ten percent of the weight of the carriage and followed the carriage for about 8 mm in its downward travel after release of the latch. The spring assembly appears as the knurled and threaded barrel located just above the latch in figure 7.

The range of the acceleration spring adjustment was such that it was possible to adjust from a condition where the silica tube separated only momentarily

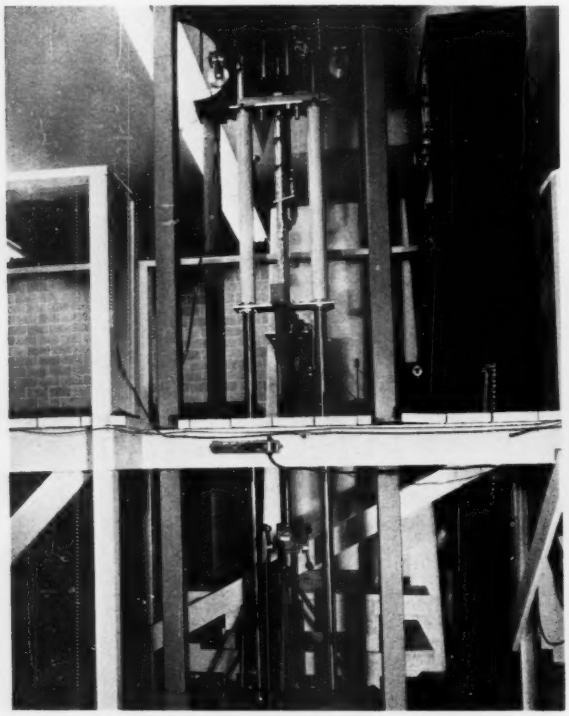

FIGURE 6. *General view of gravity machine.*

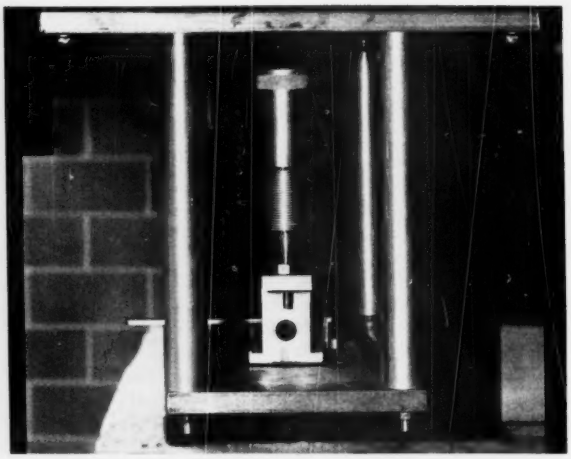

FIGURE 7. *Latch assembly with accelerating spring.*

from the supporting cone to a condition where the last aperture on the silica tube was no longer in line with the vacuum chamber optical window at the time it passed the sensing station. The actual operating condition was chosen at an intermediate value where the observed transit times were independent of the accelerating spring adjustment.

The vacuum chamber was attached to the carriage of the apparatus by centering screws so arranged that the upper and lower flanges of the chamber each rested against two adjustable screw stops on the longitudinal and transverse axes of the carriage. At each end a locking screw acting along a line at 45° to the screw stops held the flange in firm contact. This arrangement permitted the entire vacuum chamber to be removed from the carriage and then replaced without disturbing the alinement.

In the process of alining the vacuum chamber in the carriage, rotational orientation was established by observing the superposition of the images of a point light source reflected from the upper optical window of the chamber and from a glass flat in contact with the upper cross plate of the carriage. The optical axis of the sensing station was alined to be perpendicular to the same reference plane.

The apparatus was provided with a pneumatic receiving cylinder on the lower plate of the frame and a plunger attached to the lower crossplate of the carriage to bring the carriage to a stop at the end of its fall. The plunger was machined to fit the cylinder with a radial clearance of about 0.5 mm. A lubricated O-ring in a groove in the plunger completed the air seal between cylinder and plunger. The receiving cylinder was 56 cm long and 10 cm in diameter. A 5-m length of high-pressure type rubber tubing was connected to the cylinder through a port at the lower end. The other end of the tubing was connected to a closed-end section of larger diameter tubing. This combination provided damping to reduce the tendency of the carriage to rebound after being brought to a stop.

2.5. Optical System

The optical system of the position sensing aparatus is shown in figure 8 with the photomultiplier cell housing slightly retracted. This assembly was mounted on a steel bracket attached to a concrete pier directly behind the gravity apparatus (see figs. 3 and 6). The lens, a 100-mm microscope objective lens, focussed an image of the aperture plate edge on a slit mounted in the focal plane of a microscope eyepiece in the viewing system housing. This arrangement permitted an observer to focus the instrument by eye and to aline the slit with respect to the image. Once the alinement was completed, the optical system was terminated by the photomultiplier cell mounted in the sliding housing and making a light-tight seal to the viewing housing. The slit in the viewing system was approximately 4.5 mm long and 0.075 mm wide. The width of the slit was not critical and could have been much narrower since the output of the photomultiplier reached a maximum value in a 10-μm travel of the silica tube. As the magnification of the viewing

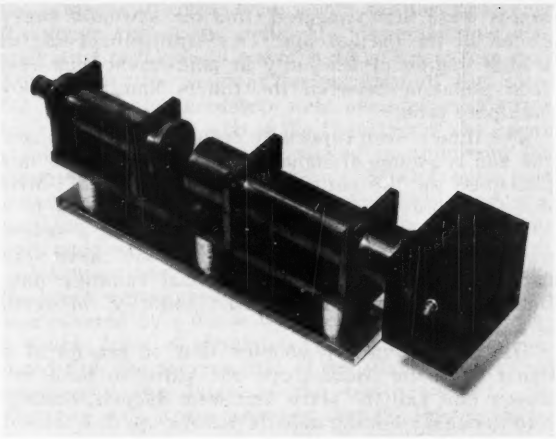

FIGURE 8. *Optical system with photomultiplier assembly.*

lens was approximately unity, a slit 10 to 12 μm wide would have been adequate. The wider slit was chosen in preference, however, since during the preliminary adjustment by eye, a narrow slit produces diffraction patterns making alinement and focussing of the images difficult.

The photomultiplier tube used was a 10-stage, head-on tube having a maximum response in the spectral region of 400 to 500 nm. The tube was operated at a cathode potential of 900 V. The photomultiplier tube anode was connected directly into a coupling amplifier. The coupling amplifier provided a low-capacitance, 51,000 Ω load on the photomultiplier anode. The anode potential was 6 V. The output of the coupling amplifier was connected to a 90-Ω terminated coaxial cable leading to the timing system.

The light source was an incandescent filament, galvanometer lamp operated at 6 V, direct current. The lamp had a straight, helical coil filament. The lamp was housed in a case having a lens on a focussing mount. The lens projected a roughly parallel beam of light which, with a vacuum chamber window in line with the axis, passed through the chamber window, through the transparent portion of the fused silica tube and provided a uniform illumination to the aperture edge plates mounted on the opposite side of the silica tube. The light source was mounted on a special telescope stand to facilitate levelling and positioning.

2.6. Electronic System

The power supplies employed for the apparatus included a low voltage direct current power supply for the light source and a high voltage direct current power supply for the photomultiplier tube. The signals from the photomultiplier tube were coupled by a coaxial cable into the input amplifier of a fast-rise cathode ray oscilloscope. The triggering circuit of the oscilloscope was adjusted to start the sweep circuit at some potential level of the linearly rising (negative) signal from the photomultiplier tube. The

timers were then triggered from the sawtooth sweep circuit of the oscilloscope. This arrangement offered a high degree of flexibility in adjustment plus very good isolation between the timers and the photomultiplier tube.

The timers were especially designed for the apparatus and sequence of signals employed. A master unit contained all the gating circuits required, a 1-MHz thermostatted quartz crystal oscillator coupled to a 10× frequency multiplier, the shaper, and a seven-place decimal counting unit. A second slave unit carried another seven-place decimal counting unit. Both counting units had a least count of one-tenth of a microsecond.

The timers were so coupled that on receipt of a signal from the oscilloscope the gates to both the master unit and the slave unit were opened, starting both decimal counting units. Upon receipt of a second signal, the gate to the decimal counting unit in the master timer was closed, leaving the gate to the slave unit open. The receipt of a third signal closed the gate controlling the slave unit.

The timers were provided with an optional circuit such that an interval displayed on the indicator panel could be retained while the gates were reset for a new timing sequence. Subsequent intervals were then added to the intervals already displayed. This circuit was not employed in the measurements on the falling silica tube but was utilized in assessing the errors of the gating circuits as described later.

3. Reference Standards

3.1. Length

The standard of length for the determination was an invar, 1-m line standard having an H-shaped cross-section. The scale was fabricated and ruled by the Société Genevoise d'Instruments de Physique of Geneva, Switzerland, in 1959. The scale was ruled in 1-mm intervals with line widths of about 5 μm. The coefficient of expansion of the invar was determined as 0.00000123 per degree Celsius.

The lengths of 0–300 mm and 0–1000 mm intervals on the scale have been compared to the standards of the United States periodically since the scale was received in February 1960. The results are shown in table 1. It was considered that the scale was very stable for an invar standard and that the results indicated no progressive drift in the lengths. Accordingly, the means of all of the reported corrections have been applied to the measurements of the fused silica tubes in the gravity determinations.

3.2. Time

The standard of time for the determination was based on the National Bureau of Standards frequency standards, since only time intervals were measured. The crystal controlled oscillator of the master timer was compared to a 1,000-Hz signal derived from the Bureau's quartz oscillator, which, in turn was compared on a daily basis to the WWV frequency standard.

TABLE 1. *Calibrations of invar line standard No. 5727*

Date of calibration	Corrections to nominal lengths		Estimated limits of error
	0 to 300-mm interval	0 to 1000-mm interval	
	m × 10 $^{-6}$	m × 10 $^{-6}$	m × 10 $^{-6}$
September 1960	−0.37	+1.16	±0.20
October 1961	[a]	+1.10	±.20
November 1962	−.22	+1.55	±.40
April 1964	+.03	+1.55	±.30
December 1965	−.20	+1.29	±.30
Mean correction	−0.19	+1.33	
Standard deviation	.17	.21	

[a] No determination made of 0 to 300-mm interval.

The comparison of the master timer with the 1,000-Hz reference signal was accomplished by starting the timer with a single sweep of the oscilloscope triggered from the reference signal. After an interval of approximately 100 seconds the oscilloscope sweep was reset and again triggered by the 1,000-Hz signal. Even though the interval displayed was not exactly 100 seconds, it was some integral multiple of 1,000 μs. Since the difference between the crystal oscillator of the timer and the frequency standard never exceeded 50 μs in 100 s, there was no ambiguity in determining the relative error of the timer frequency base.

The crystal oscillator was checked prior to each free-fall determination and again after it. Although, as indicated above, the oscillator was always maintained within 5 parts in 10^8, the observed corrections were applied to all time interval measurements.

4. Techniques of Measurement

4.1. Length

Measurements of the two lengths, L_1 and L_2, were carried out using the same apparatus employed in the free-fall determinations. The weight of the carriage was balanced by means of the steel tapes running over the frame pulleys with appropriate weights on the other ends of the tapes. The invar length standard was attached in holders beside the vacuum chamber in such a position that the rulings on the speculum surface could be viewed by a reading microscope attached to the support table for the position sensing apparatus. A fine motion drive was attached to a guide rod and served to advance the carriage by the small motions required.

Basically the procedure consisted of moving the carriage to a position where the lower aperture on the silica rod was in a position with respect to the sensing station such that the output signal from the photomultiplier cell was at the same potential as that which would trigger the oscilloscope-timer combination. At this point a reading was taken on the zero ruling of the invar scale with a filar micrometer on the reading microscope. The carriage was then moved on to bring the second aperture into line with the sensing station and a microscope reading taken

on the 300-mm graduation of the invar scale. The process was repeated again for the upper aperture and the 1,000-mm graduation.

It will be seen that this process is one of measuring how far the silica tube must be moved to produce the triggering signals rather than of measuring its length. This method of measurement has the advantage of including the effects of vacuum on the silica scale as well as any possible displacement of the images by the optical windows of the vacuum chamber. More important, since there are complex diffraction effects at a shadow edge, the measurement is related directly to the conditions present in the experiment and measures directly the quantity sought.

The reading microscope used for the observations on the invar scale was mounted on the base plate for the optical system. Provision was made for the microscope base to be attached on either side of the position sensing system. The microscope was mounted on a special base with a rack and pinion focussing control and a fine adjustment screw. The microscope tube length was 215 mm with a 22.5-mm objective and a 12.5×-filar micrometer eyepiece. The filar micrometer eyepiece was equipped with double cross-hairs spaced the equivalent of 12 μm in the object plane. The micrometer drum was graduated into 100 divisions per revolution. The reading microscope was calibrated on an auxiliary scale and had a factor of 1.112 μm per division. During observations the micrometer drum was read to one tenth of a division. In no case was it necessary to measure differences exceeding 50 divisions with the filar micrometer eyepiece.

During length measurements it was necessary to locate the carriage in a position where the output from the phototube amplifier was at the potential required to trigger the timing system. A direct current voltmeter with a trimmer was connected in parallel to the output of the amplifier and adjusted so that it indicated full scale at the maximum output of the amplifier. The triggering potential was then set to be at the half scale reading. The indication was such that the small graduations on the voltmeter corresponded to movements of about 0.2 μm at the carriage. The position could be set to a small fraction of a voltmeter division with the aid of the fine-motion drive. The meter was slow enough in response to mask the effects of photomultiplier tube noise and building vibration.

The fine-motion drive which made possible the adjustment of the carriage to the final position for reading the length standard consisted of a hinged brass clamp which could be opened, slipped around a steel guide rod and locked in place. A bronze spring provided sufficient frictional drag on the smooth rod to hold the clamp against the 100- or 200-g unbalanced weight of the carriage, yet permitted the clamp to be slid by hand as a coarse adjustment. Attached to the clamp was a flat wedge, driven by a fine thread screw, actuating a small push rod to move the carriage.

4.2. Temperature

The invar length standard was equipped with two mercury-in-glass thermometers, one mounted near the center of the 0 to 30-cm length and the other near the upper end of the scale. The thermometers were graduated to 0.2 deg Celsius and had errors less than 0.02 °C at the ambient temperature of the room (22 °C). The thermometers were mounted against the back surface of the web of the H-section of the length standard; the bulbs were packed in aluminum foil compressed against the surface of the invar and covered by 6 mm of cork sheet up to the graduated portions of the stems. The exposed portions of the cork pads were covered with a layer of aluminum foil.

A similar thermometer was mounted in contact with the lower section of the vacuum chamber. The chamber was covered by a 6-mm layer of cork sheet topped by a double layer of aluminum foil. While it was recognized that the temperature of the silica tube was not necessarily the same as the temperature of the chamber wall, it was assumed that the tube temperature maintained a reasonably constant relationship to it, once thermal equilibrium was established. The temperature of the vacuum chamber walls during length measurements averaged about 0.2 °C less than that during the free fall measurements. This difference probably was caused by the larger number of pieces of electronic equipment operating during the free fall measurements.

4.3. Compensation for Guide Curvature

The two guide rods, previously described, on which the carriage ran were of a special case-hardened steel, centerless ground and selected for straightness. The diameters were 63.47 ± 0.020 mm and the rods were straight within 80 μm per meter. These tolerances were quite adequate for operation in the free-fall phase of the experiment but the slight curvature of the rods was sufficient to make an appreciable error in the length measurement. The error is proportionate to the product of the angle of rotation of the carriage and the distance between the axis of the invar scale and the silica tube.

If the position of the silica tube and the invar scale are interchanged with respect to the direction of rotation, the algebraic sign of the error is reversed. Thus the mean of two measurements with the scale interchanged between them should be free of the error due to curvation of the guide rod, provided that the rotation of the carriage is the same in both sets of measurements.

The carriage of the gravity apparatus was provided with duplicate sets of holders for the invar scale, one set on each side of the vacuum chamber equidistant from the centerline of the silica tube. A length measurement consisted of two sets of measurements, one for each location of the invar scale. The final computed lengths from each set were averaged to obtain a working value. Ordinarily the first set of measurements was made at the start of a day. Upon completion of the first set, the invar scale was transferred to the opposite set of holders; about five hours later the second set of measurements was made. The order in which the two positions were occupied was reversed on alternate days of length measurement.

Analysis of the length measurements made on four different fused silica rods indicated that the length deviation due to curvature of the guide rod was about 1.6 μm at the 30-cm length and about 0.7 μm with opposite sign at the 1-m length.

5. Experimental Procedure

5.1. Length Measurements

In the plan of the experiment, length measurements and free-fall measurements were made on alternate days. A set of length measurements consisted of ten independent determinations of the two lengths, the silica tube being reseated and realigned and the reading microscope refocussed between determinations. At the conclusion of the set the invar length standard was transferred to the opposite side of the carriage and, after a lapse of about five hours, a second set of ten measurements was made.

The procedure in each determination was always the same. After reseating the tube and focussing the microscope, the thermometers were read and the temperature recorded. The carriage was then moved to a position where the first or lower aperture was at the reference level as indicated by the meter connected to the output of the photomultiplier tube amplifier. The zero graduation of the invar scale was centered between the cross-hairs of the filar eyepiece and the filar drum reading recorded to the nearest tenth of a division. The carriage was then moved to the second aperture position and the corresponding filar reading recorded. The process was repeated for the third aperture and the carriage returned to the first aperture position where the initial reading was repeated.

For the calculation of the two lengths, any change between the first and final lower aperture readings was assumed to be due to thermal drift, and values corresponding to the second and third aperture readings were obtained by interpolation with respect to the average time required for the operation. Any run in which the first and final lower aperture readings changed by more than 2 μm was discarded as such changes were apt to be caused by actual movement of the silica tube in its seat.

The lengths of the 30-cm and 1-m aperture distances were computed from the observed filar readings, the calibrated lengths of the invar standard intervals and the temperature correction for the invar standard (1.23×10^{-6} per degree Celsius). The measured lengths of the silica tube aperture intervals were corrected to 22 °C for comparison using an experimentally determined coefficient of 0.64×10^{-6} per degree Celsius. Since the temperature at which the free-fall measurements were made was close (within 0.2 °C) to that of the length measurements, coefficients of expansion were not determined separately for each of the four silica tubes used in the experiment.

5.2. Timer Adjustments

During the free-fall determinations, the times for the passage of the 30-cm length interval and for the 1-m interval were obtained from the two seven-decade timers already described. The smallest unit of time so displayed was one-tenth microsecond. Two corrections were applied to the time measurements. A correction for frequency of the crystal oscillator was applied, although it was negligible compared to other sources of error. A correction for differential delay in opening and closing of the gate circuits was also necessary. The indication in the unit which displayed the time interval for the 1-m length was consistently short by nearly one-tenth of a microsecond due to an electronic delay in opening the counting gate for this bank.

The gating errors for time interval meters were assessed by presenting the system with a series of pulses generated by a decimal dividing network and a crystal controlled test oscillator. The pulses were generated at intervals of 10 ms and the timers measured the time for a single and double pulse interval. A total of one hundred such measurements were summed in the counter banks of the timers. Since the mean of such a group of measurements tends to eliminate random effects, the result should reflect the systematic error in the time measurement system. It is assumed that the pulse source contained only random variations since it was a continuous system and the test oscillator was synchronized with the time interval crystal frequency to better than one part in ten million.

5.3. Free-Fall Measurements

Free-fall measurements were made on days alternating with length measurements. The free-fall measurements normally consisted of two sets of 16 determinations, one set being made at the start of the day and one set at the end of the day.

The first steps in the free-fall measurements entailed determinations of the crystal frequency error and the mean gating errors for both channels. The timing system was connected to the 1,000-Hz reference signal and the time for approximately 100,000 cycles measured. The input and triggering circuit used was the same as that used for the photomultiplier cell. The departure from the nominal multiple of 1,000 μs indicated the crystal frequency error in 100 s. Single cycle measurements of the period of the 1,000-Hz standard signal, as received, all fell within a band of ± 0.2 μs, about the average value of the period. A group of measurements over 100 s (approximately 10^5 cycles) showed a standard deviation of 0.9 μs, approximately one part in 10^8. After the crystal frequency error was measured, single and double individual period measurements were made on a decade divider pulse signal at a frequency of 100 Hz. The timers were operated to total 100 such measurements and the mean gating errors computed from the two sums indicated by the timers.

After these values had been recorded, the valve in the vacuum pump line was closed and the pump disconnected. The vacuum pressure was read, the gage indicator disconnected, and the timing system connected to the cable of the photomultiplier cell.

At this point the system was ready for the time measurements on the falling silica tube. The silica tube was alined in the vacuum chamber by means of the upper guide bearing mechanism and the guide bearing was retracted and locked in place. The vacuum chamber wall temperature was recorded and the release latch opened, permitting the carriage to fall. At the conclusion of the fall the carriage was immediately returned to the latched position and the two time intervals recorded. The silica tube was realined in the chamber and the apparatus was ready for the next determination.

During the set of measurements, the wall temperature of the vacuum chamber was recorded for every fifth drop of the carriage. At the conclusion the vacuum pressure was read and the frequency and gate error measurements repeated. The entire set of measurements required about three-quarters of an hour.

6. Results

6.1. Experimental Data

Four different fused silica tubes were included in the experiment. There were five sets of length measurements for each tube, a set consisting of two sub-sets made with the invar length standard on alternate sides of the vacuum chamber as outlined in the section on length measurements. Bracketted between each pair of sets of length measurements were two sets of free-fall measurements. A set of free-fall measurements consisted of about sixteen individual free falls of the apparatus. A few sets contained only fifteen observations and some sets contained as many as twenty-one. Since five sets of length measurements provide four adjoining pairs, there were normally eight sets of free-fall measurements for each tube.

There were two exceptions to this general rule. In the case of tube No. V, four free-fall measurements were included between the first two pairs of sets of length measurements, changing the total to twelve. In the case of tube No. VI, a readjustment of the optical system of the position sensing station became necessary after the conclusion of the third set of length measurements. The adjustment was made and a new set of length measurements inserted to go with the succeeding free-fall measurements.

A summary of the length measurements for the four silica tubes is given in table 2. Each entry in the table represents the mean of two sub-sets of 10 independent measurements. From the standard deviations of the individual sub-sets an estimate was made of the average standard deviation of the measured length intervals reported in the table. The standard deviations were approximately 0.14 μm for both the 30-cm and the 1-meter intervals. It is evident that the variations in length appearing in the table are partly random and partly due to real changes. In order to obtain adjusted length values corresponding to the free-fall measurements the data were treated as though all differences were real and as though the changes took place at a uniform rate during the course of the intervening free-fall operations. Accordingly, the adjusted length intervals were calculated by linear interpolation between adjacent measured length intervals. The adjusted values were then corrected from 22 °C to the observed chamber temperature for each set of free fall measurements. The adjusted and corrected length interval values appear in table 3.

TABLE 2. *Measured length intervals for fused silica tubes*

Tube no.	Date	Measured lengths at 22 °C	
		L_2	L_1
		Meter	*Meter*
III	May 21, 1965	0.999 950 16	0.299 953 04
	May 24	950 32	953 62
	May 26	949 22	953 53
	May 28	949 44	953 67
	Jun 2	949 66	953 92
IV	Jun 4	1.000 018 29	0.299 993 42
	Jun 7	017 60	993 34
	Jun 9	017 58	993 37
	Jun 11–12	018 25	993 26
	Jun 21	017 75	993 32
V	Apr 13	1.000 021 39	0.300 012 10
	Apr 16	022 48	012 48
	Apr 29	021 55	012 12
	May 3	022 13	012 04
	May 5	023 14	012 18
VI	May 7	1.000 050 76	0.300 018 34
	May 10	050 20	018 48
	May 12	049 70	017 98
	May 14	049 62	022 14
	May 17	049 66	021 50
	May 19	049 51	021 49

Note: Between the observations on the dates of May 12 and May 14 an adjustment was made to the lens diaphragm of the viewing system.

The time intervals presented in this table are the mean times determined from each set of free-fall observations after correction for both frequency and gating errors as described in the section on time measurements. The corresponding values of the acceleration due to gravity are calculated from the relationship

$$g = \frac{\frac{L_2}{t_2} - \frac{L_1}{t_1}}{\frac{1}{2}(t_2 - t_1)}.$$

The values in the final column are the standard deviations of the gravity values computed from the distribution of the pairs of individual free-fall time measurements about the two mean intervals for each set of free-fall observations. The standard deviation of an individual free-fall determination may be calculated by multiplying the standard deviation of the mean by the square root of the number of observations in the set, given in parentheses.

The mean values of the gravity measurements for each of the four tubes are presented in table 4. The standard deviations for the means were calculated from the distributions of the individual set means. The final result was computed as the unweighted mean of the four tubes. The mean of the 36 individual sets gives the same value.

TABLE 3. *Free-fall time and length measurements*

Tube No.	Date 1965	Eastern standard time	Chamber temperature	Adjusted lengths corrected to chamber temperature		Mean time intervals from free-fall observations		Mean acceleration	Standard deviation of mean and number of observations
				L_2	L_1	t_2	t_1		
			°C	Meter	Meter	Second	Second	cm/s²	cm/s²
III	May 22	719/735	21.98	0.999 950 19	0.299 953 18	0.348 391 11	0.155 733 04	980.1006	0.0009 (16)
	22	1958/2016	22.12	950 36	953 50	394 77	735 92	.1007	.0011 (16)
	25	718/735	22.12	950 12	953 62	395 19	736 39	.1019	.0011 (16)
	25	1417/1435	22.14	949 59	953 58	398 52	738 96	.1012	.0015 (15)
	27	747/805	22.18	949 32	953 57	389 84	732 47	.1025	.0010 (16)
	27	1512/1533	22.07	949 50	953 67	394 05	735 52	.0997	.0016 (16)
	29	730/748	22.20	949 63	953 77	393 86	735 40	.0998	.0011 (16)
	29	1938/1957	22.20	949 73	953 90	394 47	736 06	.1028	.0010 (16)
IV	Jun 5	710/734	22.19	1.000 018 24	0.299 993 44	0.348 358 59	0.155 711 97	980.1009	0.0008 (16)
	5	1937/1955	22.18	017 89	993 39	361 20	714 09	.1026	.0006 (16)
	8	749/815	22.15	017 70	993 38	365 96	717 66	.1011	.0007 (16)
	8	1450/1530	22.12	017 66	993 38	369 53	720 38	.1011	.0007 (16)
	10	805/821	22.08	017 85	993 37	370 44	721 10	.1022	.0005 (15)
	10	1402/1422	22.16	018 13	993 31	370 38	720 98	.1021	.0005 (17)
	19	735/800	22.35	018 34	993 35	361 81	714 41	.1016	.0010 (16)
	20	919/936	22.21	018 01	993 34	364 30	716 28	.1002	.0007 (15)
V	Apr 14	812/825	22.20	1.000 021 66	0.300 012 19	0.348 606 28	0.155 906 84	980.1000	0.0007 (16)
	14	1515/1527	22.16	021 90	012 27	610 50	910 06	.1003	.0007 (15)
	15	806/820	22.14	022 16	012 37	613 76	912 45	.0987	.0007 (16)
	15	1704/1720	22.00	022 34	012 43	613 83	912 62	.1009	.0008 (16)
	26	1418/1438	22.06	022 40	012 45	614 45	913 07	.1006	.0005 (15)
	27	756/830	22.12	022 21	012 36	620 33	917 60	.1016	.0008 (16)
	27	1605/1621	22.08	021 95	012 28	622 82	919 53	.1019	.0008 (16)
	28	745/810	22.17	021 78	012 19	622 82	919 53	.1020	.0006 (16)
	30	739/759	22.15	021 80	012 13	626 86	922 61	.1025	.0011 (16)
	30	1458/1515	22.20	022 11	012 10	629 23	924 22	.1002	.0010 (16)
	May 4	711/724	22.20	022 51	012 12	629 71	924 59	.1013	.0009 (16)
	4	1450/1516	22.22	023 03	012 18	629 21	924 29	.1039	.0005 (16)
VI	May 8	653/733	22.22	1.000 050 76	0.300 018 42	0.348 267 64	0.155 646 73	980.1019	0.0008 (16)
	8	1924/1948	22.24	050 49	018 49	271 03	649 31	.1007	.0008 (21)
	11	712/730	22.18	050 20	018 39	275 95	652 88	.0974	.0009 (16)
	11	1517/1542	22.17	049 93	018 13	279 74	655 93	.1013	.0008 (15)
	15	733/802	22.14	049 74	022 01	310 18	680 52	.1007	.0009 (21)
	15	1545/1610	22.17	049 74	021 69	304 69	676 30	.1020	.0016 (20)
	18	757/814	22.15	049 72	021 53	313 35	682 81	.1016	.0008 (16)
	18	1522/1541	22.18	049 67	021 52	310 71	680 64	.0986	.0011 (16)

TABLE 4. *Summary of gravity values*

Tube No.	Number of sets	Mean acceleration due to gravity	Standard deviation of the mean
		cm/s²	cm/s²
III	8	980.1012	0.0004
IV	8	980.1015	.0003
V	12	980.1012	.0004
VI	8	980.1005	.0006
Unweighted mean of four tubes		980.1011	0.0002

7. Sources of Bias

There are several potential sources of systematic error in an experiment of this type. Although the amounts of error contributed cannot always be evaluated accurately, limits can usually be set for them. It is considered that the principal contributions to error in the results of this measurement are the following: longitudinal vibration of the falling tube, electrostatic and magnetic forces, residual air in the vacuum chamber, lateral deflection of the falling object, effects from the optical windows of the chamber, time constants of the electronic circuits, and uncertainty in the length standards and measurements.

7.1. Longitudinal Vibration

At the instant of release the fused silica tube rests on the support cone which, upon release, moves downward with an acceleration about 10 percent in excess of gravity. It is reasonable to expect that the release of the slight compression of the silica tube would cause it to vibrate longitudinally while falling. As the displacement of the various parts of the tube would cause an error in time indication, the magnitude of the error is worth examining.

The largest amplitudes would be those due to the first mode of vibration in which there is a maximum amplitude at the extremities of the tube and a node at the center. For a fused silica tube or rod with density 2210 kg/m³, modulus 7.2×10^{10} N/m², and a length of one meter, the undamped frequency of the first mode is about 2850 Hz, corresponding to a period of 350 microseconds. The static compression of the tube relative to the center of mass would be 0.113 μm and the maximum harmonic acceleration under these conditions would be 3620 cm/s². Since this acceleration is greater than that of the support (approximately 1080 cm/s²), the surfaces cannot separate until the elastic deformation is reduced to a point where the sum of the harmonic acceleration and the acceleration of the center of mass is less than 1080 cm/s².

Assuming the limiting case in which the acceleration of the center of mass prior to separation is assumed to be zero, the separation would occur at about 71 μs after the release is initiated, approximately 81 percent of the first quarter period. At this point the common velocity of the two parts is determined by the velocity of the uniformly accelerated support, about 0.0765 cm/s. The resultant undamped amplitude of vibration of the fused silica tube corresponding to this speed and displacement would be 0.045 μm. The maximum effect of such an amplitude would result in an error less than 0.0003 cm/s^2 in an individual measurement. Such an error represents the upper limit possible. The calculation has not included motion of the center of mass of the silica tube which would necessarily occur with a consequent reduction in the harmonic velocity at the time of separation. Furthermore, the silver conductive coating on the tube would add considerably to the damping of the vibration.

It is considered that errors of the above magnitude would not occur consistently in a long series of measurements and can thus be considered negligible.

7.2. Electrostatic Forces

It has been the experience of most investigators in free-fall gravity experiments that electrostatic forces constitute a major source of difficulty. The separation of any two surfaces, particularly in a vacuum, usually leaves them in a charged condition. It is not necessary for the surfaces to slide in order to produce the charges. If one or both surfaces are poor conductors, the charges may remain highly localized and the electrostatic forces arising from the interaction of the intense fields may be quite substantial. The introduction of radioactive materials into the chamber offers little help as the gas pressure is too low to afford many ions and the time too short for them to dissipate the charges effectively.

In some early experiments with the apparatus described here, a fused silica rod was provided with a polytetrafluoroethylene tip. The charge generated by the separation of the tip from its seat was sufficient to draw the falling rod several millimeters out of its path during the 0.5-s fall.

The electrostatic charge problem can usually be solved by making the entire falling object electrically conductive. In the case of the fused silica tubes employed in this experiment, the objective was attained by coating the transparent tubes with silver conductive paint of the type used for printed circuit assemblies. The end-to-end resistance of the tubes ranged from 4 to 10 Ω. The tubes were coated on the outsides leaving uncoated only small areas in line with the slit apertures. Since it was possible to vary the separation between the tube and the support cone during the fall by changing the force applied by the initial accelerating spring, it could be ascertained that any remaining electrostatic attraction was below the limit of detection.

7.3. Magnetic Forces

Magnetic forces are not usually a substantial factor in free-fall gravity measurements provided the falling object can be constructed of nonferromagnetic materials. In the experiment described here, three of the tubes employed contained small amounts, less than 300 mg each, of steel in the form of thin plates for the aperture edges. The other tube, No. III, contained no ferromagnetic materials. Since the magnetic field of the earth was fairly uniform along the line of fall of the silica tube, it is considered that the net effect of magnetic attraction on the tube was negligible.

Effects caused by eddy currents would likewise be small. An analysis by E. C. Lloyd [3] of the National Bureau of Standards expresses the average ratio of the force due to eddy current losses to the gravitational force, F_m/F_g, for a conducting tube falling through a magnetic field discontinuity which is short compared to the length of the tube.

$$\frac{F_m}{F_g}=\frac{A^2t\sigma(\Delta H)^2}{1.27m(\Delta l)}\times 10^{-12}$$

where A = area enclosed by the tube, square meter,
t = time of fall, second,
σ = circumferential conductivity of the tube, mho/meter,
m = mass of the tube, kilogram,
Δl = length of the magnetic discontinuity, meter,
ΔH = change in magnetic field strength, ampere/meter.

For the experiment described here, $A=1.87\times 10^{-4}$m^2, $t=0.35$s, $\sigma=100$ mho/m, $m=0.1$ kg. If one assumes a value for Δl of 0.01 m and for ΔH of 12 A/m,

$$\frac{F_m}{F_g}=1.3\times 10^{-13}.$$

7.4. Residual Air

The principal effects of air on a falling object are the buoyant forces due to the density gradient in the air and the viscous drag resulting from relative motion of the object. The buoyant effect with fused silica is less than 600 parts in one million at atmospheric pressure and, since it varies in direct proportion to the pressure, can be considered negligible at pressures below 16 N/m^2. In the experiment the pressure at no time exceeded 1.5 N/m^2. The average pressure during the 36 sets of free-fall measurements was 0.4 N/m^2.

The viscous drag effects of air on a falling object are more complex. At pressures above 100 N/m^2 the inertial effects of the gas tend to be the predominant factor, while at lower pressures the predominant factor tends to be momentum transfer from molecular collisions with the object. Both effects overlap and there are no sharp boundaries between them. Cook [16] (Section 5.3) has discussed several cases and has shown that, at low pressures for a rod of radius r and density ρ, the ratio of the molecular forces to the gravitational forces would be expected to be less than

$$\frac{F_m}{F_g}=\frac{C\alpha}{2\rho rg}U$$

[3] Informal communication to the author, January, 1962.

where α is the gas density, C is the average molecular velocity, and U is the object speed. The gas pressures present in this experiment were such that the Stokes law forces would be expected to be of the same order of magnitude or less.

If $\alpha = 5 \times 10^{-12}$ kg/m^3, $C = 5 \times 10^2$ m/s,

$$r = 7.5 \times 10^{-3} \text{ m}, \rho = 2 \times 10^{-3} \text{ kg/m}^3,$$

and $U = 2 \times 10^{-3}$ m/s, the ratio would be of the order of

$$\frac{F_m}{F_g} = 0.014 \times 10^{-6}.$$

From the estimate above it would be expected that the total effect due to residual air would be less than 0.03 parts in a million.

In the earlier course of the experiment a few determinations were made with atmospheric pressure in the vacuum chamber. Since the air in the chamber is being accelerated downward at approximately the acceleration due to gravity it might be expected that the buoyant effect would be very small. For the limited number of tests conducted, results at atmospheric pressure did not differ significantly from those obtained at the normal pressures of 0.2 to 0.5 N/m^2.

7.5. Deflection of the Falling Object

Any lateral impulse imparted to the falling tube would cause it to rotate about a horizontal axis through its center of mass. Since the reference slits lie both above and below this point and in a plane about 8 mm closer to the viewing microscope, the amount of error depends on the plane of rotation.

Rotations in a vertical plane perpendicular to the optical axis were measured by photographing the falling tube with a 25-μm wire stretched vertically across the upper slit. The photographs were made through the microscope of the optical sensing system, using a short-duration flash synchronized with the falling tube. The photographs showed random departures on both sides of the average line of fall varying up to a maximum of 0.2 mm.

Rotation in the plane containing the optical axis could not be measured, but there was no evidence from the sharpness of focus of the photographs that the motion exceeded that in the other plane.

The motion observed in the photographs was probably due to a combination of both lateral translation and rotation at the center of mass. Lateral translation would theoretically contribute no error.

A computation of the error due to pure rotation of the maximum observed amount was made for motion both in the plane of the optical axis and perpendicular to it. The fact that the aperture plates were located off the axis of the tube makes the computation slightly different for the two planes. The computed magnitudes of the errors were approximately the same for both cases, however, about $8 \times 10^{-8} g$.

Errors due to rotation in the plane containing the optical axis are positive or negative according to the direction of rotation and thus are not likely to contribute systematic error. Rotation in a plane perpendicular to the optical axis always results in a value of gravity which is too high, but it would be expected that the average systematic error would not exceed 0.05 mGal. It did not appear feasible to apply a correction for this error as it could not be determined which part of the 0.2-mm maximum displacement of the wire image was due to rotation and which part was due to lateral translation.

7.6. Ground Motion

No attempt was made to measure seismic ground motion during the observations. It is considered that the greatest effect would arise from microseisms with periods on the order of 0.7 s. It was considered preferable to operate the release without regard to the existing amplitude and phase of the ground motion rather than to observe the seismic motion and time the release for optimum conditions. In effect this represents accepting a larger but purely random variability in preference to a smaller but less purely random one.

One source of ground movement which can operate to produce systematic bias, however, is the shock wave resulting from the release of the falling object. In the present experiment, the mass of the moveable carriage with the vacuum chamber was of the order of 22 kg.

The transient disturbance introduced by the release of the 22-kg carriage was studied with the aid of a Johnson-Matheson seismometer having a frequency range of approximately one to five cycles per second. The measurements indicated that the pier to which the position sensing station was attached experienced a sharp upward impluse from the release of the car and returned to its original level within about 70 to 80 ms. The amplitude of the motion was on the order of 0.15 to 0.2 μm. The motion appeared to be heavily damped as there was no appreciable overshoot on the return. Random motion of the pier due to other disturbances within the building at times produced motions of the same order of magnitude.

Since the time measurements for the gravity determination were not initiated until about 118 ms after release it is believed that the systematic effect of the shock wave from the release of the carriage was negligible.

7.7. Effects from Optical Windows

The vacuum chamber was equipped with three pairs of optical windows to permit observations on the fused silica tube inside. The windows, previously described, were 4.5 mm thick. It was at first considered that since any optical displacements which they produced were included in the static length measurements they were not likely to be the cause of systematic error. This assumption proved to be far from correct.

Initial measurements made with the apparatus produced results which showed a long-term, quasi-periodic variability which could not be accounted for

by any reasonable assumption of either errors in the measurements or secular changes in gravity.

During these measurements the vacuum chamber was over-constrained in its attachment to the carriage, the flat parallel ends of the chamber rested between the two parallel cross members of the carriage with a light friction fit and were secured against lateral movement by centering screws. The latch from which the carriage was suspended was attached directly to the upper cross-member of the carriage just above the vacuum chamber. It was suspected that the chamber was being loaded eccentrically by distortions of the carriage frame resulting from release of the latch. If such eccentric loading should cause some elastic bending of the vacuum chamber during the fall with a resultant rotation of the optical windows, the effect could be significant.

The displacement of the image of an object viewed through a plane-parallel glass plate is sensitive to tilt of the plate. The displacement for small angles of tilt is on the order of

$$d = T\theta\left(1-\frac{1}{N}\right)$$

where T is the plate thickness, θ is the angle of tilt and N is the index of refraction. For a thickness of 4.5 mm and an index of refraction of 1.5 a rotation of one minute of arc will produce an apparent displacement of about 0.4 μm.

On the hypothesis that sufficient flexure of the chamber was taking place to produce window rotations of this order of magnitude, and that the amount of flexure would vary with slight differences of temperature between the brass chamber and aluminum alloy carriage, the vacuum chamber mount was redesigned. The chamber was slightly shortened to produce a positive clearance at the upper end in the carriage and a single point support was provided at the lower end on the central axis of the chamber.

The modification effectively eliminated the long-term variations in the observations. Later, when the apparatus was moved from the older site in the East Building of the Bureau to the new Gaithersburg site where the observations reported here were made, the carriage itself was modified. The connection between the latch and the carriage was made through two independent yokes which were attached to the carriage at points directly above the two vertical tubular structures. This arrangement eliminated the flexing of the cross-members supporting the vacuum chamber.

7.8. Time Constants of the Circuits

The 10-stage photomultiplier tube used in the measurements had a spectral sensitivity peak in the 400- to 500-nm range and was always used in the dark-to-light transition condition. Connection to the coupling amplifier circuit was less than 5 cm long and unshielded to minimize capacitance loading of the anode. The anode current was limited to 0.1 mA at full illumination. The entire phototube circuit through the coaxial cable connections to the timer panel was capable of following illumination rise times at least five times greater than those provided by the gravity apparatus.

7.9. Uncertainty in the Length Standard

Of the two standards employed in the measurements, length and frequency, the length standard was by far the more critical in terms of the difficulty in obtaining the desired precision in its calibrations. The standard, an H-section scale of invar was ruled by the Société Genovoise. The 1-m length was graduated into 1-mm intervals. The width of the engraved lines was approximately 5 μm. Only the 0-, the 300-, and the 1000-mm lines were used in the measurements. The calibrations of the scale were limited to the intervals defined by those lines.

Table 1 shows the results of the calibrations of the scale made by the Length Section of the National Bureau of Standards. No determination was made of the 300-mm interval in the 1961 calibration because of the very small change observed in the 1000-mm interval. The table shows that the standard deviations over the five-year period compare very favorably with the estimated limits of error for the individual determinations. Since the scale was in active use over the greater part of the five-year period, it was concluded that the stability was excellent with no significant drift. The mean corrections were selected as giving the most reliable values for the lengths of the two intervals.

Some estimate of the effect of the different length determinations obtained for the invar scale can be made by computing a series of gravity values in which the successive length corrections are the only variable. Using the adopted mean corrections as a reference, the calibrations of 1960, 1962, 1964, and 1965 would have resulted in gravity values differing from the reference level by $+0.5$, $+0.7$, -1.0, and -0.2 mGal respectively. The standard deviation of the mean correction would be 0.4 mGal. This result illustrates one disadvantage in the use of an intermediary standard in a measurement requiring the greatest possible accuracy.

7.10. Uncertainty in the Length Measurements

As previously indicated in Section 4.1, a determination of the two lengths, L_1 and L_2, of a silica tube consisted of ten measurements of each length with the invar scale on one side of the carriage and ten measurements of each length with the scale on the other side. The two sets were averaged to give the final value. The individual sets showed good internal consistency even though a set required about one hour to complete. The standard deviation of a single length determination of either the 300-mm or the 1000-mm interval was usually on the order of 0.6 or 0.7 μm; thus the standard deviation of the mean of ten would be on the order of 0.2 μm. As indicated earlier, there was usually some evidence of real change in the interval lengths over the complete series of free-fall experiments.

An interesting side effect in the length measurement is the small error due to the relative shortening of the

invar scale and the silica tube when they are supported at rest in vertical positions. The length desired is, of course, that of the silica tube in its relaxed condition in free fall. The length of the invar scale is determined in the length laboratory in a horizontal position while supported at the Bessel (Airy) points. Neglecting the slight droop of the bar between the support points, it can be considered in a relaxed condition during this comparison. If now the scale and the tube are supported on their lower ends in a vertical position, both will be compressed slightly under their own weight. The changes in lengths are in proportion to the ratio of the densities of the materials to their respective moduli of elasticity.

The decrease in length of a rod or tube standing on its lower end is given by the relationship

$$\Delta L = \frac{\rho g}{E} \int (L_0 - y) dy$$

where ΔL is a change in length, ρ is the density, and E is the modulus of elasticity. If the origin is taken as the bottom of the tube, at $y = L_0$ the integral has the value

$$\Delta L = 0.5 \frac{\rho g}{E}$$

and at $y = 0.3 L_0$ the integral is

$$\Delta L = 0.255 \frac{\rho g}{E}.$$

The fused silica used in the tubes had a density of approximately 2210 kg/m^3 with a modulus of 7.2×10^{10} N/m^2. Invar has a density of approximately 8000 kg/m^3 and a modulus of 14.8×10^{10} N/m^2. The computed corrections for the tubes and invar length standard are as follows:

	30-cm interval	1-meter interval
	μm	μm
Invar	−0.14	−0.26
Silica	−0.08	−0.15
Difference	−0.06	−0.11

Although these corrections are below the level of significance in the measurements, the differences were systematic and were applied in the adjustment of the lengths of the fused silica tubes.

Since the temperature of the silica tube was not measured directly, the assumption was made that it tended to remain at some relatively stable level in relation to the temperature of the vacuum chamber which surrounded it. Some indication of the validity of this assumption can be obtained from an auxiliary set of measurements made on a brass tube of identical size and construction as the fused silica tubes from which the formal determination was made.

The brass tube was subjected to an identical set of alternating length measurements and free-fall measurements as were the fused-silica tubes. The set of experiments with the brass tube followed immediately upon the conclusion of the determinations with the four silica tubes. The decision was made at the outset that regardless of what result was obtained with the brass tube, the result would not be included in the value of gravity to be reported.

The length intervals for the brass tube were measured at vacuum chamber temperatures ranging from 21.88 to 22.00 °C and corrected to 22 °C using a coefficient of thermal expansion of 18.5×10^{-6} per degree Celsius. The results are given in table 5.

TABLE 5. *Measured length intervals for brass tube*

Date	Measured lengths at 22 °C	
	L_2	L_1
	Meter	*Meter*
July 2, 1965	0.999 733 06	0.299 962 06
July 7	734 23	962 30
July 12	734 50	962 18
July 14	734 34	961 94
July 16	734 16	962 02

Brass has a temperature coefficient such that a change of 0.1 °C would change the 1-m length by nearly 2μm. The table indicates that, aside from a single shift between the first two measurements of the 1-m interval, the brass tube showed as good repeatability as the fused silica tubes. Since the temperature coefficient of thermal expansion of brass is about 27 times that of fused silica, the evidence appears to substantiate the assumption that the temperature of the falling object followed that of the vacuum chamber reasonably well.

7.11. Uncertainty in the Final Result

From the foregoing discussion of systematic error it is concluded that the principal known source of error of a systematic nature lies in the uncertainty in the value of the length standard. The uncertainty in the time standard is too small to affect the final result significantly.

Effects such as seismic disturbances, lunar and solar tides and random errors in the time and length measurements are included in the variability of the gravity values shown in tables 3 and 4. The uncertainty in the final result is considered to be due principally to the contributions of this variability and the uncertainty in the evaluation of the invar length standard.

From the standard deviations of 0.00021 cm/s^2 for the length and time measurements and of 0.00039 cm/s^2 for the length standard, it is estimated that the uncertainly in the final result is represented by a standard deviation of 0.00045 cm/s^2.

8. Comparison with Other Gravity Values

The mean value of 980.1011 cm/s^2 given in table 4 is that determined directly from the measured parameters of the experiment. Since there is a gravity

gradient of approximately 0.0003 cm/s²/m, it is necessary to know the effective height at which the machine determines the value. An expression has been derived by Preston-Thomas et al. [10] by which the effective elevation above the optical axis at which gravity is determined can be computed. The effective height, H, can be expressed as:

$$H = H_0 - g\left[\frac{1}{12}\left(\frac{t_2^3 - t_1^3}{t_2 - t_1}\right) + \frac{\Delta t}{6}\,(2t_2 + 2t_1 + 3\Delta t)\right]$$

where H_0 = elevation of the center of gravity of the silica tube above the optical axis at the time of release,
Δt = time from the instant of release to the instant of initiation of the time measurements,
t_2 = time for the 1-meter interval,
t_1 = time for the 30-cm interval.

In the apparatus H_0 had the value 56.8 cm, Δt was 0.1184 s and t_2 and t_2 were given typical values of 0.3486 and 0.1559 s respectively. The resulting value of the effective height above the optical axis is 14.2 cm.

To establish a permanent reference point for the absolute value at a location suitable for gravity meter measurements, a location on the floor of the same room was selected as shown in figure 9. The absolute measurement site is designated NBS–1 and the reference site is designated NBS–2.

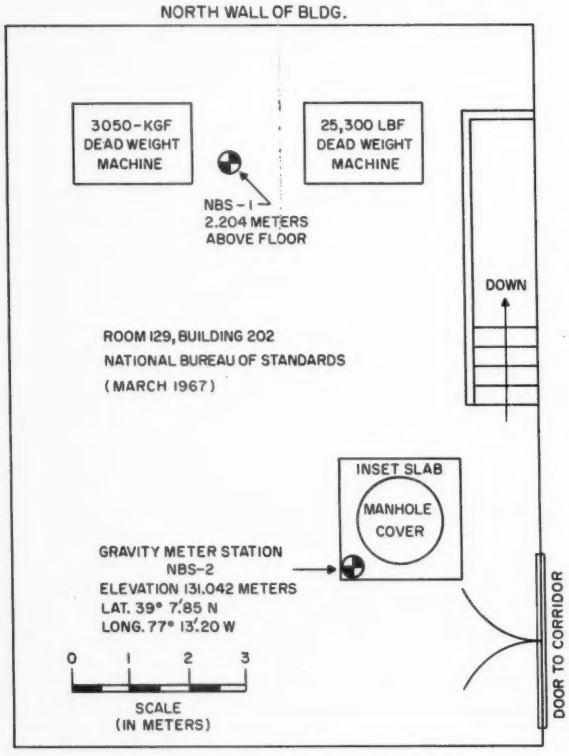

FIGURE 9. *Gravity reference station.*

The elevation of NBS–2 was established by a first order survey by the Levelling Branch of the Coast and Geodetic Survey, Environmental Science Services Administration, U.S. Department of Commerce.

Gravity meter connections linking NBS–1 and NBS–2 to the national gravity base in the Department of Commerce Building were made in November 1965 by the Gravity and Astronomy branch of the Coast and Geodetic Survey. These connections also included the station in the sub-subbasement of the East Building where Heyl's absolute measurement had been made.

A summary of the gravity differences taken from the report of the Coast and Geodetic Survey is given in table 6. The differences are referred to the national gravity base, specifically the top of the east elevated pier in the gravity room of the Commerce Building. The gravity meter observations were made with three gravity meters in a double loop including two other stations in the area. The standard error for the stations NBS–1 and NBS–2 was 0.03 mGal and that for the sub-subbasement of the East Building was 0.02 mGal.

TABLE 6. *Gravity differences from national gravity base*

Station description	Gravity value at the station minus gravity value at the national gravity base in the Department of Commerce Building
	mGal
Support for optical axis of absolute gravity machine, Station NBS–1	−3.59
Permanent reference on floor of Room 129, Bldg. 202, Station NBS–2	−2.97
Floor of the sub-subbasement of the old NBS East Bldg.	−19.46

The optical axis of the absolute gravity apparatus was 12.1 cm above the support plate which, in turn, was 220.4 cm above the floor. The machine, therefore, measured gravity at a point 232.5 + 14.2 cm above the floor. An adjustment of + 0.0007 cm/s² based on the observed gravity gradient of − 0.28 mGal/m of elevation was applied to the absolute result to correct it to station NBS − 2. The absolute value of gravity for station NBS − 2, as determined by the experiment, and the coordinates of NBS − 2 are:

$g = 980.1018$ cm/s²,
Lat = 39°07.85′ north,
Long = 77°13.20′ west,
Elevation = 131.042 m above mean sea level.

A comparison to the Potsdam system may be made from the gravity meter connections to the national gravity base in the Department of Commerce Building. If a Potsdam value of 980.1180 cm/s² is assigned to that station, the corresponding value for NBS − 2 would be 980.1150 cm/s². The NBS absolute result is 13.2 mGal less than this. This result is in general agreement with the results of other recent absolute gravity measurements.

9. Conclusion

A measurement of the absolute value of the acceleration due to gravity has been made and referenced to a permanent gravity meter station on the grounds of the National Bureau of Standards near Gaithersburg, Maryland. The value established for the reference station is 980.1018 cm/s² with a standard deviation of 0.0005 cm/s². This result, transferred to the top of the east elevated pier in the gravity room of the Department of Commerce Building, Washington, D.C., gives a value of 980.1048 cm/s² with the same standard deviation.

The author is deeply indebted for the helpful advice and assistance given by the staff of the National Bureau of Standards during the course of the work. He is particularly indebted to Mr. J. H. Troxell, who made the length measurements during the final determination.

10. References

[1] P. G. Roll, R. Krotkov, and R. H. Dicke, The equivalence of inertial and passive gravitational mass, Ann. Phys., **26,** 442–517 (1964).

[2] A. H. Cook, The absolute determination of the acceleration due to gravity, Metrologia, **1,** 84–114 (1965).

[3] F. Kühnen and P. Furtwängler, Bestimmung der absoluten Grösze der Schwerkraft zu Potsdam (Veröffentlichung des K. Preuszischen geodätischen Institutes, N. F. no. 27) Berlin: P. Stankiewicz, 1906.

[4] P. R. Heyl and G. S. Cook, The value of gravity at Washington, J. Res. NBS **17,** 805–39 (1936)RP946.

[5] J. S. Clark, An absolute determination of the acceleration due to gravity, Phil. Trans. Roy. Soc. London, Ser. A., **238,** 65–123 (1939).

[6] H. L. Dryden, A reexamination of the Potsdam absolute determination of gravity, J. Res. NBS, **29,** 303–14 (1942)RP1502.

[7] H. Jeffreys, On the absolute measurement of gravity, Monthly Notices Roy. Astron. Soc., Geophysical Suppls., **5,** 398–408 (1949).

[8] P. N. Agaleĭskiĭ and K. N. Egorov, Rezul'taty absoliutnykh opredeleniĭ uskoreniia sily tiazhesti v punkte VNIIM (Leningrad), Izmeritel Tekhn., Vol. for 1956, no. 6, 29–34.

[9] A. I. Martsiniak, "Opredelenie absoliutnoi velichiny uskoreniia sily tiazhesti po padeniiu zhezla v vakuume," Izmeritel Tekhn. Vol. for 1956, no. 5, 11–15.

[10] H. Preston-Thomas and others, An absolute measurement of the acceleration due to gravity at Ottawa, Can. J. Phys. **38,** 824–52 (1960).

[11] Å. Thulin, Une détermination absolue de *g* au pavillon de Breteuil, par la méthode de la chute d'une règle divisée, Ann. Géophys. **16,** 105–27 (1960).

[12] J. E. Faller, An Absolute Interferometric Determination of the Acceleration of Gravity. Thesis, Princeton University, 1963.

[13] A. H. Cook, A new absolute determination of the acceleration due to gravity at the National Physical Laboratory, England, Phil. Trans. Roy. Soc. London, Ser. A., **261,** 211–252 (1967).

[14] C. Volet, L'intensité de la pesanteur déterminée par l'observation de la chute d'un corps, Comptes rendus de l'Académie des sciences, **224,** 1815–16 (1947).

[15] A. Sakuma, Etat actuel de la nouvelle détermination absolue de la pesanteur au Bureau international des poids et mesures, International Association of Geodesy, Bulletin géodésique, n.s., no. 69, 249–60 (1. sept. 1963).

[16] A. H. Cook, Recent developments in the absolute measurement of gravity, International Association of Geodesy, Bulletin géodésique, n.s. no. 44, 34–59 (1. juin 1957).

(Paper 72C1–264)

JOURNAL OF RESEARCH of the National Bureau of Standards—C. Engineering and Instrumentation
Vol. 72C, No. 1, January–March 1968

Deflection of Thin Circular Elastic Plates Under Symmetrically Distributed Loading

A. F. Kirstein and R. M. Woolley

Institute for Basic Standards, National Bureau of Standards, Washington D.C. 20234

(November 16, 1967)

A special application of Bassali's solution for transverse flexure of thin elastic plates supported at several points is presented for the case of concentric symmetrically distributed load. Equations for deflection are presented for the case where the point supports lie within the loaded area. Under special conditions the numerical results from these equations coincide with those of Nadai's.

Key Words: Bassali's theory, deflection, elasticity, flexure, point supports, symmetrically distributed load, thin plates.

1. Introduction

Previous work [1][1] dealt with the deflection of centrally loaded thin circular elastic plates on equally spaced point supports in which the supports were located along a concentric circle outside of the central loaded area. A sequel to this previous work is presented in this paper where the case in which the point supports lie within the loaded area is considered.

Theoretical work given by Bassali [2] is specialized to develop expressions for deflection which consider the symmetrically distributed load in general and the uniformly distributed load in particular.

Previous experimental results [1, 3] have been shown to be in good agreement with the results of other specialized treatments of Bassali's theory for plates having thicknesses to span radii ratios up to 0.08 with span radii to plate radii ratios as small as 0.63. Even though no experimental results are presented in this paper, no lesser agreement between experimental and theoretical results should be expected for the case considered herein.

List of Symbols

x, y rectangular Cartesian coordinates
$r = \sqrt{x^2 + y^2}$, radial polar coordinate
θ arctan (y/x), polar coordinate angle
c radius of the plate
b radius of transversely loaded area of plate (Region 1)
a span radius, of circle on which supports lie
h thickness of the plate

[1] Figures in brackets indicate the literature references at the end of this paper.

m number of support points ($m \geq 3$)
$\alpha = 2\pi/m$, polar angle between support points
$\theta_s = s\alpha$, polar angle subtended by the sth support point ($s = 1, 2, \ldots, m$)
$\varphi_s = \theta - \theta_s$
$p_1 = p_0 r^{n-2}$, transverse load intensity over Region 1
$p_2 = 0$, transverse load intensity over Region 2
$P_0 = 2\pi p_0 b^n/n$, total load on the plate
$b' = b\sqrt{n/(n+2)}$
$\rho = r/c$
$t = a/c$
$q = b/c$
$q' = b'/c$
$r_s' = c^2/a$
ν Poisson's ratio
$\kappa = (3+\nu)/(\nu-1)$
E modulus of elasticity
$D = Eh^3/12(1-\nu^2)$, the flexural rigidity
w_1 deflection of the plate within Region 1
w_2 deflection of the plate within Region 2
w_c deflection at the center of the plate.

2. Deflection of the Circular Plate

The theoretical expressions for the deflection of a plate were obtained from Bassali's work [2] and a previous specialization [1] of his work which dealt with the deflection of centrally loaded thin circular elastic plates on equally spaced point supports. The previous case considered that the point supports were located along a concentric circle outside of the central loaded area (in Region 2). For the case presented here the point supports lie within the loaded area (Region 1). Figure 1 shows the concentric arrangement of the circular plate and defines Regions 1 and 2.

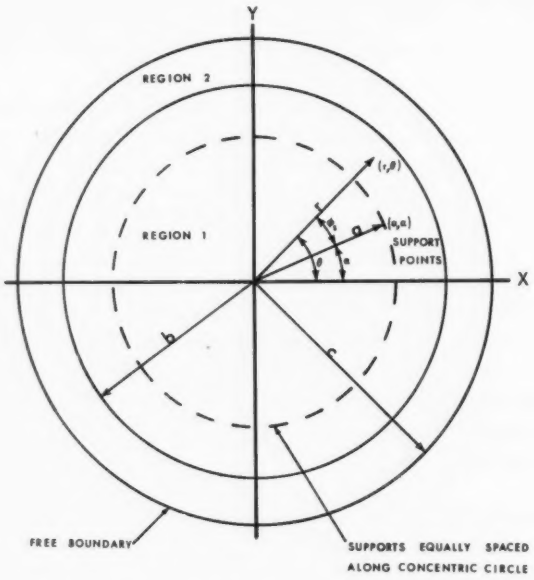

FIGURE 1. *Concentric arrangement of the circular plate.*

Previously developed [1, 2] general expressions pertaining to symmetrical bending are presented here as eqs (1) to (7). For the case considered here, the development follows the same general reasoning. The deflections of the plate in Regions 1 and 2 are represented by

$$w_1 = w_0 + \frac{P_0}{8\pi D}\left[(r^2+b'^2)\ln q - \frac{1}{m}\sum_{s=1}^{m} R_s^2 \ln\frac{R_s}{c} + \left(1-\frac{1}{n}\right)(r^2-b^2) + \frac{4(r^{n+2}-b^{n+2})}{n(n+2)^2 b^n}\right] \tag{1}$$

where n is the load distribution parameter, and

$$w_2 = w_0 + \frac{P_0}{8\pi D}\left[(r^2+b'^2)\ln\rho - \frac{1}{m}\sum_{s=1}^{m} R_s^2 \ln\frac{R_s}{c}\right], \tag{2}$$

respectively, where

$$w_0 = \frac{P_0}{8\pi m\kappa D}\left[\sum_{s=1}^{m} R_s^2 \ln\frac{R_s'}{r_s'} + (\kappa^2-1)c^2\,\mathrm{Re}\,\{L_m(\zeta)\} + \frac{m(1-\rho^2)(a^2+\kappa b'^2)}{\kappa+1}\right] + \gamma_1 x + \gamma_2 y + \gamma_3, \tag{3}$$

and

$$R_s^2(\rho,\theta) = a^2\left(1+\frac{\rho^2}{t^2} - 2\frac{\rho}{t}\cos\varphi_s\right) \tag{4}$$

$$\frac{R_s^2}{c^2} = \rho^2 - 2\rho t\cos\varphi_s + t^2 \tag{5}$$

$$\frac{R_s'^2}{r_s'^2} = 1 - 2\rho t\cos\varphi_s + \rho^2 t^2 \tag{6}$$

$$\mathrm{Re}\,\{L_m(\zeta)\} = -\sum_{n=1}^{\infty}\left[\frac{(\rho t)^n}{n^2}\sum_{s=1}^{m}\cos n\varphi_s\right] + \frac{1}{2}\sum_{s=1}^{m}(1-\rho t\cos\varphi_s)\ln(1-2\rho t\cos\varphi_s+\rho^2 t^2)$$
$$-\rho t\sum_{s=1}^{m}\sin\varphi_s \arctan\frac{\rho t\sin\varphi_s}{1-\rho t\cos\varphi_s}. \tag{7}$$

For the case in which the point supports lie within the loaded area (Region 1), i.e., $t \leq q$, the deflection, w_1 is taken to vanish at a point support, z_k. By setting eq (1) equal to zero, $r=a$, and $\rho=t$ an expression for w_0 is found to be

$$w_0 = -\frac{P_0}{8\pi D}\left[(a^2+b'^2)\ln q - \frac{1}{m}\sum_{s=1}^{m} R_s^2(a,\theta_k)\ln\frac{R_s}{c}(a,\theta_k)\right.$$
$$\left. + \left(1-\frac{1}{n}\right)(a^2-b^2) + \frac{4(a^{n+2}-b^{n+2})}{n(n+2)^2 b^n}\right]. \tag{8}$$

Noting that the central plane of the undeformed plate shown in figure 1 is taken to lie in the $x-y$ plane, i.e., $\gamma_1=\gamma_2=0$, eqs (3, 4, 5, 6, and 8) may be combined to give

$$\gamma_3 = \frac{P_0}{8\pi\kappa D}\left[a^2\{A_m(t)+(1-\kappa^2)B_m(t)\} - \kappa(a^2+b'^2)\ln q + \kappa\left(1-\frac{1}{n}\right)(b^2-a^2)\right.$$
$$\left. + \frac{4\kappa(b^{n+2}-a^{n+2})}{n(n+2)^2 b^n} - \frac{(1-t^2)(a^2+\kappa b'^2)}{\kappa+1}\right] \tag{9}$$ [2]

[2] Bassali's expression for γ_3 is incorrect in that it contains an additional term, $+2a^2\kappa\ln t$, which does not appear in eq (9).

where

$$mA_m(t)=\sum_{s=1}^{m}(1-\cos s\alpha)[\kappa \ln 2t^2(1-\cos s\alpha)-\ln (1-2t^2\cos s\alpha+t^4)], \tag{10}$$

and

$$mt^2B_m(t)=\frac{1}{2}\sum_{s=1}^{m}(1-t^2\cos s\alpha)\ln (1-2t^2\cos s\alpha+t^4)-\frac{1}{m}\varphi(t^{2m})$$

$$-t^2\sum_{s=1}^{m}\sin s\alpha \arctan\frac{t^2\sin s\alpha}{1-t^2\cos s\alpha} \tag{11}$$

where $\varphi(z)$ is defined as $-\int_0^z \ln(1-\tau)\frac{d\tau}{\tau}$, $|z|<1$.

Under the given conditions of support it is now possible to determine the deflection of the central plane of a thin circular elastic plate when subjected to a concentric symmetrically distributed load. The intensity of the distributed load is $p=p_1=p_0r^{n-2}$ when $n\geq 2$ for Region 1 and $p=p_2=0$ for Region 2 ($n=2$ produces uniform load). The total load on the plate is $P_0=2\pi p_0b^n/n$.

3. Uniformly Loaded Plate

The solution for deflection of the uniformly loaded plate is implicit in the more general equations presented in the preceding section. Since there is some practical interest in the uniformly loaded plate on equally spaced point supports, this section presents the development of the equations.

In this case $b=c$, $q=1$, $n=2$, and $b'^2=c^2/2$. The appropriate deflection is w_1, and considering the above equalities eqs (1, 3, and 9) may be written as

$$w_1=w_0+\frac{P_0}{8\pi\kappa D}\left[-\frac{\kappa}{m}\sum_{s=1}^{m}R_s^2\ln\frac{R_s}{c}+\frac{\kappa(r^2-c^2)}{2}+\frac{\kappa(r^4-c^4)}{8c^2}\right], \tag{12}$$

$$w_0=\frac{P_0}{8\pi m\kappa D}\left[\sum_{s=1}^{m}R_s^2\ln\frac{R_s'}{r_s'}+(\kappa^2-1)c^2\,\mathrm{Re}\,\{L_m(\zeta)\}+\frac{m(1-\rho^2)\left(a^2+\frac{\kappa c^2}{2}\right)}{\kappa+1}\right]+\gamma_3, \tag{13}$$

and

$$\gamma_3=\frac{P_0}{8\pi\kappa D}\left[a^2\{A_m(t)+(1-\kappa^2)B_m(t)\}+\frac{\kappa(c^2-a^2)}{2}+\frac{\kappa(c^4-a^4)}{8c^2}-\frac{(1-t^2)\left(a^2+\frac{\kappa c^2}{2}\right)}{\kappa+1}\right]. \tag{14}$$

Combining eqs (12, 13, and 14) the deflection anywhere on the central plane of the plate is

$$w_1=\frac{P_0}{8\pi\kappa D}\left[\frac{1}{m}\sum_{s=1}^{m}R_s^2\ln\frac{R_s'}{r_s'}-\frac{\kappa}{m}\sum_{s=1}^{m}R_s^2\ln\frac{R_s}{c}+\frac{(\kappa^2-1)c^2}{m}\,\mathrm{Re}\,\{L_m(\zeta)\}\right.$$

$$\left.+a^2\{A_m(t)+(1-\kappa^2)B_m(t)\}+\frac{\kappa(r^2-a^2)}{2}+\frac{\kappa(r^4-a^4)}{8c^2}+\frac{(t^2-\rho^2)\left(a^2+\frac{\kappa c^2}{2}\right)}{\kappa+1}\right]. \tag{15}$$

Combining this and eqs (4, 5, and 6) gives

$$w_1=\frac{P_0a^2}{8\pi\kappa D}\left[\frac{1}{2mt^2}\sum_{s=1}^{m}(\rho^2-2\rho t\cos\varphi_s+t^2)\ln(1-2\rho t\cos\varphi_s+\rho^2t^2)\right.$$

$$-\frac{\kappa}{2mt^2}\sum_{s=1}^{m}(\rho^2-2\rho t\cos\varphi_s+t^2)\ln(\rho^2-2\rho t\cos\varphi_s+t^2)+\frac{(\kappa^2-1)}{mt^2}\operatorname{Re}\{L_m(\zeta)\}+A_m(t)$$

$$\left.+(1-\kappa^2)B_m(t)+\frac{\kappa}{2t^2}(\rho^2-t^2)+\frac{\kappa}{8t^2}(\rho^4-t^4)-\frac{(\rho^2-t^2)\left(1+\frac{\kappa}{2t^2}\right)}{\kappa+1}\right] \tag{16}$$

where Re $\{L_m(\zeta)\}$, $A_m(t)$, and $B_m(t)$ may be determined from eqs (7, 10, and 11), respectively.

The deflection at the center of the plate when the point supports are equally spaced along the periphery may be determined by inserting $\rho=0$, $t=1$, and Re $\{L_m(0)\}=0$ into eq (16). The result is

$$w_c=\frac{P_0a^2}{8\pi\kappa D}\left[A_m(1)+(1-\kappa^2)B_m(1)-\frac{5\kappa}{8}+\frac{\left(1+\frac{\kappa}{2}\right)}{\kappa+1}\right]. \tag{17}$$

Likewise the deflection at the periphery midway between supports may be determined from eq (16) by setting $\rho=t=1$, yielding

$$w_d=\frac{P_0a^2}{8\pi\kappa D}\left[A_m(1)+(1-\kappa^2)B_m(1)+\frac{\kappa^2-1}{m}\operatorname{Re}\{L_m(\zeta)\}\right.$$

$$\left.+\frac{1-\kappa}{m}\sum_{s=1}^{m}(1-\cos\varphi_s)\ln 2(1-\cos\varphi_s)\right]. \tag{18}$$

These cases represented by eqs (17 and 18) were considered by Nadai [4]. For comparison set $m=3$ and $\nu=\frac{1}{4}$ and we have

$$w_c=0.407\frac{P_0a^2}{Eh^3} \tag{19}$$

and

$$w_d=0.307\frac{P_0a^2}{Eh^3} \tag{20}$$

which coincide with the values obtained from Nadai's work.

4. Summary

Theoretical expressions are presented to make it possible to determine the deflection of the central plane of a thin circular elastic plate which is subjected to a concentric symmetrically distributed load when the point supports are equally spaced along a concentric circle and lie within the loaded area (Region 1).

The uniformly loaded plate is treated as a separate case, and the appropriate equations for deflection are presented. The computed deflection at the center of a uniformly loaded plate on point supports equally spaced along the periphery coincides with the results from Nadai's work.

5. References

[1] Kirstein, A. F., Pell, W. H., Woolley, R. M., and Davis, L. J., Deflection of centrally loaded thin circular elastic plates on equally spaced point supports, J. Res. NBS **70C** (Engr. and Instr.), No. 4, 227–244 (Oct.–Dec. 1966).

[2] Bassali, W. A., The transverse flexure of thin elastic plates supported at several points, Proceedings Cambridge Philosophical Society, **53,** 728–743 (1957).

[3] Kirstein, A. F., and Woolley, R. M., Symmetrical bending of thin circular elastic plates on equally spaced point supports, J. Res. NBS **71C** (Engr. and Instr.), No. 1, 1–10 (Jan.–Mar. 1967).

[4] Nadai, A., Die Verbiegungen in einzelnen Punkten unterstützter kreisförmiger Platten, Physik. Z. **23,** 366–376 (1922).

(Paper 72C1–265)

JOURNAL OF RESEARCH of the National Bureau of Standards—C. Engineering and Instrumentation
Vol. 72C, No. 1, January–March 1968

A Dynamic Method for Determining the Vapor Pressure of Carbon Dioxide at 0 °C

J. L. Edwards* and D. P. Johnson

Institute for Basic Standards, National Bureau of Standards, Washington, D.C. 20234

(October 23, 1967)

The vapor pressure of carbon dioxide at 0 °C, or at 0.01 °C, has been used as a fixed point on the pressure scale. Comparisons between laboratories may be affected equally by pressure measurements, temperature measurements, and the purity (and possibly isotope composition) of the sample. A dynamic method for establishing this pressure is described, utilizing a device similar to those used to realize the sulfur and steam points on the International Practical Temperature Scale. Advantages of the method include rapid establishment of equilibrium conditions, and the automatic purification of the carbon dioxide. Results obtained indicate a sample-to-sample reproducibility better than one part in 25,000. The method is suggested as being suitable for general use in realizing the CO_2 point of the pressure scale. This experiment yielded a value for the vapor pressure at 0 °C of 3.48516 MN m^{-2} or 26,140.8 mm Hg; at the triple point of water, 0.01 °C, it was 3.48608 MN m^{-2} or 26,147.7 mm Hg.

Key Words: Carbon dioxide, fixed point, hypsometer, pressure standard, purification, vapor pressure.

1. Introduction

The use of fixed points in pressure calibration work, besides having possible direct application in measurement problems, also provides a valuable check on the stability of the pressure scale as determined by piston gages or mercury manometers. One such fixed point is the vapor pressure of carbon dioxide at 0 °C. Six careful determinations of the "CO_2 point" have been made in the last forty years [1, 2, 3, 4, 5, 6] [1]. All of these determinations used a static method in which a pressure vessel containing purified CO_2 was placed in a cryostat of known temperature. The pressure was then measured when the vapor-liquid mixture reached an equilibrium pressure. The results of these six determinations, given later in table 3, show a scatter with a range of about 5 parts in 10,000. The precision of the individual investigations, however, was in each case reported to be 1 part in 10,000 or better. This seems to indicate that the static method is subject to systematic errors which can go undetected even in very careful work. The static method of measuring vapor pressure faces several problems: While the experimenter may use elaborate procedures to obtain pure CO_2, the samples may be contaminated after filling the pressure vessel, as by leaching materials from the walls. It is difficult to eliminate temperature gradients between the bath, the thermometer, and the interface between the liquid and vapor phases. A microscopic real or virtual leak, as by temperature fluctuations in the portions of the sample in parts of the apparatus outside the bath, will shift the temperature of the interface. Such corrections as those for gas head, capillarity and head corrections, in a mercury separator between the CO_2 vapor and the fluid used in the piston gage, may contribute susbtantial random and systematic errors. The object of the present work, therefore, is to develop an independent method of making the measurement which is less subject to systematic error. This method is suggested as being suitable for general use in interlaboratory comparisons.

*Work done in partial fulfillment of requirement for a degree of Master of Science at George Washington University. Present address: 5709 Gross Dr., Dayton, Ohio 45431.

[1] Figures in brackets indicate the literature references at the end of this paper.

2. Apparatus for the Dynamic Measurement of the Vapor Pressure of CO_2

2.1. General

The apparatus is patterned after the device used to reproduce two fixed points on the International Practical Temperature Scale—the boiling point of water and the boiling point of sulfur, and described in detail by Stimson [7]. It is similar to the "hypsometer" used by physical chemists. A schematic drawing of the CO_2 point boiler or hypsometer is shown in figure 1. In operation, liquid CO_2 in the bottom of the hypsometer

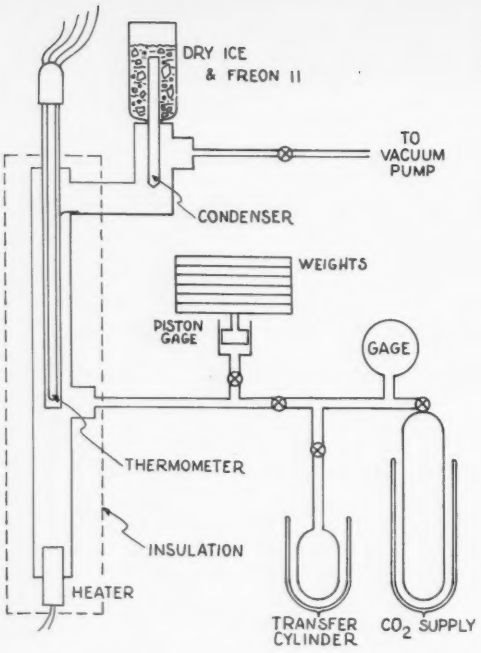

FIGURE 1. *Schematic diagram of apparatus.*

is heated to the boiling point. The rising CO_2 vapor condenses on a "cold finger" and the condensate flows down a thermometer well where the liquid and the vapor come into equilibrium and are in good thermal contact with the thermometer. The pressure at the same level is measured with a gas-lubricated piston gage operating on CO_2 directly without the need for the mercury manometer-separator used in the previous determinations.

The advantages of the dynamic method over the static method can be seen at this point. The vapor-liquid interface in the hypsometer is relatively large and is being continually renewed. This should allow for an easier attainment of equilibrium. Furthermore, the upward flow of CO_2 vapor should tend to concentrate the permanent gas impurities at the top of the hypsometer, and the condensate flowing down the thermometer well should be freq of the nonvolatile impurities which remain in the liquid at the bottom of the hypsometer. Since the pressure and temperature are measured at substantially the same level, and the temperature gradient is in a horizontal run of the connecting line, there is no head correction.

2.2. The Construction of the Hypsometer

The essential parts of the hypsometer were constructed using 1-in stainless steel tubing (type 304, 1/32-in wall thickness) and compression tube fittings. The apparatus was designed with the intention that it should be possible for any reasonably well-equipped laboratory to assemble it from commercially available parts.

The thermometer well was made with 3/8-in stainless steel tubing and was designed to hold a standard platinum-resistance thermometer, 18 inches long. The space surrounding the lower end of the thermometer was filled with liquid (Freon)[2] to improve thermal contact with the thermometer well. Stainless steel wire, 0.010-in diam, was wound around the lower two-thirds of the well, the turns separated by about one diameter of the wire. This served to slow down the flow of liquid and to provide good thermal contact between the thermometer well and both phases of the CO_2. During preliminary studies, the temperature distribution was explored with thermocouples to verify that the thermometer well was out of contact with the walls and that the liquid CO_2 from the condenser flowed down the thermometer well.

A brass reentrant plug was machined to fit a compression union. The plug was bored so that a standard 110 V, 50 W soldering element would just fit inside. The space between the interior of the plug and the heater was filled with rosin to hold the heater in position and provide thermal contact. The reentrant part of the heater plug was wound tightly over its full length with type 304, 0.010-in diam, stainless steel wire to trap gas bubbles, thereby preventing superheating of the liquid CO_2. A column of about 1 in of packing composed of very small coils of wire was placed between Nichrome screens just above the heater to act as a radiation shield between the heater and the thermometer and to further promote uniform boiling. The packing above the liquid level serves as a short fractionating column.

The condenser consisted of a brass rod, 1/2-in diam, extending about 6 in down into the hypsometer from a reducing union. A polyethylene bottle with its bottom cut off, was fitted on the upper portion of the brass rod. In operation, the condenser was cooled by filling the bottle with a mixture of Freon 11 and dry ice.

The hypsometer, insulated with about two inches of styrofoam, was placed in a 15-gal ice bath. The external connections to the supply cylinders and the piston gage were made with 1/4-in copper tubing and standard flare fittings. The small transfer cylinder shown in figure 1 has a volume of about 1200 ml. The volume of the hypsometer itself was calculated to be roughly 400 ml.

2.3. The Temperature and Pressure Measurements

The platinum-resistance thermometer used was a four-lead thermometer constructed by C. H. Myers. Its resistance was measured with a Mueller temperature bridge. The bridge had been modified by adding a 0.00001 Ω dial and by adding a bridge power supply with provision for variation of the bridge current and

[2] Certain commercial products are identified in this paper in order to specify adequately the experimental procedure. In no case does such identification imply recommendation or endorsement by the National Bureau of Standards, nor does it imply that the products or equipment identified are necessarily the best available for the purpose.

for guarding both the power supply and the galvanometer. The bridge balance was determined using a galvanometer-phototube amplifier. The galvanometer had sufficient sensitivity, with a thermometer current of 1 mA, for interpolation to 1 $\mu\Omega$ using the 0.00001 Ω dial, if desired.

The piston gage used in the measurements was one of the two NBS controlled-clearance, air-lubricated piston gages. These piston gages are regarded as primary pressure standards between 1 and 35 atm and are described briefly by Lloyd and Johnson [8]. The controlled-clearance piston gage, in general, is discussed by Johnson and Newhall [9].

A sectional view of the piston gage is shown in figure 2. The piston, 1 in in diameter, is made from Carboloy. The weights used were 50-, 10-, and 1-lb stainless steel weights. Their masses were known to about 1 ppm (part per million). At the pressure of the CO_2 point, the sensitivity of the piston gage had been previously observed to be about 1 ppm.

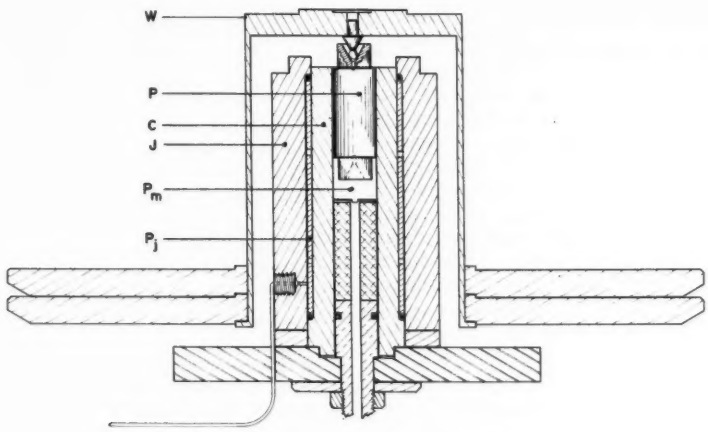

FIGURE 2. *Controlled-clearance piston gage.*
W, Weights; P, Piston; C, Cylinder; J, Jacket; P_m, Pressure to be measured; P_j, Jacket Pressure, adjusted to control clearance between piston and cylinder.

The uncertainties of the measurement are believed not to exceed the following:

	Systematic	Random
	Parts per million	
Piston gage parameters	30	
Mass and density of weights		
Piston area		
Elastic deformation		
Estimate of clearance	3	
Thermal expansion of piston	17	
Atmospheric pressure		3
Air density		1
Local gravity		
Temperature measurements—Hypsometer		
Thermometer self-heating		1
Bridge balance		5
Change of contact resistance		3
Measurements with triple-point cell		
Realization of triple point	5	
Bridge balance		3
Change of contact resistance		3
Total systematic error	55	
Resultant random error		8

Here the systematic errors are those which apply to all measurements made with this combination of instruments, and are not reduced by replication of the experiment. The random errors are those which are believed to be independent of each other and of the systematic errors; they are combined as the square root of the sum of the squares. The total uncertainty would be about 56 ppm, or about 1.5 mm Hg.

3. Experimental Procedure

3.1. Purification and Filling

One of the features desired for a fixed point procedure is that reproducible results be obtainable with material which is readily obtainable, and any necessary purification be done by methods within the resources of the ordinary standards or research laboratory. The pressure to be realized from the fixed point should be insensitive to residual impurities in the range covered by the procedure.

Accordingly commercial carbon dioxide in 20-lb cylinders was used in this experiment. The cylinder of CO_2 was set in an insulated container and the lower half cooled with dry ice until the pressure in the cylinder had fallen to the triple point. In the meantime the apparatus, at room temperature, was evacuated to a pressure of about 1 mm Hg, and then

rinsed by a flow of gas drawn from the top of the supply cylinder. During this time the supply pressure dropped to just above the atmospheric pressure, so that most of the CO_2 was in the solid form. The apparatus was again evacuated. The transfer cylinder was cooled below the temperature of the supply tank, and filled with CO_2. About 12 hr were required. Then the transfer cylinder was warmed to room temperature and the apparatus filled to a pressure of about 60 bars. Most of the permanent gas impurities were believed removed from the supply tank and the apparatus during the rinsing.

During the preliminary operations, the apparatus was filled several times, and the carbon dioxide in the supply tank was melted and frozen three times. While a small amount of permanent gas may have been entrapped in the CO_2 crystals in the first freezing, this would be released on melting, and removed on the next cycle. By the time the apparatus was filled for the first run, the CO_2 must have been quite free of permanent gas impurities. Most of the condensible impurities were retained in the supply cylinder during the sublimation. The content of water vapor, which might be particularly troublesome, is greatly reduced by sublimation, since at −78 °C the ratio of the vapor pressure of water to that of carbon dioxide is about 1 to 10^6, as compared with about 1 to 5700 at 0 °C.

3.2. Vapor Pressure Measurements

These were performed as follows: Ice was packed into the bath around the hypsometer, dry ice and Freon 11 (monofluoro-trichloromethane, used because it is nontoxic, nonflammable, and does not foam if dry ice is added rapidly) was put into the condenser, and the heater power adjusted until the hypsometer temperature was approximately 0 °C. This power, about 40 W, was such that the CO_2 was vaporized at a rate on the order of ½ liter per hour. This was sufficient to provide a thin layer of condensed liquid flowing over the entire external surface of the thermometer well. Several hours were allowed to establish a steady state. The piston gage was leveled, and the pressure in the jacket set at the optimum value as determined from the calibration curves of the gage. The weights corresponding to a desired pressure were placed on the piston, and the piston and weight assembly then rotated by hand. The valve connecting the piston and the hypsometer was opened. The heater power was increased slightly until the piston gage lifted and was in a "floating" condition; that is, until the vapor pressure of the CO_2 equaled that determined by the piston gage. While the piston gage was floating, the temperature at the bottom of the thermometer well was determined with the platinum resistance thermometer. It was found necessary to make small adjustments in heater power to maintain the piston gage in a floating condition during the 20 to 30 min required for making a series of normal and reversed readings with the thermometer bridge. By removing a 1-lb weight from the piston gage, the above process could be repeated at another pressure. In this manner, the temperatures corresponding to four different vapor pressures near the ice point were determined.

The other four sets of vapor pressure measurements were made to determine the effect of varying the CO_2 flow rate within the hypsometer and to investigate the effect of using unpurified CO_2.

For these runs, a fresh cylinder of commerical CO_2 was used. This gas had been produced by the decomposition of limestone. The supplier's estimate of the impurity content was as follows:

Nitrogen	0.1%
Oxygen	.03%
Argon	.001%
Water	.002% or less
Oil	.0004%, approx.

Runs 2 and 3 were made with gas drawn from this supply cylinder at room temperature with no purification of any kind.

For run 2 the measurements were made at the same flow rate as for run 1. For run 3, the area of the cold finger in contact with the cooling mixture was reduced. The heater power, and the flow of liquid were reduced by approximately a factor of ten. The reduced flow was maintained for run 4 but the unpurified CO_2 was discarded and the hypsometer refilled with CO_2 sublimed from the supply cylinder in the manner described above. Finally, for run 5 the sublimed CO_2 was used with the full cooling power and flow rate.

The piston gage temperature and the atmospheric pressure were recorded before and after each vapor pressure measurement, and the platinum-resistance thermometer was calibrated before and after each set of measurements, using a water triple-point cell prepared in the standard manner. The data reduction procedure for the piston gage was that given by Cross [10]. The vapor pressure at 0 °C was found for each of the five sets of measurements by fitting the pressure to a quadratic equation in the temperature using the OMNITAB least squares solution [11].

4. Results

The experimental data are shown in table 1. For each observation the temperature value is the mean of five to ten readings made while the pressure was under the control of the piston gage. The residuals are the deviations of these observations from the smooth quadratic curve.

Two parameters of the quadratic fits for the five runs, i.e., the pressures at 0 °C and the slopes, are summarized in tables 2 and 3. In these tables the standard deviations represent the precision of the pressure at 0 °C for each run, as calculated from the residuals of table 1.

Table 2 compares the results with three samples of CO_2. Run 2, made with gas containing more than 0.13 percent impurities agreed quite closely with runs 1 and 5, made with gas which was relatively pure.

TABLE 1. *The experimental results*

T(°C)*	P (bars)	P (mmHg)	Residuals (mmHg)
Run No. 1, sublimed CO_2, normal flow			
0.21511	35.0515	26290.8	−0.1
.11991	34.9633	26224.6	+0.2
.02516	34.8751	26158.5	−0.2
−.07146	34.7868	26092.3	+0.1
Run No. 2, CO_2 not purified, normal flow			
0.21422	35.0488	26288.8	+0.1
.11923	34.9609	26222.8	−0.1
.02404	34.8732	26157.1	−0.1
−.07094	34.7862	26091.8	−0.2
−.16632	34.7000	26027.1	+0.5
−.26131	34.6126	25961.6	−0.2
Run No. 3, CO_2 not purified, reduced flow			
0.12189	34.9644	26225.4	0.0
.02739	34.8774	26160.2	+0.1
−.06769	34.7899	26094.6	0.0
−.16297	34.7027	26029.2	0.0
−.25875	34.6154	25963.7	0.0
Run No. 4, sublimed CO_2, reduced flow			
0.20062	35.0353	26278.7	−0.4
.00995	34.8583	26145.9	+1.8
−.08011	34.7705	26080.0	−1.0
−.17460	34.6831	26014.5	−1.2
−.27284	34.5958	25949.0	0.8
Run No. 5, sublimed CO_2, normal flow			
0.20486	35.0398	26282.0	−0.2
.11046	34.9526	26216.6	−0.2
.01577	34.8654	26151.2	0.0
−.07942	34.7778	26085.6	0.0
−.17450	34.6904	26020.0	0.0
−.27077	34.6022	25953.8	0.0
.01596	34.8658	26151.5	+0.1
.20595	35.0414	26283.2	+0.2

*Means of five to ten temperature observations at each pressure.

TABLE 2. *Observed values for the vapor pressure of carbon dioxide at 0 °C*

Run No.	Pressure (bars)	Pressure (mmHg)	Std. dev. of pres. (mmHg)	Slope (mmHg/°C)	Std. dev. of slope (mmHg/°C)
1	34.8523	26141.4	0.24	689.7	3.1
2	34.8514	26140.7	0.21	687.9	0.9
5	34.8510	26140.4	0.09	690.9	0.4
Mean	34.8516	26140.8		689.5	

TABLE 3. *Test at reduced flow rates*

Run No.	Pressure (bars)	Pressure (mmHg)	Std. dev. of pres. (mmHg)	Slope (mmHg/°C)	Std. dev. of slope (mmHg/°C)
3	34.8520	26141.2	0.04	689.5	0.4
4	34.8466	26137.1	1.24	701.3	5.5

Table 3 shows the effect of reducing the CO_2 flow rate by a factor of ten. Run 4 was relatively erratic and gave a low mean pressure, compatible with intermittent coverage of the well with liquid. Since operation at this reduced flow rate is not to be recommended, both runs 3 and 4 were excluded from the result to be reported.

These results are compared with those of other authors in table 4. Much of the previous work was reported in mm Hg (the conventional mm Hg is the pressure corresponding to the height of a fluid of density 13.5951 g/cm², under normal gravity, 9.80665 m/sec²). The value, 26,132.2 reported by Roebuck and Cram was given in terms of the value 13.5955 for the density of mercury; here it has been adjusted to the conventional mm Hg. Michels et al., and Greig and Dadson reported the value at the triple point of water; the numbers in parentheses were calculated from the reported value and slope.

It is tempting to interpret the differences between the various measurements as indicating differences in the pressure scales of the laboratories. Thus, O. C. Bridgeman included data from ten piston gages, with calibrations made at the Massachusetts Institute of Technology from 1911 to 1926, and Meyers and Van Dusen included data gathered at the National Bureau of Standards between 1919 and 1931. But a close reading of the latter paper shows that more is involved.

TABLE 4. *Determinations of the CO_2 point to date*

Investigator	Year	Bars 0.00 °C	Millimeters of mercury 0.00 °C	Millimeters of mercury 0.01 °C	Reference
Bridgeman	1927	34.8567	26.144.7		[1]
Meyers and Van Dusen	1933				[2]
Equation			26.141.7		
MIT measurements			26.141.2		
NBS measurements		34.8498	26.139.5		
Roebuck and Cram	1933	34.8411	26.133.0		[3]
Michels, et al.	1950	(34.8467)	(26.137.2)	26.144.0	[4]
Edmister, et al.	1964	34.8499	26.139.6		[5]
Greig and Dadson	1966	(34.8472)	(26.137.6)	26.144.5	[6]
This paper	1966	34.8516	26.140.8	26.147.7	–

Three values taken from the paper of Meyers and Van Dusen are shown in the table. The first is from an equation which was chosen to represent the vapor pressure of the liquid over the full range from the triple point to the critical point. The form of this equation is largely determined by observations made during 1920 on two samples prepared the previous year. The second was measured during 1927 at MIT on NBS sample No. 1. The numerical value was not stated in the paper, but the point is plotted on the graph in which Meyers and Van Dusen compared the equation and their experimental results. The third value was observed during 1929 at the NBS on the same sample. It will be seen that the measurements at MIT on the NBS and MIT samples differ by twice as much as the measurements by the two laboratories on the NBS sample, and that the difference between the two laboratories was less than the estimated systematic errors (0.01% for the NBS) in the pressure measurements.

The difficulties of realizing a temperature of 0.000 °C in an ice bath are substantial. The ice point is defined at the temperature of melting pure ice in contact with water which is saturated with air. Pure water is in equilibrium with pure ice at atmospheric pressure and a temperature of 0.003 °C. This temperature difference corresponds to 2.1 mm of mercury at the CO_2 point. Since freshly melted ice is free of air, the conditions of the definition are hard to realize. The investigators both at MIT and the NBS were fully aware of these difficulties and it is probable that their temperatures did not differ by more than 0.0005 °C.

Apparently, at least part of the difference between the values published by the two laboratories must be charged to the preparation of the samples of carbon dioxide. Both laboratories took elaborate precautions to avoid chemical contamination. The gas was obtained by decomposition of sodium bicarbonate, dried with P_2O_5, and then sublimed five to eight times. In addition, at the NBS, the liquid was cooled by evaporation several times to obtain the solid. While substantial amounts of chemical contaminants seem unlikely, the possibility of isotope separation cannot be ruled out.

Recent determinations of the CO_2 point, including those made in Europe [4, 6], are lower than this measurement by an amount which slightly exceeds the sum of the uncertainties estimated by the various authors. This difference may be systematic as between the static and dynamic methods. However, one point with regard to the gas-lubricated piston gage should be mentioned. Carbon dioxide cools substantially on expansion. If this cooling reduces the temperature of the piston significantly, the effective area would be decreased and the apparent pressure increased. Estimates based on the Joule-Thompson coefficient and thermal conductivity of CO_2, the rate of leak, and the clearance indicate that this effect would not exceed 0.1 deg in temperature or 2 ppm in the pressure. This point could be verified by operation of the piston gage with helium, which has a positive Joule-Thompson coefficient.

5. Conclusions

In the use of the vapor pressure of CO_2 as a means of calibration, at least three factors are of comparable importance, i.e., pressure measurement, temperature measurement, and preparation of the sample.

Measurement of the vapor pressure of CO_2 by the dynamic method appears to be insensitive to impurities, at least at the level found in commerically available CO_2 in gas cylinders. The use of a gas-lubricated piston gage eliminates the need of fluid or diaphragm separators with the associated possible systematic errors.

The authors are indebted to J. L. Cross and his associates who furnished the piston gage and temperature measuring equipment and determined their parameters.

6. References

[1] O. C. Bridgeman, A fixed point for the calibration of pressure gages. The vapor pressure of liquid carbon dioxide at 0 °C. J. Amer. Chem. Soc., **49**, 1174–1183 (May 1927).

[2] C. H. Meyers and M. S. Van Dusen, The vapor pressure of liquid and solid carbon dioxide, J. Res. NBS **10**, 381 (1933) RP538.

[3] J. R. Roebuck and Winston Cram, A multiple column mercury manometer for pressure to 200 atmospheres, Rev. of Sci. Instr., **8**, 215 (1937).

[4] A. Michels, et al., The vapor pressure of liquid carbon dioxide, J. Appl. Phys. **16**, 501 (1950).

[5] W. C. Edmister, H. G. McMath, and R. C. Lee, Pressure comparisons for dead weight piston gages and vapor pressure of carbon dioxide, Oklahoma State University, unpublished paper (1964).

[6] R. G. P. Greig and R. S. Dadson, The vapour pressure of carbon dioxide at 0.01 °C, Brit. J. Appl. Phys., **17**, 1633 (1966).

[7] H. F. Stimson, Precision resistance thermometry and fixed points, precision measurement and calibration, **II**, Heat and mechanics, NBS Handbook 77, 40 (1964).

[8] E. C. Lloyd and D. P. Johnson, Static and dynamic calibrations of pressure-measuring instruments at the National Bureau of Standards, Automatic and remote control, p. 274 (Proceedings of the First International Congress of the International Federation for Automatic Control, Moscow) (Butterworths, London, 1960).

[9] D. P. Johnson and D. H. Newhall, The piston gage as a precise pressure-measuring instrument, Trans. ASME. **75**, 301 (1953).

[10] J. L. Cross, Reduction of Data for piston gage pressure measurements, NBS Mono. 65 (1963).

[11] J. Hilsenrath et al., OMNITAB, a computer program for statistical and numerical analysis, NBS Handbook 101 (1966).

(Paper 72C1–266)

JOURNAL OF RESEARCH of the National Bureau of Standards—C. Engineering and Instrumentation
Vol. 72C, No. 1, January–March 1968

An Adiabatic Saturation Psychrometer

Lewis Greenspan and Arnold Wexler

Institute for Basic Standards, National Bureau of Standards, Washington, D.C. 20234

(November 17, 1967)

An adiabatic saturation psychrometer for measuring the humidity of gases, as well as the vapor content of vapor-gas mixtures, is described. The instrument behaves in accordance with predictions deduced solely from thermodynamic considerations. With water-air, water-hydrogen, carbon tetrachloride-hydrogen, carbon tetrachloride-oxygen and toluene-air systems, at room temperature, atmospheric pressure, and gas flow rates of 1.3 to 5.2 liters per minute, measured wet-bulb temperatures agree with calculated "thermodynamic wet-bulb temperatures" to within the accuracy of the measurements and the uncertainties in the published thermodynamic data used in the computations. For the water-air system, the systematic and random errors due to these sources are estimated at 0.027 deg C and 0.019 deg C respectively. The agreement between the calculated and measured wet-bulb temperature is 0.029 deg C, which at a dry-bulb temperature of 25 °C and an ambient pressure of 1 bar is equivalent to an uncertainty in relative humidity which varies from 1/8 to 1/4 percent. The time constant is a function of the gas flow rate; at flow rates of 3.75 to 5.2 liters per minute, the time constant is of the order of 3/4 minute.

Key Words: Adiabatic saturation, gas mixtures, humidity, hygrometer, mixing ratio, moist gas, psychrometer, psychrometric factor, saturation, thermodynamic wet-bulb temperature, vapor content, wet-bulb.

1. Introduction

The psychrometer is one of the oldest and most common instruments for measuring the humidity of moist air. In its elemental form it consists of two thermometers; the bulb of one is covered with a wick and is moistened; the bulb of the other is left bare and dry. Evaporation of water from the moistened wick lowers its temperature below the ambient or dry-bulb temperature. The wet-bulb temperature attained with the conventional psychrometer is dependent on many factors in addition to the moisture and temperature state of the gas [1–4].[1] Although attempts have been made to develop a theory that would correctly interrelate the parameters affecting the behavior of the conventional psychrometer, there is no theory which completely describes its performance. In the well-known convection or adiabatic saturation theory [5–10], the principles of classical thermodynamics exclusively are used to derive a formula that predicts the humidity of a moist gas from wet- and dry-bulb thermometer measurements. Unfortunately the conventional psychrometer, even under steady-state conditions, is an open system undergoing a nonequilibrium process which cannot be depicted completely by classical thermodynamic theory. It is fortuitous that the formulas so derived yield results that are in nominal agreement with empirical facts for water vapor-air mixtures. When these formulas are applied to other vapor-gas mixtures, they fail to predict the correct vapor content.

The wet-bulb thermometer of a psychrometer in a steady-state condition experiences simultaneous heat and mass transfer. Although theories based on heat and mass transfer laws lead to equations which have a structural similarity to those derived from thermodynamic reasoning as well as to those of empirical origin, they also involve the ratio of thermal to mass diffusivities [3, 11–21]. Even these equations, which yield results in closer agreement with experimental data, do not completely depict all psychrometric behavior. For the water-air system, the ratio of thermal to mass diffusivity is close to one, accounting, in part, for the nominal agreement between the predictions based on the convection theory with those based on heat and mass transfer laws. In general, this ratio is greater than one [11, 22].

It would be advantageous to have an adequate theoretical basis for the behavior of the conventional psychrometer, but lacking a rational theory which accurately and fully describes the operation of the conventional psychrometer, one can invert the problem and inquire whether a psychrometer can be built which will behave in accordance with the postulates of classical thermodynamics. It appears that such a psychrometer can be designed and constructed and

[1] Figures in brackets indicate the literature references at the end of this paper.

that its behavior can be predicted by thermodynamic reasoning and expressed in mathematical form.

2. Theoretical Considerations

Consider a closed system undergoing an isobaric quasi-static process in which compressed liquid (or solid) at pressure P and temperature T_w is introduced into a gas at pressure P, temperature T, and mixing ratio[2] r to bring the gas adiabatically to saturation at pressure P, temperature T_w, and mixing ratio r_w. The term "gas" as used here and elsewhere in this paper is intended to include a gaseous mixture of which one constituent or component is a permanent gas or mixture of permanent gases and the second constitutent or component is the vapor of the compressed liquid involved in the psychrometric process and manifests itself as a product of evaporation. Since the process is adiabatic and isobaric the sum of the enthalpies of the various phases within the system are conserved, thus the initial and final enthalpies are equal, leading to the following equation:

$$h(P, T, r) = h(P, T_w, r_w) - (r_w - r) \cdot h'_w(P, T_w) \tag{1}$$

where

$h(P, T, r)$ = The enthalpy of $(1+r)$ g of gas mixture at pressure P, temperature T and mixing ratio r, that is, the enthalpy of a mixture consisting on 1 g of the vapor-free gas and r g of the vapor component;

r = the mass of vapor in the original gas mixture per unit mass of vapor-free gas with which the vapor is associated;

$h'_w(P, T_w)$ = the enthalpy of 1 g of pure compressed liquid (or solid) of the vapor component at pressure P and temperature T_w;

$h(P, T_w, r_w)$ = the enthalpy of $(1+r_w)$ g of gas mixture saturated with respect to the second or vapor component at pressure P and saturation temperature T_w, that is, the enthalpy of a gas mixture containing one gram of vapor-free gas and r_w g of the vapor component; and

$r_w = r_w(P, T_w)$ = the mass of vapor component of the gas mixture per unit mass of vapor-free gas of the mixture when it is saturated with respect to the vapor component at pressure P and temperature T_w.

The "thermodynamic wet-bulb temperature" is defined [23] as the solution for T_w in eq (1).

In order to facilitate the mathematical development we introduce the following additional notation:

$\Delta T = (T - T_w)$ = The wet-bulb depression;

$h(P, T_w, r)$ = the enthalpy of $(1+r)$ g of gas mixture at pressure P, temperature T_w (the same as the "thermodynamic wet-bulb temperature" of the original gas mixture), and mixing ratio r (the same as the mixing ratio of the original gas mixture);

$h(P, T, 0) = h(P, T, r=0)$ = the enthalpy of 1 g of the pure first (vapor-free) component of the mixture at pressure P and temperature T; and

$h(P, T_w, 0) = h(P, T_w, r=0)$ = the enthalpy of 1 g of the pure first component of the mixture at pressure P and temperature T_w.

[2] In several of the engineering disciplines r is called the humidity ratio.

Let

$$F = F(P, T, T_w, r) = [h(P, T, r) - h(P, T_w, r)] \tag{2}$$

and

$$C_{p,m} = \frac{[h(P, T, 0) - h(P, T_w, 0)]}{(T - T_w)} = \frac{1}{(T - T_w)} \int_{T_w}^{T} C_p dT \tag{3}$$

where

C_p = the specific heat at constant pressure of the pure vapor-free component.

Also let

$$C_{pv,m} = \frac{[h(P, T, r) - h(P, T_w, r)] - [h(P, T, 0) - h(P, T_w, 0)]}{r(T - T_w)} \tag{4}$$

and

$$L_{v,r} = \frac{[h(P, T_w, r_w) - h(P, T_w, r) - (r_w - r)\, h'_w(P, T_w)]}{(r_w - r)} \tag{5}$$

From the above definition, it will be clear that $C_{p,m}$ represents the mean specific heat at constant pressure of the pure vapor-free first component over the temperature range from T_w to T. The entity $C_{pv,m}$ may be interpreted as the "effective" specific heat at constant pressure P of the vapor component of the mixture taken as a mean over a temperature range from T_w to T and at a mixing ratio of r. Finally, $L_{v,r}$ may be understood as the "effective" latent heat of vaporization (or sublimation) of the vapor component of the mixture at constant pressure P and constant temperature T_w. It will be seen that $L_{v,r}$ is taken as a mean while $(r_w - r)$ gram of vapor component evaporates into the gas mixture from a plane surface of its liquid phase per gram of first component. Both mixture and liquid must be at the same pressure P and temperature T_w, the gas mixture having a mixing ratio r initially and attaining a mixing ratio r_w finally as a result of the process of evaporation.

It should be noted that the "effective" specific heat $C_{pv,m}$ and the "effective" latent heat of vaporization $L_{v,r}$ both differ from their counterparts pertinent to the pure phase of the second (vapor) component owing to the interactions between the molecules of the first and second components of the gas mixture, and due to other small effects [24].

By adding to the function F each of the quantities $h(P, T, 0)$ and $h(P, T_w, 0)$, both with positive and negative signs, respectively, one obtains the useful identity

$$\begin{aligned} F &= [h(P,T,r) - h(P,T_w,r)] \\ &= [h(P,T,r) - h(P,T,0)] - [h(P,T_w,r) - h(P,T_w,0)] \\ &\quad + [h(P,T,0) - h(P,T_w,0)]. \end{aligned} \tag{6}$$

When one subtracts $h(P, T_w, r)$ from both the left-hand and right-hand members of eq (1), it is obvious that the left-hand member transforms to the function F. Therefore, the right-hand member of eq (1) *minus* $h(P, T_w, r)$ is also equal to F, so that we can equate this difference to eq (6) which yields the relationship

$$\begin{aligned} &[h(P,T_w,r_w) - h(P,T_w,r)] - (r_w - r)h'_w(P,T_w) \\ &\quad = [h(P,T,r) - h(P,T,0)] \\ &\quad - [h(P,T_w,r) - h(P,T_w,0)] \\ &\quad + [h(P,T,0) - h(P,T_w,0)]. \end{aligned} \tag{7}$$

Inspection reveals that the product $(r_w - r)L_{v,r}$ is equal to the left-hand member of eq (7), while the sum of the products $(T - T_w)C_{p,m}$ and $r(T - T_w)C_{pv,m}$ is equal to the right-hand member of eq (7). On making these substitutions in eq (7) it transforms to

$$(r_w - r)L_{v,r} = [C_{p,m} + rC_{pv,m}](T - T_w). \tag{8}$$

On introducing the "psychrometric factor" A and the ratio B defined by

$$A = C_{p,m}/L_{v,r} \tag{9}$$

$$B = C_{pv,m}/L_{v,r} \tag{10}$$

substituting these in eq (8), and solving it for r, one finds

$$r = \frac{r_w}{[1 + B\Delta T]} - \frac{A\Delta T}{[1 + B\Delta T]} \tag{11}$$

where $\Delta T = T - T_w$.

Solving eq (11) for A one obtains

$$A = \frac{r_w - r[1 + B\Delta T]}{\Delta T}. \tag{12}$$

The "psychrometric factor" A as defined by eq (9) is identically equal to the "psychrometric factor" A as given by eq (12).

For the case where the initial mixing ratio of the gas is zero, eq (12) reduces to

$$A = \frac{r_w}{\Delta T}. \tag{13}$$

If the vapor and the gas separately and admixed with one another obey the ideal gas laws, eq (11) becomes

$$r = \frac{r_w}{(1 + B'\Delta T)} - \frac{A'\Delta T}{(1 + B'\Delta T)} \tag{14}$$

or, alternately, in terms of vapor pressure,

$$e = \frac{e_w}{(1 + B'\Delta T)} \frac{(P - e)}{(P - e_w)} - \frac{(P - e)A_0\Delta T}{(1 + B'\Delta T)} \tag{15}$$

where

$$A_0 = \frac{M_g}{M_v} \frac{C'_p}{L'_v} \tag{16}$$

$$A' = \frac{C'_p}{L'_v} \tag{17}$$

$$B' = \frac{C'_{pv}}{L'_v} \tag{18}$$

and

e = the partial pressure of the vapor component in the original gas mixture;
e_w = the saturation vapor pressure of the liquid phase of the vapor component at temperature T_w;
P = the total pressure;
C'_{pv} = the pure phase specific heat of the vapor at constant pressure;
L'_v = the pure phase latent heat of vaporization of the vapor;
C'_p = the specific heat of the vapor-free gas at constant pressure;

A_0 = the so-called "psychrometric constant" (which appears in most formulas for the conventional psychrometer [3]);
M_g = the molecular weight of the vapor-free gas component; and
M_v = the molecular weight of the vapor component.

When e and e_w are small compared to P and $B'\Delta T$ is small compared to one, which is the case for the water-air system at dry-bulb temperatures T up to about 45 °C, eq (15) reduces to

$$e = e_w - A_0 P \Delta T \tag{19}$$

which is identical to the classical equation often used to represent the behavior of the conventional psychrometer.

It does not appear feasible to construct a practical psychrometer that is an embodiment of a closed system undergoing the ideal adiabatic isobaric saturation process which serves as the basis of eq (1). On the other hand, an open system undergoing a steady-flow process would appear to be operationally feasible, and such a system was constructed and its performance investigated. The aim was to approach ideal conditions as closely as practical, namely to bring compressed liquid (or solid) to pressure P and temperature T_w, to evaporate it into a gas stream at pressure P, temperature T and mixing ratio r, and to bring the gas adiabatically to saturation at pressure P, temperature T_w, and mixing ratio r_w. This system then becomes an adiabatic saturator operating at constant pressure. If nothing enters to violate the conditions of eq (1), the adiabatic saturator becomes an "adiabatic saturation psychrometer" since measured values of P, T, and T_w can be inserted into eq (11) to obtain the mixing ratio of the entrant gas stream. It was realized that practical and theoretical matters, such as heat exchanges due to radiation and conduction, and pressure drop associated with flow, would be among the factors limiting the possibility of attaining the ideal, especially in view of the desire to keep the apparatus simple for ease of construction. It was left, therefore, to experiment to serve as the indicator of how close the actual psychrometer conformed to theory.

3. Background

In 1922, W. K. Lewis performed several experiments in which a dried gas was bubbled through a volatile liquid in a Dewar flask containing glass beads, the gas being discharged into the liquid through a vacuum-jacketed glass inlet tube. For water-air, water-carbon dioxide, toluol-air and chlorbenzol-air the gas substantially became saturated and the liquid (as well as the effluent gas) eventually reached a steady-state temperature that was essentially the "thermodynamic wet-bulb temperature." The readings of wet-bulb temperature in the experiments using water, toluol and chlorbenzol as the liquid were independent of air velocity and of the amount of air contact with the liquid. This was not the case in the experiments with liquids of higher vapor pressure. The discrepancy probably was due to incomplete saturation and incomplete heat transfer between the gas and liquid rather than lack of constancy of the wet-bulb temperature as Lewis assumed.

Nanda and Kapur [28] performed similar experiments, bubbling dried air into a Dewar containing such liquids as acetone, methyl alcohol, ethyl alcohol, and butyl alcohol. After a considerable length of time, the liquid temperature approached the "thermodynamic wet-bulb temperature."

We also repeated these experiments, and in doing so found it necessary to use a vacuum-jacketed glass inlet tube, such as Lewis had used, for bubbling the gas through the liquid in the Dewar flask. With this inlet tube, which reduced precooling of the inlet gas prior to discharge into the liquid, steady-state temperatures of the liquids were obtained, which were in close agreement with calculated "thermodynamic wet-bulb temperatures," provided the gas flow was very low and only after extended continuous flow, usually hours.

Although "thermodynamic wet-bulb temperatures" could be obtained with the Dewar flask, the low gas flow rates, and the extremely long time necessary to reach steady-state conditions at these flow rates, seemed to preclude its use as a practical instrument for measuring humidity.

Carrier and Lindsay [25], and Dropkin [14] constructed large scale, engineering-type apparatus for obtaining adiabatic saturation. The essential feature of these devices was the provision for passing air over surfaces moistened with water that had been precooled to, or close to, the wet-bulb temperature, within well-insulated ducts. The experiments performed by these investigators were limited to the water-air system.

In 1961, J. D. Wentzel described a psychrometer which apparently measured the "thermodynamic wet-bulb temperature" of water-air with high accuracy [29]. In his instrument, Wentzel attempted to saturate adiabatically a stream of test air (whose humidity was to be measured) with water vapor in a fashion that appeared to approach the idealized steady-flow adiabatic process. Basically his instrument consisted of a vacuum-insulated glass tube, the inner walls of which were silvered to reduce radiation effects. The tube was partially filled with a moistened natural sponge through which the air flowed. Makeup water was added intermittantly, in one design, and continuously in a second design. In the latter version, the continuous flow of makeup water was precooled by an essentially equivalent instrument through which part of the gas stream was channeled. To preclude the possibility of drying of the sponge, excess makeup liquid was used. Wet-bulb temperatures were measured with thermocouples imbedded in the moistened sponge. Wet-bulb temperature measurements for the water-air system corresponded very closely to "thermodynamic wet-bulb temperatures." It is well known, however, that the wet-bulb temperature for moist air as measured with a conventional psychrom-

eter nominally is not very different from the "thermodynamic wet-bulb temperature" so that further demonstration is required to establish that a psychrometer is undergoing a true thermodynamic wet-bulb process. This could have been accomplished by the use of liquid-gas systems other than water-air for which the wet-bulb temperature as indicated by a conventional psychrometer, and the "thermodynamic wet-bulb temperature" differ appreciably.

L. P. Harrison [26] has proposed three psychrometer designs for measuring "thermodynamic wet-bulb temperature," each design involving the employment of three concentric tubes so arranged as to insure intimate contact between gas and liquid and therefore to insure adiabatic saturation.

We first duplicated Wentzel's instrument with some modifications. Whereas Wentzel successfully had employed natural sponges as his saturating element, we were unsuccessful in the use not only of natural but also of artificial sponges because of the tendency for the liquid to be blown out by the gas stream. Only when we finally resorted to cotton cheesecloth did the instrument operate satisfactorily. Various liquid-gas systems were tried and although wet-bulb temperatures approaching "thermodynamic wet-bulb temperatures" were obtained, these were not sufficiently close to one another to form the basis of an accurate measuring system. The best results were achieved with the water-air system. The major defect in the instrument appeared to be the lack of sufficient precooling of the liquid so that it would feed into the saturating element at, or very close to, the "thermodynamic wet-bulb temperature." With the water-air system the operation of an adiabatic saturation psychrometer is less sensitive to the liquid feed temperature than it is with some other liquid-gas systems.

We then developed an instrument utilizing vacuum-jacketed glass tubes, as in the Wentzel instrument, but employing a different saturating element and a novel feed arrangement that precools the liquid very close to the wet-bulb temperature. "Thermodynamic wet-bulb temperatures" were closely approached with various liquid-gas systems, as well as with water-air.

4. Description

The instrument is shown in figures 1 and 2. It consists of a vacuum-jacketed glass saturator tube, A, that is surrounded by a glass Dewar flask, B. Within the saturator tube is a thermocouple, C, for measuring dry-bulb temperature, wicking, D, for saturating the gas stream, and a feed tube, E, through which liquid is introduced for moistening the wicking. A thermocouple, F, for measuring wet-bulb temperature is located beyond the outlet end of the saturator tube. The saturator tube is centered and held in the Dewar flask by a stopper, G. There is a pressure tap, H, at the outlet end of the saturator tube and an exit flow line, I, through which the effluent gas leaves the instrument. The test gas enters at the inlet end of the saturator tube, flows through the saturator tube, emerges at the outlet end of the saturator tube, reverses direction, flows over the exterior surface of the saturator tube and discharges through the exit flow line and micrometer valve, J.

The main component is the saturator tube fabricated with double walls, with the space between the walls evacuated and sealed. The tube is silvered to reduce radiation effects, is 13 in long, and has an o.d. of ½ in and an i.d. of 0.15 in. It is within this saturator tube that the "thermodynamic wet-bulb process" occurs.

The liquid feed system comprises a graduated reservoir, K, a preliminary heat exchanger, L, a main heat exchanger, M, and a feed tube, E. Liquid flows from the reservoir, through the heat exchangers, the feed tube, and onto the wicking. The reservoir is mounted on a vertical rod. Its elevation can be adjusted to provide the required head of liquid to maintain the flow necessary for complete and continuous moistening of the wicking. The preliminary heat exchanger is a 12-ft

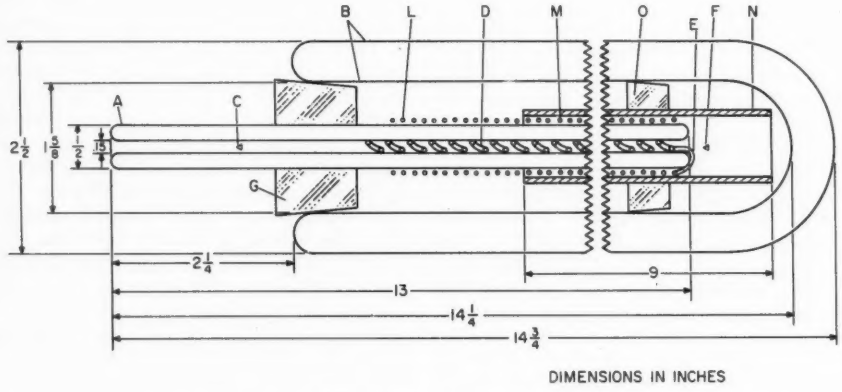

FIGURE 1. *Adiabatic psychrometer—principal section*
A. Vacuum-jacketed glass saturator tube; B. glass Dewar flask; C. Dry-bulb thermocouple; D. Cotton wicking; E. liquid feed tube; F. wet-bulb thermocouple; G. saturator tube rubber stopper; L. preliminary heat exchanger; M. main heat exchanger; N. flow guide; O. flow guide cork stopper.

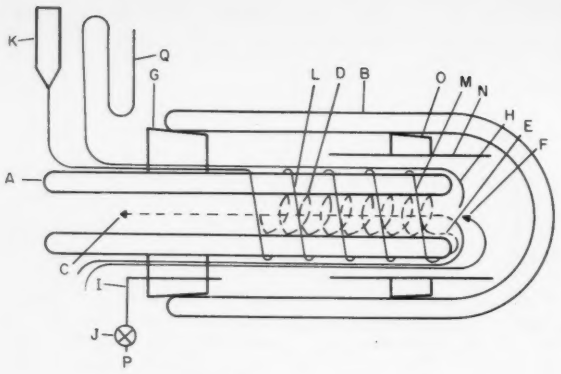

FIGURE 2. *Adiabatic psychrometer—schematic*
A. Vacuum-jacketed glass saturator tube; B. glass Dewar flask; C. dry-bulb thermocouple; D. cotton wicking; E. liquid feed tube; F. wet-bulb thermocouple; G. saturator tube rubber stopper; H. static pressure tap; I. exit flow line; J. micrometer exhaust valve; K. graduated reservoir; L. preliminary heat exchanger; M. main heat exchanger; N. flow guide; O. flow guide cork stopper; P. vacuum source; Q. oil manometer.

length of polytetra fluoroethylene tubing, with an o.d. of about 0.045 in and an i.d. of about 0.021 in, loosely wound for 6 in around the outside of the saturator tube, connected at one end to the reservoir and at the other end to the main heat exchanger. The latter is a 5-ft length of stainless steel tubing, with an o.d. of 0.0355 in and an i.d. of 0.023 in, wound into a $\frac{5}{8}$-in diam helix that fits over the outlet end of the saturator tube for a distance of 4 in. The feed tube is fabricated from 2 ft of the same PTFE tubing as used in the preliminary heat exchanger. It is wound into a helix which fits inside the saturator tube and extends inward for 10 in from the outlet end.

The feed tube is covered with a close-fitting sleeve of cotton wicking. One end of the sleeve terminates $\frac{1}{2}$ in inside the outlet end of the saturator tube; the other end is tied tightly with cotton thread immediately beyond the discharge port of the feed tube.

The wet- and dry-bulb thermocouples are made from calibrated No. 40 copper and constantan wires encased in PTFE tubing like that described above. The dry-bulb thermocouple junction is located $1\frac{1}{2}$ in inside the inlet end of the saturator tube and upstream of the wicking; the wet-bulb thermocouple junction is located just beyond the outlet end of the saturator tube downstream of the wicking. Both junctions are placed along the axis of the saturator tube.

A silvered glass Dewar flask, 12 in long and with an i.d. of $1\frac{5}{8}$ in, encloses most of the saturator tube. The saturator tube fits tightly within a concentric hole in a No. 9 rubber stopper which, in turn, fits snugly into the mouth of the Dewar flask. The two sets of thermocouple wires, the preliminary heat exhanger, the pressure line, and the exit gas flow line are fed separately through, and tightly fitted in, holes in the stopper.

Within the Dewar flask is a glass tube, N, 9 inches in length, $\frac{7}{8}$-in o.d., and $\frac{1}{16}$-in thick, that is, in turn, supported by a cork stopper, 0. The saturator tube with its associated components is positioned concentrically inside the glass tube. The latter serves as a flow guide for channeling the gas over the surface of the main heat exchanger. It reduces the size of the annulus through which the gas flows and improves the heat transfer between the liquid in the main heat exchanger and the gas.

The exit flow line is connected to a micrometer valve and then to a vacuum source, *P*. The pressure line is connected to an oil manometer, *Q*. which, in conjunction with a barometer which measures ambient atmospheric pressure, yields the absolute pressure at the outlet end of the saturator tube. A potentiometer and null detector are used to measure the emfs generated by the thermocouples. The saturator assembly is maintained in a horizontal orientation.

The saturator tube is constructed with a vacuum jacket to reduce heat transfer between its interior and its surroundings. The outer Dewar flask serves the purpose of providing additional thermal insulation from the ambient atmosphere for the test gas. The design of the liquid-feed tube and wicking combination is intended to provide a large evaporative area to the flowing gas while reducing as far as practical the pressure drop and total liquid heat capacity. The liquid-feed heat exchanger provides for the automatic precooling of the liquid by the gas which has been brought to the wet-bulb temperature by the moistened wicking. Counter flow of gas and liquid is used to obtain the maximum heat exchange. It was intended that the total heat capacity of the heat exchanger and its contained liquid should be as small as possible. The preliminary liquid-feed heat exhanger is not considered to be part of the thermal capacity of the main heat exchanger and is a slight embellishment for heat exchange purposes. The liquid reservoir height adjustment is used to control the rate of liquid feed. Both thermocouples were located so as to be exposed only to and in contact with the gas stream.

5. Operating Procedure

The instrument is operated by establishing a continuous flow of sample gas and liquid. After steady-state conditions are reached, the wet- and dry-bulb temperatures and the pressure are measured.

The test gas is fed to the saturator tube at atmospheric pressure. Because of the use of glass in the construction of the saturator tube and the Dewar flask and the use of stoppers for assembling and sealing these components, the maximum pressure within the psychrometer is limited to about 1 atm. The outlet port of the micrometer valve is attached to a vacuum source. The micrometer valve is calibrated in terms of air flow over the range 0 to 6.2 liters per minute. By means of a density correction, the equivalent flow is obtained for any other gas. Thus, by an appropriate micrometer setting any desired flow within this range can be established through the psychrometer. Since the valve functions as a variable critical flow orifice, the volumetric flow through the psychrometer, for a given micrometer setting, is essentially constant.

The height of the reservoir is set so as to produce a liquid flow rate that is approximately three times that

required to completely saturate the vapor-free test gas. This liquid flow rate is measured by timing the change in volume of the liquid in the graduated reservoir. If drying occurs in any part of the wicking, a temperature transient is propagated through the saturator that upsets the thermal equilibrium of the instrument and yields an erroneous wet-bulb temperature. Excess liquid insures that the wicking is always completely moistened; the excess is carried through the saturator by the flow of gas and collects in the Dewar flask where it can be drained manually or automatically. Since the liquid enters and emerges from the saturator tube at essentially wet-bulb temperature, the enthalpies of the excess liquid flowing into and out of the saturator are essentially equal and therefore do not contribute to the overall enthalpy balance as given in eq (1).

5.1. Tests

Since eq (1) represents an interrelation among parameters P, T, T_w, and r such that $f(P, T, T_w, r)=0$, then if any three parameters, say P, T, and r are measured and inserted into the equation, the fourth, T_w, can be calculated. If, in addition, a measurement is also made of T_w, the calculated and observed "thermodynamic wet-bulb temperatures" can be compared. Such a comparison offers a measure of the conformance of psychrometer behavior with theory.

Equation (12) may be expressed in the form

$$\frac{C_{p,\,m}}{l_{w,\,r}}=\frac{r_w-r[1+B\Delta T]}{\Delta T} \tag{20}$$

in which the right- and left-hand sides are different functions of the same parameters, that is,

$$A_1(P, T, T_w, r)=A_2(P, T, T_w, r). \tag{21}$$

By inserting the same set of measurements of the parameters (P, T, T_w, r) into A_1 and A_2 these two functions can be calculated and compared. Such a comparison offers an alternate method of checking whether the psychrometer performs in accordance with theory. It should be recognized that A_1 and A_2 are alternate expressions of the "psychrometric factor."

A series of experiments was performed with the psychrometer, with various liquid-gas systems, to obtain experimental or observed values of the wet-bulb temperature which is given the notation $(T_w)_{obs}$. With the same values of parameters P, T, and r, the "thermodynamic wet-bulb temperature" was calculated. To differentiate it from the observed value it is given the notation $(T_w)_{calc}$. Because of the difficulty of generating vapor-gas mixtures of known mixing ratios to supply to the psychrometer, only dry, vapor-free gases were used. Thus, in each case the mixing ratio r of the gas was zero. All experiments were performed at room temperature (about 25 °C), except for four test points with water-air which were performed at about 37 °C, and at atmospheric pressure (about 1 bar). The flow rate of the test gas mixture was varied over the range 0.8 to 6.2 liters per minute. The possible implications due to the restriction $r=0$ will be discussed later.

The following systems were selected for the experiments: water-air, water-hydrogen, carbon tetrachloride-oxygen, carbon tetrachloride-hydrogen, and toluene-air. The gases were obtained from a commercial source in steel cylinders compressed to a pressure of about 120 atm. The carbon tetrachloride was of spectro grade, the toluene of reagent grade, and the water of distilled grade purity. These systems encompass a range of thermal to mass diffusivity ratios of 0.9 to 4.5 as shown in table 5.

The experimental setup is shown in figure 3. The gas from a cylinder, R, was passed through a high pressure reducer, S, and a low pressure reducer, T, in series, a drier filled with phosphorous pentoxide, U, and a stainless steel heat exchanger, V, immersed in a temperature-controlled liquid bath, W, and then fed into the psychrometer, X, at a pressure of about 1 atm. The desired gas flow rate was obtained by the appropriate setting of the micrometer on the exhaust valve, J. The reservoir, K, was filled with the test liquid and its elevation adjusted so that the liquid flow rate was approximately three times as great as that calculated as necessary to completely saturate the test gas at the wet-bulb temperature.

Tests were also performed to determine the speed of response of the instrument. Using air as the sample gas, and water as the liquid, the psychrometer was subjected to a nominal step-function change in mixing ratio at a dry-bulb temperature of 25 °C and at an ambient atmospheric pressure of about 1 bar. Dry air was fed to the psychrometer. After steady-state conditions were reached, the connection feeding the dry air to the inlet of the saturator tube was quickly removed and ambient (room) air was drawn in producing an increase in mixing ratio. The procedure was then reversed producing a decrease in mixing ratio. The emf from the wet-bulb thermocouple was fed to a precision potentiometer. The unbalance of the potentiometer was amplified and recorded as a function of time. After nulling the potentiometer for the steady-state initial wet-bulb temperature condition, a trace was obtained of the wet-bulb temperature change produced by the step-function change in mixing ratio.

5.2. Results

A comparison is shown in table 1 between the observed and calculated "thermodynamic wet-bulb temperatures," $(T_w)_{obs}$ and $(T_w)_{calc}$, for the several liquid-gas systems that were investigated. The absolute pressures P in the region of the wet-bulb thermocouple are given in column 1. Column 2 lists the approximate flow rates of the gas at the inlet end of the psychrometer, that is, at temperature T. Columns 3 and 4 list the observed (measured) dry- and wet-bulb temperatures. The calculated wet-bulb temperatures, obtained by solving eq (23) or (24) (see appendix) for T_w, are given in column 5. The differences between the observed and calculated wet-bulb temperatures, $|(T_w)_{obs}-(T_w)_{calc}|$, are tabulated in column 6.

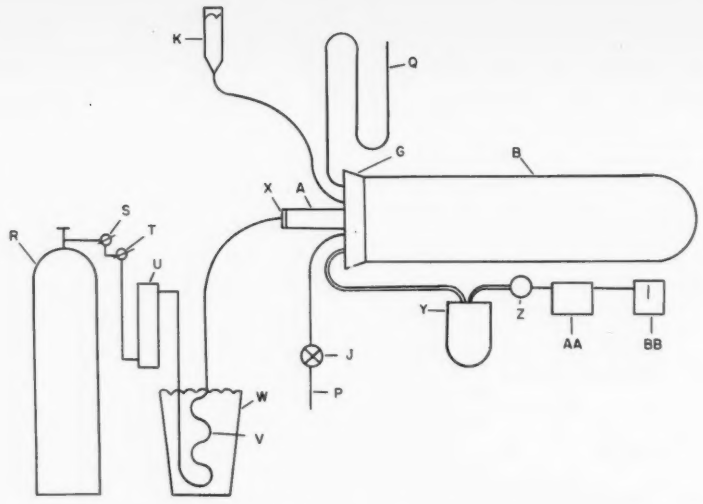

FIGURE 3. *Test setup—schematic*

J. micrometer exhaust valve; K. graduated reservoir; P. vacuum source; Q. oil manometer; R. compressed gas cylinder; S. high pressure reducer; T. low pressure reducer; U. drier; V. heat exchanger; W. temperature-controlled liquid bath; X. psychrometer; Y. reference junction ice bath; Z. thermocouple selector switch; AA. precison laboratory potentiometer; BB. null indicator.

Columns 7 and 8 of table 1 give values of the "psychrometric factor" $A_2=\frac{r_w}{\Delta T}$ and $A_1=\frac{C_{p,m}}{L_{v,r}}$ respectively, for the various liquid-gas systems studied. The differences (A_2-A_1) are given in column 9 while the percentage difference $\frac{(A_2-A_1)}{A_2}$ 100 are given in column 10.

Since in this imperfect world one cannot expect perfect agreement between experimental and theoretical values, it is desirable to have some criteria by which the reasonableness of the agreement can be assessed. An error analysis was therefore made to obtain estimates of the accuracy of the calculated "thermodynamic wet-bulb temperature" using the observed, or measured parameters P, T, and r. It is apparent that an iterative method must be used to solve eq (23) or (24) for T_w. Furthermore, the parameters P, T, T_w, and r must be known or assumed in order to obtain values of the enthalpy functions $h(P, T, r)$, $h(P, T_w, r)$, $h(P, T_w, r_w)$ and $h'_w(P, T_w)$, the latent heat of vaporization function $L'_v(T_w)$ and the saturation mixing ratio function $r_w(P, T_w)$. Not only do the measurement errors in P, T, and r enter into estimation of the error in $(T_w)_{calc}$, but experimental and other systematic uncertainties in the enthalpies, latent heats of vaporization and saturation mixing ratios must be accounted for. A similar analysis was made to obtain estimates of the accuracy of the psychrometric factors A_1 and A_2 using the observed parameters P, T, T_w, and r. Details of the analyses are given in the appendix, along with the sources of the thermodynamic data and physical constants used in the calculations. The results of the analyses are presented in tables 2, 3, and 4.

The parameters used in the computation of $(T_w)_{calc}$, A_1 and A_2 are listed in column 1 of table 2. The nominal magnitudes of the parameters are given in column 2. Estimates of the systematic and random errors in these parameters are given in columns 3 and 4 while the corresponding systematic and random errors in the wet-bulb temperature difference $[(T_w)_{obs}-(T_w)_{calc}]$ and in the psychrometric factor difference (A_2-A_1) produced by the estimated errors in these parameters are given in columns 5, 6, 7, and 8. Thus, for example, an estimated systematic error of 0.01 deg C in T for the water-air system produces a corresponding systematic error or 0.005 deg C in $[(T_w)_{obs}-(T_w)_{calc}]$ in the water-air system. The estimated overall systematic error in $[(T_w)_{obs}-(T_w)_{calc}]$ was obtained by summing the individual systematic errors listed in column 5. Similarly the estimated overall systematic error in (A_2-A_1) was obtained by summing the individual systematic errors in column 7. The estimated overall random error in $[(T_w)_{obs}-(T_w)_{calc}]$ and in (A_2-A_1) was obtained by computing the root-mean-square value of the individual random errors in columns 6 and 8, respectively. The estimated overall errors may be considered as guesses of the differences between $(T_w)_{obs}$ and $(T_w)_{calc}$ and between A_2 and A_1 which may be expected to occur due to systematic and random errors, provided the psychrometer otherwise acted in accordance with eq (1).

Table 3 lists, for each liquid-gas system, the average of $[(T_w)_{obs}-(T_w)_{calc}]$ and an estimate of the standard deviation of the average. Estimates of the overall systematic error and the overall random error, given in table 2, are repeated here for convenience in making comparisons. Table 4 gives similar values for (A_2-A_1).

TABLE 1. *Comparison between wet-bulb temperatures and psychrometric factors*

Pressure P	Flow	Dry-bulb temperature T	Wet-bulb temperature			Psychrometric factor			
			Observed $(T_w)_{obs}$	Calculated $(T_w)_{calc}$	Difference $[(T_w)_{obs}-(T_w)_{calc}]$	$A_2=\frac{f_w}{\Delta T}$	$A_1=\frac{C_{p,m}}{L_{v,T}}$	Difference (A_2-A_1)	Percentage difference $\frac{(A_2-A_1)}{A_2}\times 100$
Bars	Liter per minute	deg C	deg C	deg C	deg C	10^{-3}/deg C	10^{-3}/deg C	10^{-3}/deg C	%
Water—Air									
0.9745	1.4	24.80	7.87	7.86	0.01	40.65	40.57	0.08	0.2
.9737	1.4	24.73	7.81	7.82	−.01	40.54	40.57	−.03	−.1
.9816	1.4	24.62	7.80	7.83	−.03	40.42	40.57	−.15	−.4
.9806	1.4	24.65	7.82	7.84	−.02	40.49	40.57	−.08	−.2
1.0002	1.4	25.11	8.24	8.21	.03	40.76	40.59	.17	.4
0.9943	2.1	37.07	13.25	13.26	−.01	40.71	40.75	−.04	−.1
.9948	2.1	37.01	13.19	13.24	−.05	40.53	40.75	−.22	−.5
.9943	2.1	37.02	13.27	13.24	.03	40.88	40.75	.13	.3
0.9978	2.1	37.02	13.23	13.27	−.04	40.56	40.75	−.19	.5
1.0000	2.1	24.98	8.15	8.14	.01	40.61	40.58	.03	.1
1.0005	2.1	25.02	8.16	8.17	−.01	40.55	40.58	−.03	−.1
1.0008	2.1	25.02	8.18	8.17	.01	40.64	40.59	.05	.1
1.0008	2.1	25.08	8.22	8.20	.02	40.70	40.59	.11	.3
1.0007	2.1	25.17	8.25	8.24	.01	40.65	40.59	.06	.1
0.9818	6.2	24.88	8.07	7.95	.12	41.19	40.58	.61	1.5
.9829	6.2	24.85	8.10	7.95	.15	41.38	40.58	.80	1.9
Water—Hydrogen									
0.9718	5.2	24.40	7.60	7.58	0.02	576.8	575.0	1.8	0.3
.9807	5.2	24.29	7.57	7.60	−.03	573.1	575.0	−1.9	−.3
.9823	5.2	24.25	7.56	7.59	−.03	572.8	575.0	−2.2	−.4
.9851	5.2	24.40	7.63	7.68	−.05	571.2	575.0	−3.8	−.7
Carbon tetrachloride—Oxygen									
0.9929	1.3	24.52	−8.50	−8.52	0.02	416.8	416.1	0.7	0.2
.9714	1.9	24.67	−8.73	−8.72	−.01	415.6	416.0	−.4	−.1
.9876	1.9	24.66	−8.56	−8.53	−.03	415.1	416.1	−1.0	−.2
.9878	1.9	24.45	−8.66	−8.60	−.06	413.8	416.0	−2.2	−.5
.9870	1.9	24.41	−8.69	−8.62	−.07	413.6	416.0	−2.4	−.6
1.0114	0.8	24.26	−8.17	−8.39	.22	424.8	416.3	8.5	2.0
Carbon tetrachloride—Hydrogen									
1.0061	2.1	23.93	−8.71	−8.83	0.12	6.519	6.451	68	1.0
0.9970	2.1	23.82	−8.83	−8.97	.14	6.531	6.450	81	1.2
.9839	2.9	24.18	−8.96	−9.00	.04	6.471	6.449	22	.3
.9843	2.9	24.20	−8.98	−8.99	.01	6.453	6.449	4	.1
.9848	2.9	24.12	−9.01	−9.01	.00	6.447	6.448	−1	−.0
Toluene—Air									
0.9981	1.4	25.47	6.79	6.84	−0.05	236.8	238.2	−1.4	−0.6
.9986	1.4	25.37	6.74	6.80	−.06	236.5	238.2	−1.7	−.7
.9923	1.4	25.15	6.65	6.64	.01	238.4	238.2	0.2	.1
.9930	1.4	25.13	6.65	6.64	.01	238.5	238.2	0.3	.1
.9764	2.1	25.58	6.65	6.70	−.05	236.8	238.2	−1.4	−.6
.9784	2.1	25.54	6.62	6.70	−.08	236.0	238.2	−2.2	−.9
1.0056	0.8	25.09	6.90	6.73	.17	242.9	238.3	4.6	1.9
1.0075	0.8	24.98	6.90	6.70	.20	243.9	238.3	5.6	2.3

If the errors in $(T_w)_{obs}$ and $(T_w)_{calc}$, or in A_2 and A_1, were solely random, then the average of the appropriate difference, for a given liquid-gas system, would tend toward zero. Since the averages are not equal to zero, one would expect that these values are experimental measures of the systematic errors and should therefore have the same magnitudes as the estimates of the overall systematic errors. The standard deviations of the differences about these averages, on the other hand, are indicators of the experimental random errors and so, correspondingly, should have a close relationship to the estimates of the overall random errors.

It can be observed from table 3 that the average values of $[(T_w)_{obs}-(T_w)_{calc}]$ are smaller than the estimates of the overall systematic errors of $[(T_w)_{obs}-(T_w)_{calc}]$. This is also the case for (A_2-A_1) as shown in table 4. This is probably due to an overly conservative estimate of the individual systematic errors of the parameters (especially f_w) and the fact that summing the corresponding individual systematic errors of the appropriate differences gives a maximum.

It can be observed further from tables 3 and 4 that the estimates of the standard deviations are considerably greater than the estimates of the over-

TABLE 2. *Error analysis*

Parameter	Nominal magnitude of parameter	Estimated error of the parameter		Estimated error of $[(T_w)_{obs} - (T_w)_{calc}]$ due to parameter error		Estimated error of $(A_2 - A_1)$ due to parameter error	
		Systematic	Random*	Systematic	Random	Systematic	Random
				deg C	deg C	10^{-5}/deg C	10^{-5}/deg C
Water – Air							
$(T_w)_{obs}$, °C	8.	0.01	0.015	0.010	0.015	0.052	0.08
T, °C	25.	.01	.024	.005	.011	.024	.06
P, bar	1.0		.0002		.002		.01
M_r, g/g mol	18.01534	.00006		.000		.000	
M_g, g/g mol	28.9645	.0009		.000		.000	
f_w	1.004	.0008		.006		.033	
e_w, bar	0.0107	.0000043		.003		.016	
C_p, J/g °C	1.0	.00036		.003		.015	
h'_w, J/g	33.	.025		.000		.000	
h_r, J/g	2.516	.084		.000		.001	
Estimated overall error				.027	.019	.14	.10
Water – Hydrogen							
T_w, °C	8.	0.01	0.015	0.010	0.015	0.74	1.11
T, °C	25.	.01	.024	.005	.011	.35	0.83
P, bar	1.0	.01	.0002		.002		.12
M_r, g/g mol	18.01534	.00006		.000		.00	
M_g, g/g mol	2.01594	.00001		.000		.010	
f_w	1.	.005		.039		2.91	
e_w, bar	0.0104	.0000042		.003		.23	
C_p, J/g °C	14.2	.00042		.000		.02	
L_r, J/g	2.483	1.76		.005		.40	
Estimated overall error				.062	.020	4.65	1.39
Carbon Tetrachloride – Oxygen							
T_w, °C	−9.	0.01	0.015	0.010	0.015	0.37	0.56
T, °C	25.	.01	.024	.003	.008	.12	.31
P, bar	1.0		.0002		.002		.09
M_r, g/g mol	53.82315	.002		.000		.00	
M_g, g/g mol	31.9988	.0001		.000		.00	
f_w	1.	.005		.057		2.14	
e_w, bar	0.027	.000093		.038		1.46	
C_p, J/g °C	.92	.000167		.002		0.9	
L_r, J/g	214.	1.09		.055		2.14	
Estimated overall error				.165	.017	6.32	.65
Carbon Tetrachloride – Hydrogen							
T_w, °C	−9.	0.01	0.015	0.010	0.015	6.0	8.9
T, °C	25.	.01	.024	.003	.008	2.0	4.7
P, bar	1.0		.0002		.002	.1	1.3
M_r, g/g mol	153.82315	.002		.000		.1	
M_g, g/g mol	2.01594	.00001		.000		.0	
f_w	1.	.005		.056		33.2	
e_w, bar	0.027	.000091		.038		22.6	
C_p, J/g °C	13.4	.00406		.000		0.2	
L_r, J/g	214.	1.09		.054		32.9	
Estimated overall error				.161	.017	97.0	10.1
Toulene – Air							
T_w, °C	7.	0.01	0.015	0.010	0.015	0.27	0.40
T, °C	25.	.01	.024	.004	.010	.13	.31

TABLE 2. *Error analysis*—Continued

Parameter	Nominal magnitude of parameter	Estimated error of the parameter		Estimated error of $[(T_w)_{obs}-(T_w)_{calc}]$ due to parameter error		Estimated error of (A_2-A_1) due to parameter error	
		Systematic	Random*	Systematic	Random	Systematic	Random
		deg C		deg C		10^{-3}/deg C	10^{-3}/deg C
Toulene Air—Continued							
P.....bar	1.0		.0002		.002		.05
M_v.....$\frac{g}{g\ mol}$	92.14181	.00008		.000		.00	
M_a.....$\frac{g}{g\ mol}$	28.9645	.0009		.000		.01	
f_w	1.	.005		.049		1.20	
e_w.....bar	0.014	.000014		.010		.24	
C_p.....$\frac{J}{g\ °C}$	1.00	.00036		.002		.07	
L_v.....$\frac{J}{g}$	423.	.88		.021		.40	
Estimated overall error				.096	.018	2.32	.51

*Estimated standard deviation of an observation.

TABLE 3. *Summary of wet-bulb temperature differences* $[(T_w)_{obs}-(T_w)_{calc}]$

System	Average	Standard deviation of the differences about the average	Estimated overall systematic error Δ_s	Estimated overall random error* Δ_r	Estimated total error $(\Delta_s+\Delta_r)$	Rejection criterion $(\Delta_s+3\Delta_r)$
	deg C	deg C	deg C	deg C	deg C	deg C
H_2O-Air	+0.015	0.053	0.027	0.019	0.046	0.084
H_2O-Air (Restricted flow)	−.003	.026	.027	.019	.046	
H_2O-H_2	−.021	.033	.062	.020	.082	.122
CCl_4-O_2	+.013	.108	.165	.017	.182	.216
CCl_4-O_2 (Restricted flow)	−.029	.035	.165	.017	.182	
CCl_4-H_2	+.060	.064	.161	.017	.178	.212
C_7H_8-Air	+.018	.109	.096	.018	.114	.150
C_7H_8-Air (Restricted flow)	−.038	.042	.096	.018	.114	

*Estimated standard deviation of an observation.

TABLE 4. *Summary of psychrometric factor differences* (A_2-A_1)

System	Average	Standard deviation of the differences about the average	Relative average	Estimated overall systematic error Δ_s	Estimated overall random error* Δ_r	Estimated total error $(\Delta_s+\Delta_r)$
	10^{-3}/deg C	10^{-3}/deg C	%	10^{-3}/deg C	10^{-3}/deg C	10^{-3}/deg C
H_2O-Air	+0.08	0.27	.19	0.14	0.10	0.24
H_2O-Air (Restricted flow)	−.01	.12	−.02	.14	.10	.24
H_2O-H_2	−1.6	2.4	−.27	4.65	1.39	6.04
CCl_4-O_2	+0.5	4.0	+.12	6.32	0.65	6.97
CCl_4-O_2 (Restricted flow)	−1.1	1.4	−.26	6.32	.65	6.97
CCl_4-H_2	+35.	37.	+.25	97.	10.	107.
C_7H_8-Air	+0.5	3.0	+.21	2.3	0.5	2.8
C_7H_8-Air (Restricted flow)	−1.0	1.0	−.43	2.3	.5	2.8

*Estimated standard deviation of an observation.

all random errors. The overall random errors were based on estimates of the individual random error to be expected in measurement of each of the parameters in a system in static equilibrium. The measurements were made in a dynamic system under conditions close to steady-state, but with some fluctuation of inlet temperature. Since the thermocouple emfs were not read simultaneously and since the wet-bulb thermocouple does not respond to changes in inlet temperature as rapidly as does the dry-bulb thermocouple, it is likely that the actual random temperature errors were greater than that estimated. That the standard deviation was approximately two- to three-fold the estimated overall (static) random error, does not seem disturbing, but does indicate that some contributory effects were not accounted for.

Examining the data in table 1, one finds that there are several sets of measurements which yielded excessively large individual differences in $[(T_w)_{obs}-(T_w)_{calc}]$.

The criterion was established to reject any difference which exceeded the sum of the estimated overall systematic error plus three times the estimated overall random error in $[(T_w)_{obs}-(T_w)_{calc}]$. It was assumed that such large differences represented anomalous behavior of the psychrometer. The application of this criterion led to the rejection of two sets of data for the water-air system, one set of data for the carbon tetrachloride-oxygen system, and two sets of data for the toluene-air system. These rejected sets of data included all experiments performed at the lowest and highest flow rates, that is, at 0.8 and 6.2 liters per minute, and none within the flow rate range of 1.3 through 5.2 liters per minute.

Average differences and estimates of the standard deviations of the average differences were recomputed excluding the rejected differences, and are given in tables 3 and 4 under the heading "restricted flow." Whereas the average algebraic differences initially were positive in sign for the water-air, carbon tetrachloride-oxygen, and toluene-air systems, after applying the rejection criterion, the sign in each case was negative. The magnitude of the average algebraic difference decreased by a factor of five for the water-air system, but doubled for the carbon tetrachloride-oxygen and toluene-air systems. The new ("restricted flow") estimates of the standard deviations were smaller by a factor of about two to three

and agreed more closely with the estimates of the overall random error.

It appears that the rejection process eliminated both low and high flow-dependent systematic errors. This is to be expected since at very low flows heat losses to the ambient atmosphere become a noticeable fraction of the heat supplied by the test gas. At very high flows, incomplete saturation and incomplete heat exchange apparently occur.

Corrections or error estimates could be made for radiative or conductive heat losses, incomplete saturation, change of kinetic energy of the gas stream, heat supplied by incoming liquid or other factors that might tend to affect the performance of the psychrometer. In designing this instrument, an attempt was made to make these sources of error as negligible as feasible, so that corrections would not need to be applied. Since the purpose of these tests was to determine how well the instrument actually performed its intended function as an adiabatic saturation psychrometer, such corrections were not made in this evaluation.

Though on the average the measured wet-bulb temperatures differ little from the calculated wet-bulb temperatures, there is a prevalence for the measured temperature to be lower than the calculated temperature for the "restricted flow" cases. This probably stems from the fact that the true f_w-factor is greater than unity whereas a value of one was used for all systems except water-air in determining $(T_w)_{calc}$.

For the water-air system, for which the f_w-factor is known and therefore was used, $(T_w)_{calc}$ is much closer to $(T_w)_{obs}$ on the average than for any other system.

The response time traces obtained appeared to have the general shape of exponential functions as one would expect. The time constant τ was obtained by measuring the time required for the wet-bulb temperature to undergo 63 percent of its total change for each test condition. Figure 4 is a plot of these measured time constants against gas flow rate for the two conditions tested. The time constant is a function of gas flow rate. At flow rates of 3.75 to 5.2 liters per minute the time constant is about $^3/_4$ of a minute.

Although the temperature of the liquid at the point where it discharges onto the wicking was not measured, several calculations were made to obtain estimates of how close this temperature approached the "thermodynamic wet-bulb temperature." For example, with water flowing at a rate calculated to be three-fold that required to saturate an air flow of $1^1/_2$ liters per minute at inlet conditions of zero mixing ratio, 25 °C dry-bulb temperature, and 1 bar pressure, the liquid feed temperature was calculated to be 0.2 °C higher than "thermodynamic wet-bulb temperature." This, it was estimated, would elevate the wet-bulb temperature by approximately 0.008 °C. If the inlet relative humidity of the gas were higher, the other inlet and flow conditions remaining unchanged, the absolute temperature error in the liquid feed would be less, but the percentage error in the experimental psychrometric factor, would be the same.

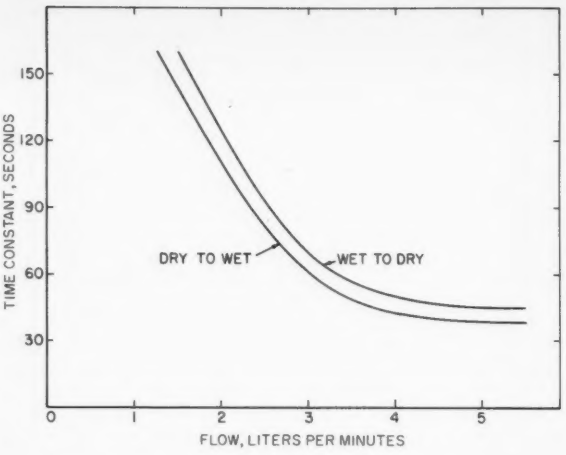

FIGURE 4. *Time constant versus inlet gas flow rate for water-air system.*

It is important to reiterate that the adiabatic saturation psychrometer behaves very differently from conventional types of psychrometers. This is shown in table 5 which compares the psychrometric factor ratios A_2/A_1 at $r=0$ obtained at NBS with the adiabatic saturation psychrometer and with three types of conventional thermocouple psychrometers corrected for radiation losses; it also lists ratios based on results reported by other investigators on conventional psychrometers. The ratio is essentially unity for the adiabatic saturation psychrometer for the five systems listed; it differs significantly from unity for the conventional types of psychrometer, although for the water-air system the magnitude of the difference is smaller than for the other systems.

TABLE 5. *Typical psychrometer performance*

System	Ratio of thermal to mass diffusivities	Ratio of psychrometric factors, A_2/A_1						
		NBS instruments				Other instruments		
		Adiabatic saturation psychrometer[a]	Thermocouple psychrometer A[b]	Thermocouple psychrometer B[b]	Thermocouple psychrometer C[b]	Arnold [11][b]	Sherwood [12]	Lewis [13]
H_2O-Air	0.9	1.000	1.14	1.04		0.95	1.21	
H_2O-H_2	1.7	0.997	1.64	1.47	1.53			
CCl_4-O_2	3.0	.997	2.33		2.23			
CCl_4-H_2	4.5	1.005			2.79			
C_2H_6-Air	2.6	0.996		2.07	1.96	1.77	2.08	2.5

[a] Shielded against radiation.
[b] Corrected for radiation.

6. Discussion and Conclusions

The theoretical basis governing the operation of this instrument has been demonstrated at room temperature, atmospheric pressure, and over the flow range of 1.3 through 5.3 liters per minute, by tests with several liquid-gas systems subject to the re-

striction that the data were limited to the condition $r=0$. Since zero mixing ratio produces the maximum wet-bulb depression for any given dry-bulb temperature, and since such effects as radiative and conductive heat losses tend to have a greater influence with increasing depression, the $r=0$ condition subjects the psychrometer to its severest experimental test. Use of the gas temperature just beyond the outlet end of the saturator tube rather than the temperature of the moistened wicking as the wet-bulb temperature further increases the assurance that this instrument is producing "thermodynamic wet-bulb temperatures." Since essentially all cooling of the incoming gas occurs by heat transfer from the gas to the moistened wicking, the average temperature of the moistened wicking must of necessity be equal to or less than the average temperature of the exit gas. It is possible under some circumstances (for example, where the ratio of thermal to mass diffusivity is less than 1) for the moistened wicking to be cooled below the "thermodynamic wet-bulb temperature," but it is extremely unlikely that the average temperature of the exit gas could be as low as the "thermodynamic wet-bulb temperature" without satisfying the postulates that form the theoretical basis for eq (1).

Although the intended use of this instrument is to measure the water vapor content of gases, it is possible to use it for the determination of other vapors in gases and perhaps for the determination of f_w for particular vapor-gas combinations. The latter might be done by controlling inlet gas temperatures in such a way as to produce wet-bulb temperatures which correspond to those at which the vapor pressure and latent heat of evaporation of the liquid are well known.

Due to the difficulty of producing known vapor concentrations in gases other than zero, this instrument was only tested at the condition $r=0$. Its performance characteristics, therefore, have been demonstrated only at this condition. We believe however, that the characteristics would not be altered significantly were the psychrometer operated at $r>0$. Furthermore, as mentioned above, for any given dry-bulb temperature, $r=0$ produces the minimum wet-bulb temperature and subjects the psychrometer to the maximum radiative and conductive heat losses, and hence is the most severe condition under which to test the behavior of a psychrometer.

It is of interest to predict how well one could measure the water vapor content of air with this psychrometer. Whereas the magnitude of the error in wet-bulb temperature probably is related directly to the difference between wet- and dry-bulb temperatures, we will use for our prediction the error obtained at $r=0$ which is in all likelihood maximum since the wet- and dry-bulb temperature difference is maximum, and handle it as though it were a fixed error although it is likely smaller at higher relative humidities. For our estimate of this error we will use the average value of $[(T_w)_{obs}-(T_w)_{calc}]$ plus one standard deviation of this quantity obtained from the "restricted flow" test points. This should give us a one-sigma error estimate. Assuming a dry-bulb temperature of 25 °C, a total pressure of 1 bar, and using the above error in wet-bulb temperature, it is estimated that the psychrometer can be used to determine the relative humidity to within ¼ percent. Table 6 gives the error estimates in both the mixing ratio and relative humidity determination at various inlet relative humidities.

TABLE 6. *Estimated instrument error for water vapor-air system at 25 °C, 1 bar pressure and various relative humidities*

RH	Δr	ΔRH
%	g vapor/g vapor-free gas	%
0	0.000025	0.13
20	.000029	.15
40	.000034	.17
60	.000038	.19
80	.000043	.21
100	.000049	.23

The suggestions and criticisms of L. P. Harrison, ESSA, Weather Bureau, Silver Spring, Md., are gratefully acknowledged.

7. Appendix. Computations and Sources of Constants

$(T_w)_{calc}$ was computed for each experimental point by solving one of the following equations in an iterative manner, using measured values of P and T:

$$h(P, T, 0)=h(P, T_w, r_w)-r_w h'_w(P, T_w) \quad (22)$$

$$h(P, T, 0)=h(P, T_w, 0)+r_w L'_v. \quad (23)$$

A_2 was computed for each experimental point equating A_2 to A in eq (13) into which the measured values of P, T, and T_w were substituted. A_1 was computed for each experimental point by using one of the following equations into which the measured values of P, T, and T_w were substituted;

$$A_1=\frac{r_w[h(P, T, 0)-h(P, T_w, 0)]}{\Delta T[h(P, T_w, r_w)-h(P, T_w, 0)-r_w h'_w(P, T_w)]} \quad (24)$$

$$A_1=\frac{[h(P, T, 0)-h(P, T_w, 0)]}{\Delta T L'_v} \quad (25)$$

where A_1 is the equivalent of A in eq (9).

Equations (22) and (24) were used for the water-air system and are exact. Equations (23) and (25) are approximations and were used for all other systems because neither the gas mixture enthalpy $h(P, T_w, r_w)$ nor the "effective" latent heat of vaporization $L_{v,r}$ for these systems was known.

In all cases r_w was determined by solution of the following equation:

$$r_w = \frac{M_v}{M_g} \frac{f_w e_w}{(P - f_w e_w)} \tag{26}$$

where f_w = a function of pressure and temperature for a given liquid-gas system.[3]

Each of the individual errors in $(T_w)_{calc}$ is associated with an error in one of the parameters entering into its calculation. The error in $(T_w)_{calc}$ was obtained by solving eq (22) or (23), as appropriate, using the parameter value plus its estimated error in the calculation and subtracting $(T_w)_{calc}$ from the result. The individual errors in $(A_2 - A_1)$ were obtained by solving equations (13) and (24) or (25) as appropriate, using the parameter value plus its estimated error in the calculation along with the values of $(T_w)_{calc}$ obtained from prior computation. The solution of these equations gives the error directly since $A_2 - A_1 = 0$ at $(T_w)_{calc}$ when there are no errors.

The results of the error computations are given in table 2.

Water-Air System. $h(P, T, r)$, $h(P, T_w, r)$ and $h(P, T_w, r_w)$ were obtained by solution of the following equation:

$$h = \frac{7}{2} R [T + \frac{8}{7} r \frac{M_a}{M_v} (T + 1354.74)] + \Delta h$$

$R = 0.068557$ ITcal-K^{-1}(g dry air)$^{-1}$ or 0.28703 J-K^{-1} (g dry air)$^{-1}$.

and Δh was obtained from table 85 of the Smithsonian Meterological Tables [31].

Values of h'_w were linearly interpolated from a table given by Goff [24] and values of f_w were obtained by linear interpolation in both T and P from values given in Table 89 of the Smithsonian Meteorological Tables [31]. The saturation vapor pressure of water was obtained by solution of an equation given by Goff [32]. The estimated errors in these parameters are given in table 2.

Water-Hydrogen System. $h(P, T, 0)$ and $h(P, T_w, 0)$ were obtained for vapor-free hydrogen by linear temperature interpolation of the tabulated values given by Hilsenrath [33]. Values of L'_v were obtained from steam tables [34]. In the absence of data on the factor f_w at the experimental test conditions, a value of unity was assumed for f_w. Values of e_w were obtained in the same manner as with the water-air system. The estimated errors in these parameters are given in table 2.

Carbon Tetrachloride-Oxygen System. $h(P, T, 0)$ and $h(P, T_w\ 0)$ were obtained for vapor-free oxygen by linear temperature interpolation of tabulated values given by Hilsenrath [33]. Values of L'_v were obtained by linear interpolation from the tabulation in the International Critical Table [35]. A value of unity was ascribed to f_w and vapor pressures were calculated from the following equation given by Hildebrand [36]:

$$e_w = \text{Antilog}\,[6.89406 - \frac{1219.58}{227.16 + T_w}] \text{ mm Hg}$$

or

$$e_w = 0.0013332 \text{ Antilog}\,[6.89406 - \frac{1219.58}{227.16 + T_w}] \text{ bars.}$$

The estimated errors in these parameters are given in table 2.

Carbon Tetrachloride-Hydrogen System. Enthalpies were obtained as in the water-hydrogen system and all other parameters were obtained as in the carbon tetrachloride-oxygen system. The estimated errors in these parameters are given in table 2.

Toluene-Air System. $h(P, T, 0)$ and $h(P, T_w, 0)$ were obtained for vapor-free air by linear interpolation of tabulated values given by Hilsenrath [33]. Values of e_w were obtained from the equation of Rossini [37]:

$$e_w = \text{Antilog}\left[6.95464 - \frac{1344.800}{219.482 + T_w}\right] \text{ mm Hg}$$

or

$$e_w = 0.0013332 \text{ Antilog}\left[6.95464 - \frac{1344.800}{219.482 + T_w}\right] \text{ bars.}$$

A value of unity was assigned to f_w and L'_v was computed from the equation given by Scott [38]:

$$L'_v = \frac{11637 - 4.823\ T_w - 1.260 \times 10^{-2} T_w^2}{92.141}$$

where T_w is given in degrees Kelvin. According to Scott, this formula is applicable over the temperature range of 298 to 410 °K. However, since it was used to extrapolate values of L'_v at 280 °K, allowance for this fact was made in estimating the error in L'_v. The estimated errors in these parameters are given in table 2.

8. References

[1] Monteith, J. L., Error and Accuracy in Thermocouple Psychrometry, Proceedings of the Physical Society, B **LXVII**, 217 (1954).

[2] Bindon, H. H., A Critical Review of Tables and Charts Used in Psychrometry, Humidity and Moisture **1**, 3 (Reinhold Publishing Corp., New York, 1965).

[3] Harrison, L. P., Some Fundamental Considerations Regarding Psychrometry, Humidity and Moisture **3**, 71 (Reinhold Publishing Corp., New York, 1965).

[4] Wylie, R. G., Psychrometry, Report PA-4, Commonwealth of Australia, Commonwealth Scientific and Industrial Research Organization, National Standards Laboratory, Division of Physics, University Grounds, Sydney, Australia, July 1949.

[5] Ivory, J., On the hygrometer by evaporation, Philosophical Magazine **60**, 81 (1822).

[6] August, E. F., Uber die Verdunstungskälte und deren Anwendung auf Hygrometrie, Ann. der Physik und Chemie **5**, 69 (1825).

[7] Apjohn, J., Formula for inferring the dewpoint from indications of the wet-bulb hygrometer, Phil. Mag. **6**, 182 (1835).

[8] Apjohn, J., On the theory of the moist bulb hygrometer, Trans. Roy. Irish Acad. **17**, 275 (1837).

[3] The saturation vapor pressure of a liquid substance in the presence of an inert gas differs from that when the pure substance alone is present. The factor f_w accounts for this difference. It is defined as $f_w(P, T_r) = \frac{X_r P}{e_w}$ where X_r is the mole fraction of the vapor in a vapor-gas mixture under saturation at temperature T_w and total absolute pressure P.

[9] Whipple, F. J. W., The wet and dry bulb hygrometer: The relation to theory of the experimental researches of Awberry and Griffiths, Proc. Phys. Soc. London **45,** 307 (1933).
[10] Carrier, W. H., Rational psychrometric formulae, Am. Soc. Mech. Engrs. Trans. **33,** 1005 (1911).
[11] Arnold, J. H., The theory of the psychrometer. II. The effect of velocity, Physics **4,** 334 (Sept. 1933).
[12] Sherwood, T. K. and Comings, E. W., On experimental study of the wet-bulb hygrometer, Trans. Am. Inst. Chem. Eng. **28,** 88 (1932).
[13] Lewis, W. K., The evaporation of a liquid into a gas—a correction, Mech. Eng. J. **55,** 567 (1933).
[14] Dropkin, D., The Deviation of the Actual Wet-Bulb Temperature from the Temperature of Adiabatic Saturation, Cornell University Engineering Experiment Station, Bulletin No. 23 (July 1936).
[15] Brun, E. and Lions, M., Sur la theorie generale du psychrometrie et sur une methode simple d'etude experimentale des lois de diffusion forcie, C.R.A.S. (Paris) **222,** 1071 (1946).
[16] Kawata, S. and Omori Y., An investigation of thermocouple psychrometer I, J. Phys. Soc. Japan **8,** No. 6, 768 (1953).
[17] Maxwell, J. C., Diffusion, Encyl. Brit. 9th Ed. VII, 218 (1877).
[18] Mieghem, J. Van, La Thermodynamique du Thermometre Mouille, Bull. Classe Sci. Acad. Roy. Belgi. Bruxilles **27,** 85 (1941).
[19] Svennson, A., Verdunstung und Abkühlung oder Erwärmung in dem Laminaren Gasstrom von Konstanter Geschwindigkeit. Anwendung auf Assmansche Aspiration-psychrometer, Arkiv. f. Mat. Astron. och Physik. Stockholm, Hafte 4, **22A,** 23 (1932).
[20] Threlkeld, J. L., Thermal Environmental Engineering, Prentice-Hall, Inc., Englewood Cliffs, N.J. (1962).
[21] Weber, S., Psychrometrets Teori, Dansk Videnskobernes Selsk, Mathem-fys. Medd **3,** No. 19 (1921).
[22] Arnold, J. H., The theory of the psychrometer. I. The mechanism of evaporation, Physics **4,** 255 (July 1933).
[23] Goff, J. A., Standardization of thermodynamic properties of moist air—final report of working subcommittee, International Joint Committee on Psychrometric Data, ASHVE Journal Section, Heating, Piping and Air Conditioning **55,** 118 (1949).
[24] Goff, J. A., and Gratch, S., Thermal properties of moist air, ASHVE Journal Section, Heating, Piping and Air Conditioning **51,** 334 (June 1945).
[25] Carrier, W. H. and Lindsay, D. C., The temperature of evaporation of water into air, Trans. of Am. Soc. Mech. Eng. **46,** 739 (1924).
[26] Harrison, L. P., Proposal for an Experimental Triple-tubed Adiabatic Saturator to Measure Thermodynamic Wet-Bulb Temperature as a Limit Approached During the Saturation Process, Humidity and Moisture **1,** 33 (Reinhold Publishing Corp., New York, 1965).
[27] Lewis, W. K., The Evaporation of a Liquid into a Gas, Trans. Am. Soc. Mech. Engrs. **44,** 325 (1922).
[28] Nanda, V. S. and Kapur, R. K., A note on the thermodynamics of the wet- and dry-bulb hygrometer, Indian J. Phys. **31,** 391 (1948).
[29] Wentzel, J. D., An instrument for the measurement of the humidity of air, American Society of Heating, Refrigeration and Air Conditioning Engineers Journal **66,** 67 (Nov. 1961).
[30] Harrison, L. P., Fundamental Concepts and Definitions, Humidity and Moisture **3,** 3 (Reinhold Publishing Corp., New York, 1965).
[31] Smithsonian Meteorological Tables, Smithsonian Institution, Washington, D.C. (1951).
[32] Goff, J. A., Saturation Pressure of Water on the New Kelvin Scale, Humidity and Moisture **3,** 289 (Reinhold Publishing Corp., New York, 1965).
[33] Hilsenrath, J., et al., Tables of thermal properties of gases, NBS Circ. 564 (1955).
[34] Bain, R. W., Steam Tables, Department of Scientific and Industrial Research, National Engineering Laboratory, East Kilbride, Scotland (1964).
[35] International Critical Tables (McGraw-Hill Book Co., Inc., New York, N.Y., 1928).
[36] Hildenbrand, D. L. and McDonald, R. A. The Heat of vaporization and vapor pressure of carbontetrachloride; the entropy from calorimetric data, J. Phys. Chem. **63,** 1521 (1959).
[37] Rossini, F. D., et al., Values of Physical and Thermodynamic Properties of Hydrocarbons and Related Compounds (Carnegie Press, Pittsburgh, Pa., 1953).
[38] Scott, D. W., et al., Toluene thermodynamic properties, molecular vibrations and internal rotation, J. Phys. Chem. **66,** 911 (1962).

(Paper 72C1–267)

JOURNAL OF RESEARCH of the National Bureau of Standards—C. Engineering and Instrumentation
Vol. 72C, No. 1, January–March 1968

An Injection Method for Self-Calibration of Inductive Voltage Dividers

Wilbur C. Sze

Institute for Basic Standards, National Bureau of Standards, Washington, D.C. 20234

(November 14, 1967)

A self-calibration or "boot-strapping" injection method for determining the voltage ratio and phase angle deviations of inductive voltage dividers utilizes specially constructed transformers for step and differential voltage injections without reference to the fundamental electrical units or standards. Construction details of transformers, derivation of equations, and systematic evaluation of uncertainties are presented. Calibration of certain ratios involving a combination of dial settings on several decades can be obtained as readily as that of a single decade. The accuracy of the results obtainable at 10 kHz is within 2×10^{-7} of input for deviations less than 10 ppm of input and within 1×10^{-6} for deviations up to 100 ppm of input. This same calibration technique can readily be used to cover a frequency range from 1 to 20 kHz.

Key Words: Calibration, in-phase deviation, inductive voltage divider, measurements, quadrature deviation, ratio calibration, transformer, two-stage voltage transformer, voltage divider, voltage ratio.

1. Introduction

Since voltage ratio is a dimensionless quantity, one may reasonably expect that it can be accurately determined in any laboratory without reference to any standards or fundamental electrical units. It is also reasonable to assume that the limitations on the order of accuracy obtainable depend primarily on the knowledge and ingenuity of the developer and to a lesser extent on the commercially available equipment.

At the National Bureau of Standards, a new calibration method has been developed for determining the in-phase and quadrature deviations of inductive voltage dividers. The advantages of this technique are: (1) the test dividers may be calibrated as either three-terminal or four-terminal networks; (2) the test circuit imposes zero burden on the test divider; and (3) certain combinations of dial settings involving several decades can readily be calibrated.

The purpose of this paper is: (a) to describe a self-calibration or "boot-strapping" method; (b) to show the construction details of special transformers for step and differential voltage injections; and (c) to analyze various factors affecting the accuracy of the measurements.[1] In this paper, the discussion is primarily centered at 10 kHz. However, the same method of calibration and technique of design can readily be used to cover a broad frequency range from 1 to 20 kHz.

2. Inductive Voltage Divider Circuits

Inductive voltage dividers are basically "three-terminal" devices; that is, they consist of two terminals for voltage input and an adjustable intermediate tap or output terminal. However, commercial type dividers are generally provided with two "common" terminals for convenience in

[1] This work was supported in part by the Metrology Engineering Center, Bureau of Naval Weapons, Pomona, Calif.

making connections (fig. 1). The voltage differences between the "common" terminals in such "four-terminal" devices, due to internal pickup and impedance of the connecting wire, may be significantly large at high operating frequencies and may vary with the settings of the dials. In order to prevent the introduction of electrostatically induced voltages into the connecting lead, a copper shield has been added over it in the dividers used in this study. In figure 3, this shield and the case of the divider are electrically connected to the "common" terminal located near the "input" terminal.[2] The maximum measured voltage difference $\alpha''_{lCx}+j\beta''_{Cx}$ (fig. 3) is reduced by addition of the shielding to the connecting wire from about 5×10^{-7} to less than 3×10^{-8} of the input voltage. Further reduction can be achieved by shielding the output terminals (i.e., replacing them with coaxial type).

It is not necessary to add the shield in order to calibrate the divider with the method described here. However, it is a convenience in the calibration procedure particularly if the divider is to be used as a reference standard for calibration of other working dividers.

Throughout the discussion in this paper, the "common" terminal located near the "input" terminal will be disignated as the "reference" point for all voltage measurements, see figure 3.

3. Method of Measurement

3.1. Description of Circuit

Figure 2 shows the schematic circuit diagram simplified by omission of the guard circuits and shielding arrangements. D_1 and D_2 represent the test inductive voltage dividers whose in-phase and quadrature deviations are being determined. D_1 and D_2 can be calibrated simultaneously or one can be treated as an auxiliary. Their input terminals are connected together with a short coaxial lead, the impedances of which, from the junction point to the input terminals of each divider, must be very small relative to the divider input impedances. Their output "common" terminals are connected together with a low resistance lead.

The calibration circuit uses three toroidal transformers: one transformer for injection of step voltage, the second for injection of differential voltage, and a third for null detection.

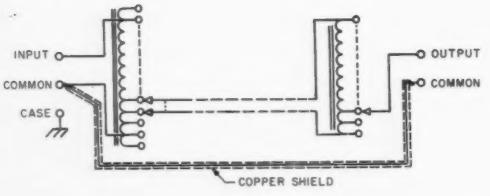

FIGURE 1. *Typical "four-terminal" divider circuit (shown with copper shield added by NBS).*

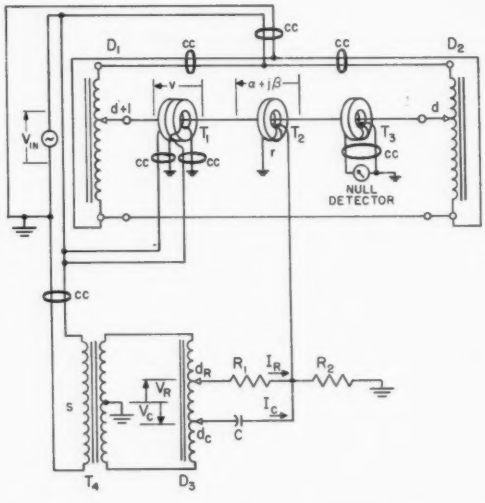

FIGURE 2. *Schematic circuit diagram (simplified by omission of the shielding arrangements and guard circuits).*

[2] On some commercial dividers, the case ground terminal is located near the "output" terminal. A suitable lead may then be used to connect the case to the "common" terminal located near the "input" terminal.

Transformer T_1 (each primary winding is represented by one-turn in figure 2 for simplicity) injects a voltage, v (approximately equal to that corresponding to one step of the decade being calibrated) into the lead connecting the "tap" output terminals of the two dividers. When T_1 is energized, the tap setting, $d+1$, of divider D_1 is set one step higher than the tap setting, d, on the corresponding decade of divider D_2. Inductive voltage divider D_3, injects, through the R-C network and transformer T_2, in-phase and quadrature differential balancing voltages, $\alpha+j\beta$, in the same connecting lead.

The detector circuit consists of a tuned null-indicator and a specially constructed shielded transformer, T_3, to match the impedance and to isolate the detector from the measuring circuit.

Transformer, T_4, is also specially constructed with an accurate voltage ratio, s, of either 1:1 or 1:2. The midpoint of the secondary is grounded so that either polarity can be obtained from the outputs of D_3 without the necessity of altering the circuit.

3.2. Calibration Procedure

When calibrating commercial type inductive voltage dividers which have only one adjustable output terminal, two such dividers, shown as D_1 and D_2 in figures 2 and 3, must be used. The procedure is as follows: First, determine the voltage, $\alpha''_n+j\beta''_n$, corresponding to balance with both dividers at a given setting, d, with the transformer T_1 deenergized; second, determine the balancing voltage, $\alpha'_n+j\beta'_n$, required with T_1 energized and the tap setting on divider D_1 one step higher. Repeat these two measurements on each of the ten settings to provide a "boot-strapping" calibration of the decade.

3.3. Coaxial Chokes

In order to realize the desired accuracy, coaxial chokes are required in various branches of the circuit. These reduce the small but troublesome loop and ground currents to insignificant values. The use of coaxial chokes in related applications has been discussed by Thompson, Homan, and Cutkosky [1, 2, 3, 4].[3] Each coaxial choke consists of an appropriate number of turns of a coaxial cable threaded through a high permeability toroidal core, located and shown as "cc" in figures 2 and 4. The operating principle is as follows: When the currents in the outer and center conductors of a coaxial lead are equal but in opposite directions, no flux is generated in the core. If either a loop, pickup, or leakage current causes an unequal flow of currents in the coaxial lead, a flux is generated in the core which in turn produces a high impedance in the particular path. Thus the undesirable current is reduced to a negligible value.

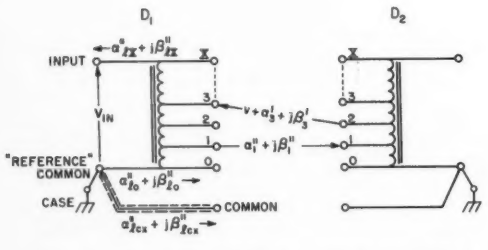

FIGURE 3. *Circuit for self "boot-straping" calibration.*

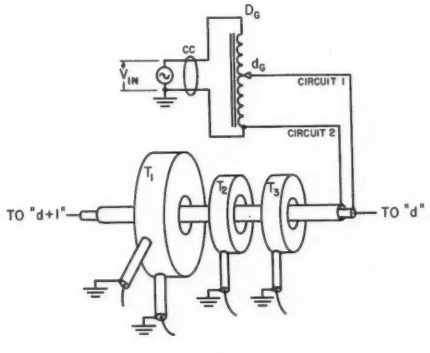

FIGURE 4. *Guard circuit.*

[3] Figures in brackets indicate the literature references at the end of this paper.

3.4. Guard Circuits

It is imperative to the success of this "boot-strapping" method that the step-voltage injector transformer, T_1, maintain precisely the same value of voltage, v, in its secondary winding regardless of the dial settings of the test dividers. This requirement necessitates that the lead connecting the output terminals of the test dividers be doubly guarded as shown in figure 4, to eliminate errors from capacitance currents.

A guard inductive voltage divider, D_G, is used to supply the voltages of the guard circuits. Circuit 1 is connected to the "tap" output terminal of the guard divider, with its dials set corresponding to that of the adjacent test divider (i.e., $d = d_G \neq d+1$). Circuit 2 is connected to the "common" output terminal which is at ground potential. Thus the voltage between the center conductor and circuit 1 is approximately zero regardless of the dial settings on the test dividers, and no significant capacitive current should exist. The same is true between the cases of transformers (T_1, T_2, and T_3) and circuit 2. The leakage current between circuits 1 and 2 constitutes a variable load on the guard divider which is independent of the measurement circuits.

A voltage difference approximately equal to v exists between the case of transformer T_1 and that portion of the circuit 2 between it and the "tap" output terminal of divider D_1. The leakage current constitutes a load on T_1. However, this leakage remains at a constant value throughout the "boot-strapping" test procedure and does not affect the test results.

4. Theoretical Relations

By definition, the voltage ratio of a divider is the ratio of the output terminal voltage, V_{out}, to the input terminal voltage, V_{in}, which can be expressed as

$$\frac{V_{out}}{V_{in}} = d + a + jb$$

where d is the nominal ratio or setting of the dials, a is the in-phase deviation, and b is the quadrature deviation. Both deviations are expressed as fractions of input or unity.

4.1. Differential Injection Voltage, $\alpha + j\beta$

The equations for the in-phase and quadrature differential injection voltages, $\alpha + j\beta$, will be derived first from the R–C network in figure 2 as follows:

$$V_R = I_R R_1 + r(\alpha + j\beta),$$

$$V_C = -I_C \left(j\frac{1}{\omega C}\right) + r(\alpha + j\beta),$$

and

$$r(\alpha + j\beta) = (I_C + I_R)\frac{R_2 Z}{R_2 + Z} \approx (I_C + I_R)\, R_2$$

where Z is the impedance of transformer T_2, referred to its primary side, and r represents its voltage ratio. Since the circuit described here, $Z \gg R_2$, the above approximation is justified.

By solving for I_R and I_C from the first two equations and substituting in the third,

$$r(\alpha + j\beta) = \frac{V_C R_1^2 + V_R \left(\frac{1}{\omega C}\right)^2 \left(1 + \frac{R_1}{R_2}\right) + jR_1 \left(\frac{1}{\omega C}\right)\left[V_C \left(1 + \frac{R_1}{R_2}\right) - V_R\right]}{R_1^2 + \left(\frac{1}{\omega C}\right)^2 \left(1 + \frac{R_1}{R_2}\right)^2}.$$

It is convenient to express V_C, V_R, and $\alpha+j\beta$ on a per-unit-input basis. V_C/V_{in} and V_R/V_{in} may be expressed as $\frac{1}{s}(d_C-0.5)$ and $\frac{1}{s}(d_R-0.5)$, respectively, where d_C and d_R are dial settings of divider D_3 and s represents the voltage ratio of T_4. (The necessity for subtracting 0.5 from the dial readings of D_3 arises from the fact that the center tap of the secondary winding of T_4 is grounded.) Then by multiplying the above equation by p and separating real and imaginary terms,

$$p\alpha=\frac{1}{sr}\left[\frac{(d_C-0.5)\,R_1^2+(d_R-0.5)\left(\frac{1}{\omega C}\right)^2\left(1+\frac{R_1}{R_2}\right)}{R_1^2+\left(\frac{1}{\omega C}\right)^2\left(1+\frac{R_1}{R_2}\right)^2}\right]\approx(d_R-0.5)\left(\frac{R_2}{srR_1}\right)$$

and

$$p\beta=\frac{1}{sr}\left[\frac{\frac{R_1}{\omega C}\left[(d_C-0.5)\left(1+\frac{R_1}{R_2}\right)-(d_R-0.5)\right]}{R_1^2+\left(\frac{1}{\omega C}\right)^2\left(1+\frac{R_1}{R_2}\right)^2}\right]\approx(d_C-0.5)\left[\frac{R_2}{sr\left(\frac{1}{\omega C}\right)}\right]$$

where $p=1/V_{in}$.

The above approximations are justified[4] since $\frac{1}{\omega C}\approx R_1$ and $R_1\gg R_2$.

4.2. In-Phase and Quadrature Deviations, $a+jb$

In figure 3, V_{in} represents the input terminal voltage, v the step-injection voltage of transformer T_1; $\alpha'_n+j\beta'_n$ and $\alpha''_n+j\beta''_n$ the small balancing voltages from transformer T_2; $\alpha''_{l0}+j\beta''_{l0}$ the voltage drop between the "reference" terminal and the "tap" output terminal when the dial of the decade under test is set on 0; and $\alpha''_{lX}+j\beta''_{lX}$ the voltage drop between the "high" input terminal and the "tap" output terminal when the dial is set on X. The voltage drop, $\alpha''_{lCx}+j\beta''_{lCx}$, measured between the "common" terminals in general depends on the dial settings. The subscript x identifies the dial setting. Then from figure 3 (note assigned voltage polarities), the equation for a four-terminal voltage ratio is derived as follows:

$$V_{in}=\alpha''_{l0}+j\beta''_{l0}+10v+\sum_{n=1}^{10}\alpha'_n+\sum_{n=1}^{10}j\beta'_n+\sum_{n=0}^{9}\alpha''_n+\sum_{n=0}^{9}j\beta''_n+\alpha''_{lX}+j\beta''_{lX}$$

and the voltage ratio for any setting x on the top decade can be expressed as

$$\frac{V_{out}}{V_{in}}=\frac{\alpha''_{l0}+j\beta''_{l0}-\alpha''_{lCx}-j\beta''_{lCx}+xv+\sum_{n=1}^{x}\alpha'_n+\sum_{n=1}^{x}j\beta'_n+\sum_{n=0}^{x-1}\alpha''_n+\sum_{n=0}^{x-1}j\beta''_n}{V_{in}}$$

$$=\frac{\frac{x}{10}+\left(\alpha''_{l0}+j\beta''_{l0}-\alpha''_{lCx}-j\beta''_{lCx}+\sum_{n=1}^{x}\alpha'_n+\sum_{n=1}^{x}j\beta'_n+\sum_{n=0}^{x-1}\alpha''_n+\sum_{n=0}^{x-1}j\beta''_n\right)\frac{1}{10v}}{1+\left(\alpha''_{l0}+j\beta''_{l0}+\sum_{n=1}^{10}\alpha'_n+\sum_{n=1}^{10}j\beta'_n+\sum_{n=0}^{9}\alpha''_n+\sum_{n=0}^{9}j\beta''_n+\alpha''_{lX}+j\beta''_{lX}\right)\frac{1}{10v}}.$$

[4] Except for some change in notation, the above analysis has been presented elsewhere [5].

Since $10v \approx V_{in}$ for the top decade, and with $\frac{1}{V_{in}} = p$ as previously defined, a rearrangement of terms leads to $\frac{V_{out}}{V_{in}} = d + a + jb$

$$\approx \frac{x}{10} + \left[p\alpha''_{l0} - p\alpha''_{lCx} + \sum_{n=1}^{x} p\alpha'_n + \sum_{n=0}^{x-1} p\alpha''_n - \frac{x}{10}\left(p\alpha''_{l0} + \sum_{n=1}^{10} p\alpha'_n + \sum_{n=0}^{9} p\alpha''_n + p\alpha''_{lX} \right) \right]$$

$$+ j\left[p\beta''_{l0} - p\beta''_{lCx} + \sum_{n=1}^{x} p\beta'_n + \sum_{n=0}^{x-1} p\beta''_n - \frac{x}{10}\left(p\beta''_{l0} + \sum_{n=1}^{10} p\beta'_n + \sum_{n=0}^{9} p\beta''_n + p\beta''_{lX} \right) \right]$$

If three-terminal voltage ratios are desired, the term $\alpha''_{lCx} + j\beta''_{lCx}$ is omitted from the above equations, and the "common" output terminal is ignored.[5]

The foregoing derivation is for determining the voltage ratios of the top decade of divider D_1. By addition of a series of measurements of the internal voltage drops of divider D_2, a similar expression can be derived for determining the voltage ratios of D_2.

For calibration of lower decades, using step-voltage injection transformers of appropriate ratios, similar equations can be derived.

5. Description of Components

T_1, T_2, T_3, and T_4 are specially constructed shielded transformers using high magnetic permeability strip wound toroidal cores to insure close magnetic coupling and to conserve space in the circuit. The shields minimize the susceptibility to magnetic pickup from stray fields in the laboratory.

The two-stage step-injection voltage transformer T_1 is shown in detail in figure 5. This transformer injects a voltage v which is closely equal to that of one step of the test decade. The principle involves a double circuit: one to provide a rough voltage and the other to correct it. The theory of operation is discussed by Cutkosky [6]. In figure 5, the voltage applied to winding 1 can be thought of as a rough generator which supplies excitation current to the transformer to obtain an approximation of the desired voltage ratio. The voltage applied to winding 2 then corrects this approximate voltage ratio. The number of turns for windings 1 and 2 is governed by the decade of the divider to be calibrated (i.e., 10 turns for the top or 10^{-1} decade; 100 turns for the 10^{-2} decade, etc.). Each winding is wound in a single, equally distributed layer from 0° to 360°, and the wire is brought along the core from 360° back to the point of origin. Thus no loop is formed, and

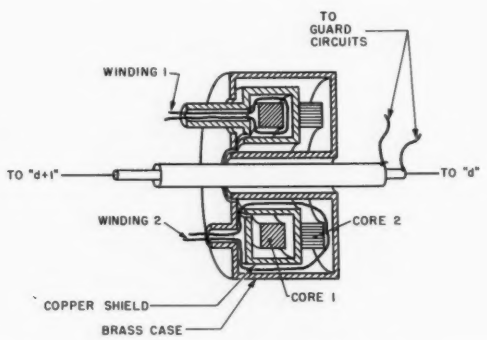

FIGURE 5. *Two-stage step-injection voltage transformer "T_1".*

[5] $\alpha''_{n'x} + j\beta''_{n'x}$ is measured with transformers, T_2 and T_3, connected between the "common" terminals in figure 1.

susceptibility to stray magnetic pickup is greatly reduced. (This same technique is applied in winding all other transformers.) One-mil (0.025 mm) thick supermalloy-type strip toroidal cores of 38.1 mm ID, 63.5 mm OD, and 12.7 mm H are used. A copper eddy current shield 20-mil (0.51 mm) thick between windings 1 and 2 reduces the stray magnetic fields in the region of winding 2 caused by excitation current in winding 1, and hence improves the accuracy of the voltage ratio. The brass case is for electrostatic shielding.

Figure 6 shows the details of construction of transformers T_2 and T_3 as a single unit. They are identical and interchangeable. Each consists of a 100-turn primary winding on a 1-mil (0.025 mm) thick supermalloy-type strip toroidal core of 38.1 mm OD, 25.4 mm ID, and 6.4 mm H. The shielding arrangements are such that the cross capacitances at the gaps are reduced to a minimum [7]. However, if the technique were to be used for calibration of dividers with large in-phase and quadrature voltage deviations which would require a significantly higher value for R_2, the cross-sectional area of the core of the transformer designated as T_2 (differential voltage injection) would have to be increased, so that the current through the primary of T_2 would remain insignificant in comparison with that through R_2 (i.e., $Z \gg R_2$).

Figure 7 shows the construction of transformer T_4. It consists of a toroidal core of the same dimensions as that used for T_1, a secondary winding which is sandwiched between two copper eddy-current shields, two parallel sections (100-turns each) of primary winding, and an overall Mu-metal case. The sandwich design improves the accuracy of the voltage ratio. The midpoint of the secondary winding is grounded. Two versions of T_4 have been made, one with a 100-turn secondary and the other with a 200-turn secondary, in order that voltage ratios, s, of 1:1 and 1:2 can be selected.

The inductive voltage divider, shown as D_3 in figure 2, actually consists of two commercial type units in parallel, one for in-phase voltage injection and the other for quadrature voltage injection. Each consists of three inductive decades and a continuously adjustable resistive divider.

C is a three-terminal capacitor having a very small dissipation factor. R_1 and R_2 are three-terminal, low-reactance decade resistors of 10×1 kΩ and 10×10 Ω, respectively. For 10 kHz calibrations, if an air capacitor of 1592 pF is used for C, $s = 1{:}1$, $R_1 = 10$ kΩ, and $R_2 = 10$ Ω, one step on the top decades of D_3 represents a difference of 1 ppm-in in in-phase or quadrature deviation.[6]

The detector circuit consists of a preamplifier and a cathode-ray oscillograph. A narrow band-pass filter is used to discriminate against noise before the first stage of amplification. A double elliptical pattern, suggested by Clothier, is shown on the oscillograph to indicate balance condition [8]. The unbalance voltage from the calibration circuit is impressed on the vertical plates. On the horizontal plates is placed a signal of the same frequency, whose phase can be adjusted so that the angular departure of the major axis of the elliptical pattern represents in-phase

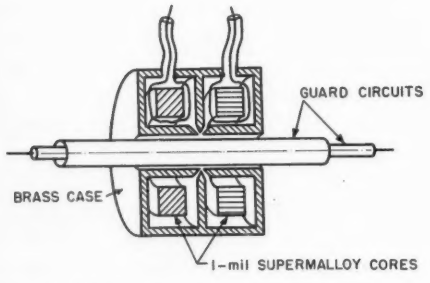

FIGURE 6. *Injection-detection transformers "T_2" and "T_3".*

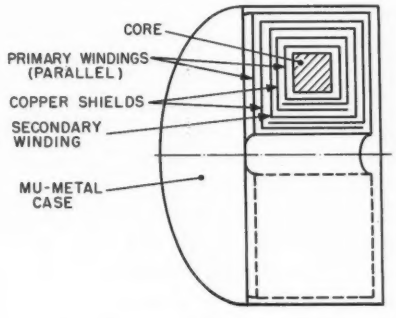

FIGURE 7. *Shielded transformer "T_4".*

[6] ppm-in (parts-per-million of input or unity).

unbalance and opening along the minor axis quadrature unbalance. At balance, the figure appears to be a single line. An unbalance voltage of 100 pV is easily observed.

6. Ratios Involving a Combination of Several Decades

For simplicity of presentation, sections 3 to 5 are written for the calibration of an individual decade. However, one may readily apply the same technique to calibration of voltage ratios involving a combination of dial settings on several decades of the test divider.

The turns ratio of the 2-stage step-injection voltage transformer, T_1, determines the voltage v (see figs. 2 and 5) which in turn governs the size of the step interval of the dial settings of the test dividers; i.e., if windings 1 and 2 were to consist of 40 turns each, the turns ratio would be 40:1, and the interval of the dial setting, 0.025. Forty separate balances of $\alpha'_n + j\beta'_n$ and of $\alpha''_n + j\beta''_n$ would then provide a "boot-strapping" calibration at dial settings of 0.025, 0.05, 0.075, etc.

7. Two-Stage Multitap Single-Range Dividers

The claimed accuracy of results has been verified by construction of two-stage single-range dividers, whose taps are all brought out to external connectors. Their construction is similar to the voltage transformer shown in figure 5, but both guard circuits and the center conductor are omitted, and a Mu-metal shield substituted for the copper shield. Figure 8 shows the arrangement of external connectors on a 20-section and a 40-section divider.

For the 20-section divider, winding 1 (fig. 5) consists of 100 turns and winding 2 of 5 turns of a 20-wire cable. The wires in the cable are connected in series, and the junctions are made at the connectors on the cover. The 2-stage 40-section is similarly constructed.

Since a single divider can be self-calibrated providing all the taps are brought out externally, D_1 and D_2 of figure 2 can be thought of as a single divider. The in-phase and quadrature voltage deviations of these two special dividers were obtained with both 10:1 and 20:1 voltage ratio step-injection transformers, T_1, and the 40-section divider was also calibrated with a 40:1 voltage ratio T_1.

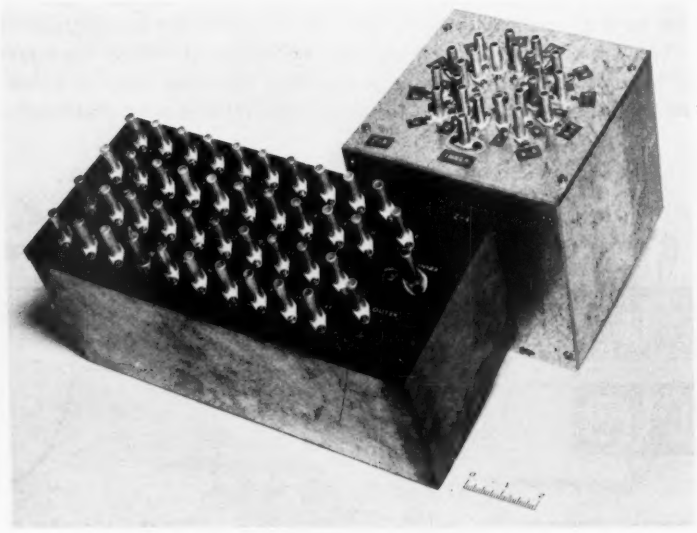

FIGURE 8. *Two-stage single-range dividers.*

Since the high input terminal and the highest output terminal are located immediately adjacent to one another and are connected together with a very short copper bus, and the same is true for the low input and "0" output terminals, the voltage differences, $\alpha''_{l0}+j\beta''_{l0}$ and $\alpha''_{lX}+j\beta''_{lX}$ are thus reduced to zero. Therefore, the calibration procedure required obtaining $\alpha'_n+j\beta'_n$ balances only.

These single range dividers were: (1) further calibrated in combination with commerical type dividers in the self-calibration circuitry and (2) used for comparison calibration in the comparator circuitry [5] to verify that the accuracy of measurements obtainable by the self-calibration or "boot-straping" technique.

The results obtained on approximately 1300 separate measurements are too voluminous to show here. In general, about 80 percent of the measurements agreed to within 1×10^{-7} ppm-in, while the lack of agreement exceeded 2×10^{-7} ppm-in in only about 2 percent of the approximately 1300 separate measurements. These close agreements also indicated that the method of measuring $\alpha''_{l0}+j\beta''_{l0}$, $\alpha''_{lX}+j\beta''_{lX}$, and $\alpha''_{lCx}+j\beta''_{lCx}$ as outlined previously is correct.

8. Consideration of Errors

An examination of uncertainties requires a systematic evaluation of all possible errors and a careful appraisal of all components of the measuring circuit as well as a justification of estimations, even though in this case one would expect most of the associated errors and uncertainties to be negligible.

The first source of errors to be considered is the differential voltage injection circuit. Approximations are made in developing the expressions for obtaining the in-phase and quadrature deviations, $\alpha+j\beta$, where the effects of the residual of the decade resistors and the dissipation factor of the capacitors are ignored. Approximate magnitudes of these errors have been obtained by adding the estimated equivalent residual reactance across R_1 and R_2 and estimated series resistance to C. These errors have been found to be negligible.

Another justifiable approximation is omitting the impedance, Z, of transformer T_2 from the expression for $\alpha+j\beta$. Since $Z\approx2.5\times10^4$ ohms and $R_2=10\ \Omega$, the current through Z is relatively insignificant. Calibration (with appropriate output loading) of the pair of inductive voltage dividers, D_3, introduces another source of uncertainty. However, experience indicated that errors in them should not exceed 0.5 ppm-in. Uncertainties in obtaining the voltage ratio correction due to excitation and variable load currents of the transformers T_2 and T_4 should not exceed 0.5 ppm of indicated ratio. However, since the injection voltage, $\alpha+j\beta$, rarely exceeds 0.002 percent of the input voltage, the overall uncertainty, including the errors caused by the associated leads, contacts, and imperfect shields, is estimated to be <0.05 ppm-in.

The second source to be considered is the step-voltage injection circuit. As indicated before, it is imperative that the injection voltage, v, of T_1 be constant throughout the "boot-strapping" calibration. This requires an extensive guard arrangement. Since both guard circuits and the lead connecting the "tap" output terminals constitute the secondary windings of T_1, any leakage current is a secondary load on T_1. The uncertainties from this source are determined as outlined in section 7 to be <0.06 ppm-in.

The third and largest source of uncertainty to be appraised is the guard arrangement. The primary function of the guard circuits is to intercept or eliminate any leakage currents, and their secondary function is to prevent electrostatic pickups. Because of the nature of the terminals used on the commercial test dividers, the shields at either end are not as complete as they could be; and because neither a detector nor a quadrature voltage is used to balance the voltage between guard circuit 1 and the center conductor, a small leakage current exists. These errors are estimated to be about 0.08 ppm-in for in-phase and 0.10 ppm-in for quadrature deviations.

A significantly large error is inherent in obtaining the measurements $\alpha''_{lCx}+j\beta''_{lCx}$ if the internal lead connecting the "common" terminals is not shielded. Proper shielding as indicated in section 2 should reduce the uncertainty to <0.01 ppm-in.

The last to be considered are miscellaneous errors from all other sources not covered previously, such as pickup from stray fields in the laboratory, harmonics in power supply, loop currents in the circuits, lead resistance, contacts, and imperfect shieldings. These uncertainties are estimated to be < 0.05 and < 0.07 ppm-in for in-phase and quadrature deviations, respectively.

Finally, an appropriate multiple of the standard deviation of the results obtained in repeated calibrations should be added to the combination of the systematic errors estimated above [9, 10].

Source of errors	Uncertainties to in-phase deviations "a"		Uncertainties to quadrature deviations "b"	
	m	m^2	m	m^2
	ppm-in		*ppm-in*	
From $\alpha+j\beta$ injection circuit	0.05	0.0025	0.05	0.0025
From v injection circuit	.06	.0036	.06	.0036
From guard arrangement	.08	.0064	.10	.0100
Miscellaneous	.05	.0025	.07	.0049
From $\alpha''_{H:x}+j\beta''_{H:x}$ measurements	.01	.0001	.01	.0001
Σm^2		0.0151		0.0211
$[\Sigma m^2]^{1/2}$	.12		.15	
$3\times$ standard deviation	.06		.06	
Maximum error	0.18		0.21	

The maximum error values indicated in the table are for "a" and "b" deviations of < 10 ppm-in.

9. Conclusion

A high-accuracy self-calibration method has been developed for measuring the in-phase and quadrature voltage deviations of inductive voltage dividers at 10 kHz. An overall uncertainty within 2×10^{-7} parts of input is achieved for dividers with deviations of less than 1×10^{-5} parts of input, and 1×10^{-6} is attainable for deviations up to 1×10^{-4} parts of input.

This same calibration technique can readily be used to cover a frequency range from 1 to 20 kHz.

These high accuracy measurements are made without reference to any standards or fundamental electrical units.

Calibration of voltage ratios involving certain combinations of dial settings on several decades can be obtained as readily as on a single decade.

The author acknowledges the valuable help and suggestions received from Robert D. Cutkosky, Absolute Electrical Measurements Section, NBS. R. J. Berry contributed skillfully in constructing the components.

10. References

[1] The precision measurement of transformer ratios, R. D. Cutkosky and J. Q. Shields, IRE Trans. Instr. **I-9**, No. 2, 243–250 (Sept. 1960).

[2] The precise measurement of small capacitances, A. M. Thompson, IRE Trans. Instr. **I-7**, Nos. 3 and 4, 245–253 (Dec. 1958).

[3] A.C. bridge methods for the measurement of three-terminal admittances, A. M. Thompson, IEEE Trans. Instr. Measr. **IM-13**, No. 4, 189–197 (Dec. 1964).
[4] Applications of coaxial chokes to ac bridge circuits, D. N. Homan, in press.
[5] Comparator for calibration of inductive voltage dividers from 1 to 10 kHz, Wilbur C. Sze, ISA 1966 Conference, Paper No. 12.3–2–66, October 24–27, 1966, New York.
[6] Active and passive direct-reading ratio sets for the comparison of audio-frequency admittances, R. D. Cutkosky, J. Res. NBS **68C** (Engr. and Instr.) No. 4, 227–236 (Oct.–Dec. 1964).
[7] The NBS gas thermometer II. Measurements of capacitance to a grounded surface with a transformer ratio-arm bridge, L. A. Guildner and R. E. Edsinger, J. Res. NBS **69C** (Engr. and Instr.) No. 1, 13–18 (Jan.–Mar. 1965).
[8] A cathode-ray oscilloscope bridge balance display, W. K. Clothier, J. Sci. Instr. **43**, pp. 264–265 (April 1966).
[9] An analysis of errors in the calibration of electrical instruments, F. L. Hermach, AIEE Trans. Comm. and Elctn., Paper 61–63, May 1961.
[10] Experimental statistics, M. G. Natrella, NBS Handbook 91, Chap. 23, Aug. 1, 1963.

(Paper 72C1–268)

JOURNAL OF RESEARCH of the National Bureau of Standards—C. Engineering and Instrumentation
Vol. 72C, No. 1, January–March 1968

Bolometric Voltage and Current (Bolovac) Standard for High and Microwave Frequencies

M. C. Selby*

Institute for Basic Standards, National Bureau of Standards, Boulder, Colo. 80302

(October 31, 1967)

A standard of voltages and currents for lumped-constant, coaxial, and other circuits operating in the TEM mode has been developed. Its approximate potential ranges are 1 MHz to 20 GHz in frequency, 0.05 to 10 volts, and 5 microamperes to 10 amperes. The principle may be used with bolometric, thermoelectric, photoelectric or other sensing elements consisting of thin film conducting or semiconducting disks located in the transverse plane of the TEM mode. Application and advantages are described and a comprehensive error analysis is presented. Figures illustrating construction details of one of the models of the Bolovac are included.

Key Words: Current measurement, measurement voltages, microwave current, microwave voltages, transmission-line voltages, voltage measurements.

1. Introduction

The first National Bureau of Standards (NBS) equipment to standardize sinusoidal voltages at frequencies up to 1 GHz employed a two-thermistor-bead bolometer head of special design. It was developed at the NBS [1] [1] in the middle forties and was reproduced in other laboratories in the USA and abroad. A dynamometer type standard for rf current was also developed at the NBS; its principle and theory was analyzed [2] and an experimental model was built years ago. The construction of an improved instrument was recently completed [3]; a similar instrument, based on the same principles, was also built and put into operation in Japan.

The original NBS voltage standard has a frequency range of about 1 to 1000 MHz, a voltage range of about 20 mV to 1.5 V, and an approximate range of uncertainties of 0.3 to 2 percent. The rf current standard has a frequency range of about 1 to 1000 MHz, a current range of about 0.5 to 100 A, and a range of uncertainties of 0.3 to 1 percent.

A new type bolometer head was developed at the NBS within the last several years for both voltage and current standardization having a considerably higher upper frequency and wider dynamic ranges at accuracies equal and potentially exceeding those above. This head will be described here and will be referred to as the "Bolometric Voltage and Current Standardization Head" or "Bolovac" for brevity. The basic principle and potential capabilities of the Bolovac will be discussed here in the front sections. The following sections will indicate the critical elements of the device and the results obtained with the first models. The error analyses in this paper are generally limited to first order errors and uncertainties; higher order uncertainties are reserved for future analytical study and experimental verifications employing improved structural features of the Bolovac. Sources of overlooked uncertainties and possible means of their determination or elimination will be briefly discussed in the appropriate sections.

The Bolovac may be described as a source of known voltage and a sink of a known amount of current. It employs a disk-type bolometer split along one of its diameters and placed in a cylindrical coaxial line. It presently has a frequency range up to 10 GHz, a voltage range of about 0.1 to 5 V and a current range of about 5 to 200 mA. Its potential frequency and dynamic ranges are much wider; e.g., it can be used to 20 GHz and higher, to 10 V and to 10 A or higher depending partly on frequency. The principal advantages of the Bolovac are listed below and its limitations are discussed and analyzed later in the text.

The principal advantages of the Bolovac are as follows:

It serves as a standard of both voltage and current.

It has the widest frequency range of any standard of its kind known to date.

It employs a new type bolometer, namely, a split disk or disk sectors; other types, e.g., solid disks, barretters and semiconductors may also be employed for certain frequency and dynamic ranges. The disk may be made of metal, metal oxide, or carbon, depend-

*Radio Standards Engineering Division, Boulder, Colo. 80302.

[1] Figures in brackets indicate the literature references at the end of this paper.

ing upon the frequency range and accuracy desired. It may be a thin film deposited on a substrate or a relatively thick conducting disk supported by a substrate. These disks have a wider range of resistance (fractions of an ohm to 1,000 Ω or higher) than the present day high-frequency thermistors (having an approximate range of 5 to 100 Ω). The disks generally have positive temperature coefficients of resistivity as against generally negative ones for thermistors; this reduces the danger of overloading the bolometers in the absence of current-limiting impedances in the biasing and rf sources. Because the rf impedance of these disks is essentially equal to their d-c resistance over a wide frequency range, the Bolovac assembly may be used for some pulsed voltage and current measurements, e.g., as bolometric detectors.

It has potentially wider voltage and current ranges than the previous standards; its ability to measure currents down to 5 mA or lower with the accuracies indicated is of particular importance in view of present needs.

It provides a tool to measure microwave power transmitted down a uniform line with a potential accuracy comparable to the best present calorimetric techniques.

It eliminates the tedious and expensive thermistor matching problem required with the previous standard head. Thermistors must be matched with rf applied; the Bolovac disk sections are matched only at d-c.

It is relatively simple in construction, much more rugged, and more reliable than thermistors. It may be used with a number of types of available bolometer bridges and d-c or low frequency measuring instrumentation depending upon the desired accuracies.

The principle and construction can be used directly in ammeters, e.g., for measuring base currents in vertical antennas, etc. The split disk type Bolovac retains the advantage of the two-thermistor mount in that it eliminates measurement errors associated with single thermistor mounts; the latter require stubs or other equivalent isolation components in the d-c or audio biasing circuitry.

It is relatively simple to operate and maintain (by comparison, for example, with a dynamometer type instrument requiring nonvibrating supports and fine suspensions, or with mounts employing fragile thermistor beads with their 1-mil diam leads).

2. Principle and Analysis

Consider a conductive-film disk placed in a plane perpendicular to the axis of a uniform cylindrical coaxial lossless line energized by a source as illustrated in figure 1a. It will be shown below that, when the film thickness is smaller than one-fifteenth of the depth of the current penetration for the material, the equivalent circuit of the disk and the line for all practical purposes is that shown in figure 1b. In 1b V_m is the rf voltage across the disk and is equal to the product of the d-c resistance of the disk and the rf current through it. The disk impedance may be made essentially equal to its d-c resistance for frequencies to 20 GHz and higher. Here V_m is detected and measured employing the well-known bolometric technique; other techniques, e.g., thermoelectric or photoelectric techniques may also be used for this purpose. If we employ the bolometric technique, we measure the rf power dissipated in the disk and we can compute the rf voltage across it at the frequencies in question and with accuracies approaching those of d-c measurements. For an assumed, unperturbed TEM field in the line at R_m, the measurement of V_m is not affected by any other combinations of network elements shunting R_m; one of these elements may be the imput impedance of a voltmeter under calibration. The rf current through the disk, I_m, is measured by making Z_r much higher than R_m, in which case the transmission line current, I_i, approaches the value of I_m as Z_r approaches infinity.

The disk may be considered a coaxial-line section of length d and characteristic impedance

$$Z_{0_m} = \eta_m \frac{1}{2\pi} \ln \frac{r_1}{r_2} \tag{1}$$

where η_m is the intrinsic impedance of the metallic or semiconducting medium having a permittivity ϵ_m, permeability μ_m, and conductivity σ_m; r_1 and r_2 are the respective large and small radii of the line conductors.

At all frequencies under consideration here for media such as copper, silver, nickel, tantalum, carbon, etc. [4, 5],

$$\eta_m = \left(\frac{j\omega\mu_m}{\sigma_m + j\omega\epsilon_m}\right)^{1/2} \cong (1+j)\left(\frac{\omega\mu_m}{2\sigma_m}\right)^{1/2} \tag{2}$$

and the propagation constant

$$\gamma_m = [j\omega\mu_m(\sigma_m + j\omega\epsilon_m)]^{1/2} \cong (1+j)\left(\frac{\omega\mu_m\sigma_m}{2}\right)^{1/2} \tag{3}$$

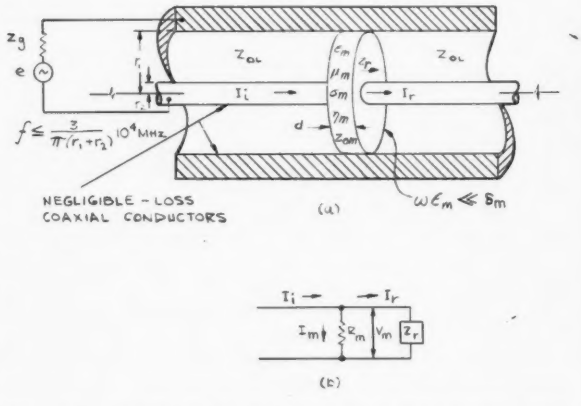

FIGURE 1. *(a) Conductive-film disk placed in plane perpendicular to air-dielectric cylindrical coaxial line;* $d \ll r_2$: $\omega\epsilon \ll \sigma_m$, *(b) equivalent circuit of 1a for skin depth* $\delta_m \geq 15d$.

because $\omega\epsilon_m$ (which has a value of 1.1 mhos per meter at 20 GHz for copper for example) is negligible compared with σ_m (5.8×10^7 mhos per meter).

Therefore

$$Z_{o_m} = (1+j)\left(\frac{\omega\mu_m}{2\sigma_m}\right)^{1/2} \frac{1}{2\pi} \ln \frac{r_1}{r_2}. \tag{4}$$

The d-c resistance of the disk is given by

$$R_m = \frac{1}{2\sigma_m \pi d} \ln \frac{r_1}{r_2} \tag{5}$$

and the depth of current penetration into the solid metal of the film at a frequency f, is

$$\delta_m = \left(\frac{1}{\sigma_m \pi f \mu_m}\right)^{1/2}. \tag{6}$$

Substituting (5) and (6) into (4),

$$Z_{0_m} = (1+j) R_m \frac{d}{\delta_m} \tag{7}$$

and

$$\gamma_m = (1+j)\frac{1}{\delta_m}. \tag{8}$$

From transmission line theory the output voltage, V_m, of the disk line section having a characteristic impedance of Z_{0_m} is the product of the transfer impedance Z_t and the input current I_i:

$$Z_t = \left(\frac{1}{Z_r}\cosh \gamma_m d + \frac{1}{Z_{o_m}} \sinh \gamma_m d\right)^{-1}$$

$$= \left\{\frac{1}{Z_r}\cosh\left[(1+j)\frac{d}{\delta_m}\right] + \frac{1}{R_m}\frac{\sinh\left[(1+j)\frac{d}{\delta_m}\right]}{(1+j)\frac{d}{\delta_m}}\right\}^{-1}. \tag{9}$$

Making use of available tables [6] one can show that for values of $\frac{d}{\delta_m} \leq 0.07$ we have in the worst case

$$(1+j)\frac{d}{\delta_m} = 0.1 \underline{/45°},$$

$$\frac{\sinh (0.1 \underline{/45°})}{0.1 \underline{/45°}} = 1.00000 \underline{/0.096°}.$$

$$\text{Cosh } (0.1 \underline{/45°}) = 1.00001 \underline{/0.287°}$$

Whence

$$Z_t = \left[\frac{1}{Z_r}(1.00001 \underline{/0.3°}) + \frac{1}{R_m}(1.00000 \underline{/0.1°})\right]^{-1}.$$

Thus we see that for a ratio of $\frac{d}{\delta_m} = 0.07$ one of the components of Z_t will change in magnitude in terms of $\frac{1}{Z_r}$ by about 0.001 percent and will be shifted by 0.3° in phase; the other component will remain essentially the same in magnitude and will be shifted in phase by 0.1°. These phase shifts are sufficiently small to be neglected; the magnitudes will be in error by less than 0.01 percent if we accept the value R_m to be as shown in figure 1b, i.e.,

$$Z_t = \left[\frac{1}{Z_r} + \frac{1}{R_m}\right]^{-1} = \frac{Z_r R_m}{Z_r + R_m}. \tag{10}$$

This indicates that the film need not be thinner than about one-fifteenth of the skin depth of the given metal at the maximum frequency of interest for a possible error of 0.01 percent from this cause. It will be shown below that in all practical cases this may be accomplished with a reasonable safety factor.

It also follows from (10) or from the equivalent circuit of figure 1b that

$$\text{for } Z_r \gg R_m, \qquad I_i \cong \frac{V_m}{R_m}. \tag{11}$$

A high Z_r may be obtained by effectively terminating the line in a quarter wave section or in a parallel resonant LC circuit properly placed in the circuit.

One could arrive at eq (10) by simply showing that the disk impedance is resistive for $d \leq 0.07\delta_m$; however, the more rigorous approach eliminates the question of the possible effect of the metal disk upon the TEM field distribution at the boundary planes of the air and metallic disk. It is not immediately apparent that the presence of the metallic disk will not perturb the radial electric field lines; one might be concerned with the capacity effect between the individual elements of the resistive disk and between each element of the disk and the transmission line conductors. One might also question the perturbation effect of the disk upon the concentric magnetic field lines because each element of the disk has its own external inductance.

The configuration of figure 1a can be treated as a composite of three cascaded transmission line sections of uniform diameters and infinite-conductivity conductors. This case has been analyzed in textbooks [7]. Results show that for coaxial-line inner and outer radii, a and b, essentially no energy will be propagated along the line at modes other than the TEM at wavelength smaller than

$$\lambda = \pi(b+a).$$

This approximate formula gives the critical frequency to within 8 percent. Furthermore, no higher modes can be produced by the presence of the film and substrate of the disk from the present TEM field; there are no longitudinal components of the electric and magnetic fields and the presence of the disk (the

Z_{0_m} section) does not introduce capacitive or inductive components into the system (except of those of its intrinsic characteristic impedance). This may not be the case when there are step discontinuities at the interfaces because of line diameter changes; the effect in this latter case will be discussed further on.

One may also heuristically show that the presence of the disk will not distort the field. This effect is negligible because of the circular and axial symmetry of the structure. For each electric and magnetic field line contributed by a given element of the disk, there is an equal and opposite field line contributed by another element located diametrically opposite the first, and the two cancel each other [8]. The effect of the substrate (insulator) upon which the metal film is deposited will also be discussed later on.

3. Description of the Bolovac

The heart of the Bolovac is a conductive bolometric film deposited on one face of an insulating disk (substrate). The film is split along one of the disk diameters, thus forming two bolometer elements of approximately semicircular or disk sector shapes. This disk is mounted in a specially constructed assembly permitting the following electrical connections: (1) the two bolometers are connected in series for the biasing energy and in parallel for the rf energy; (2) the plane where the standardizing rf voltage appears is located essentially at the input plane of the rf voltage indicating device being calibrated; (3) the plane through which the rf standardizing current is flowing is located essentially at the output plane of the current indicating device being calibrated. The distances from the rf-voltage or rf-current reference planes to the reference planes of the devices being calibrated is of the order of 1 to 2 mils. This distance is the thickness of the dielectric required to form a capacitance to isolate the biasing from the rf powers entering the Bolovac. Details of the disk and Bolovac assembly are shown in the figures below. The term "disk" below applies to the finished unit.

In principle the disk need not be split and the Bolovac may indeed be constructed with nonsplit disks. The relative advantages of splitting the disk are as follows. When bolometry is used, one generally needs to supply biasing power to the bolometer. Splitting the disk (dual element) eliminates the need of rf chokes or coaxial stubs required for a d-c return path. The d-c resistance of the chokes interferes with the precision and convenience of bridge operations. Stubs have to be tuned and require capacitors at the "shorted" end. Biasing currents should generally not be allowed in the rf current meters under calibration. Splitting the disk makes this possible. In case of the Bolovac, splitting the disk improves the bridge sensitivity generally by a factor of four. When the thermoelectric or photoelectric principle is used, generally no biasing power is needed, and solid disks may be preferable; however, the applications of these principles may introduce other difficulties particularly in the choice of materials and fabrication of the disks.

Figure 2a shows the basic circuit of the Bolovac applied for rf voltage standardization, one of the possible biasing arrangements (in this case a d-c source) and a symmetrical measuring bridge. The analysis and computation are identical to those presented for the voltage standardization bridge employing thermistors [1].

The voltage, V_{rf}, applied to the unknown being calibrated is given for the symmetrical bridge by

$$V_{rf}=\frac{R_T}{2(R_T+R_b)}\left[(V_{R2}-V_{R1})(2V_0-V_{R2}-V_{R1})\right]^{1/2}. \tag{12}$$

Here V_{R1} and V_{R2} are the respective voltage drops across the adjustable resistance in series with the d-c source before and after rf power is applied to the Bolovac with the bridge balanced in both cases. R_T and R_b are the respective Bolovac and bridge arm resistances as shown in figure 2a.

Figure 2b shows a schematic of the circuit arrangement with the Bolovac used for current standardization. The basic difference between figures 2a and 2b is that in 2a the standard V_{rf} is obtained at the output terminals of the Bolovac, whereas in 2b the standard current, I_{rf}, is obtained at the input terminals to the Bolovac. The schematic shows a thermoelement being calibrated in terms of the rf current entering the Bolovac. A constant-current d-c biasing source is shown in this case [9] and I_{rf} is given for a symmetrical bridge by

$$I_{rf}=[2I_s\, I_{dco}-I_s^2]^{1/2}. \tag{13}$$

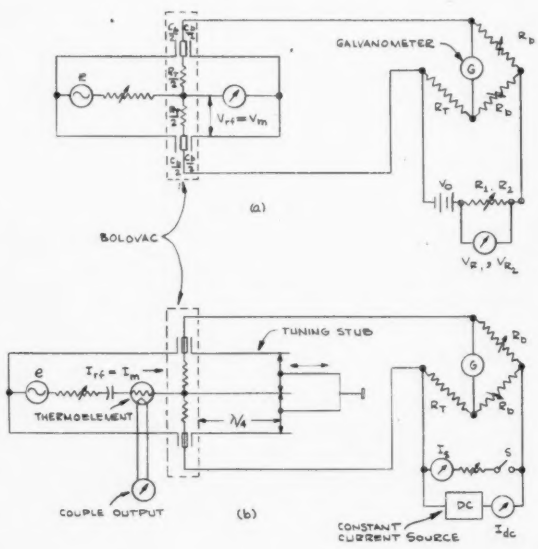

FIGURE 2. *Schematic diagram showing the applications of the Bolovac for (a) voltage standardization, and (b) current standardization.*

Here I_{dco} is the d-c biasing current in the bridge at initial balance (without rf) for I_s = zero, and I_s is the amount by which the I_{dco} was reduced for final balance (with rf) with switch S closed.

In both voltage and current cases it is assumed that the two sections of the Bolovac disk have been adjusted for equal resistance. Correction factors may be used if these resistances are not exactly alike; it will be shown later that this requirement is not critical. It is, of course, apparent that either of the two shown and other biasing arrangements may be used for both rf voltage and current standardization.

Figure 3 shows the top view and cross section of a Bolovac disk. The substrate of the disk may be made of any suitable insulating material such as quartz, Pyrex, or high thermal-conductivity ceramic (to allow higher current carrying capacity for the conducting film). Electrodes may be fired or evaporated on the cylindrical surfaces and, if necessary, at their rims to make sure of good contact with the conductors of the coaxial line system. A thin conducting film is then deposited on one of the flat surfaces. The radial gaps between the two halves of the circular film may be produced by a mask during evaporation or by removing parts of the film after evaporation. The gaps extend to the center electrode ring interconnecting these halves of the film in series for the biasing current and in parallel for the rf current as was pointed out above. As stated before, the film may

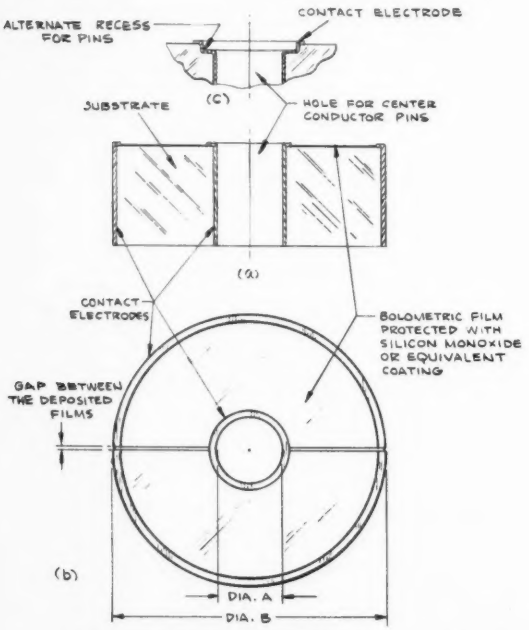
ALTERNATE RECESS FOR PINS
CONTACT ELECTRODE
(c)
SUBSTRATE
HOLE FOR CENTER CONDUCTOR PINS
(a)
CONTACT ELECTRODES
BOLOMETRIC FILM PROTECTED WITH SILICON MONOXIDE OR EQUIVALENT COATING
GAP BETWEEN THE DEPOSITED FILMS
(b)
DIA. A
DIA. B
NOTE: FOR BEST RESULTS DIAMETERS A & B SHOULD BE THE SAME AS THE CORRESPONDING DIAMETERS OF THE COAXIAL LINE SYSTEM WITH THE RESISTIVE FILM COVERING UNIFORMLY THE ENTIRE SPACE BETWEEN THE CYLINDRICAL CONDUCTORS.

FIGURE 3. *Bolovac bolometric disk (a) cross-section, (b) top view, (c) alternate recess for pin to avoid a discontinuity.*

be made of noble metals, chromium, nickel, tantalum, metal oxides, or carbon, etc. The width of the annulus of the film should, as closely as possible, be equal to the spacing between the coaxial conductors to reduce step discontinuities to a minimum. One must be cautious with some materials for the films to make certain the capacities between the particles (sometimes referred to as the "Boella" effect) will not introduce a reactive component even with sufficiently thin films. It may, however, be possible to determine by measurement the departure of the value of rf resistance of the bolometer elements from their d-c values and introduce an appropriate correction in the computed values of the voltages or currents. The art of film and electrode deposition and of disk substrate fabrication has recently attained a degree of perfection sufficient for the objectives in question here. A brief appraisal of the limitations and likely errors from disk fabrication imperfections is given in the appendix. The first disks for the Bolovac were made at the NBS. The substrates were cut in the instrument shops and the electrodes and films were deposited employing sputtering or evaporation and firing. The most stable NBS disks to date had platinum films with power resistivity constants of the order of two ohms per watt. Parameters of the disk and their correlation to the performance results will be discussed in the section on error analysis.

The Bolovac consists of a core and an auxiliary rf bypassing capacitor when needed. The core has two disk-supporting semicircular or rectangular metal plates sandwiched between two other "ground" metal plates. Figures 4, 5, and 6 show the details of the core and capacitor ring assembly and are self-explanatory. The bolometer disk is clamped, soldered, or cemented between two half disks forming an extension of the biasing electrodes; the clamping may be accomplished by means of plastic or insulated steel bolts. The insulation between the outside "ground" plates and the inside composite plate is the dielectric of the rf bypassing capacitors C_b shown in figure 2; the outer plates are thus the common ground of the system for the rf power. Referring to figure 4a the rf power is fed into the bottom plate and the standardizing voltage appears in the plane A of the bolometric film. The input plane to the voltmeter under calibration is in plane A′ a specified distance of 1 to 2 mils away from A. It is, therefore, imperative to design the disk pin and plate receptacle dimensions to maintain this spacing between the two planes, particularly for frequencies of 1 GHz and higher. With the quality of rf connectors continuously improving, and especially with the new precision sexless connectors currently being standardized, this requirement should not present any serious problems.

Again, referring to figure 4a, for current standardization, the top plate of the core may be replaced by another plate incorporating the enclosure for the current-measuring device to be calibrated. Or an adapter may be built to enable the connection of such a housing without removing the entire top plate; an example

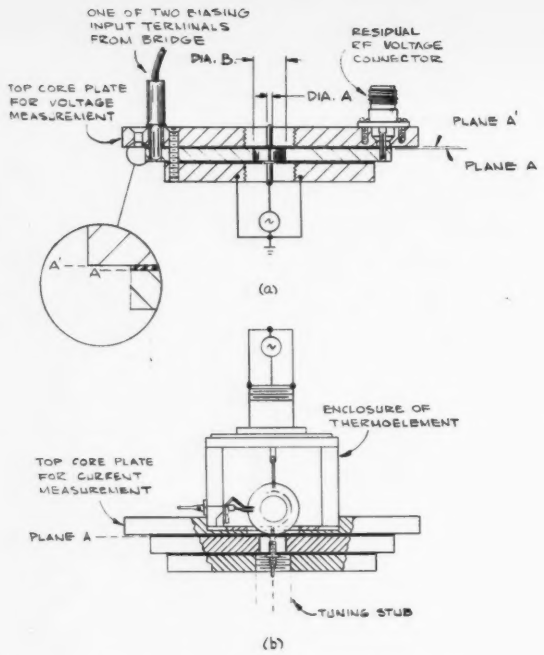

FIGURE 4. *Structural components of the Bolovac; (a) core cross section for voltage measurement, (b) core cross section for current measurement.*

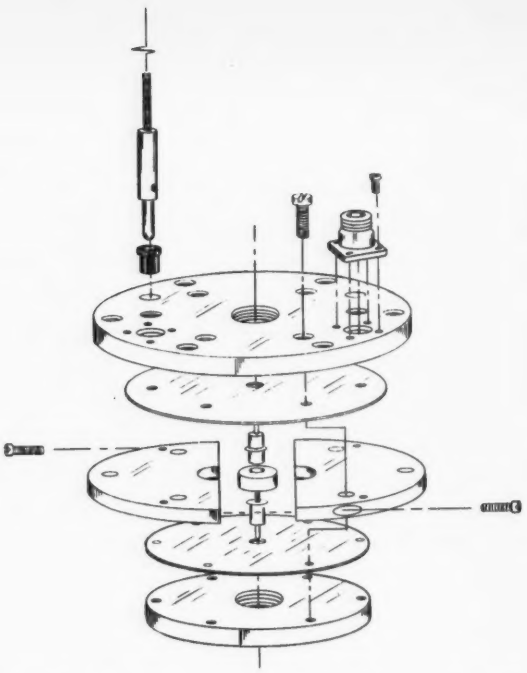

FIGURE 5a. *Exploded view of core for voltage standardization.*

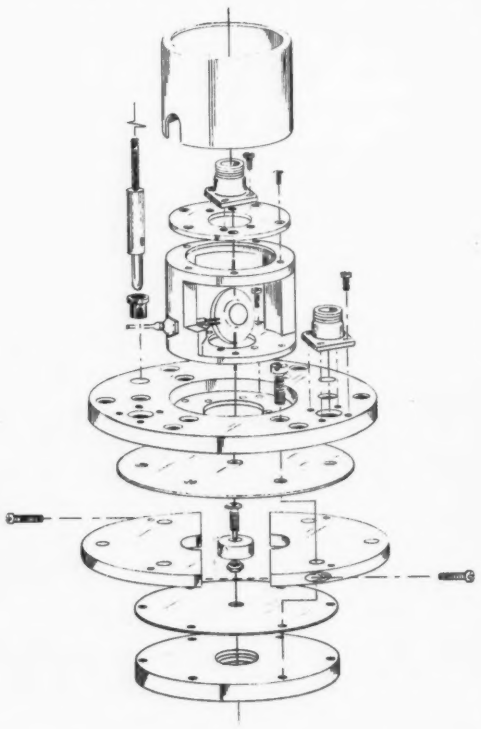

FIGURE 5b. *Exploded view of core for current standardization.*

of such an adapter is shown in figure 4b. The top plate with one kind of an enclosure for a certain type of thermoelement is shown in this figure. The rf current enters the core via the input into the housing and the standardizing current crosses reference plane A in which the film is located. The output reference plane of the current-sensor in its housing is thus essentially in plane A irrespective of how far the thermoelement is actually located from A. One must, however, reproduce this reference plane A when the enclosure of the "current meter" is removed from the Bolovac and put into use. The effect of the impedance in plane A as seen by the "current meter" and of the mechanical discontinuity upon the TEM mode are discussed under error analysis. For current standardization, the "output" port of the core is used for attaching an adjustable shorting line, a low-capacity shielding cap, or a tuned LC tank to terminate the system in a high impedance Z_r as discussed in the previous section. In some cases one may use a tube, equivalent to an outer conductor of the line, of sufficient length to prevent radiation from this end of the core. The latter may prove more economical than a shorting stub provided the value of the terminating impedance is high enough for the desired accuracy.

Figure 5 shows exploded views of the core assembly for voltage and current standardization.

The capacity C_b of the core itself (see fig. 2) is of the order of 2000 pF between each outer ground plate and the composite inner plate. In order to keep the effective impedance of C_b at a value sufficiently low

so that the rf voltage drop across it does not introduce serious errors, particularly at low frequencies (discussed under error analysis), the additional ring-shaped capacitor mentioned above was constructed; this ring is generally not needed for current measurements. It consists of additional ground and center plates with a large number of fixed capacitors imbedded into the center plates. Thus, the value of C_b is increased to about 60,000 pF. The construction details are shown in figure 6. One may use the core with or without the ring depending on the frequency. Other structures are, of course, possible in order to increase the value of C_b of the core and ring, and one may increase it further by adding fixed capacitors, for example, at the outside rim of the ring. The application of anodized aluminum plates or other similar techniques may be considered to obtain the largest value of C_b per unit volume and weight of the structure.

Type N rf connectors on the two sides of the core (fig. 4a) may be used for measuring the biasing potentials as well as for probing the rf voltage mentioned above across C_b when wanted.

Figure 6 shows an exploded assembly of C_b and figure 7 shows a perspective view of the assembled core with the voltage plate and the capacitor ring. Figure 8 shows the voltage and current center conductor pins used with the disk. Figures 9a, b, etc., show photographs of the components and assemblies described above. The auxiliary C_b assembly may, of course, have shapes other than the ring type used here.

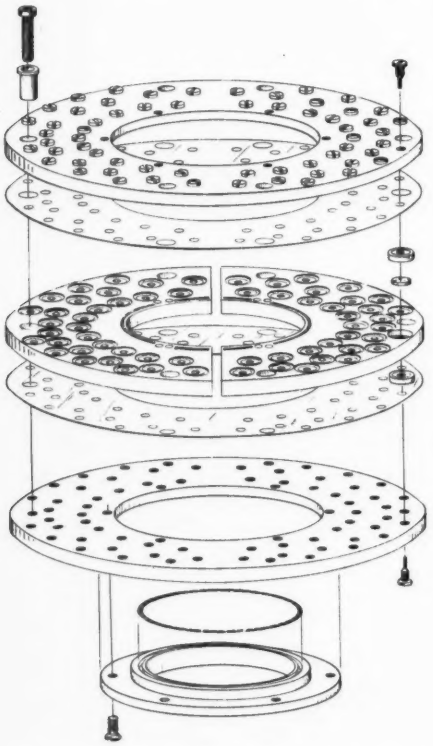

FIGURE 6. *Exploded view of ring-shaped auxiliary capacitor.*

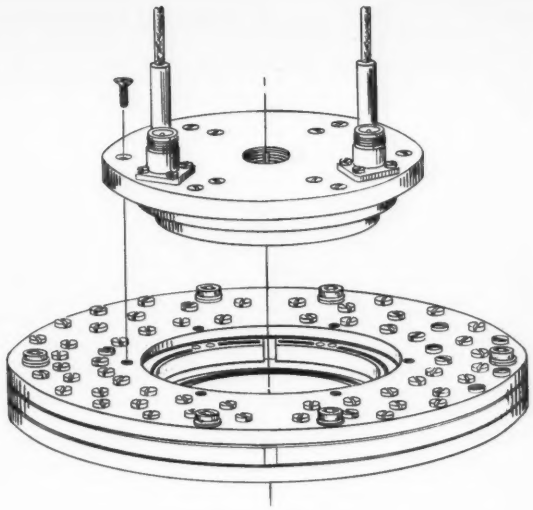

FIGURE 7. *Core (with voltage plate) and auxiliary capacitor of Bolovac.*

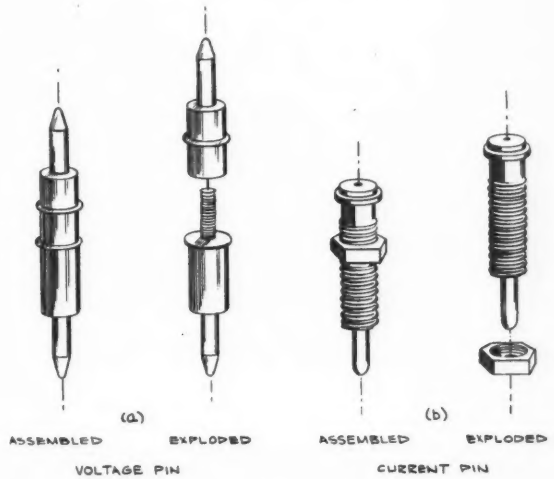

FIGURE 8. *Center conductor pins of Bolovac disk; (a) for voltage measurement, (b) for current measurement.*

4. Results and Error Analysis

4.1. Results

Most of the measurements were made at voltage and current levels at which intercomparisons with power standards in a 50-Ω system could be made directly (without auxiliary attenuation or amplification). Calorimetric power measurements served as

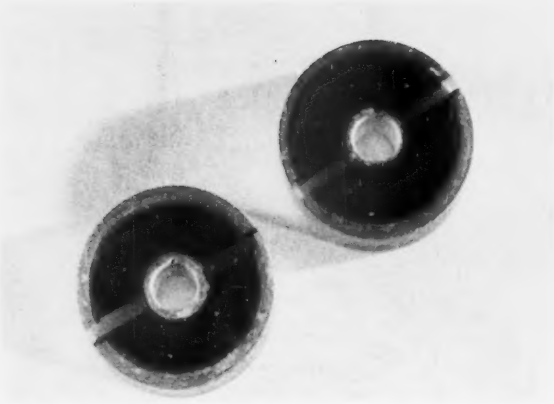

FIGURE 9a. *Bolovac split-film resistors and substrates (disks).*

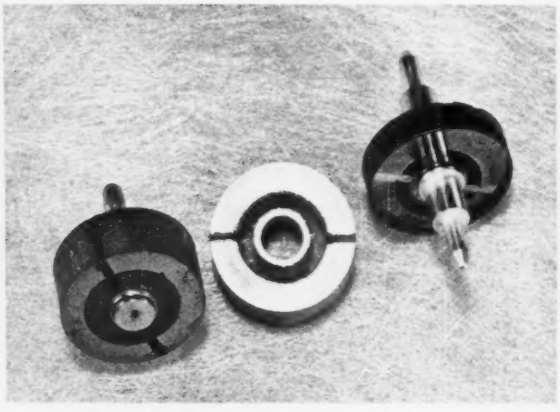

FIGURE 9b. *Disks without and with voltage and current coax-conductor pins.*

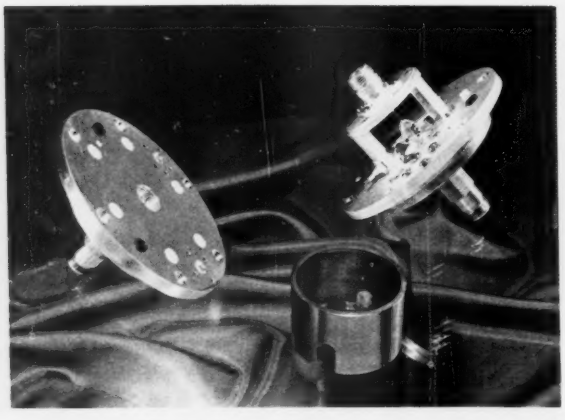

FIGURE 9c. *Voltage and current cores assembled.*

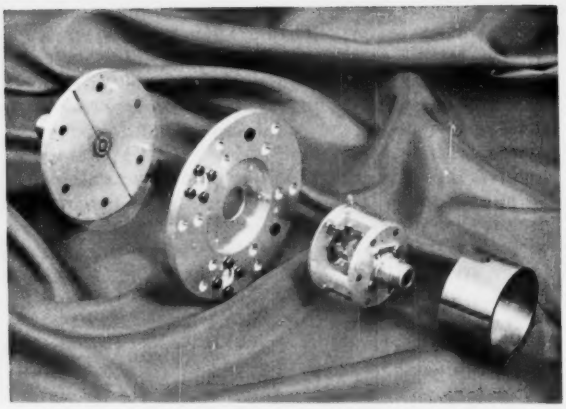

FIGURE 9d. *Current core exploded.*

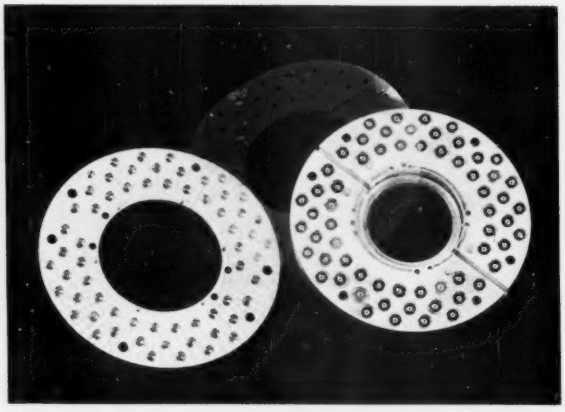

FIGURE 9e. *Auxiliary capacitor with top plate and insulator removed.*

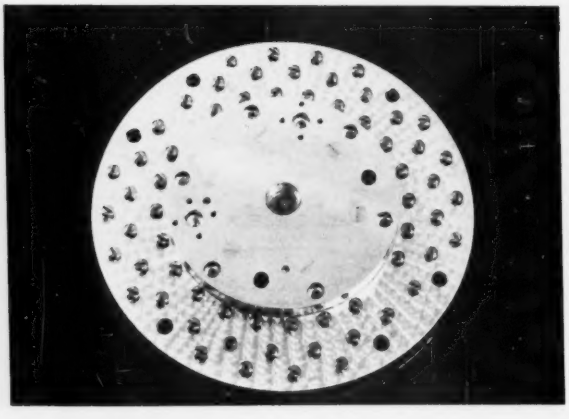

FIGURE 9f. *Voltage core and auxiliary capacitor.*

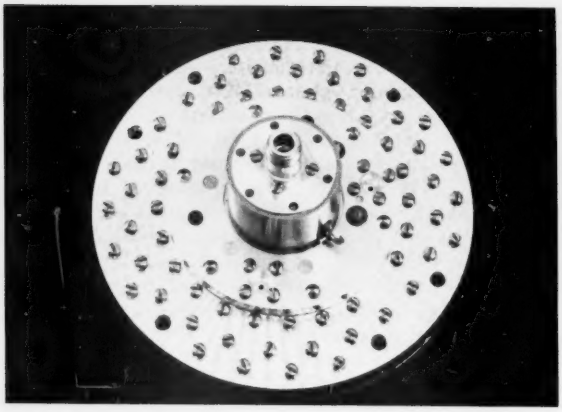

FIGURE 9g. *Current core and auxiliary capacitor.*

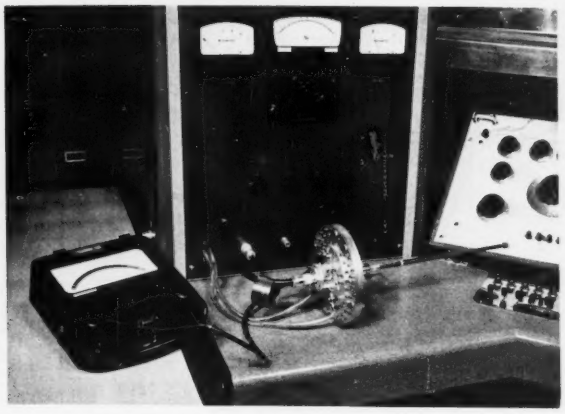

FIGURE 9j. *Bolovac set up to calibrate thermoelement.*

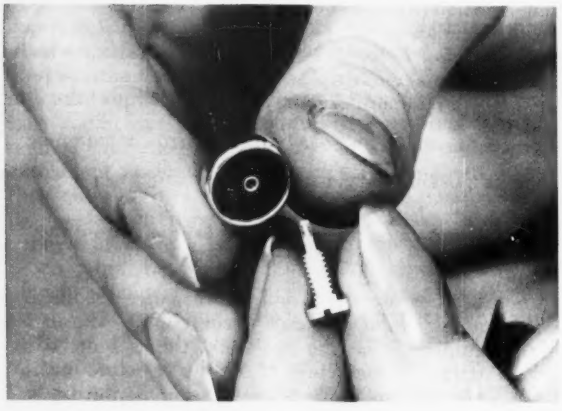

FIGURE 9h. *Capacitor disk and grounding-electrode bolt (beryllium-copper split contact pin).*

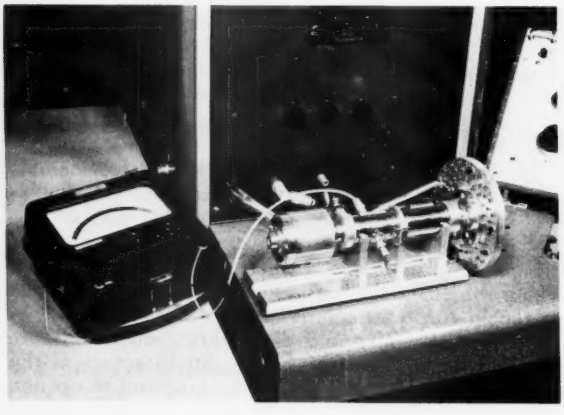

FIGURE 9i. *Bolovac set up to calibrate ATVM.*

independent direct or indirect comparisons for both voltage and current. Intercomparisons with thermistor mounts at frequencies to 1 GHz and between a number of Bolovac cores and disks above 1 GHz served as quasi-independent techniques; the latter furnished confidence in the quality of the disks and the assemblies of the system as a whole. In addition, intercomparisons were made employing two independent bridge consoles, one a constant dc-voltage biasing type, the other with constant dc-current biasing. The agreement at voltage levels of about 0.2 to 1.5 V was 1 percent or better to 2 GHz, 2 percent at 4 GHz and 4 percent at 8 GHz. The agreement in measuring currents of 5 to 75 mA (in 5 to 200 mA thermoelements) was 1 percent or better to 1 GHz. Reproducibility of current measurements was within 1 percent at 2, 3, and 4 GHz; comparison with power was not made at these frequencies because of resonances exhibited by the thermoelements, apparently as a result of residual inductances and shunt capacities of the heaters.

Figure 10 shows calibration curves of these thermoelements obtained, to our knowledge, for the first time over the frequency range and to the accuracies given above.

A conservative estimate of the uncertainties of the measured voltages and currents in terms of assumed true values is equal to the above figures on the agreements. It is felt that a several-fold improvement over the above results may be achieved because our efforts to date to perfect the Bolovac and the measuring system were at best only moderate.

To prevent misinterpretation of the following "error analysis" it is advisable to define terms as used here. An "error in mathematics" is defined as "the difference between the true value and the calculated or observed value" [10]. A "result" may be corrected for a given "error." Because the "true" value is never known, the absolute magnitude of the "error" can only be approximately determined. A result is known to an estimated plus or minus "uncertainty"; the result cannot be corrected for an "uncertainty." The "un-

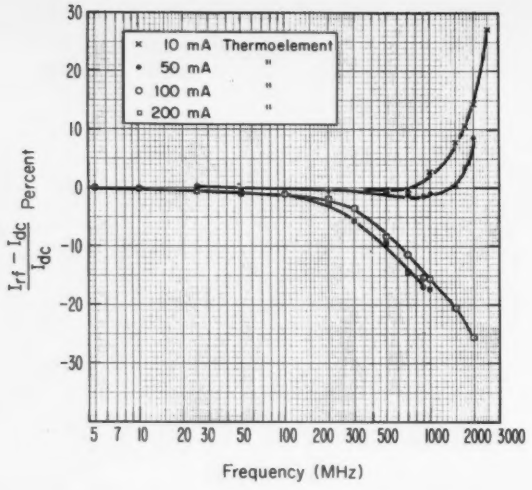

FIGURE 10. *Calibration of the UHF thermoelements with Bolovac.*

certainty" may consist of a number of uncertainties of parameter values entering an equation and includes the uncertainty in the "error." "Uncertainty" is often referred to as "limits of error."

The results of the technique described here are subject to the following sources of uncertainties:

Approximations in the analytical steps leading to eqs (10), (11), (12), and (13).

Uncertainty of values of bridge components, biasing source instability, limits of bridge sensitivity, balancing galvanometer noise, and rf source instability.

Quality of bolometric disk and its substrate.

Standing waves and discontinuities in the transmission line.

Input impedance of the resonant circuit or of quarter wave coaxial line section shunting R_m for current measurements.

Residual impedances in the ground system.

An assessment of the uncertainties contributed by these sources follows.

4.2. Effect of Approximations Leading to eqs (10) to (13)

It was shown earlier that the magnitude of the voltage or current may be in error by less than 0.01 percent if the disk-film thickness, d, is 7 percent of the skin depth, δ_m. In practice the ratio $\frac{d}{\delta_m}$ is always smaller than 0.07.

The resistance, and the depth of current penetration into the annular resistor is given by [4, 5, 11].

$$R_m = \frac{1.724 \times 10^{-8} \rho_m/\rho_c}{2\pi d} \ln \frac{r_1}{r_2} \text{ ohms} \qquad (14)$$

$$\delta_m = \frac{0.0661}{f^{1/2}} \left(\frac{1}{\mu_{mr}}\right)^{1/2} \left(\frac{\rho_m}{\rho_c}\right)^{1/2} \text{ meters} \qquad (15)$$

where d is in meters, f is in Hz, μ_{mr} is relative permeability of the conductor ($\mu_{mr} = 1$ for copper and other nonmagnetic materials); ρ_m/ρ_c = relative resistivity (in terms of copper at 20 °C, $\rho_c = 1.724 \times 10^{-8}$ Ωm).

For $\frac{r_1}{r_2} = 2.3$ ($Z_0 = 50$ ohms),

$$\frac{d}{\delta_m} = 3.46 \times 10^{-8} \frac{1}{R_m} \left(\frac{\rho_m}{\rho_c} \mu_{mr} f\right)^{1/2}. \qquad (16)$$

Assuming an extreme pessimistic case of $R_m = 0.1\ \Omega$ at 20 GHz for copper,

$$d \cong 0.05\delta_m.$$

It follows from eq (16) that higher values of R_m may be realized by using higher resistivity materials without changing the ratio of $\frac{d}{\delta_m}$. When materials of sufficient resistivity are not available, one may reduce the film thickness, d, in order to increase R_m. However, d cannot be reduced beyond the point at which the film stops behaving as a solid conductor. When this limit is reached, one may have to compromise for higher ratios of $\frac{d}{\delta_m}$, and consequent narrower frequency range or possibly larger penetration error.

4.3. Uncertainty Introduced by Bridge Assembly Components

Uncertainties were introduced into the results by the random drift of the d-c power supply, the error in the values of the d-c resistors, the random drift and temperature coefficient of the d-c resistors during the time it took to make a measurement, the uncertainty in measuring d-c voltages before and after rf was applied to the bridge, and the d-c imbalance of the two halves of the disk resistors [12]. An estimate of the limiting uncertainty from these sources is ±0.06 percent. Another source of uncertainty was the limited stability of the rf sources during a measurement, which is estimated as ±0.01 percent. The outside limits of the uncertainties introduced by these causes are thus ±0.07 percent.

4.4. Quality of Bolometric Disk and of Its Substrate

Two parameters of the film and substrate assembly will affect the uncertainty of the results. The first is the film sensitivity designated by γ_m (ohms/watt), the incremental resistance as a function of power dissipated in the disk. The second is the film stability which will affect the signal to noise ratio of the bridge galvanometer, particularly at low levels of V_m. As already stated, film and disk fabrication details are outside the scope of this paper. Such factors as the quality of the substrate surfaces, aging and protection of the films, migration of contact electrode metals into the film, uniformity of the film thickness, etc.,

have been apparently well under control and should contribute negligible uncertainty in the results. Some information on the state of the art of film deposition and of the uncertainties imposed by its limitations are discussed in the appendix. Thermal noise of the disks (of the order of 200 μV for a bandwidth of 10 GHz for a 200 Ω disk at room temperature) may also be neglected at the voltage and current levels here under consideration, particularly for "single" frequency or narrow band applications.

However, the uncertainty is affected considerably by γ_m because the bridge sensitivity (expressed as the galvanometer deflection for a given voltage or current increment in the disk) is directly proportional to γ_m [12]. The results shown above were obtained with platinum film disks; their γ_m values in the assembly were about 1 to 3 Ω/W. Some chromium, nickel, and gold disks were also fabricated at the NBS without great improvement of γ_m; in one case of a 50 Ω (200 Ω d-c) nickel unit, γ_m was 9 Ω/W. Measurements of carbon films indicated a γ_m of 2 to 7. There is evidence that values of 10 Ω/W and higher are obtainable in laboratories outside the NBS. Our platinum units were considerably more stable and had a much longer life than the chromium or nickel units. It seems rather difficult to predict the value of γ_m because the temperature coefficient of the conductivity of films is a pronounced function of their thickness. The temperature coefficient is negative for values below about 100 Å, then crosses the zero line and becomes positive as the thickness increases [13]. For two disks having the same temperature coefficients of resistivity it seems more promising to use higher resistivity metals or alloys because a thicker film will be realized for a given disk resistance. This may insure greater stability.

There will be an error in the measured voltage or current if the resistances or the values of γ_m of the two halves of the film-disks are not equal. This error has been discussed in the past [1, 12, 14, 15] and is approximately proportional to the product of (1) the fractional difference of the initial resistances, and (2) the fractional difference of the γ's. A practical case in our experience is a 25-Ω (100-Ω d-c, nominal) platinum disk, which has been in use for close to 2 years to date; fractional differences in the resistances stayed constant at 0.4 percent, and in the γ's at 4 percent, which yield a possible error of 0.008 percent in voltage or current. A pessimistic figure of 0.01 percent from this source is used in the summation of the errors. In case of large fractional differences this error may be reduced by applying corrections. Also, a large difference in γ's may be compensated by reducing the difference of the resistances, and vice versa. Another way of avoiding this source of error is to make one half of the film out of a material having a relatively low γ as compared with that of the other half [12].

4.5. Effect of Standing Waves on Voltage Measurement

Assuming uniform diameters of the coaxial system, the error introduced in the voltage, V_x, applied at the input plane of an unknown voltmeter is obviously a function of (1) the VSWR, S_x, looking into its input port, and of (2) the distance, x, between the Bolovac film, R_m, and the above plane. This distance is 1 or 2 mils. High input impedance voltage monitors may have S_x values of 200 at 1 GHz [16]. The voltage ratio distribution in a lossless transmission line is given by

$$\frac{V_x}{V_m}=\frac{1}{\cos \beta x+j\frac{Z_0}{Z_x}\sin \beta x}. \tag{17}$$

For infinite input impedance of a voltmeter, this results in a possible error of 0.01 percent at 10 GHz and of 0.02 percent at 20 GHz. It is therefore desirable to keep the distance between the two planes in question to a minimum.

4.6. Effect of Resonant Tank Impedance Shunting R_m on Current Measurements

The input impedance, Z_s, of quarter wave, air dielectric, shorted, coaxial tuning stubs may be computed from [17]:

$$Z_s=11.11(f)^{1/2}bF\frac{1}{n}, \tag{18}$$

where:

$f \equiv$ frequency in Hz,
$b \equiv$ inner radius of outer conductor in cm,
$F \equiv$ a constant found in figures 4 to 15 of the given reference,
$n \equiv$ odd number of quarter waves on the stub.

For $n=1$, at 1 GHz, and a 50-Ω stub, with $b=0.64$ cm, Z_s is approximately 100,000 Ω and the likely errors for R_m values at 25, 50, and 100 Ω are 0.025, 0.05, and 0.1 percent, respectively. One may use larger characteristic impedance stubs to reduce this error. For example, one may double the outer conductor radius and reduce the inner conductor radius to half of the 50-Ω stub, and thereby reduce the corresponding above errors to 0.005, 0.01 and 0.02 percent.

Stubs may be used down to 50 MHz. At lower frequencies, lumped constant tanks may be preferable; obviously the highest possible Q values with the lowest value tuning capacitors should be used. Errors in this case may be kept below 0.05 percent.

In either case the effect of the shunt impedance, Z_s, may be corrected for, once the value of Z_s is determined.

4.7. Effect of Standing Waves on Current Measurements

Standing waves are at present a more critical source of error in current than in voltage measurements. The reason is the relatively large dimensions and high effective characteristic impedances of the present day current sensing devices. For example, so called

"UHF" vacuum thermoelements are nearly always used at high frequencies. Bolometers, such as cylindrical resistors and themistors, have been used on rare occasions. Solid state thermoelements were recently developed for frequencies up to about 60 MHz, and bead type thermoelements were developed some years ago at the Bell Telephone Laboratories [18]. It is assumed that at the frequencies considered here, the current measuring devices are enclosed in a box approximating a coaxial structure with the current sensing element in series with the center conductor. Except for the case of thermistors and other beads (having diameters of the order of 0.1 to 1 mm), the current sensing elements are long relative to the shorter wavelengths involved here. The UHF thermoelements have a glass envelope of about 2 cm in diameter and heater diameters starting at about 10 or 20 μ (for the 5 mA current carrying capacity); the heaters are about 1 cm in length [19]. The uncertainties in calibrating these types of thermoelements are briefly discussed here as an illustration of the procedure in error evaluation.

Figure 11 shows a typical UHF feed-through type thermoelement mounted in a metallic tube. Planes D, H, and A are at the input end, middle, and output end of the heater, respectively. The Bolovac film is in plane C. The heater and its input and output leads form the center conductor of a coaxial system terminated by the Bolovac disk, R_m. This disk is, in turn, terminated by a negligible admittance. The effect of the discontinuities in the thermoelement coax system is negligible for the case at hand, at least

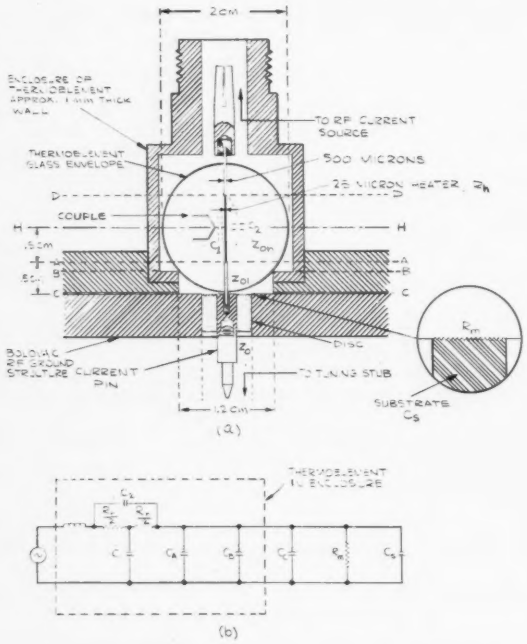

FIGURE 11. *UHF thermoelement under calibration by the Bolovac.*
Dimensions are approximate for use only as an illustration.

to 5 GHz, as shown below. Current standing waves are present along the line formed by the heater (Z_{0h}) and the section formed by the output lead of the thermoelement (Z_{01}). This second section is assumed to be uniform for the sake of simplicity. The heater section must be treated as a lossy line, because of the relatively high center conductor resistances, while the lead section may be considered lossless.

As previously indicated, the Bolovac-disk effective rf resistances may be of the order of 0.1 Ω up to the value of Z_0. For the dimensions shown, Z_{0h} is approximately 400 Ω and Z_{01}, 220 Ω. It follows that for all resistance values of the Bolovac disk up to 200 Ω there will be a current maximum in plane C.

Two effects of the standing wave need be considered in the heater, one caused by the nonuniform longitudinal distribution of the rf heater current, which may affect its temperature gradients. The other effect is the lower heater current as compared with that in planes A and C.

To determine a pessimistic error versus frequency for the given physical dimensions, we apply the following well-known, low-loss, shorted (the higher the losses, the lower the effect) equation to the line section Z_{0h}:

$$\frac{I_x}{I_A} = \cosh \alpha x \cos \beta x + j \sinh \alpha x \sin \beta x. \tag{19}$$

Here I_x and I_A are the respective currents entering the planes at x and A; x is the distance from plane A toward the current source.

Assuming the case of a relatively low-loss line where the phase velocity β is the same as in the air dielectric of the Z_0 line, the attenuation factor α introduced by heater resistances of the order of 10 Ω or less is

$$\alpha_{oh} = \frac{r_h}{2\,Z_{oh}}, \tag{20}$$

where r_h = heater resistance in ohms per meter.

For a typical 25 mA thermoelement, $r_h \cong 1{,}000\ \Omega/\text{m}$ and $Z_{oh} \cong 400\ \Omega$, as stated above;

$$\therefore\ \alpha_{0h} = 1.25 \text{ nepers per meter.}$$

Under these conditions the current distribution is, to a good approximation, the same as for a lossless shorted line, i.e.,

$$\frac{I_x}{I_C} = \cos \beta x \tag{21}$$

where I_C is the rf current in the Bolovac disk and x is the distance from C towards the source. Direct computation of the impedances and current ratio for the dimensions given (at 1 GHz and assuming $R_m \ll Z_{01}$), results in

$$\frac{I_A}{I_C} \cong 0.995$$

$$\frac{I_H}{I_C} \cong 0.978$$

$$\frac{I_D}{I_A} \cong 0.956.$$

One may assume that the current is uniform along the heater and has a value of the current at the middle of the heater, or 0.978 I_C. One can show that the error in this assumption will not exceed 0.2 percent. Based upon the distance between planes H and C, one may therefore calculate the value of $I_H (I_H = 0.978 I_C)$ with an estimated uncertainty of 0.2 percent. It is evident from eq (19) that this error will be lower as the heater resistance is increased.

One may also compute the top limit of R_m for a given error for values above 200 Ω; in our experiments R_m did not exceed 50 Ω. It also follows from the above that the length of the heater plus the leads seem to limit these thermoelements to frequencies below 1.5 GHz. Our observations and manufacturers data indicate the presence of resonances at frequencies above 1.5 GHz for these thermoelements for the current ratings of 5 to 1,000 mA; this is apparently a result of the residual inductance of the heater and of the shunt capacity across it. These thermoelements may therefore be used as indicators at frequencies above 1.5 GHz, but may be objectionable as calibrated instruments at higher frequencies because of likely instabilities.

It is, of course, apparent that the errors introduced by the standing waves are entirely avoidable when R_m is made equal to the load impedance of the current sensor (in its enclosure) at its final application. This is so because the current entering the load will be calibrated for a given output of the couple and will be accurately reproduced irrespective of a possible difference between I_C and I_H.

To summarize, for the above VHF thermoelements enclosed in 2-cm diam tubes and mounted at the Bolovac disk the error in assuming the corrected heater current equal to the Bolovac current will not exceed 0.4 percent at frequencies to 1 GHz; this error would not exceed 5 percent at 3 GHz, but the residual resonances may interfere above 1 GHz. For frequencies above 1 GHz it seems best to use smaller current indicators. The source of error introduced by standing waves can be easily eliminated by using a value of R_m sufficiently close to the intended load impedance of the thermoelement.

4.8. Effect of Discontinuities on Current Measurements

Figure 11 shows typical discontinuities as a result of steps in the nominally coaxial assembly of a thermoelement under calibration. The thermoelement may be enclosed in a metal box in such a way that the output-current lead length from the glass envelope of the thermoelement to the Bolovac disk is of the order of a millimeter. It is important to evaluate the effect of the shown discontinuities on current measurements because currents there are not continuous. Equivalent circuits representing the effects of these types of step discontinuities have been comprehensively evaluated in the past [20]. The results there show that the discontinuities can be accounted for by placing a capacitor at the plane of the discontinuity, provided the transverse dimensions of the line are a small fraction of the wavelengths transmitted. The equivalent circuit of figure 11a is shown in figure 11b omitting series inductances because these have been accounted for above in exploring the effect of the standing waves.

We consider the capacities C_1, between the heater and the thermocouple, and C_2, between the thermoelement leads, a part of the thermoelement assembly; their effect is independent of the connection to the Bolovac and is lumped into the thermoelement assembly characteristics to be determined by the calibration measurements. C_A in plane A, introduced by the discontinuity at the joint of the heater to the thermoelement output lead, is negligible; so is the capacity at the input end of the heater [20]. The capacitance C_s, contributed by the change in the dielectric medium, is lumped into the impedance terminating R_m and thus becomes part of the quarter-wave stub tuner or of another tank. Therefore, it seems sufficient to evaluate the effect of the discontinuities in planes B and C.

The housing may enclose the thermoelement on all sides except for an opening at the current output; in this case the discontinuity in plane B is part of the housing and only the discontinuity in plane C is to be evaluated. Or the housing may be left open at the side in contact with the Bolovac; in this case there is no discontinuity in plane B. The equivalent capacities were looked up for both cases. C_c turns out to be about 0.06 pF for the first case of the complete enclosure and about 0.1 pF for the second case. Because the capacitive current is in quadrature with the current in the disk, the error in the worst second case could be 1.4 percent at 5 GHz, with a 50-Ω disk, and about 0.05 percent at 1 GHz. In the case of a complete enclosure the error at 5 GHz would be reduced to about 0.5 percent. As the disk resistance is reduced, the error is reduced; for example, with a 10-Ω disk, the error at 5 GHz for a partial enclosure will be 0.05 percent.

A possible presence and effect of higher modes as a result of the above discontinuities is subject to further investigation. It is felt that the effect is negligible in our case, at least to 1 GHz; experimental evidence to that effect was obtained at 1 GHz. Two precalibrated thermoelements (in individual enclosures) were connected in tandem and the currents agreed well within the accuracies indicated. One must recall that the effect of suspected higher modes may always be reduced to any desired level by providing sufficiently long uniform line sections between the planes of the discontinuities and the reference plane of the current.

The conclusion is that a maximum enclosure of the thermoelement and a lowest practicable disk resistance will keep the error from this source to a negligible value even at 5 GHz. Reducing the physical

size of the current sensor will further reduce this error. The case of the thermoelement is presented only as an example; effects of discontinuities may be similarly computed for other current sensors.

4.9. Effects of Residual Impedances in the Ground System

It was indicated above that the rf bypass capacitor C_b (fig. 2) of the Bolovac may be a source of error because of its own impedance, particularly at or close to the frequency at which it may resonate with the distributed inductance of the assembly's ground system. C_b may also be a source of higher modes. Figure 12 shows the likely equivalent circuit of this part of the system where L_1 and L_2 represent residual inductances of connecting bolts, of lumped capacitors, and ground circuits. C_n is the capacity between the insulated ground plates. Figure 12a shows the equivalent circuit of a grounded rf source, the Bolovac (neglecting its residual ground inductances), and a grounded voltmeter being calibrated. Figure 12b is the equivalent of figure 12a with the Bolovac ground plates insulated from each other. L_1 is the combined residual inductance of the bolts used to ground the center electrodes of the 1,000 pF capacitors and of any other residual inductance of the capacitors. Figure 12c is the same as figure 12b except the ground plates are interconnected with metal bolts and/or brackets having a total inductance of L_2. Figure 12d is the same as 12b assuming an effective common laboratory ground which would normally short out L_2 but which generally cannot be realized at high frequencies. The two halves of the metal-film disks comprising R_m are shown in figure 12a in series with their respective rf bypassing capacities, 1/2 C_b. For negligible L_1, $C_b = C_b' + C_n$. The reactances of C_b and the residual ground inductance on the input side may be considered a part of the impedance of the rf source and does not affect results as long as they remain sufficiently stable.

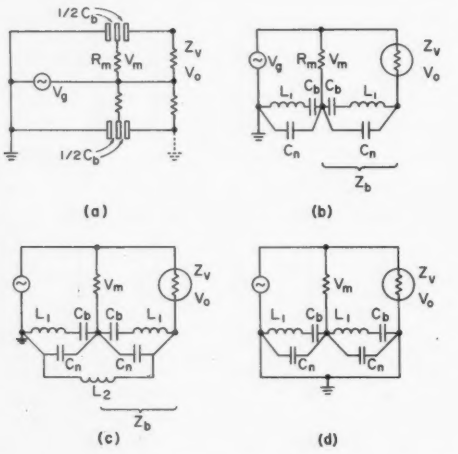

FIGURE 12. *Circuits of Bolovac, RF source, and voltmeter under calibration.*

(a) Equivalent circuit of setup when RF source and voltmeter have one terminal connected to common laboratory ground; residual inductances neglected. (b) Equivalent circuit with Bolovac ground plates insulated from each other; L_1 is residual inductance of C_b. (c) Same as (b) except ground plates are interconnected with metallic bolts and/or brackets. (d) Same as (b) assuming an effective common laboratory ground which generally cannot be realized at high frequencies.

On the other hand, the impedance of C_b in series with the output side of the disk may affect results. Observations indicated that the circuits shown in figure 12b and c, and not d, are the likely equivalents at frequencies above, say, 100 MHz, where effect of the residual inductances becomes appreciable in the particular assembly tested. The input impedance, Z_v, of the device under calibration and the ground impedance, Z_b, appear as a voltage divider across the known voltage, V_m. V_0 should, therefore, be lower than V_m by an amount depending upon the relative value of Z_b/Z_v. This may be appreciable at a frequency, f_r, at which the ground reactance elements are at resonance. With ground plates insulated from each other, such a resonance apparently did exist at approximately 550 MHz. C_b of the core and auxiliary capacity ring was approximately 0.06 microfarads (μF). V_m was greater than V_0 by several percent. It is evident from figure 12d that if the common laboratory ground were effective at the high frequencies, and when both the generator and voltmeter were grounded, V_0 would be larger than V_m. This was not the case. With the outer ground plates noninsulated (i.e., interconnected with metal bolts), f_r was about 300 MHz, and there were evidences of other resonances. Therefore, these plates were insulated from each other in our working assembly. In order to verify these deductions, a special voltage indicating device was constructed in such a way that it could be connected to the output of the Bolovac with and without the presence of the capacitor C_b at the output. This voltmeter consisted of two half sections insulated from each other for dc, but common for rf. It was then calibrated with and without the output C_b in the circuit to observe the ground effects. The only appreciable differences in the calibration values were at 550 and 300 MHz indicated above.

A search of our models to date for resonances has not revealed any of an appreciable magnitude at frequencies to 8 GHz, except the one at about 550 MHz with the C_b ring. The value of C_b of the cores without the ring was approximately 2000 pF. This permitted the application of our cores without the C_b ring down to frequencies of about 100 MHz for the uncertainties cited above. Cores as well as rings with different values of C_b may, of course, be readily designed depending on frequency ranges of interest. Small diameter cores with relatively large value of C_b may be obtained with modern techniques, e.g., employing anodized electrode surfaces. Our cores used 1-mil thick mylar insulators.

Further experimental study of the effect of C_b as a radial transmission line is perhaps in order. Available information on such a line [21] suggests that its characteristic impedance is fairly well approximated by the characteristic impedance of a coaxial line. The latter is assumed to have the same conductor separa-

tion as the radial line and a mean radius equal to the mean radius of the radial line section. In our case this characteristic impedance in the Bolovac core would be of the order of 0.01 to 0.1 Ω. Despite such a low value of the characteristic impedance, the effective input impedance into the radial line section may still be appreciable at resonance frequencies. A possible way of eliminating this source of uncertainty seems to be to coat the disk surfaces of C_b with some lossy compound, like carbon; this should reduce the input impedance of the radial section to a negligible value at resonance frequencies as well. As was stated before, an error may be introduced by the ratio of the input impedance of the radial line section to the input impedance of the voltmeter under calibration and not by the magnitude of the former.

It is readily apparent from figure 2 that measurements of rf currents are not affected by ground residuals nor by the value of C_b. The rf current enters the Bolovac disk from the center conductor, and its value is determined from the value of V_m measured by the bridge. It returns via C_b to the source. Therefore, the auxiliary capacitive ring is not essential for rf current measurement. It should thus prove relatively simple and economical to build Bolovacs for frequencies above, say, 100 MHz, particularly for practicable accuracies of 1 to 5 percent.

It is, of course, obvious that this error may be reduced to a negligible value even at resonance by making C_b sufficiently large. However, this error can be avoided without the additional expense of increasing C_b in one of three ways: (1) the core may be used without the ring so that f_r may be materially shifted away from the desired calibration frequency; (2) a shift of f_r may be obtained by decreasing C_b of the ring by a sufficient amount, e.g., by breaking the contacts of some of the disk capacitors to ground; (3) f_r may be shifted by temporarily shorting the ground plates of the ring. In the latter case, for a given L_2 and residual losses, the greater the value of C_b, the lower f_r and the lower the value of the parallel resonance resistance and whence the lower the error in V_0.

Because it is rather difficult to predict residual parameters of a ground system and a likely f_r, it is best to search for such f_r's experimentally whenever a new variation of the Bolovac is designed. For example, one or more coaxial outlets may be installed to observe the voltage V_b across C_b, as we have done. The sharpness of a peak of V_b as V_m is kept relatively constant will indicate the presence of f_r, and the ratio of V_b/V_m will indicate its possible detrimental effect. A measurement of V_b will also indicate a possible error in V_0 in case the value of C_b is too low for the lower end of the desirable frequency range. The likely error will, of course, be a function of the ratio of Z_b/Z_0; for example, at 3 MHz for C_b equal to approximately 0.06 μF, the reactance, X_b, is approximately 0.28 Ω, which is negligible compared to modern rf voltmeter input impedances. Even for a 50-Ω resistive input impedance the error should not exceed 0.013 percent because the voltage drop across X_b is in quadrature with that across Z_0. To search for f_r and to measure V_b it seems best to use good grade rf connectors with a voltmeter which will not introduce its own resonance effects. Once the values of f_r and of V_b/V_m have been found and steps determined to eliminate ground effect errors, these connectors may be removed or may be employed as bridge connecting terminals; however, their presence makes it possible to check the ground conditions at any time.

4.10. Summary of Errors

The uncertainties analyzed above may be conservatively summarized in percent of measured levels as shown in table 1 for voltage and table 2 for current. The uncertainties 1, 2, 3, and 4 of table 1 hold for current measurements in typical enclosed present day UHF vacuum thermoelements. Three other causes are listed in table 2. It is evident that wider ranges of voltage magnitudes and of frequencies may be realized with a given Bolovac at the sacrifice of some uncertainty.

TABLE 1. *Summation of errors in voltage measurements*

Source	Percent
1—Approximations in derived equations showing that the rf voltage drop across the resistive film is equivalent to the d-c voltage drop	±0.00
2—Magnitudes and instabilities of bridge components and biasing source	±.06
3—R-f source instability	±.01
4—Quality of bolometric disk and substrate	±.01
5—Effect of standing waves on voltage at 10 GHz (at 20 GHz—0.020)	±.01
6—Effect of residual parameters in the ground system (total limits of uncertainty)	±.00
Total limits of uncertainty for voltages of 0.1 to 5 V at 10 MHz to 10 GHz	±.09
Same to 20 GHz	±.10

TABLE 2. *Summation of errors in current measurements*

Source	Percent
1–4 Listed for voltage	±0.09
7—Effect of standing waves and nonuniform heater current at 1 GHz with correction applied for any R_m to 200 Ω	±.40
Same, if R_m is equal to the intended load of the thermoelement	±.00
8—Effect of discontinuities to 1 GHz for $R_m = 50$ Ω and maximum enclosure of the thermoelement	±.05
Same for $R_m = 10$	±.01
9—Estimated average effect of resonant tank impedance shunting R_m	±.05
Conservative total limit for frequencies to 1 GHz and $R_m \leq 50$	±.60
Same for $R_m \cong$ intended load	±.10

5. Comparison With Power Measurements

It may be instructive at this point to discuss the overall uncertainties in measuring voltage and current in a plane A arrived at in tables 1 and 2 as compared with the uncertainties of the power measurements

against which the results are cited here. A thorough analysis of this issue is beyond the scope of this paper. Only the apparent major causes of the discrepancy are indicated as follows.

The power measurement uncertainties above 1 GHz were ± 1 to ± 2 percent at best because a precalibrated bolometer power meter was used in this case. A calibration factor in terms of a calorimetric power standard was determined and the reading obtained with the meter was corrected accordingly. Direct comparison with the calorimetric power standard might have reduced the uncertainty to ± 0.5 to ± 1 percent. Because this was not yet done, the estimated uncertainty of our results of the voltage measurements is conservatively put at ± 1 percent to 2 GHz, ± 2 percent to 4 GHz, and ± 4 percent to 8 GHz. These are the differences or disagreements, stated previously, between the Bolovac and the power-bolometer results.

Another reason for caution is the relatively small number of Bolovac disks tried so far in our laboratory. The differences between results of individual disks and the reproducibility of readings were within 1 percent. No effort was made to improve the bridge operation via a sufficiently careful calibration of its components to warrant the figures of uncertainty listed in the table.

The difference between determination of power transmitted along a transmission line employing voltage measurements as against other methods may be pointed out here. The multiple probe method of measuring power (and impedance) in TEM transmission lines was recommended years ago [22]. The reason for neglecting it might well have been the inability of measuring voltages with sufficient accuracy. With the latter difficulty remedied within the limits indicated here, it seems advisable to reconsider the method particularly for application in secondary standardization laboratories and field measurements. The method holds promise for better accuracies and greater economy. Power may be computed by measuring voltages at three probes spaced one-eighth wavelength apart. Only one voltage need be accurately known; the voltages at the other probes enter the equation simply as ratios to the first. It was shown above that the voltage in a given plane A, in a coaxial line, may be determined with an uncertainty of 0.09 percent. Assuming the uncertainty in the value of the characteristic impedance of presently available coaxial low-loss-precision line sections of ± 0.05 percent, one can readily show that the power transmitted may be determined to an uncertainty of about ± 0.2 percent over a wide range of standing wave ratios. This can be done without replacing the load of the system by a calorimeter, and indeed, without disturbing the system once probes have been installed and a voltmeter in combination with the probe section has been precalibrated for the purpose. Probe sections are needed for each frequency (or a band of frequencies with correction curves). However, the same voltmeter may be used for all frequencies. It may be one of a number of 50-Ω input-impedance voltmeters or power meters presently available for frequencies up to 2 GHz or higher. The voltmeter need not be permanently connected to the probe line section and can be used for other purposes in the laboratory or system installation.

The objective of this discussion is not to advocate voltage measurements in place of widely used power measurement techniques. The need of measuring power as a basic quantity is beyond dispute. However, one should be aware of the multiple probe method and its potentialities. An up-to-date survey of power measurements [23] lists ± 2 percent as the lowest presently attainable uncertainty for feedthrough power meters at frequencies to 10 GHz. The lowest uncertainty in calibrating the effective efficiency of a bolometric power meter, using a calorimeter as the basic method, is ± 0.2 percent. The latter involves complicated, relatively costly equipment, and has a long time constant. It would thus seem that the multiple probe method has a fair margin of safety in terms of uncertainty, particularly for use with field equipment and systems where accuracies of 1 percent are needed. Another advantage of the multiple probe method is the ability to measure impedances with the system in operation; an addition of a fourth probe makes this possible. Still other advantages are the relatively large voltage and power ranges that can be measured with one voltmeter and the relatively high decoupling factor, or low incident power absorbed by the probe and voltmeter.

6. Conclusion

Hopefully this paper, describing the Bolovac basically, will be followed by another on applicational steps, details, precautions, and additional results as well as on further perfection of the device. Throughout the development steps of the Bolovac, to date, the emphasis was on proving the validity and practicability of the principle and technique. No particular effort was made towards achieving optimum or potential accuracy, nor on establishing limits of voltage and current magnitudes, and a top limit of frequency. Considerable improvement is anticipated in the quality of the disks, particularly in their current-carrying capacity, sensitivity, and stability. Intercomparison with the dynamometer type ammeter [3] and with more accurate power measurements is pending. However, the results obtained so far amply illustrate the superior value of the Bolovac as an instrument for both high and medium accuracy calibrations of voltage, current, and possibly power meters over a wide frequency range.

Appreciation is hereby expressed to the Radio Standards Laboratory and to the NBS for the opportunity of developing the Bolovac; to P. A. Hudson, P. E. Werner and (the late) P. London for their splendid cooperation in disk developments; to W. J. Blank and R. P. Chariton for performing countless painstaking observations and measurements; to D. Holt for his assistance in the computation of the inductance of

a short and wide rectangular film, and to C. M. Allred and C. C. Cook for critical and constructive reviews of the paper.

7. Appendix

One may reasonably question the effect of the imperfections of the film-resistor disk on the purity of the TEM mode. The nonuniformity of (1) the film thickness and of (2) the width of the annular ring may cause an effective residual inductance and thus introduce an error in the deduction that the disk impedance is purely resistive. A third possible source of uncertainty is the effective discontinuity introduced by the contact electrodes to the film. The likely limiting errors as a result of the above three imperfections will here be briefly analyzed.

The up-to-date state of the art on depositing resistive films and electrodes on substrate (preferably polished) surfaces indicates that the thickness uniformity of the film can be maintained to 1 to 2 percent over a 2 sq in area [5, 22, 25]. Registration tolerances in the order of 0.0002 in (5×10^{-4} cm) of true position are obtained with photo-resist techniques [25]. The resistances of the two halves of the film (e.g., of platinum) may be made equal to 0.1 percent; the coefficient, γ, may be equal to within the same degree as the thickness (because γ is a function of the thickness [13]). With tantalum or chromium on polished glass the γ's may be equal to within 0.1 percent. The tolerances are, naturally, a function of the resistance values desired; deposition rates can be controlled down to a few angstroms per minute [22]. Practical thickness limitations (at which the film characteristics approach those of the bulk of the material) vary widely with materials and are of the order of 50 to 200 angstroms [13].

Effect of film thickness variation on disk inductance. The area of the 7-mm diam substrate over which the film is deposited is approximately 0.075 sq in. On the basis of the above tolerances one may expect a thickness variation of about 0.03 percent. It will be assumed below that one half of the annulus differs in thickness from the other half, but each half is uniformly thick over its surface. To obtain a pessimistic evaluation, the effect of thickness differences of 0.03, 0.1, and 1 percent were considered.

To determine the effective residual inductance caused by the thickness differences one must compute the inductance of half an annulus (having the shape of half a washer) with radial currents, as shown in figure 13a. No analytical expression for the inductance of this case is available and the derivation of a suitable equation presents a problem beyond the scope of this paper. A conservative evaluation was therefore made on the basis of figure 13b. The film in figure 13b is identical to that of figure 13a assuming an infinite radius of the coaxial line. It may be looked upon as a film resistor located in the transverse plane of a strip line with a center conductor and two outer "ground" conductors; the fringing fields are neglected. The

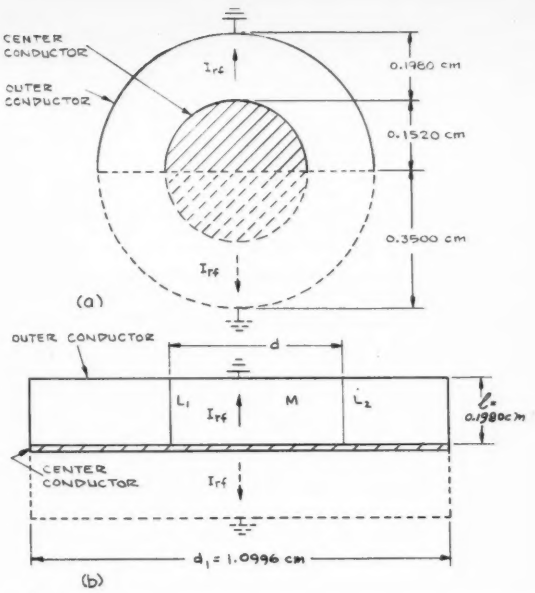

FIGURE 13. *Bolovac coaxial transverse film and approximate equivalent film in strip line.*

inductance of half of the film (between the center conductor and one of the outer conductors) can be computed for the transverse currents. Because of the dimensional configuration, conventional formulas derived for long conductors (for which $l \gg d$) cannot be used. Instead, the inductance was determined from an equation derived by Hoer and Love [26] using an electronic computer. Inductance values were computed for 1000-Å thick films differing in thickness by ± 0.03, 0.1, and 1 percent. The inductance was 2.24908×10^{-4} microhenries (μH) for the 1000-angstrom film. The differences in the inductance were as follows:

Thickness difference	Difference in L
Percent	*Microhenries*
+0.03	-9.39×10^{-9}
−0.03	$+1.06 \times 10^{-8}$
+0.1	-3.20×10^{-8}
−0.1	$+3.42 \times 10^{-8}$
+1	-6.60×10^{-8}
−1	$+3.43 \times 10^{-7}$

One may show that the approach chosen is a pessimistic one as follows. Assume two conductive fibers (comprising two elements of the film) located a distance, d, from each other as illustrated in figure 13b. L_1, L_2, and M are their respective self and mutual inductances. The combined inductance of the two filaments in parallel with currents flowing in the same direction is given by [27].

$$L_t = \frac{L_1 L_2 - M^2}{L_1 + L_2 - 2M}$$

here $L_1 = L_2 = L$

and $$L_t = \frac{L + M}{2}.$$

In the limit as $d \to \infty$, $M \to 0$, and $L_t \to \frac{L}{2}$. As $d \to 0$, $M \to K$, $L_1 L_2 \to KL$, $K \to 1$ and $L_t \to L$.

The presence of the mutual M increases L_t. In the case of a cylindrical coaxial line (fig. 13a), the value of M will always be smaller than for the corresponding filaments of case 13b because of the relative angular positions of the filaments; indeed M will be zero between filaments located at right angles to each other. Therefore L_t will always be smaller in case 13a than in case 13b; so will the differences in L as a result of differences in thickness. Therefore, the deductions for case 13b safely hold for case 13a.

The effective inductance of the entire annular film of 13a and of the top and bottom halves of 13b is the difference between the inductances of the two halves and is equal to the figures given above for the differences in the thicknesses chosen.

The likely difference at the present state-of-the-art is of the order of 0.03 percent. For a 1000-Å thick film the conservatively computed effective inductance might thus be as high as 1.06×10^{-8} μH.

Again assuming a further pessimistic value of a thickness difference of one percent, the effective inductance may be as high as 3×10^{-7} μH. This corresponds to a reactance of about 3.8×10^{-2} Ω at 20 GHz. This quadrature component in series with, say, a 10-Ω film may introduce an error of 7×10^{-4} percent in the assumption that the rf impedance of the film is equal to its dc resistance. One should, perhaps, point out again that this is an "error" and in principle may be corrected for, if indeed the rf impedance can be measured with the required precision. The likely error may of course be computed for other film thicknesses and resistances. The higher the resistance of the film, the thinner it is and the higher may be the effective inductance. However, it enters as a quadrature component in the impedance. Thus, the overall error is not likely to be appreciable for any value of the film resistances and frequencies here under consideration.

Effect of variation of width of film. It was indicated above that the registration tolerances of the film are at present of the order of 5×10^{-4} cm of true position. The incremental film width variation for a 7-mm, 50-Ω coaxial line is thus approximately ± 0.5 percent. The inductance for radial currents is approximately proportional to the width of the annulus (i.e., to the "length" of each elemental filament). Assuming in the limit that one half of the annulus differs in "length" from the other half by 0.5 percent and taking again the above example of the 1000-angstrom film having an inductance of 2.25×10^{-4} μH, the effective inductance of the annulus might be about 11.25×10^{-7} μH. This might contribute an error of about the same magnitude as that of the difference in thickness, and again, a correction can be applied.

Effect of discontinuities introduced by contact electrodes. It was stated previously that registration tolerances may permit deposition of electrodes on the substrate to within 5×10^{-4} cm. Because of requirements associated with securing the position of the disk in the coaxial structure (e.g., by means of soldering, conductive epoxy cement, clampings, etc.), we will allow a conservative width of the electrodes on the disk surface of 15×10^{-3} cm. The computed [19] equivalent shunt capacity introduced by these electrodes in a 7-mm, 50-Ω line is approximately 15×10^{-3} pF. The effect of the equivalent quadrature shunt reactance at 10 GHz on current measurements employing a 50-Ω film will be approximately 0.11 percent. With lower film resistances (most likely to be used for current standardization), the uncertainty is correspondingly lower. As was indicated previously, these discontinuities do not introduce uncertainties in voltage standardization; higher modes, if any, should be sufficiently attenuated along the uniform line sections normally present in input connectors to high frequency voltmeters.

8. References

[1] M. C. Selby and L. F. Behrent, A Bolometer bridge for standardizing radio-frequency voltmeter, J. Res. NBS **44**, 15–30 (Jan. 1950) RP2055.

[2] Electrodynamic ammeter for very high frequencies, NBS Tech. News Bull. **34**, No. 7, 103–104 (July 1950.)

[3] N. V. Frederick, An absolute electrodynamometer for high frequency currents (to be published).
Y. Aida, Research on the primary standard of current using short-circuited-ring for high frequencies, Researches of the Electrotechnical Laboratory, Japan, No. 639, pp. 1–93 (1963). (In Japanese).

[4] J. D. Ryder, Networks, Lines and Fields, Ch. 10, (Prentice Hall, Inc., New York, 1962).

[5] E. Keonjian, Microelectronics, pp. 181–191, 256, 257 (McGraw-Hill Book Co., Inc., New York, N.Y., 1963).
L. Braun and D. E. Lood, Precision thin-film cermet resistors for integrated circuits, Proc. IEEE **54**, No. 11, 1521–1527 (Nov. 1966).

[6] A. E. Kennelly, Tables of Complex Hyperbolic and Circular Functions (Cambridge, Mass., Harvard University Press, 2d ed., 1927).

[7] J. J. Karakash, Transmission Lines and Filter Networks, pp. 116–125 (The Macmillan Co., New York, 1950).
T. Moreno, Microwave Transmission Design, p. 69 (Dover Publication, Inc., New York, 1958).

[8] M. C. Selby, Accurate radio-frequency microvoltages, Trans. of AIEE, Pt. 1, Communication and Electronics **72**, 158–164 (May 1953).
R. D. Cutkosky, Evaluation of the NBS unit of resistance based on a computable capacitor, J. Res NBS (Phys. and Chem.) **65A**, No. 3, 147–158 (May–June 1961).

[9] M. C. Selby, C. M. Allred, P. A. Hudson, I. S. Berry, High frequency power measuring bridge circuit, Pat. No. 2,833,620, (April 21, 1959).

[10] IRE Dictionary of Electronics Terms and Symbols. The Inst. of Radio Engineers, p. 54 (1961). For a comprehensive analysis of "imprecision," "systematic error," "uncertainty," etc., see: C. Eisenhart, Realistic evaluation of the precision and accuracy of instrument calibration systems, J. Res. NBS **67C** (Engr. and Instr.) No. 2, 161–187 (Apr.–June 1963). H. H. Ku, Statistical Concepts in Metrology, Ch. 2, Handbook of Industrial Metrology, sponsored by Amer. Soc. of Tool and Mfg. Engrs. (Prentice Hall, Inc., New York, N.Y. 1967).

[11] Reference Data for Radio Engineers, p. 129 (IT&T Corp., New York, 4th ed., 1957).
[12] M. C. Selby, Single-bolometer series-parallel circuit for accurate voltage and power measurement, 19th Annual ISA Conference and Exhibit (Oct. 1964), Preprint No. 21, 6-1-61.
[13] W. Lewis, Thin Films and Surfaces, pp. 27, 69-71 (New York, Chemical Publishing Co., 1950).
[14] I. A. Harris, A coaxial film bolometer for the measurement of power in the UHF band, Inst. of Elec. Eng., Part B, **107,** 67-72 (Jan. 1960).
[15] Glenn F. Engen, A dc-rf substitution error in dual-element bolometer mounts, IEEE Trans. on Instrumentation and Measurement, **IM-13,** Nos. 2 & 3, 58-64 (June-Sept. 1964).
[16] M. C. Selby, W. J. Blank, and R. P. Chariton, Voltmeter calibration to 1 GHz, WESCON/65, Session 8, pp. 1-12.
[17] F. E. Terman, Electronic and Radio Engineering, pp. 106-107 (McGraw-Hill Book Co., Inc., 4th ed., 1955).
[18] C. G. Montgomery, Technique of Microwave Measurements, Radiation Laboratory Series No. 11, p. 189 (McGraw-Hill Book Co., Inc., New York, N.Y., 1947).
[19] M. J. O. Strutt and K. S. Knol, Measurements of currents and voltages down to a wavelength of 20 centimeters, Proc. IRE **27,** No. 12, 783-789 (Dec. 1939).
[20] J. R. Whinnery, H. W. Jamieson and T. E. Robbins, Coaxial line discontinuities, Proc. IRE **32,** No. 11, 695-709, (Nov. 1944).
[21] S. Ramo and J. R. Whinnery, Fields and waves in modern radio, 2d ed., pp. 395-401 (John Wiley & Sons, New York, N.Y., 1953).
G. L. Ragan, Microwave transmission circuits, R. L. Series #9, (1948), 1st ed., pp. 100-114, 407-455.
[22] M. C. Selby, Voltage measurement at high and microwave frequencies in coaxial systems, proc. IEEE **55,** No. 6, 877-882 (June 1967).
R. A. Schrack, Radio-frequency power measurements, NBS Circ. 536, p. 11 (Mar. 16, 1953).
D. D. King, Measurements at Centimeter Wavelength, pp. 197-199 (D. van Nostrand Co., Inc., N.Y., 1952).
F. E. Terman and J. M. Pettit, Electronic Measurements, pp. 197-199 (McGraw-Hill Book Co., Inc., New York, N.Y., 1952).
M. Sucher and J. Fox, Handbook of Microwave Measurements, pp. 122-131 (Interscience Publishers, 3d ed., New York, 1963).
[23] A. Y. Rumfelt and L. B. Elwell, Radio Frequency Power Measurements, Proc. IEEE, **55,** No. 6, 837-850 (June 1967).
[24] J. W. Nickerson and R. Moseson, Low-energy sputtering, Research and Development **16,** No. 3, 53-57, (Mar. 1965).
[25] D. Hyndman, Basic thin film techniques, Electronic Design, pp. 86-93 (July 20, 1964).
[26] C. Hoer and C. Love, Exact inductance equations for rectangular conductors with applications to more complicated geometries, J. Res. NBS **69C** (Phys. and Chem.) No. 2, 127-137, equations (14) and (19). (June 1965).
[27] F. Langford-Smith, Radiotron Designer's Handbook, 1953, 4th ed., RCA, Harrison, N.J., p. 148.
NBS Circular C74, Radio Instruments and Measurements, p. 18, (1937), Superintendent of Documents, Washington, D.C.

(Paper 72C1-269)

JOURNAL OF RESEARCH of the National Bureau of Standards—C. Engineering and Instrumentation
Vol. 72C, No. 1, January–March 1968

An Admittance Meter Technique to Measure the Complex Permeability at VHF

A. L. Rasmussen* and C. M. Allred**

Institute for Basic Standards, National Bureau of Standards, Boulder, Colo. 80302

(October 24, 1967)

An admittance meter technique may be used in evaluating and comparing accurately and conveniently the complex permeability of magnetic materials from 30 MHz to ~ 100 MHz. The admittance meter has three coaxial lines fed from a common source at a common junction point, two lines being terminated by shorts and the third by 50Ω. The currents in the lines are detected by three electrically connected parallel loops each located close to the common junction point of the lines. The loops are adjustable to one minute of rotation and follow closely a sine law. The complex permeability of a sample is derived from measurements with a sample in and out of one of the shorted coaxial lines. The estimated error from 30 MHz to 100 MHz is from ~ 1 to ~ 10 percent for sample inductance from $3 \cdot 10^{-9}$ to 10^{-7} H and sample resistance $5 \cdot 10^{-1}$ to $10^{2}\Omega$. Error of inductance is ~ 1 percent from 30 MHz to 200 MHz for low-loss samples using calibrated sample data. Using precision 50Ω, low-contact resistance lines, the sample impedance error attainable is estimated as ~ 1 percent for the above limits of impedance and measurements can be extended to above 100 MHz. The equations for the inductance and the resistance of the sample are expressed in terms of calibrated values for the settings of two loops, the calibrated resistance value of the 50Ω termination, the calibrated or calculated impedance components of the sample line, and the inductance of an equivalent air core.

Key Words: Admittance meter, attenuation calibration, lossy magnetic materials, magnetic measurement methods, permeability, rf magnetic materials, VHF bridge, VHF magnetic materials.

Definitions of Symbols

Y_1 = Line 1 admittance terminated by a short.
Y_2 = Line 2 admittance terminated by 50Ω.
Y_3 = Line 3 admittance terminated by a short.
K_1 = Relative loop output which is a function of the angle of loop rotation in the corresponding numbered line.
K_2 = Same as above. A primed symbol refers to data *with* a sample in line 3.
K_3 = Same as above. A primed symbol refers to data *with* a sample in line 3.
L = Sample inductance.
R = Sample resistance.
ω = Angular frequency.
L_3 = Inductance of line 3 without a sample inside.
R_2 = Resistance of line 2.
L_a = Calculated inductance of an equivalent air core.
R_3 = Resistance of line 3 without a sample inside.
μ' = Real component of initial permeability.
μ'' = Imaginary component of initial permeability.
$\tan \delta = \mu''/\mu' = R/\omega L$.

*Radio Physics Division, Radio and Microwave Materials, Boulder, Colo. 80302.
**Radio Standards Engineering Division, HF Electrical Standards, Boulder, Colo. 80302.

1. Introduction

A technique based on the principles of a familiar admittance meter [1] [1] may be used in evaluating and comparing accurately and conveniently the complex permeability of magnetic materials from 30 MHz to ~ 100 MHz. Such an instrument is relatively simple to calibrate; and, utilizing a null method, "lossy" materials are easier to evaluate than they would be if resonant cavity techniques were used. The technique is evaluated and data discussed.

2. The Admittance Meter and Its Calibration

The admittance meter discussed here (see fig. 1) has three coaxial lines fed from a common source at a common junction point, two lines being terminated by shorts and the third by 50Ω. In the commercially available model one line is terminated by its characteristic impedance (50 Ω), another by a reactance, and the third by the unknown admittance. The current in each line in these instruments is sampled near the common junction point by a loop through the mutual coupling between the loop and the center conductor of the line. The mutual coupling which closely follows a sine law, is adjustable by rotating the loop about an axis perpendicular to the center conductor of its respective line. The outputs of the loops are connected in parallel and fed into a sensitive tuned null detector.

The experimental model used in the technique described here was originally designed and constructed at NBS for use in some very special rf power measurements, and a more stable instrument with better impedance matching could easily be designed to better meet the needs required in the technique under discussion if the time and funds were available. Nevertheless, in spite of some difficulties, the technique was adequately evaluated and found to have merit.

In order to explain the measurement technique and loop calibration, the basic equations for the admittance meter are developed and discussed. As shown in figure 1, the two shorted lines are designated as 1 and 3, and the 50 Ω line as 2. The currents in lines 1, 2, and 3 are

$$i_1 = VY_1$$

$$i_2 = VY_2$$

$$i_3 = VY_3.$$

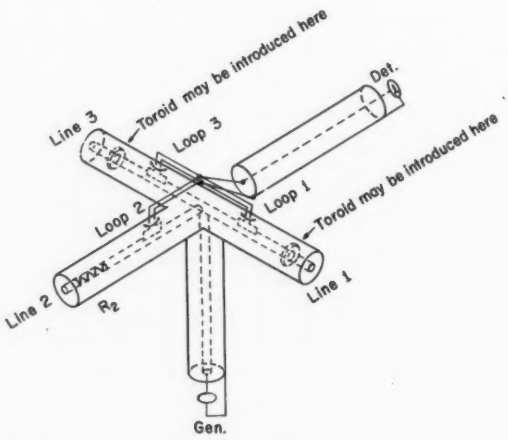

FIGURE 1. *Schematic of the admittance meter circuit used.*

[1] Figures in brackets indicate the literature references on page 87.

The outputs of the loops are, respectively,

$$v_1 = K_1 i_1$$

$$v_2 = K_2 i_2$$

$$v_3 = K_3 i_3$$

where the proportionality constant K is a function of the angle of loop rotation. The functional relationship is to a close approximation, $K = k \sin \theta$. The three outputs are combined and the K's are adjusted for a null where

$$v_1 + v_2 + v_3 = 0$$

and hence

$$K_1 Y_1 + K_2 Y_2 + K_3 Y_3 = 0. \tag{1}$$

The K_1 values for the instrument used are proportional to the sines of angles of $+90°$ to $-90°$; K_2, from $+5°$ to $-90°$; and K_3 from $-5°$ to $+90°$. Angles are adjustable to one minute of rotation.

Measurements of a sample can be made by (1) holding K_1 constant and adjusting loops 2 and 3 for the conditions with and without a sample in line 3, or (2) a sample in one line can be compared with a sample in the other coaxial line. We chose to use method (1). Method (2) is especially useful if the two coaxial lines are identical both electrically and physically.

It can be shown (see appendix A) that the equations for the inductance and the resistance of a sample in line 3 are

$$L = \frac{(K_3'/K_3)(1/\omega L_3)}{\omega[((K_2' - K_2)/K_3)^2 (1/R_2)^2 + (1/\omega L_3)^2]} - L_3 + L_a, \tag{2}$$

$$R = \frac{-(K_3'/K_3)((K_2' - K_2)/K_3)(1/R_2)}{((K_2' - K_2)/K_3)^2 (1/R_2)^2 + (1/\omega L_3)^2} - R_3 \tag{3}$$

when the following assumptions are made:

1. $K_1 Y_1 =$ constant during the measurement with and without a sample in line 3. K_1 may have a wide range of values. Setting loop 1 determines the setting of loop 3 and vice versa.

2. $R_2 = 50\ \Omega$ and its VSWR ≈ 1.005. See appendix A.

3. Precision 50 Ω lines with low contact resistance terminations are used. The lines used did not have these characteristics; therefore, the term $R_3/\omega^2 L_3^2$ should be added to $-((K_2' - K_2)/K_3)(1/R_2)$ whenever this expression appears in eqs (2) and (3). See appendix A. In addition to the correction from R_3, other corrections for transformed impedances should be made. However, none were necessary for the accuracy of the data in this paper.

For a low-loss sample where $\omega L \gg R$, we can simplify the equations to

$$L = L_3[(K_3'/K_3) - 1] + L_a \tag{4}$$

$$R = -(K_3'/K_3)((K_2' - K_2)/K_3)(1/R_2)(\omega L_3)^2 - R_3 \tag{5}$$

when the expression $((K_2' - K_2)/K_3)^2 (1/R_2)^2 \ll (1/\omega L_3)^2$. As in assumption 3 above, $R_3/\omega^2 L_3^2$ must be added to $-((K_2' - K_2)/K_3)(1/R_2)$ in eq (5). If L and R of a high- or low-loss sample are known, one can find L_3 and R_3 using eqs (2) and (3) or (4) and (5). L_3 can also be calculated from the dimensions of a precision line.

Finally, the complex permeability is (using the L and R values of eqs (2) and (3) or (4) and (5)):

$$\mu' = \frac{L}{L_a} \tag{6}$$

$$\mu'' = \frac{R}{\omega L_a} \tag{7}$$

and the loss tangent

$$\tan \delta = \frac{\mu''}{\mu'} = \frac{R}{\omega L}. \tag{8}$$

Calibration of the loop outputs shows they closely follow a sine law, deviating somewhat when the angles are $\lesssim 10°$. "Calibrated values" include the relative outputs of the loops to each other. In general data are a little more accurate using a sine law and the relative output calibration. However, results on samples reported in this paper come from completely calibrated loop data.

Calibration of the voltage output of the loops is performed using the circuit shown in figure 2. To a first order approximation, the voltage in each loop is proportional to the admittance in the corresponding numbered line.

A signal in Branch 1 is matched to a signal in Branch 2 by balancing a loop output to the attenuator output of opposite phase. This loop is terminated in 50 Ω. The two other loops are set to zero output and their corresponding lines to infinite impedance. The zero output angle of each loop is found electrically.

Angles are calibrated by reading the angle to a resolution of one minute and the attenuator to ± 0.001 dB accuracy. Voltage ratios are derived from measuring the decibel change from a reference angle. Calibration of the loop output may be calculated from the voltage ratios. Relative output is found by measuring the change in attenuation from one loop to another.

Loop calibration was checked at 30 MHz using two 50 Ω terminations accurate to ± 0.5 percent. They were compared to each other using lines 1 and 2, 1 and 3, and 2 and 3 with the loops set at several different angles, and generally agreed within 0.5 percent.

The precision of loop 3 measurements when evaluating samples was ~ 0.1 percent, and for loop 2, ~ 1 percent for "lossy" samples. Sample data are independent of the loop angles used (except when they were close to zero). At 30 MHz, the input power was ~ 0.25 W and at 100 MHz, ~ 0.1 W.

3. Interpretation of Measurements

Using the instrument described and treating line 3 impedances as lumped circuit quantities, the estimated error from 30 to 100 MHz is from ~ 1 percent to ~ 10 percent for sample inductance

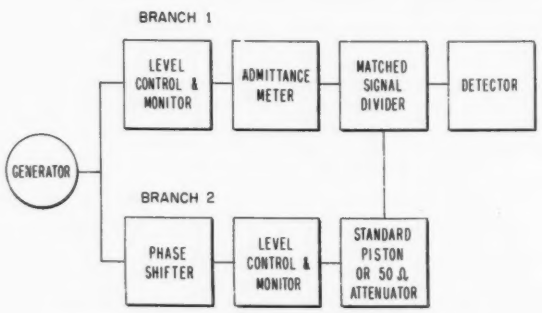

FIGURE 2. *Schematic of circuit used to calibrate loops.*

Standard piston attenuator used at 30 MHz only. 50 Ω attenuator used at 30 MHz and 100 MHz.

from $3 \cdot 10^{-9}$ to 10^{-7} H and sample resistance $5 \cdot 10^{-1}$ to $10^{2}\Omega$. Error for inductance is ~ 1 percent from 30 to 200 MHz for low-loss samples using calibrated sample data, figure 3. Using precision 50 Ω lines with low contact resistance terminations in place of the present lines, it is estimated the effect of the present mismatch could be reduced from the observed ~ 10 percent to ~ 1 percent. It is also estimated that measurements could be extended to lower resistances and higher frequencies.

Low-loss sample data ($\mu' \sim 10$ and $\tan \delta \sim 10^{-2}$) are shown in table 1 and figure 3. In table 1, sample inductance at 30 MHz, $\Delta L = (\mu' - 1)L_a$, or from eq (4), $\Delta L = (L - L_a)$, is compared to calibrated sample inductance values. These are constant over the frequency range used. The samples were calibrated using an adjustable length precision coaxial line functioning at a small fraction of a wavelength at low frequency and as a half wavelength cavity at high frequencies [2]. The losses, $\sim 5 \cdot 10^{-3}\Omega$, are not reported because of the poor precision in the contact resistance of line 3. Inductance data shown in table 1 agree within 1 percent, the estimated error of the calibrated samples.

Figure 3 may be used to evaluate the inductance of low-loss samples from loop data. A sample may be identified as having low loss by showing only a small change in loop 2 when placing a sample in line 3. Transformed line impedances cause the curves shown to decrease their slope with frequency.

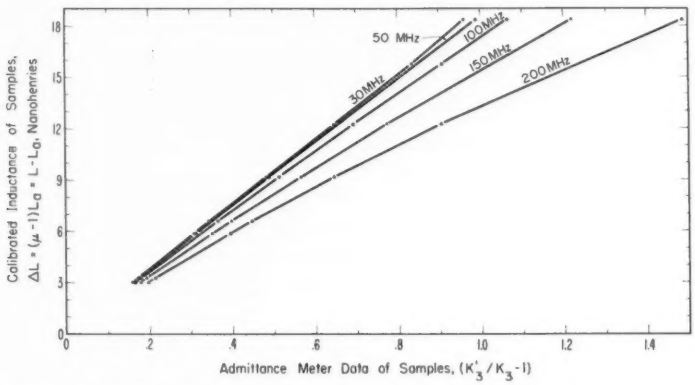

FIGURE 3. *Calibrated inductance* $(\mu' - 1)L_a$ *of low-loss samples versus* $[(K'_3/K_3) - 1]$, *admittance meter loop data of samples, at 30, 50, 100, 150, and 200 MHz.*

Table 1 data are used to get ΔL. The graph may be used to find the permeability of a low-loss sample using admittance meter data.

TABLE 1. *Inductance data of samples using the admittance meter at 30 MHz compared to data using an adjustable length precision coaxial line (1 MHz) or coaxial cavity (100 MHz) for samples whose permeability is constant to several hundred MHz.*

	Inductance $\Delta L = (L - L_a) = (\mu' - 1)L_a$		
Sample	Admittance meter* (30 MHz)	Adjustable length coaxial line (1 MHz)** or coaxial cavity (100 MHz)**	Coaxial line or cavity frequency
1	$3.05 \cdot 10^{-9}$ H	$3.03 \cdot 10^{-9}$ H	1 MHz
2	3.27	3.27	1 MHz
3	5.61	5.66	1 MHz
4	6.21	6.22	1 MHz
5	6.56	6.59	100 MHz
6	9.12	9.17	100 MHz
7	12.25	12.25	100 MHz
8	18.52	18.35	100 MHz

*Using $(L - L_a) = L_3[(K'_3/K_3) - 1]$, eq (4) of the text. Sample with $\Delta L = 5.87 \cdot 10^{-9}$ H (1 MHz) was used to calibrate L_3.

**$\Delta L = (\mu' - 1)L_a$, the change in length of the line equivalent to the inductance change introduced by the sample placed at the end of the line. The cavity operates at ½ wavelength.

High-loss sample data using the admittance meter and other techniques are shown in table 2, and figure 4, parts a, b, c, and d. Techniques used for comparison to admittance meter data are the rf permeameter [3] (a calibrated transformer in which the sample is part of the secondary) on a Schering bridge or the Q-meter and the adjustable length coaxial cavity operating at a ½ wavelength [2]. Since the latter is a resonance technique, it is not particularly adaptable to measuring

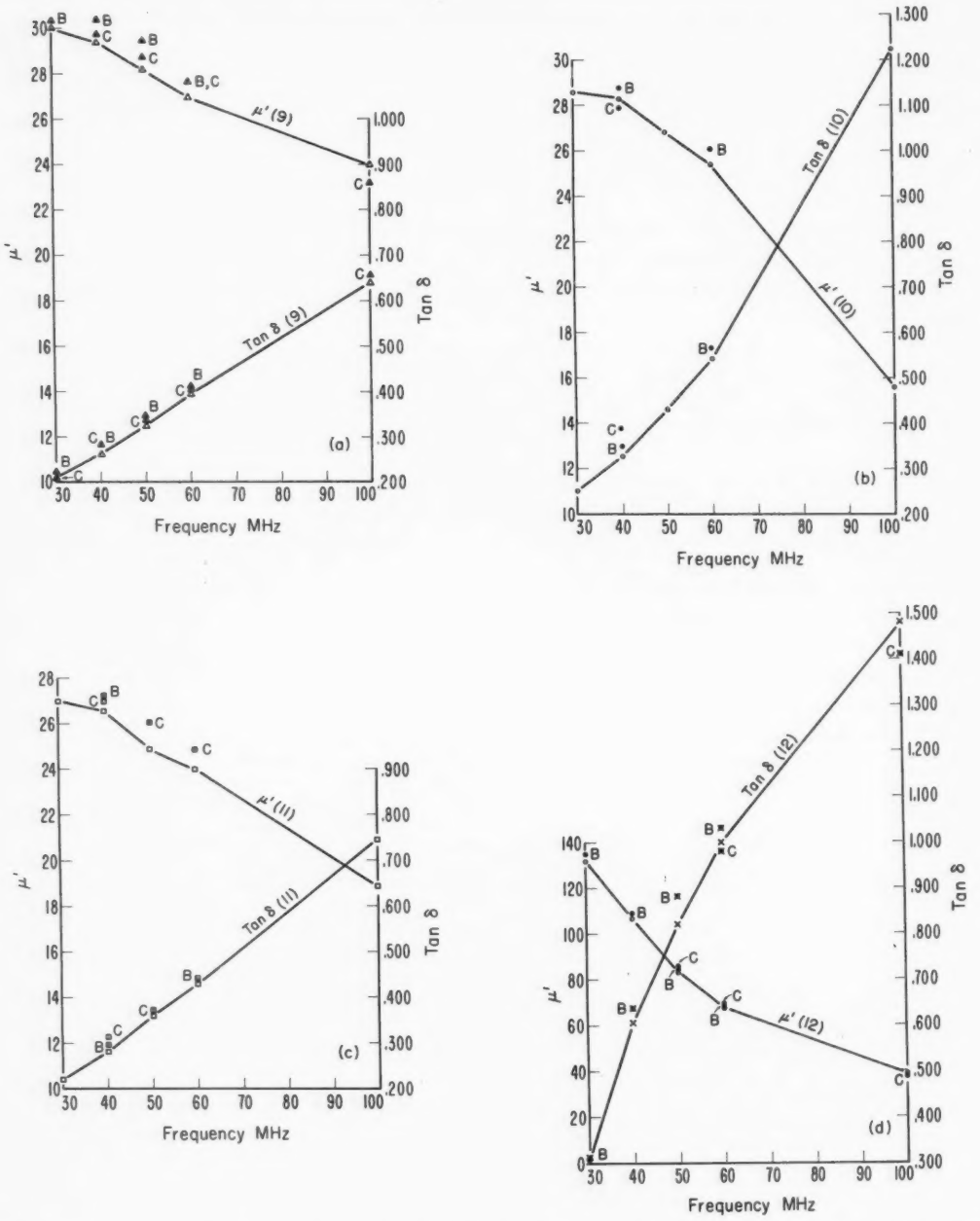

FIGURE 4. *Permeability (μ') and loss tangent ($\tan \delta = \mu''/\mu'$) versus frequency (MHz) of lossy materials using the admittance meter (A), the permeameter (B), and coaxial cavity (C).*

These data are also found in table 2.

TABLE 2. *Initial permeability (μ') and loss tangent ($\tan \delta = \mu''/\mu'$) of "lossy" materials using the admittance meter compared to other techniques*

Equations (2), (3), (6), and (8) of the text were used with the changes of eqs (2) and (3) indicated in assumption 3. The L_3 value calibrated at 30 MHz was used for all the admittance meter data.

Frequency	Method*	Sample 9		Sample 10		Sample 11		Sample 12	
		μ'	$\tan \delta$	μ'	$\tan \delta$	μ'	$\tan \delta$	μ'	$\tan \delta$
30 MHz	A	30.0	0.212	28.6	0.252	27.0	0.222	132	0.302
	B	30.4	.221					135	.310
	C	30.9 (28 MHz)	.206						
40	A	29.4	.262	28.3	.327	26.6	.283	107	.605
	B	30.4	.281	**28.8	**.349	**27.2	**.296	109	.635
	C	29.8	.283	27.9	.390	27.0	.314		
50	A	28.2	.326	26.8	.431	24.9	.360	83.4	.819
	B	29.5	.345					84.8	.881
	C	(1) 28.8	.332			26.1	.371	85.7	.816
		(2) 28.7	.344						
60	A	27.0	.395	25.4	.543	24.0	.431	68.1	.999
	B	27.7	.406	**26.1	**.566	**24.9	**.442	68.3	1.03
	C	27.7	.400					69.2	0.983
100	A	24.0	.640	15.6	1.22	18.9	.747	38.8	1.48
	B								
	C	(1) 23.2	.646					37.2	1.47
		(2) 23.25	.666					39.8	1.36

*Method A – Admittance meter.
**Method B – RF permeameter-Schering bridge or Q-meter (the permeameter is a calibrated transformer in which the sample is part of the secondary).
Method C – Adjustable length coaxial cavity. See second footnote of table 1.

"lossy" materials. It is seen that there is relatively good agreement between the admittance meter data and data using the other techniques from 30 to 100 MHz. At 100 MHz, the impedance transformation affecting μ' and tan δ values of sample 12 in a precision 50 Ω line of equivalent length to the coupling loop is ~ 10 percent and ~ 5 percent, respectively. It is pointed out that the 30 MHz calibration of L_3 was used to 100 MHz. The agreement of the data is better than the percentages just given implying that some errors cancel in the system described.

The authors thank Clarence C. Cook and Robert A. Lawton for valuable discussions with them, and Leonard B. Schmidt for making some measurements.

4. References

[1] R. A. Soderman, Impedance measurements in the 50 to 2000 Mc range, Radio & Television News **46,** Radio-Electronic Engineering Section, 3–6, 25 (July 1951).

[2] R. D. Harrington, Cavity techniques for permeability measurements in the VHF region, Proc. Electronic Components Conf., 27–29 (May 1955).

[3] R. D. Harrington and A. L. Rasmussen, Magnetic core permeability measurement techniques, Magnetic Core Conf., Proc. **7,** 11–24 (June 1965).

5. Appendix A

Assuming lumped circuit conditions, eqs (2) and (3) in the text for the sample inductance (L) and sample resistance (R) are derived as follows. K_1 and Y_1 are held constant and loops 2 and 3 are adjusted for the conditions with and without a sample in line 3.

Without a sample in line 3, we have

$$K_1Y_1 + K_2Y_2 + K_3Y_3 = 0. \tag{A1}$$

With a sample in line 3, we have

$$K_1Y_1 + K_2'Y_2 + K_3'Y_3' = 0. \tag{A2}$$

Subtracting eq (A1) from eq (A2), we have

$$(K_2'-K_2)Y_2+K_3'Y_3'-K_3Y_3=0 \tag{A3}$$

where

$$Y_2=\frac{1}{R_2+j\omega L_2}=\frac{R_2-j\omega L_2}{R_2^2+\omega^2L_2^2} \tag{A4}$$

$$Y_3=\frac{1}{R_3+j\omega L_3}=\frac{R_3-j\omega L_3}{R_3^2+\omega^2L_3^2} \tag{A5}$$

$$Y_3'=\frac{1}{(R_3+R)+j\omega(L_3+L-L_a)}=\frac{R_3+R-j\omega(L_3+L-L_a)}{(R_3+R)^2+\omega^2(L_3+L-L_a)^2}. \tag{A6}$$

Separating the real and imaginary parts in eqs (A4), (A5), and (A6) and substituting them in eq (A3), we have

$$(K_2'-K_2)\frac{R_2}{R_2^2+\omega^2L_2^2}+K_3'\frac{(R_3+R)}{(R_3+R)^2+\omega^2(L_3+L-L_a)^2}-K_3\frac{R_3}{R_3^2+\omega^2L_3^2}=0 \tag{A7}$$

and

$$(K_2'-K_2)\frac{L_2}{R_2^2+\omega^2L_2^2}+K_3'\frac{(L_3+L-L_a)}{(R_3+R)^2+\omega^2(L_3+L-L_a)^2}-K_3\frac{L_3}{R_3^2+\omega^2L_3^2}=0. \tag{A8}$$

From eqs (A7) and (A8) we get

$$K_3'\frac{(R_3+R)}{(R_3+R)^2+\omega^2(L_3+L-L_a)^2}=K_3\frac{R_3}{R_3^2+\omega^2L_3^2}-(K_2'-K_2)\frac{R_2}{R_2^2+\omega^2L_2^2} \tag{A9}$$

and

$$K_3'\frac{(L_3+L-L_a)}{(R_3+R)^2+\omega^2(L_3+L-L_a)^2}=\frac{K_3L_3}{R_3^2+\omega^2L_3^2}-(K_2'-K_2)\frac{L_2}{R_2^2+\omega^2L_2^2}. \tag{A10}$$

Equations (A9) and (A10) yield

$$\frac{R_3+R}{K_3\dfrac{R_3}{R_3^2+\omega^2L_3^2}-(K_2'-K_2)\dfrac{R_2}{R_2^2+\omega^2L_2^2}}=\frac{L_3+L-L_a}{K_3\dfrac{L_3}{R_3^2+\omega^2L_3^2}-(K_2'-K_2)\dfrac{L_2}{R_2^2+\omega^2L_2^2}}. \tag{A11}$$

Solving for (L_3+L-L_a) in eq (A10) after substituting the expression for (R_3+R) found from eq (A11), we have

$$L_3+L-L_a=\frac{\dfrac{K_3'}{K_3}\left(\dfrac{L_3}{R_3^2+\omega^2L_3^2}-\dfrac{(K_2'-K_2)}{K_3}\dfrac{L_2}{R_2^2+\omega^2L_2^2}\right)}{\left(\dfrac{R_3}{R_3^2+\omega^2L_3^2}-\dfrac{(K_2'-K_2)}{K_3}\dfrac{R_2}{R_2^2+\omega^2L_2^2}\right)^2+\omega^2\left(\dfrac{L_3}{R_3^2+\omega^2L_3^2}-\dfrac{(K_2'-K_2)}{K_3}\dfrac{L_2}{R_2^2+\omega^2L_2^2}\right)^2}. \tag{A12}$$

Substituting (L_3+L-L_a) from eq (A12) into eq (A11) we get

$$R_3+R=\frac{\dfrac{K_3'}{K_3}\left(\dfrac{R_3}{R_3^2+\omega^2L_3^2}-\dfrac{(K_2'-K_2)}{K_3}\dfrac{R_2}{R_2^2+\omega^2L_2^2}\right)}{\left(\dfrac{R_3}{R_3^2+\omega^2L_3^2}-\dfrac{(K_2'-K_2)}{K_3}\dfrac{R_2}{R_2^2+\omega^2L_2^2}\right)^2+\omega^2\left(\dfrac{L_3}{R_3^2+\omega^2L_3^2}-\dfrac{(K_2'-K_2)}{K_3}\dfrac{L_2}{R_2^2+\omega^2L_2^2}\right)^2}. \tag{A13}$$

If line 3 without a sample has low-loss, $\omega L_3 \gg R_3$ and $\omega^2 L_3^2 \gg R_3^2$, the latter being a correct approximation for even a lossy line; consequently, R_3 and R_3^2 may be neglected.

If line 2 and R_2 have a VSWR ≈ 1.005, L_2 and $\omega^2 L_2^2$ may be neglected for $R_2^2 \gg \omega^2 L_2^2$.

Therefore eqs (A12) and (A13) become

$$L_3 + L - L_a = \frac{\dfrac{K_3'}{K_3}\left(\dfrac{1}{\omega L_3}\right)}{\omega\left[\left(\left(\dfrac{K_2' - K_2}{K_3}\right)\dfrac{1}{R_2}\right)^2 + \left(\dfrac{1}{\omega L_3}\right)^2\right]}$$

$$R_3 + R = \frac{-\dfrac{K_3'}{K_3}\left(\dfrac{K_2' - K_2}{K_3}\right)\dfrac{1}{R_2}}{\left(\left(\dfrac{K_2' - K_2}{K_3}\right)\dfrac{1}{R_2}\right)^2 + \left(\dfrac{1}{\omega L_3}\right)^2}$$

which are eqs (2) and (3) in the text.

It should be noted that if R_3 cannot be neglected, but if $\omega^2 L_3^2 \gg R_3^2$ then

$$\frac{R_3}{R_3^2 + \omega^2 L_3^2} \approx \frac{R_3}{\omega^2 L_3^2}$$

which is the approximation leading to the correction mentioned in assumption (3) in the text following eqs (2) and (3).

(Paper 72C1-270)

JOURNAL OF RESEARCH of the National Bureau of Standards—C. Engineering and Instrumentation
Vol. 72C, No. 1, January–March 1968

Publications of the National Bureau of Standards*

Selected Abstracts

Analytical coordination chemistry; titrimetry, gravimetry, flame photometry, spectrophotometry, gas evolution and isotopic preparations, July 1965 to June 1966, Ed. O. Menis, *Tech. Note 402 (July 21, 1967), 50 cents.*

Studies in four areas of analytical chemistry: titrimetry, gravimetry, flame emission and atomic absorption, and solution spectrophotometry, are described from the standpoint of analytical coordination chemistry and applications to NBS standard reference materials. In the first two competences these investigations dealt with spectrophotometric titrations and homogeneous precipitation methods. Advances are described in the latter two areas through the unique applications of ternary complexes, displacement reactions in metal-ligand systems and the use of complexing media as "releasing agents." This approach is described for the determination of nanogram quantities of Sb, Cu, Ni, and Au in very high purity zinc by both spectrophotometric and flame procedures. Also in flame emission and atomic absorption a current table is presented for the detection limits of 70 elements. Progress of a new method is reported for the simultaneous determination of Ni, Cu, and Co by the dimethylglyoxime method. Descriptive tables of results are also given for ferrous, non-ferrous and ceramic materials which were analyzed by one of the four competences. In Another analytical area dealing with the analysis of gases in metals results of homogeneity and precision studies lead to certification of three new ferrous SRM's for their oxygen content. Also reported are the initial investigations of pyrohydrolytic separations of fluoride, nitrides and boron, separations of molybdenum from tungsten, controlled potential coulometric titration of molybdenum, and a description of improved instrumentation in flame emission and atomic absorption. Finally data are given on the preparation of stoichiometric mixtures of uranium oxide of varied isotopic composition and a list describing the variety of special analyses is included.

Key Words: Spectrophotometric titration, controlled potential coulometric, molybdenum, homogeneous precipitation, aluminum, beryllium, thermoanalytical standards, tricalcium silicate, spectrophotometry, antimony, high precision determination of nickel, simultaneous determination copper, cobalt, "releasing agents" in flame emission and atomic absorption, magnesium, ferrous SRM's, stoichiometric mixtures uranium oxide, isotope ratio determination.

Calorimetry, C. T. Armstrong, *1967 McGraw-Hill Yearbook of Science and Technology, pp. 124–127 (1967).*

The present status of calorimetry is reviewed. Several new and promising instruments for accurate calorimetry and the development of new or improved techniques for calorimetric processes are discussed. The relationship of calorimetry to the U.S. fuel technology, to the rocket propellant program, and to molecular biophysics is briefly discussed.

Key Words: Calorimetry, international, calorimetry, review, fuel calorimetry, calorimetry: biological, calorimetry: new developments.

Drawings of micrometer U-tube manometers for the ranges up to 100 mm of mercury, A. M. Thomas and J. L. Cross, *Tech. Note 420 (Aug. 26, 1967), 15 cents.*

Drawings with sufficient detail are presented so that micrometer U-tube manometers for use with mercury, oil, and water may be constructed. Measurements made with the oil manometer have an uncertainty of about 4×10^{-4} mm of Hg plus one part in 10^4 of the reading. Measurements made with the mercury manometer have an uncertainty of about 4×10^{-3} mm of Hg plus eight parts in 10^5 of the reading. The operation and an error analysis are described elsewhere.

Key Words: Manometer, micrometer, U-tube, vacuum, medium-vacuum measurements.

NBS standard frequency and time services, radio stations WWV, WWVH, WWVB, WWVL, *Misc. Publ. 236, 1967 Edition (1967), 15 cents.*

Detailed descriptions are given of eight technical services provided by the National Bureau of Standards radio stations WWV, WWVH, WWVB, and WWVL. These services are: 1. Standard radio frequencies; 2. Standard audio frequencies; 3. Standard musical pitch; 4. Standard time intervals; 5. Time signals; 6. UT2 corrections; 7. Radio propagation forecasts; and 8. Geophysical alerts. In order to provide users with the best possible services, occasional changes in the broadcasting schedules are required. This publication shows the schedules in effect on June 1, 1967. Annual revisions will be made. Advance notices of changes occurring between revisions will be sent to regular users of these services upon request. Current data relating to standard frequencies and time signals are also available monthly in the Time and Frequency Services Bulletin.

Key Words: Broadcast of standard frequencies, high frequency, low frequency, standard frequencies, time signals, very low frequency.

Standard Reference Materials: Mössbauer spectroscopy standard for the chemical shift of iron compounds, J. J. Spijkerman, D. K. Snediker, F. C. Ruegg, and J. R. DeVoe, *Misc. Publ. 260–13 (July 28, 1967), 40 cents.*

The preparation, calibration, and use of the Standard Reference Material for chemical shift of iron compounds in Mössbauer Spectroscopy is described. This standard is a properly oriented single crystal of sodium pentacyanonitrosylferrate (II) dihydrate (sodium nitroprusside). Primary standards were calibrated with a high accuracy optical Mössbauer spectrometer and secondary calibrations were made with a tandem Mössbauer spectrometer. The midpoint between the two absorption peaks in the spectrum at 25.0 °C provide a useful velocity scale calibration of the spectrometer. Descriptions of the spectrometers used and the error analysis associated with the data are given. Suggested format for reporting Mössbauer spectra and their parameters is also presented.

Key Words: Mössbauer, spectroscopy, standard, differential chemical shift, quadrupole splitting, random error, systematic error, sodium nitroprusside, iron compounds, optical Mössbauer spectrometer, tandem Mössbauer spectrometer, velocity calibration.

Standard Reference Materials: Recommended method of use of standard light-sensitive paper for calibrating carbon arcs used in testing textiles for colorfastness to light, E. Passaglia and P. J. Shouse, *Misc. Publ. 260–15 (July 21, 1967), 20 cents.*

**Publications for which a price is indicated are available by purchase from the Superintendent of Documents, U.S. Government Printing Office, Washington, D.C. 20402 (foreign postage, one-fourth additional). The NBS nonperiodical series are also available from the Clearinghouse for Federal Scientific and Technical Information, Springfield, Va. 22151. Reprints from outside journals and the NBS Journal of Research may often be obtained directly from the authors.*

The use of NBS light-sensitive paper and NBS booklets of standard faded strips in the standardization of fading lamps is described. These lamps are used to determine the fading characteristics of textiles, and the light-sensitive paper is thus useful in standardizing this procedure.

Key Words: Light-sensitive paper; Booklets of faded strips; fading characteristics; textiles; fading standardization.

Revision of the NBS tables of spectral-line intensities below 2450 Å, C. H. Corliss, *Mono. 32 Supplement (July 7, 1967), 30 cents.*
A calibration is applied to the intensity measurements of the 1400 lines below 2450 Å in the NBS Tables of Spectral-Line Intensities. Tables of the new values are presented with the lines arranged by elements and by wavelengths.

Key Words: Atomic spectra, intensities, spectral lines, ultraviolet.

Thermal-shock resistance for built-up membranes, W. C. Cullen and T. H. Boone, *Bldg. Sci. Series 9 (Aug. 21, 1967), 20 cents.*
The resistance of bituminous built-up roofing membranes to thermally induced forces is considered in terms of their strength properties such as breaking load in tension, modulus of elongation and apparent linear thermal expansion coefficient. The development of a Thermal-Shock Resistance Factor is described and values are given for three bituminous built-up membranes at temperatures of −30 °F (−34.4 °C), 0 °F (−17.8 °C), 30 °F (−1.1 °C) and 73 °F (22.8 °C). The apparent relation between the values obtained in the laboratory and the observed performance of roofing membranes in service is considered. The utilization of the Thermal-Shock Resistance Factor in the reduction of potential failures of bituminous built-up roofing membranes in service from thermally induced forces is also discussed.

Key Words: Development, roofing membrane, strength properties, thermally induced forces, thermal-shock resistance factor.

The single-engine Claude cycle as a 4.2 °K refrigerator, R. C. Muhlenhaupt and T. R. Strobridge, *Tech. Note 354 (June 1, 1967),* 45 cents.
The performance of the 4.2 °K Claude-cycle refrigerator has been computed taking into account the efficiencies of the various components. The results are presented in graphical form. These charts give the input power requirements, mass flow rates for both the compressor and expander, pertinent temperatures, and allow selection of the optimum high pressure for a given set of component characteristics.

Key Words: Claude, cyrogenics, refrigeration.

Part 1. The solid system. II. Numeric compression, P.A.D. deMaine, K. Kloss, and B. A. Marron, *Tech. Note 413 (Aug. 15, 1967), 30 cents.*
This part of NBS Technical Note 413 describes the general NUMERIC COMPRESSOR (NUPAK) Algorithm for automatically compressing (encoding) or decoding compressed numerical information, which may of course have come from graphical information. The amount of compression achieved is determined by the "lowest limit of significance," the range, and the sequential patterns of the data to be stored. The encoded information can be stored in memory or on external storage devices in a small fraction of the space normally required, and can be expanded (decoded) item-by-item whenever needed by the system.

Key Words: Numeric compression, information handling, high-speed information transmission, information storage and retrieval, systems analysis.

Part 2. The solid system. III. Alphanumeric compression, P. A. D. deMaine, K. Kloss, and B. A. Marron, *Tech. Note 413 (Aug. 15, 1967), 30 cents.*
An algorithm for compressing alphanumeric information is described. Unlike other methods which depend upon frequency of occurrence of words in a particular class of publications, this scheme is language and content independent since the information for compression is obtained from the text itself. The compressed bit stream is preceded by sufficient information for automatic reconstruction of the original bit stream whenever the system requires it. Even with this additional information required for expansion, compression rates approaching 40% have been achieved. Because this ALPHANUMERIC COMPRESSOR (ANPAK) is fully automatic and self-organizing, it can operate on information which has already been compressed via the NUMERIC COMPRESSOR (NUPAK).

Key Words: Alphanumeric compression, information handling, high-speed information transmission, information storage and retrieval, systems analysis.

Determination of trace elements in standard reference materials by neutron activation analysis, G. W. Smith, D. A. Becker, G. J. Lutz, L. A. Currie, and J. R. DeVoe, *Anal. Chim. Acta* **38,** *333–340 (1967).*
Neutron activation analysis with its high sensitivity and accuracy in trace analysis, is being used at the NBS for analysis of Standard Reference Materials. Problems affecting precision and accuracy have been encountered and solutions to four problems are discussed. First, the positive bias introduced by induced radioactivity of similar gamma-ray energy was found in the determination of interstitial argon in ultra-pure silicon. A decay curve resolution technique was used to compensate for the error. Secondly, errors due to differences in geometrical location between sample and standard during irradiation were observed. Flux gradients were determined by copper foil flux monitoring to give necessary means of correction. Thirdly, errors are caused by differences in neutron self-shielding between sample and standard during irradiation. An empirical correction method was used and computer program written for calculation. Examples are given. Finally, the problem of gamma-ray attenuation during counting of sample and standard has been explored. A theoretical and experimental study gives the necessary corrections. It is concluded that careful study is vital to assure accurate analyses by neutron activation analysis on trace elements in complex matrices such as many Standard Reference Materials.

Key Words: Neutron, activation, analysis, trace, Standard Reference Materials, accuracy, precision, similar gamma-ray energy, decay curve resolution, geometrical location, neutron self-shielding, gamma-ray attenuation.

Distillation as a tool for purification of research quantities of material, R. T. Leslie, *Ann. N. Y. Acad. Sci.* **137,** *19–29 (1966).*
Distillation can increase the purity of nearly any vaporizable mixture if sufficient effort is made. The method is invaluable for purifying relatively small quantities of material for research purposes.
The selection of the proper still column for a particular problem can be based on a knowledge of the characteristics of a few basic types of columns. Some operating procedures which favor good results can be outlined in a general way, but testing of stills by the operator using mixtures whose behaviors can be predicted under various conditions is recommended.
Some possibilities for the improvement of still columns is suggested.

Key Words: Distillation, material, purification of research quantities of materials, research quantities.

Gas phase radiolysis of cyclobutane, R. D. Doepker and P. Ausloos, *J. Chem. Phys.* **44,** *1641–1647 (Feb. 1966).*
The gas phase radiolysis of cycle-C_4H_8 and cyclo-C_4D_8 has been investigated in the presence of O_2, NO, H_2S, NH_3, and several organic compounds. From the products formed, it could be inferred that the following fragmentation processes occur:

$$C_4H_8^+ - C_3H_5^+ + CH_3$$
$$C_4H_8^+ - C_2H_4^+ + C_2H_4$$
$$C_4H_8^+ - C_2H_5^+ + C_2H_3$$
$$C_4H_8^+ - C_3H_4^+ + CH_4.$$

At 20 torr, the ion pair yields which can be ascribed to some of these processes are lower than the corresopnding ion pair yields observed in the mass spectrometer at a pressure of 10^{-5} torr.
When compounds such as NO (I.E. = 9.25 eV) or $(CH_3)_3N$ (I.E. = 7.8 eV) are added to cyclobutane, butene (I.E. = 9.13 − 9.58 eV) is a major product. On the other hand, when organic or inorganic compounds whose ionization energy is higher than that of butene

are added to cyclobutane, the yield of butene is, in most cases, negligibly small. The formation of butene can be tentatively accounted for by a ring opening of the parent ion followed by charge transfer. On the basis of this mechanism, a minimum value of 0.42 with an estimated possible deviation of ± 0.02 can be ascribed to $M(C_4H_8^+)/N$.
When an electrical field is applied in the saturation current region, during radiolysis of cyclobutane-NO mixtures, the yields of methane, ethane and butene which have the parent ion or fragments thereof as precursors, remain unchanged. On the other hand, the yields of products such as ethylene, allene, acetylene, and 1,3-butadiene whose formation is, in part, attributed to the decomposition of neutral excited molecules, are seen to increase due to increased excitation by electron impact. In the absence of an electrical field, the number of neutral excited molecule decompositions per ion pair is estimated to be $\leq 0.65 \pm 0.05$.

Key Words: Cycloalkanes; ion-molecular reactions; ion-pair yields; radiolysis; unimolecular decomposition.

Investigating ion-molecule reactions by analyzing neutral products formed in the radiolysis and photoionization of hydrocarbons, P. Ausloos, S. G. Lias, and A. A. Scala, *Adv. Chem. Ser.* **58,** *264–277 (1966).*
The analysis of neutral products produced in the radiolysis and photoionization of suitable deuterium labeled hydrocarbons or hydrocarbon mixtures provides information concerning: a) the relative rates of H^+, H^-, H_2^-, and H_2-transfer reactions; and b) the structure of the reacting ion or reaction complex. The reaction cross section of a given ion with various alkalanes is generally seen to increase with increasing polarizability of the neutral molecule. The actual increase in rate is, however, faster than that of the collision cross section given by the expression: $2\pi e(\alpha/\mu)^{1/2}$. Good quantitative and qualitative correspondence is seen between the information on reactions of parent ions obtained from gas phase radiolysis studies and that derived from photoionization experiments carried out at wavelengths slightly above the ionization energy of the molecule.

Key Words: Analysis of neutral products, ion-molecule reactions, neutral products, photoionization of hydrocarbons, radiolysis and photoionization of hydrocarbons.

Microtexture and composition of reaction products in the system kaoline-lime-water, W. C. Ormsby and L. A. Bolz, *J. Am. Ceram. Soc.* **49,** *No. 7, 364-366 (July 1966).*
Textural and compositional features of reaction products in the kaolin-lime-water system were examined by electron microscopy and electron diffraction. Electron micrographs of replicas of fracture surfaces of compacted mixtures and transmission electron micrographs of powdered compacts showed considerable attack of kaolinite particles by hydrated lime and indicated the formation of significant amounts of calcium silicate hydrate phases. Electron diffraction of reaction products confirmed the presence of calcium silicate hydrates. The presence of these hydrates is undoubtedly responsible for the stabilizing effects of lime which have previously been reported in the literature.

Key Words: Calcium silicate hydrates, composition, electron diffraction, electron microscopy, kaolin-lime-water, microtexture.

Microwave spectroscopy, D. R. Lide, Jr., *Encyclopedia of Industrial Analysis 2, 600–611 (John Wiley & Sons, Inc., New York, N.Y., 1966).*
The experimental techniques used in microwave spectroscopy are described. A brief outline of the theory of rotational spectra is given. The information on molecular structure which can be obtained from microwave studies is discussed. Some comments are made on the use of microwave spectroscopy in chemical analysis.

Key Words: Chemical analysis, microwave spectroscopy, microwave studies, molecular structure, rotational spectra, spectra-rotational, spectroscopy-microwave.

Mössbauer spectroscopy: applications to aerospace, J. R. DeVoe and J. J. Spijkerman, *Book, Radioisotopes for Aerospace, Part 2, Systems and Applications, pp. 254–269 (Plenum Press, Inc., New York, N.Y., 1966).*
The principle of the Mössbauer Effect will be discussed. A few possible applications of the technique with respect to physics and engineering in aerospace will be outlined. Of greater interest are the possible applications of the technique for determining chemical structure and solid state properties of materials. Solid phase transitions of materials subjected to severe conditions similar to that existing in space can be measured by Mössbauer Effect.
The National Bureau of Standards' Mössbauer spectrometer will be discussed and some data taken on a number of materials (such as tecktites, steels, glasses, and metal alloys) will be presented.

Key Words: Aerospace, applications, materials structure analysis, Mössbauer effect, spectrometer, standards.

Needs of American Chemical Society members for property data, H. M. Weisman, *J. Chem. Doc.* **7,** *No. 1, 10–14 (Feb. 1967).*
In August of 1965 the American Chemical Society, on behalf of the NBS Office of Standard Reference Data, sent a questionnaire to its membership asking for information on their needs for compilations of critically evaluated data. Through this questionnaire, the Office of Standard Reference Data obtained information on the preferences and needs of the chemical profession for data compilations, and equally importantly, located a substantial number of compilation activities of which it was not aware. Further, the Office of Standard Reference Data identified dozens of individuals who are both interested and competent to undertake additional projects. Approximately 16,000 replies were received. Overwhelmingly, response was that present compilations of data satisfy poorly or at best only moderately the requirements of the membership of ACS. The survey identified the properties which ACS workers most often sought in the literature as well as those data compilations most often consulted by respondents. Many worthwhile comments and suggestions were contributed as to approaches taken, compilation priorities and techniques of format and presentation.

Key Words: American Chemical Society, chemical and physical properties, compilation, data, NSRDS, Office of Standard Reference Data, questionnaire, survey, users.

Radiation and photochemistry, P. Ausloos, *Ann. Rev. Phys. Chem.* **17,** *205–236 (1966).*
A critical review of major publications on Photochemistry and Radiation Chemistry published in 1965.

Key Words: Photochemistry, radiation chemistry.

Sublimation, E. C. Kuehner and R. T. Leslie, *Encyclopedia of Industrial Chemical Analysis* **3,** *573–584 (1966).*
Sublimation is considered analogous to distillation and their advantages are compared. Methods of sublimation and types of sublimators are discussed. A section on sublimation analysis is included in which characteristics of a solid substance, such as condensation temperatures, are applied to the identification and quantitative analysis of material.

Key Words: Analogous distillation, analysis-sublimation, condensation temperatures, solid substance, sublimation, sublimators.

Simultaneous determination of copper and zinc in human lung tissue by neutron activation analysis, R. G. Keenan, J. H. Marcus, and J. R. DeVoe, *Am. Ind. Hygiene Assoc. J.* **27,** *128–134 (Mar.–Apr. 1966).*
Certain trace elements including copper and zinc are constituents of numerous enzymes and function as essential catalysts in biosyntheses. The expanded interest in these substances has supplied a demand for microanalytical techniques of increased sensitivity, accuracy and precision if meaningful conclusions are to be derived from the analytical data. This paper shows that good precision may be realized in the activation analysis of complex biological specimens with only a few one-step chemical separations.
The nuclear reactions Cu^{63} (n, γ) Cu^{64} (12.8h) and Zn^{68} (n, γ) Zn^{69m} (13.8h) were used for the analysis. The samples were irradiated in a thermal neutron flux of 10^{13} n/cm^2/sec. The copper was extracted as the acetylacetonate into chloroform from an acetate system buffered at a *p*H of 4.75. The remaining aqueous phase was extracted with chloroform to remove most of the acetylacetone dissolved in

the aqueous phase. The zinc was extracted as the dithizonate into chloroform and was back-extracted into 1% HCl for counting. Careful internal standardization was used for correction of results for variation in chemical yields.
Applications of the method to the simultaneous determination of copper and zinc in lung samples provided values of the same order of magnitude as those reported by Tipton and Cook for U.S. adults using emission-spectrographic procedures which were between 7 and 10 ppm for copper and 40 and 70 ppm for zinc. Comparison of the precision of this method with that of emission spectroscopy indicates that this activation technique has at least three times better precision.

Key Words: Biosynthesis, catalysis in biosynthesis, copper, human lung tissue, lung tissue, neutron-activation analysis.

Systematic errors in "recovery" and "detection" efficiency as related to radiochemical analysis, L. A. Currie, *Proc. 11th Annual Bio-Assay and Analytical Chemistry Meeting, Albuquerque, New Mexico, Oct. 7–8, 1965, AEC No. 651008, pp. 35 (Clearinghouse for Federal Scientific and Technical Information, Springfield, Va., 1967).*
Evidence of systematic error in the assay of thorium arose when the chemical yield from a biological sample seemed to depend upon the detection method. When α-counting and spectrophotometry were applied to different aliquots of the same sample, following chemical purification, the discordant chemical yields pointed to variations in detection efficiency. The difficulty arises because determination of the chemical yield is based upon the known disintegration rate of a "spike" which has been chemically processed, and upon the detection efficiency, which is generally determined by means of a standard which may not have been chemically processed. Thus, if the nature of the original sample or the resultant material in any way influences the final detection efficiency, the calculated recovery and its relative variance must be incorrect. Systematic errors in recovery and detection efficiency may be eliminated in one of two ways: (1) direct measurement of the "overall" yield—the product of chemical yield and detection efficiency, (2) accurate determination of both the chemical yield and the detection efficiency by such methods as isotope dilution and internal (efficiency) monitoring, respectively. Experimental illustrations are given for analyses of thorium and of carbon-14.

Key Words: Radiochemical analysis, bio-assay, systematic errors, random errors, thorium chemical yield, detection efficiency, "overall" yield, isotope dilution, carbon-14.

The crystal structure of sodium tetraborate, A. Hyman, A. Perloff, F. Mauer, and S. Block, *Acta Cryst.* **22,** *No. 6, 815–821 (June 1967).*
Single crystals of sodium tetraborate, $Na_2O \cdot 4B_2O_3$, have been synthesized and studied. The structure has been determined using the method of symbolic addition. The space group is $P2_1/a$ with unit cell dimensions: $a = 6.507 \pm 0.001$, $b = 17.796 \pm 0.002$, $c = 8.377 \pm 0.001$, and $\beta = 96°34' \pm 2'$; $Z = 4$. The structure consists of two infinite, independent, and interlinking boron-oxygen networks, each containing alternating single and double rings. The sodium atoms serve to hold the networks together through coordination with oxygen atoms.

Key Words: Boron-oxygen networks, double ring, sodium tetraborate.

Thermal decomposition of 4,4-dimethylpentene-1 in a single-pulse shock tube, W. Tsang, *J. Chem. Phys.* **46,** *No. 7, 2817–2822 (Apr. 1, 1967).*
4,4-Dimethylpentene-1 has been pyrolyzed in a single pulse shock tube. The initial process is apparently the breaking of the allylic carbon-carbon bond. The rate expression for the reaction,

$$C_4H_9-C_3H_5 \xrightarrow{k} t\text{-}C_4H_9\cdot + C_3H_5\cdot$$

has been found to be

$$k = 10^{15.8} \exp(-65{,}500/RT) \text{ sec}^{-1}.$$

Assuming no activation energy for the recombination process this leads to a value of 12 kcal for the allylic resonance energy.

Key Words: 4,4-dimethylpentene-1, allyl radicals, *t*-butyl radicals, thermal decomposition, bond energy, allylic resonance energy, single pulse shock tube, 1-butene, 4-methylpentene-1, 1,5 hexadiene.

Two National Bureau of Standards data centers: chemical kinetics and mass spectrometry, D. Garvin and H. M. Rosenstock, *J. Chem. Doc.* **7,** *No. 1, 31–34 (Feb. 1967).*
Two current information retrieval centers, one for chemical kinetics, the other for mass spectrometry are described. The methods and philosophies of operation of these programs are compared. The role of specialized information systems in promoting data evaluation, the evaluation of their usefulness as sources for reference material, the choice of techniques and possibilities for inter-center coordination are discussed.

Key Words: Chemical kinetics, mass spectrometry, information retrieval.

A new ultra-low-frequency bridge for dielectric measurements, W. P. Harris, *1966 Annual Report, Conf. Electrical Insulation and Dielectric Phenomena, National Academy of Sciences—National Research Council, Mount Pocono, Pennsylvania, 1966, pp. 72–74 (1967).*
This *is* an abstract of a talk given at the NAS–NRC Conference on Electrical Insulation and Dielectric Phenomena at Pocono Manor, Pennsylvania, October 4, 1966. It is to be included in the Annual Report of the Conference.

Keys Words: Bridge, dielectrics, dielectric measurements, electrical measurements, low frequency measurements, electrical, measurements, dielectric, ultra low frequency.

A 100 Mc/s 2 out of 3 gate, J. K. Whittaker, *Nucl. Instr. Methods* **45,** *No. 1, 138–140 (Nov. 1966).*
A zero-crossing type of discriminator with a very wide dynamic range and a short dead-time is described. When used with a 56 AVP photomultiplier with a linear dynode resistor chain, a light amplitude variation of at least 125:1 may be accommodated. The relative time shift of the output discriminator pulse is then only 200 p.s.

Key Words: Discriminator, zero-crossing, wide-range, time-invariant, picosecond, resolution.

A single axis, two crystal x-ray instrument, R. D. Deslattes, *Rev. Sci. Instr.* **38,** *No. 6, 815–820 (June 1967).*
Design features of a two crystal instrument capable of measurements of diffraction angles to of the order of 0.1 arc second are presented. The instrument is of simple geometry, employs a stable and massive chassis and derives its precision from components of general availability. Diffraction angles are generated in 1° increments by a precise indexing mechanism and interpolated by means of a sine arm driven by a micrometer.

Key Words: X-ray spectrometer, double crystal instrument, precise goniometry.

A testing and rating method for refrigerated trucks with respect to cooling load, P. R. Achenbach, C. W. Phillips, and R. W. Penny, *Annex to Proc. Intern. Inst. Refrigeration, Comm. VII, pp. 29–35 (London, England, Sept. 1966).*
A testing and rating method for refrigerated delivery trucks has been developed under the sponsorship of the U.S. Department of Agriculture and the Truck Body and Equipment Association. The method is applicable to insulated vehicles used for short-haul delivery of frozen food at a low temperature or fresh produce at a medium temperature. It involves a measurement of the steady-state transmission of heat from ambient air to cargo space under selected conditions of test and the use of a correction factor for the effect of solar radiation on a stationary vehicle. The essentials of the testing and rating procedure and of the laboratory studies carried out to develop the procedure are described.

Key Words: Air leakage, cooling load, refrigerated trucks, solar heating, testing and rating methods.

A two-crystal, vacuum monochromator, R. D. Deslattes, *Rev. Sci. Instr.* **38,** *No. 5, 616–620 (May 1967).*
Design and construction of a vacuum two crystal instrument for

high resolution spectroscopy at long wavelengths is reported. The instrument provides for coordinated rotations of both crystals source and detector. The usable scan range is 8° in Bragg angle and is limited only by the characteristics of the tangent drive system.

Key Words: X-ray spectrometer, vacuum instrument, double crystal instrument.

Air-to-air heat pumps for military housing, P. R. Achenbach, *Military Engr.* **384,** *270 (July–Aug. 1966).*
The National Bureau of Standards has performed laboratory and field studies of electric air-to-air heat pumps as a part of the technical investigations sponsored by the three agencies of the Department of Defense. These studies have developed information on the coefficient of performance and heating and cooling capacities of typical systems used for residential applications, design data useful for estimating energy usage and maximum power demand for similar installations, some information relative to the unexpectedly high rate of motor-compressor failure, and comparisons of the annual cost of year-around air conditioning using heat pumps and gas heating systems combined with conventional air conditioners for cooling. The annual cost of heating and cooling these military houses with air-to-air heat pumps averaged about $100 for a unit electric energy cost of 0.8¢/kWh.

Key Words: Air-to-air heat pumps, residential air conditioning, energy usage, annual energy cost.

An improved transportable 10 picofarad capacitor, R. D. Cutkosky and L. H. Lee, *Proc. 11e Session, Comite Con. D'Electricite, May 10–12, 1965, pp. 65–66 (May 1965).*
By design modifications improvements have been achieved in the performance of 10-pF capacitance standards with fused silica dielectric as regards voltage dependence, shock sensitivity, and stability of value. It is suggested that standards of the new design are suitable for interlaboratory comparisons of the unit of capacitance.

Key Words: Capacitance standards, fused silica dielectric, picofarad capacitor, shock sensitivity, stability of value, ten picofarad capacitor, transportable ten picofarad capacitor, unit of capacitance, volume dependence.

Comparison of the Hall-Petch parameters of zone-refined determined by the grain size and extrapolation methods, B. W. Christ and G. V. Smith, *Acta Met.* **15,** *809–816 (May 1967).*
The dependence of the lower yield strength of zone-refined iron containing 0.0020 wt. % (carbon plus nitrogen) on grain size has been investigated at room temperature. In spite of the rather limited grain size variation possible with such pure metal, a meaningful determination of the Hall-Petch parameters has been made by the grain-size method: friction stress -2.5 kg/mm^2, Petch slope -2.4 kg/mm$^{3/2}$. It is shown that tensile data obtained where the grain diameter is comparable to the minimum specimen dimension should not be included in the grain size method of analysis.
Analysis of tensile data by the extrapolation method produces Hall-Petch parameters which (1) are internally inconsistent, and (2) compare unfavorably with results of the grain size method. It is concluded that the extrapolation method in its present form is not an adequate substitute for the grain size method of evaluating the Hall-Petch parameters of iron.

Key Words: Extrapolation methods, grain size, Hall-Petch parameters, iron, zone-refined, parameters, zone-refined iron.

Discussion of the paper "flow in culverts and related design philosophies," J. L. French, *J. Hydraulics Div. Am. Soc. Civil Eng.* **93,** *No. HY1, 85–91 (Jan. 1967).*
An evaluation is made of certain conclusions advanced in a paper by Fred W. Blaisdell. The paper, entitled "Flow In Culverts And Related Design Philosophies" appeared in the Journal of the Hydraulics Division, American Society of Civil Engineers, March 1966. The present paper will form a discussion of Mr. Blaisdell's paper and will appear in a subsequent issue of the same publication.
The present discussion of Mr. Blaisdell's paper illustrates the use of tapered inlets in the design of culverts. The use of a minimum performance curve in the design of culverts is concluded to be acceptable, notwithstanding certain reservations advanced by Mr. Blaisdell. The concept of "balanced design" as applied to culverts is discussed in terms of the assessment of the risks of hydraulic overloading to the various component parts of the structure and it is concluded that the design rate of flow for the culvert and a structure or channel immediately downstream of the culvert need not be identical. And finally it was suggested that the experimental data so far presented have not demonstrated, beyond reasonable question, that the performance assigned to the hood-inlet is applicable at prototype size as well as at model size.

Key Words: Culverts, hydraulics, tapered inlets, hood inlets.

Five years of VLF worldwide comparison of atomic frequency standards, B. E. Blair, E. L. Crow, and A. H. Morgan, *Radio Sci.* **2,** *No. 6, 627–636 (June 1967).*
The VLF radio braodcasts of GBR(16.0 kHz), NBA(18.0 or 24.0 kHz), and NSS(21.4 kHz) have enabled worldwide comparisons of atomic frequency standards to parts in 10^{10} when received over varied paths and at distances up to 9000 or more kilometers. This paper summarizes a statistical analysis of such comparison data from laboratories in England, France, Switzerland, Sweden, Russia, Japan, Canada, and the United States during the 5-year period 1961–1965. The basic data are differences in 24-hr average frequencies between the local atomic standard and the received VLF radio signal expressed as parts in 10^{10}. The analysis of the more recent data finds the receiving laboratory standard deviations, $\hat{\alpha}_i$, and the transmission standard deviation, $\hat{\tau}$, to be a few parts in 10^{11}. Averaging frequencies over an increasing number of days has the effect of reducing $\hat{\alpha}_i$ and $\hat{\tau}$ to some extent. The variation of the $\hat{\alpha}_i$ with propagation distance is studied. The VLF–LF long-term mean differences between standards are compared with the recent portable clock tests, and they agree to parts in 10^{11}.

Key Words: Analysis of variance, atomic frequency standard errors, portable clock, VLF propagation.

The Bi I–II transition pressure measured with a dead-weight piston gage, P. L. M. Heydemann, *J. Appl. Phys.* **38,** *No. 6, 2640–2644 (May 1967).*
A dead piston gage was used to determine the Bismuth I–II transition pressure and the volume change at the transition. The transition pressure for one sample, believed to contain less than .001% impurities, was found to be $25{,}306 \pm 60$ bars. With another sample, of substantially less purity and of larger grain size, a transition pressure of $25{,}500 \pm 60$ bars was measured. The average relative volume change was .035.

Key Words: Free piston gage, bismuth, polymorphic phase transition, transition pressure, volume change, high pressure.

Performance criteria for building components and systems, P. R. Achenbach, *Proc. Porcelain Enamel Institute Forum, University of Illinois, Urbana, Ill., Sept. 28–30, 1966,* **28,** *176–195 (1966).*
The Building Research Division has conducted a number of technical investigations which led to the development of new test procedures for evaluating the significant performance requirements of building components and systems. These investigations have typically produced performance data which could be used by appropriate organizations in establishing criteria of acceptability. Laboratory studies of this type have been completed on underground heat distribution systems, ducts for heating and air conditioning systems, and sanitary plumbing fixtures and a similar study is in progress on exterior wall systems for residential buildings. In each of these studies the Building Research Division has collaborated with multidiscipline task groups of the Building Research Advisory Board of the National Academy of Sciences-National Research Council in developing the list of important performance characteristics in qualitative language. The work done on these projects is used to illustrate the sequence of activities required in developing performance criteria, the importance of collaboration among representatives of industry, professional societies, codes and standards organizations, and government bodies in selecting acceptable performance levels, the problems involved in devising adequate laboratory test procedures for building components made of widely-differing materials, and the incomplete state of administrative

procedures for implementation of performance criteria on a national scale.

Key Words: Performance characteristics, performance criteria, building components, laboratory procedures, codes, standards, specifications.

Transistorized current stabilizer for x-ray tubes with directly heated cathodes, K. W. Yee and R. D. Deslattes, *Rev. Sci. Instr.* **38,** *No. 5, 637–638 (May 1967).*
An instrument is described which stabilizes the emission current in x-ray tubes with directly heated cathodes. Transistors are used in the amplifier and loading circuits. Emission currents from 20 mA to 1A are maintained constant to within 0.1% for periods of about a half-hour.

Key Words: Emission, current, regulator, x-ray tube, controlled impedance, stabilizer.

Computer aided typesetting, W. R. Bozman, *Book, Advances in Computers,* **7,** *ch. 4, 195–207 (Academic Press, Inc., New York, N.Y., 1966).*
Several examples are given of typesetting prepared by a computer.

Key Words: Photocomposition, typesetting, computers, printing, automation, publication.

A comparator for thermal AC–DC transfer standards, R. S. Turgel, *Proc. 21st Annual ISA Conference and Exhibit, New York, N.Y., Oct. 24–27, 1966, ISA Preprint 12.3-1-66 (Oct. 1966).*
Thermal transfer standards play an important role in precision a-c measurements. They are calibrated by intercomparison with standards of known ac-dc difference. A comparator is described that simplifies such routine calibrations. A sequence of null balances in the measuring circuit operates a simple analog computer which indicates the result of the intercomparison directly in parts per million of ac-dc difference.

Key Words: A–C, D–C, calibration, transfer standard, thermoelement, intercomparison.

Calibration of the NBS photoelectric pyrometer of 1961, R. D. Lee, *Proc. 7th session, Comite Con. de Thermometrie, Paris, France, pp. 74–78 (Sept. 24, 1964).*
Factors affecting the reproducibility of the NBS Photoelectric Pyrometer are listed, and progress in reducing these factors are described. A calibration to realize the International Practical Temperature Scale (IPTS) above 1063 °C to 1256 °C is described. At present, the estimated uncertainty in realizing the IPTS is about 0.1 °C at 1063 °C, 0.2 °C at 1256 °C, and is predicted to be 0.8 °C at 2400 °C.

Key Words: Calibration-NBS photoelectric pyrometer of 1961, International Practical Temperature Scale, NBS photoelectric pyrometer, photoelectric pyrometer-NBS, pyrometer, photoelectric-NBS.

On long-term stability of Zener reference diodes, W. G. Eicke, Jr., and H. H. Ellis, *Proc. 11th Session, Comite Con. D'Electricite, May 10–12, 1965, pp. E–73–E–77 (May 1965).*
This paper gives a summary of a three year study of the stability of Zener Diodes either when operated intermittently or continuously. The diodes that were studied under intermittent use were in use for periods of 5 to 10 minutes with periods of two to four weeks between measurements. The diodes studied had normal voltage ranging from 8.1 to 9.2. The studies were conducted at 25.00 ± °C. The studies indicated that the Zener voltage gave stable output voltage to within 3 to 10 ppm over a three year period.

Key Words: Diodes-reference, long-term stability, reference diodes, Zener reference diodes.

Potential applications of the x-ray/density method for the comparison of atomic-weight values, R. D. Deslattes, H. S. Peiser, J. A. Bearden, and J. S. Thomsen, *Metrologia* **2,** *No. 3, 103–111 (July 1966).*
Without presenting experimental details, this report outlines and reappraises the principles involved in measurement of crystal lattice parameters and density for the determinations of atomic-weight values.
Attention is drawn to the advantages to be derived from a comparison of densities and lattice spacings with those of a crystal of mononuclidic elements, rather than from absolute measurements of x-ray spacings and density.
Errors arising from physical and chemical imperfections are discussed as are the general techniques of adequate precision for density and lattice spacings measurements.
Recent literature data is used by way of illustration to derive the effective atomic weight of calcium appertaining to a group of calcite samples from that of a group of silicon crystals (really an unsuitable "standard"). The calcium value obtained is 40.0795 ± 0.0019 (probable error); it compares with IUPAC's adopted 40.08 and a "physical value" of 40.078 from nuclidic masses and isotopic abundance measurements. There are several elements for which the x-ray/density method is judged to be potentially the most promising for atomic-weight redeterminations in the foreseeable future.

Key Words: Atomic weights, crystal densities, crystal perfection, experimental methods, lattice parameters.

Review of elementary theory of the photometry of projection apparatus, C. S. Douglas, *Illum. Eng.* **62,** *No. 4, 246–253 (Apr. 1967).*
Equations based upon simple geometric relations are developed for the illuminance produced by a projector such as a searchlight, beacon, or floodlight at a distance from the projector. When the beam is rotationally symmetrical but not collimated and the image, virtual or real, subtends a smaller angle at the point of observation than does the objective of the projector, illuminance varies inversely as the square of the distance to the image. If the angle subtended by the image is larger than that subtended by the objective, the illuminance varies inversely as the square of the distance to the objective. The distance at which the two angles are equal is defined as the critical distance. Equations relating critical distance to the radius of the source, the radius of the objective, and the magnification of the system are developed. Approximations for use when the beam of the projector is asymmetric are developed. Very good agreement was found between the computed variation of illuminance with distance and the measured variation of illuminance with distance for a projector forming a virtual image 150 feet behind the objective.

Key Words: Critical distance, illumination, light projectors, photometry, photometric distance, signal lighting.

Statistical concepts in metrology, H. H. Ku, *Book, Handbook of Industrial Metrology, ch. 2, pp. 20–54 (Prentice-Hall, Inc., Englewood Cliffs, N.J., 1967).*
These two sections of the chapter, statistical concepts of a measurement process and statistical analysis of measurement data, are part of the textbook *Handbook of Industrial Metrology* sponsored by the American Society of Tool and Manufacturing Engineers.
Beginning with the differentiation between arithmetic and measurement numbers, the properties of the latter are developed and described, leading to a discussion of precision and accuracy at the end of the first section.
A basic kit of tools for the comparison and manipulation of means and variances are given in the second section, including a collection of propagation of error formulas. The use of control chart techniques for monitoring stability is emphasized. Examples are given using actual calibration data of NBS.
Selected references are given for topics introduced but not treated in detail.

Key Words: Industrial metrology, measurement process, statistical analysis, statistical concepts.

The photometry of colored light, A. C. Wall, *Illum. Engr.* **62,** *No. 4, 239–242 (Apr. 1967).*
The photosensitor of a photometer must be corrected to have a spectral sensitivity as close as possible to the CIE photopic luminous efficiency function. A correction-by-filter technique is described, applicable to photosensitors which are used in the measurement of "colored light," which, in this paper, designates light which has a spectral distribution different from that of the light with which the photometer is calibrated. Three types of photosensitors with their associated auxiliary filters were investigated, as well as one type

of barrier-layer cell with an integral filter. The photosensitors were first calibrated by exposing them to illumination from a lamp operating at 2854 °K. Then, to test the adequacy of the spectral correction-by-filter technique, twenty-two 2-by-2-inch squares of colored glass whose luminous transmittance was computed from spectrophotometric data were placed in turn in the light beam and readings proportional to the irradiance incident on each photosensitor were taken. If the spectral correction were perfect, the ratio of the reading obtained with the filtered light to the reading with the unfiltered light would be equal to τ_s, the luminous transmittance of the filter obtained from the spectrophotometric measurements. Factors were calculated to convert the ratios obtained to τ_s for the color-corrected photosensitors and for five types of noncolor-corrected photosensitors.

Key Words: Photometry, photocells, spectral correction of phototubes, photometers, phototubes, filters.

Thermal converters used as transfer standards for the measurement of alternating current and voltage, F. L. Hermach, *Proc. 11e Session, Comite Con. D'Electricite, May 10–12, 1965, pp. E–83–E–88 (May 1965).*
This report to the Advisory Committee oulines recent progress at NBS in the development of ac-dc transfer standards (comparators) for measurements of alternating current and voltage with 20 ppm accuracy or better at audio frequencies. Electrothermic transfer standards of the thermocouple type offer good prospects of meeting this goal. Their ac-dc differences appear to be very stable. The standards can be read with high precision and are rugged and portable. Furthermore, they can readily be intercompared for ac-dc difference, to step up and down the current and voltage scale with a precision of a few ppm. They are thus worthy of consideration for international comparisons of the accuracy of alternating current and voltage measurements.

Key Words: Audio frequency, audio, standards, comparator, thermoelements, thermal converters, transfer standards, voltage comparator, voltage measurements.

Use of a laser for length measurement by fringe counting, K. E. Gillilland, H. D. Cook, K. D. Mielenz and R. B. Stephens, *Metrologia* **2,** *No. 3, 95–98 (July 1966).*
The use of a 633-nm He-Ne laser of normal neon isotopic abundance as a light source for an automatic fringe counting interferometer was found to improve the counting precision and extend the usefulness of the interferometer to the full one meter limit of its carriage travel. A 91-mm length was measured in terms of Hg^{198} and laser fringes. From the fringe counts obtained and the wavelength of the Hg^{198} line, the laser vacuum wavelength was measured to be 632.991 46 nm with a standard error of $1.1\times10-7$. With the laser wavelength so determined, wach decimeter interval of a one meter line standard was measured by counting laser fringes. All measured decimeter interval lengths agreed with the assigned values within the mutual limits of uncertainty, the largest discrepancy being less than 0.5 um. The result obtained for the total length of the line standard agreed with the assigned length of the line standard to 7 parts in 10^8, which is well within the mutual limits of uncertainty.
This method is being applied to routine calibration of line standards using a stabilized isotopic He-Ne laser.

Key Words: Automatic fringe counting interferometer, fringe counting, interferometer, laser for length measurement, length measurement.

A note on thermal expansion coefficients of rare gas solids, R. D. Mountain, *J. Phys. Chem. Solids* **28,** *1071–1073 (Dec. 29, 1966).*
Recent measurements of the thermal expansion coefficient of solid argon, krypton and xenon are shown to violate the law of corresponding states. The failure of the law of corresponding states is related to the different ways the lattice vibration spectra of these crystals change as pressure is applied to the lattice.

Key Words: Corresponding states, lattice vibration spectrum, solid argon, solid krypton, solid xenon, thermal expansion coefficient.

Annual report on spectroscopy, C. E. Moore, *Astron. J.* **71,** *No. 9, 796–797 (Nov. 1966).*
This report is furnished annually to the Astronomical Journal in order to present to astrophysicists the spectroscopic work that they are particularly interested in. It is published with the Observatory Reports and provides a brief summary of activity at the National Bureau of Standards.

Key Words: Atomic spectra, rare-earth spectra, transition probabilities, solar spectrum.

Approximate eigenfunctions of the Liouville operator in classical many-body systems. II. Hydrodynamic variables, R. J. Nossal and R. Zwanzig, *Phys. Rev.* **157,** *No. 1, 120–126 (May 5, 1967).*
A variational solution of the Liouville Equation is used to obtain collective coordinates for simple classical fluids. Comparison is made with macroscopic analogs determined from relevant hydrodynamic equations. Approximate eigenfunctions of the Liouville operator, when constructed from linear combinations of the spatial fourier transforms (fluctuations) of the mass, momentum, and energy density operators for the fluid, are found appropriate to low frequency disturbances. When time derivatives of fluctuations are included among trial functions the variational procedure provides fluid state counterparts of usual solid state phonons.

Key Words: Eigenfunctions, Liouville operator, many-body systems, hydrodynamic variables, irreversible processes.

Certificates of radioactivity standards, S. B. Garfinkel, A. P. Baerg, and P. E. Zigman, *Report of the Subcommittee on the Use of Radioactivity Standards, Natl. Acad. Sci.-Natl. Res. Council, pp. 1–11 (Dec. 1966).*
Recommendations for certificates of standards of radioactivity are presented. It is hoped that commercial producers of such standards in the United States of America will use these recommendations in the preparation of certificates which they supply with their standards.

Key Words: Certificates, commerical standards, radioactivity standards, standards accuracy, combination of errors, precision, measurements.

Deformation twinning in Ni and F.C.C. Fe-Ni alloys, R. P. Reed, *Phil. Mag.* **15,** *No. 137, 1051–1055 (May 1967).*
Using electron and optical microscopy techniques, deformation twinning has been found in Ni and fcc Fe-Ni alloys at low temperatures (76–4 °K).

Key Words: Nickel, Fe-Ni alloys, deformation twinning, low temperature.

Development of the engineering method and some simplified methods of structure shielding analysis, C. Eisenhauer (*Lecture Notes, OCD Summer Inst., Kansas State Univ., Manhattan, Kansas, 1962–1963, 1965), TR–40, Radiation Shielding–Analysis and Design Principles as Applied to Nuclear Defense Planning, V–1–V–iv (Supt. Docs. Govt. Printing Office, Washington, D.C., Nov. 1966).*
These lecture notes describe the technical basis for the procedures currently being used by the Office of Civil Defense to evaluate fallout protection in structures. The notes describe in detail how the equations and charts used in these procedures were derived from fundamental calculations of radiation shielding. Examples are given for simple structures.

Key Words: Fallout protection in structures, radiation shielding, structures.

Dielectric constants of $PbWO_4$ and $CaWO_4$, W. S. Brower and P. H. Fang, *J. Appl. Phys.* **38,** *No. 5, 2391 (Apr. 1967).*
The dielectric constants (ϵ') $PbWO_4$ and $CaWO_4$ were measured at 24.5 °C in air. Two specimens of each orientation were measured. The averages and deviations therefrom of the two measured when of the reflective dielectric constants are as follows:

$$PbWO_4\ \epsilon' \parallel a\ 23.6\pm0.3;\ \epsilon' \parallel c\ 31.0\pm0.4;$$

$$CaWO_4\ \epsilon' \parallel a\ 11.7\pm0.1;\ \epsilon' \parallel c\ \ 9.5\pm0.2.$$

Key Words: Dielectric constant, single crystal, calcium tungstate, lead tungstate.

Effect of oxygen on the photoelectron yield from tungsten in the vacuum ultraviolet, B. J. Waclawski, L. R. Hughey, and R. P. Madden, *Appl. Phys. Letters* **10,** *305 (1967).*
The effect of adsorbed oxygen on the photoelectron yield of bulk polycrystalline tungsten was studied at photon energies of 7.7, 10.2, 11.8, 16.9, and 21.2 eV. Use of ultra-high vacua $\sim 3\times10^{-10}$ torr ensured sample cleanliness prior to oxygen exposure. The photoelectron yield decreases with oxygen exposure because of the increase in the electronic work function of the tungsten photocathode. However, at $h\nu=21.2$ eV, an increase in photoelectron yield with oxygen exposure also appears and is believed to be due to photoelectron emission from the adsorbed oxygen atoms.

Key Words: Oxygen adsorption, photoelectric effect, tungsten, vacuum ultraviolet.

Effects of environment on the fracture of glass, S. M. Wiederhorn, *Proc. RIAS Conf., Baltimore, Md., June 7–8, 1965, pp. 293–317 (Gordon and Breach, New York, N.Y., 1966).*
This paper briefly reviews previous work on the topic of delayed fracture of glass, and then presents the results of a new experimental approach to the subject. Using the double-cantilever cleavage technique, it was possible to observe crack motion and to accurately measure crack velocities in glass. The temperature and stress dependence of the crack velocity indicates that the observed fracture is an activated process with an activation energy of 19,500 calories/mole. The existence of a static fatigue limit is inferred from the experimental data. Experimental results will be discussed with reference to current theories of static fatigue.

Key Words: Glass, fracture, crack propagation, static fatigue, corrosion, cleavage.

Electron beams: National Bureau of Standards and the new technology, H. W. Koch, *Science* **156,** *No. 3773, 321–328 (Apr. 21, 1967).*
High energy electron beams can now be generated with radiation powers of hundreds of kilowatts and can be measured with energy resolutions of several parts in 10^4. The importance of this new technology to science, industry, and the public is related to the measurement research and services of the National Bureau of Standards.

Key Words: Electrons, x-rays, particle accelerators, radiation power, nuclear physics, radiation processing, radiation measurement standards.

Exposure rate measurements of X- and gamma-rays with silicon radiation detectors, K. Scharf, *Health Phys.* **13,** *No. 6, 575–586 (June 1967).*
The steady-state d.c. current and voltage signals produced by x- or gamma-rays in silicon radiation detectors used either as photovoltaic cells or photodiodes are shown to be dependent on such circuit parameters as load resistance and bias voltage used in the respective exposure rate measurement. Non-linear exposure rate dependence of radiation-produced signals may result from choosing unsuitable circuit parameters and no singular value of sensitivity or signal per unit exposure rate can be ascribed to an individual detector without specifying the circuit parameters used. Measurements are reported with silicon detectors of the diffused *p-n* junction type illustrating these performance features, and a measuring method is suggested which makes it possible to measure with high precision the generated photocurrent at zero voltage applied at the detector which is independent of circuit parameters and proportional to exposure rate over a wide range. Measurements using this method are reported of exposure rates ranging up to 10^5 R/hr of 30-kV x-rays of 0.09 mm Al HVL, and from approximately 1 R/hr to 30 R/hr of ^{60}Co gamma rays.

Key Words: X-rays, gamma rays, radiation detectors, silicon, semiconducting devices, exposure rate measurements, dosimetry, radiation monitoring, radiation detection devices.

Experimental evidence concerning the conduction band of $SrTiO_3$, H. P. R. Frederiske, W. R. Hosler, and W. R. Thurber, *(Proc. Inter. Conf. Physics of Semiconductors, Kyoto, Japan, Sept. 8–13, 1966) J. Phys. Soc.* **21,** *Suppl., 32–36 (1966).*
Experimental information about the conduction band of semiconducting $SrTiO_3$ is compared with the calculated band structure. Measurements of transport properties, magnetic susceptibility and plasma frequency yield rather high average effective masses. Low-field magnetoresistance as well as piezoresistance experiments have been performed on $SrTiO_3$. Although some disagreement remains, the weight of the evidence is in favor of a many-valley structure of the lowest conduction band as predicted by theory.

Key Words: Band structure, effective mass, electronic transport properties, semiconductor, strontium titanate.

Ferromagnetic iron alloys lacking a hyperfine field at the iron site, L. H. Bennett and L. J. Swartzendruber, *Physics Letters* **24A,** *No. 7, 359–360 (Mar. 27, 1967).*
Although ferromagnetism has been reported for $TiFe_xCo_{x-1}$ when $0.3 \ll x \ll 0.7$, the Mössbauer effect shows no evidence for the existence of a localized moment at the iron site. Thus the magnetization is most likely due to a diffuse moment associated with the Ti atoms, implying itinerant ferromagnetism.

Key Words: Alloys, ferromagnetism, superconductivity, hyperfine fields, moments, titantium, cobalt, Mössbauer effect, iron.

Future spectroscopy for late-type stars, C. E. Moore, *Proc. Colloquium on Late-Type Stars, Trieste, Italy, June 13–17, 1966, pp. 15–24 (Stampato Presso, Trieste, Italy, 1967).*
The subject is reviewed with the idea of the application of spectroscopy to work on abundances. Two main topics are discussed: the general characteristics of the observed stellar spectra and the available data on laboratory spectra needed to identify the stellar lines. The impact of the developments in space technology has greatly expanded the observed range of stellar spectra. This is handled by regions, the Ultraviolet, the Visible, and the Infrared. More laboratory programs are needed to meet present needs for data on both atomic and molecular spectra. The existing programs are discussed. Encouraging progress on the analyses of selected rare-earth spectra is reported. These promise to be of great astrophysical interest.

Key Words: Spectra of late-type stars, atomic spectra, molecular spectra, solar spectra, sun-spot spectra, reference data programs, rare-earth spectra.

Report on international conference on spectroscopy, Bombay, 9–18 January 1967, C. E. Moore *(Intern. Conf. Spectroscopy, Bombay, India, Jan. 9–18, 1967), Appl. Opt.* **6,** *No. 5, 836 (May 1967).*
The First International Conference on Spectroscopy in India, was held in Bombay, January 9–18, 1967. Three International Unions, Astronomy, Physics, and Chemistry, supported the Organizing Committee in arranging for the Conference. Some 200 scientists from 13 countries attended. There were 30 invited papers and more than 100 contributed papers in all. Most of them dealt with molecular spectroscopy, but a few touched on interstellar spectra, solar spectroscopy, in the x-ray region and laser spectroscopy.

Key Words: Molecular spectroscopy, Indian Conference on Spectroscopy, International Conference on Spectroscopy.

Interpretation of the far infrared laser oscillation in ammonia, D. R. Lide, Jr., *Physics Letters* **24A,** *No. 11, 599–600 (May 1967).*
The interpretation of the laser emission spectrum of ammonia in the far infrared is considered. The P branch of the $v_2=3^s \rightarrow 2^a$ transition is shown to coincide closely with the observed laser spectrum. However, only the low K transitions are observed. Possible reasons for the absence of the expected strong $K=3$ lines are discussed.

Key Words: Ammonia, infrared, inversion, laser, molecular, spectrum.

Low-temperature heat capacity of $NdCl_3$ and $PrCl_3$, J. H. Colwell and B. W. Mangum, *J. Appl. Phys.* **38,** *No. 3, 1468–1469 (Mar. 1, 1967).*
Heat capacities of $PrCl_3$ and $NdCl_3$ have been measured between 0.3 °K and 4 °K. The dominant feature of the heat capacity curves is a broad anomaly indicating a region of extensive short-range magnetic ordering. The anomaly in $NdCl_3$ has a maximum at 0.47

°K and fits closely that of a linear Ising chain model. In addition, two small peaks appear at the same temperatures as the sharp spikes found in the magnetic susceptibility. $PrCl_3$ has a sharp peak in the heat capacity at 0.4 °K which is presumably associated with long-range ordering. The broad anomaly in $PrCl_3$ has a maximum at 0.8 °K. The magnetic entropy change for the temperature region of the measurements is approximately 80% of R $\log_e 2$ for both salts.

Key Words: Heat capacity, magnetic entropy, magnetic susceptibility, $NdCl_3$ (neodymium trichloride), $PrCl_3$ (praeseodymium trichlroide), temperature measurement.

Modulus of rupture of glass below room temperature, M. J. Kerper and T. G. Scuderi, *Am. Ceramic Soc. Bull.* **45,** *No. 9, 782–783 (Sept. 7, 1966).*
The modulus of rupture of seven different commercial glasses was determined at 0 °F (−17.8 °C) and −50 °F (−45.6 °C). The results showed that for all glasses and for all conditions of temper the modulus of rupture increased as the temperature decreased.

Key Words: Glass, strength, low temperature.

On the diffraction profiles of spectrograph slits of finite width, K. D. Mielenz, *Optik* **25,** *No. 3, 138–139 (May 17, 1967).*
In an earlier paper, the author presented a measured curve of line intensity vs. slit width, for the case of partially coherent spectrograph slit illumination. The result of a theoretical calculation is now presented which supports the experimental curve.

Key Words: Diffraction, partial coherence, spectrograph slit.

Optical properties of $SrTiO_3$ under applied stress and electric field, R. C. Casella, *Phys. Rev.* **154,** *No. 3, 743–749 (Feb. 15, 1967).*
Motivated by recent experiments on the effects on uniaxial stress on the superconducting transition and normal-state transport properties of $SrTiO_3$, we have carried out a symmetry analysis, obtaining the perturbed band structure and optical selection rules for the cases of uniaxial stress along the (111) and (001) axes and of static electric field along (001). A comparison of the last case with $BaTiO_3$ in the C_{4v} ferroelectric phase suggests a model with a reversal in the order of the valence bands in $SrTiO_3$ relative to that proposed earlier. Selection rules for polarized light are obtained for both models and criteria for deciding experimentally which is correct are stated. An example is given of how the sign of the relative energy shift of the conduction valleys with stress may be determined optically.

Key Words: Electro-optical effects, energy bands, selection rules, stress-optical effects, strontium titanate.

Oscillatory photoconductivity and luminescence in $SrTiO_3$, L. H. Grabner, *Proc. Cairo Solid State Conf., Cairo, Egypt, Sept. 3–8, 1966, Book, Interaction of Radiations with Solids, Ed. A. Bishay, pp. 155–160 (Plenum Press, Inc., New York, N.Y., 1967).*
Photocurrents and luminescence in $SrTiO_3$ oscillate at low temperatures (~ 4 °K) at a threshold of about 100 volts/cm. Voltage-current curves show negative differential resistance in the region of oscillation. We suggest that these effects are due to the field ionization, into the valence band, of a hole trapped 1 eV from the valence band. The hole is ionized by the local field (~ 10^6 V/cm) which differs from the externally applied field of 10^2 V/cm because of the high dielectric constant of $SrTiO_3$ (~ 10^4) at low temperatures.

Key Words: Electric field quenching, luminescence, negative resistivity, photoconductivity, strontium titanate.

Photographic and spectroscopic studies of exploding wires in a sealed vessel, E. C. Cassidy and K. K. Neumann (*Proc. 7th Intern. Cong. High-Speed Photography, Zurich, Switzerland, Sept. 12–18, 1965), Book, Kurzzeitphotographie, Ed. O. Helwich, pp. 178–185 (Verlag Dr. Othmar Helwich, Darmstadt, West Germany, 1967).*
Investigations of the mixing process between exploding wires and a confined air environment are described. The various high-speed framing camera, combined framing camera and drum camera, drum camera, periodic still, and ultraviolet photographic techniques employed for time resolution of the explosion are described and illustrated. The photographic results are correlated with time-resolved (by photographic and photoelectric techniques) spectroscopic observations. Results have suggested a method and suitable intervals (during the explosion) for estimating the average temperature of the exploding vapor column. A phenomenon apparently due to reflecting shock waves was observed in a later stage of the explosion.

Key Words: High-speed, photographic, time-resolved, spectrographic, exploding wires, electrical discharge.

Piezo-optical effects in solids by sample rotation, A. Feldman, *Physics Letters* **23,** *No. 11, 627–628 (Dec. 12, 1966).*
The differential absorption and reflection coefficients of uniaxially stressed Si and $SrTiO_3$ were determined by rotating the samples in a linearly polarized light beam.

Key Words: Modulation technique, optical, piezo-optical, semiconductor, silicon, strontium titanate.

Radioactivity criteria for radiation processing of foods, H. W. Koch and E. H. Eisenhower, *Book, Radiation Preservation of Foods, Advances in Chemistry Series 65 (American Chemical Society, Washington, D.C., 1967), ch. 7, pp. 87–108.*
The high-dose-level processing of foods by high-energy electrons and x-rays can induce measurable radioactivity in foods. Such radioactivity might, but fortunately need not, present a food wholesomeness problem. The amount of induced radioactivity can be controlled and limited so as to be non-measurable by limiting the maximum energy of the radiation to 10 MeV. Therefore, non-measurability is one useful criterion. Another criterion may be developed from considerations of the maximum permissible concentration of radioactivity in foods and of the deliberate or chance nature of the occurrence of the activity. The bases of the various criteria and of possible future developments are detailed by a consideration of the characteristics of photonuclear radioactivities, the detection methods and capabilities, the influence of production parameters, and the maximum permissible concentrations.

Key Words: Detection, induced radioactivity, maximum permissible concentrations, photonuclear reactions, processing, radiation, threshold energies.

Reactor physics in the resonance and thermal regions, D. T. Goldman, *J. Franklin Inst.* **283,** *No. 5, 437–438 (May 1967).*
A review of papers presented at a topic conference of the American Nuclear Society.

Key Words: Neutron, thermalization, resonance, absorption, reactor, review.

Spectroscope slit images in partially coherent light, K. D. Mielenz, *J. Opt. Soc. Am.* **57,** *No. 1, 66–74 (Jan. 1967).*
The apparatus function of prism or grating spectroscopes with finite slits is derived for the general case of partially coherent illumination of the slit. Numerical results are presented for the border cases of coherent and incoherent slit illumination, as well as for full and partial illumination of the spectroscope aperture.
The dependence of line intensity and line width on slit width, as well as the optimum slit width, are determined for each of these cases. It is shown that the performance of the spectroscope reaches an optimum when the aperture is at least fully illuminated.

Key Words: Spectroscope slit, diffraction, partial coherence slit illumination, luminosity, resolution, optimal performance.

Status of the National Standards for physical measurement, R. D. Huntoon, *Science* **150,** *No. 3693, 169–178 (Oct. 8, 1965).*
This article outlines various stages of sophistication in the development of a measurement system, from a "unit-standard" system to a consistent system in which standards are tied to atomic and molecular properties in an independently reproducible way. The present stage of development of our measurement system is discussed in this context, and predictions are made regarding its future development.

Key Words: Ampere, candela, current, degree Kelvin, International System of Units, kilogram, length, luminous intensity, mass, meter, metric system, second, standards for physical measurement, temperature, time.

The basis of our measurement system, R. D. Huntoon, *Phys. Teacher* **4,** *No. 3, 113–120 (Mar. 1966).*
This article outlines various stages of sophistication in the development of a measurement system, from a "unit-standard" system to a consistent system in which standards are tied to atomic and molecular properties in an independently reproducible way. The present stage of development of our measurement system is discussed in this context, and predictions are made regarding its future development.

Key Words: Degree Kelvin, kilogram, measurement system, meter, physical constant, second, standard, unit.

The elastic energies of non-regular hexagonal dislocation loops, R. DeWit and A. W. Ruff, Jr., *Phil. Mag.* **15,** *No. 137, 1065–1069 (May 1967).*
The elastic energies of dislocation loops have been calculated as a continuous function of shape from equilateral triangle to hexagon. A smooth decrease in energy is found in this sequence; a relatively rapid change is associated with truncation of the triangle corners. The results are compared with previous calculations for other geometric shapes. The effect of a stacking fault in the loop plane is also considered.

Key Words: Dislocation, elastic energy, loops, stacking fault.

Temperature dependence of the high-frequency moduli of vitreous B_2O_3, W. Capps, P. B. Macedo, B. O'Meara, and T. A. Litovitz, *J. Chem. Phys.* **45,** *No. 9, 3431–3438 (Nov. 1, 1966).*
Measurements of ultrasonic velocity allowed the calculation of the high frequency shear and bulk moduli of B_2O_3 from 80 °C below to 300 °C above the glass transition. The temperature dependences of these moduli were found to be consistent with a semi-empirical extension of the theory of Zwanzig and Mountain.

Key Words: B_2O_3, high frequency moduli, ultrasonic velocity.

A determination of trace amounts of iron and cobalt in the same sample by substoichiometric radioisotopic dilution analysis, A. R. Landgrebe, L. McClendon, and J. R. DeVoe (*Proc. 1964 Winter Meeting American Nuclear Society, San Francisco, Calif., Nov. 30–Dec. 3, 1964*), *Trans. Am. Nucl. Soc.* **7,** *No. 2, 337–338 (Nov. 1964).*
A method of analysis for iron and cobalt was developed for the concentration range of 10^{-3} to 10^{-8} M. The method involves using a limiting amount of EDTA to complex iron or cobalt. The noncomplexed ions were removed from solution with a cationic exchanger (Dowex 50–X8) leaving a constant amount of cobalt or iron EDTA complex in solution. Trace amounts of naturally occurring cobalt and iron were determined with good sensitivity as long as radioisotopes of high specific activity were used. N.B.S. standard reference material (671, 672, and 673) of nickel oxide were also analyzed for iron and cobalt.

Key Words: Iron, cobalt, EDTA, radioisotopic dilution, Dowex 50–X8, nickel oxide, analysis, standard reference material.

Application of radiometric techniques to quantitative paper chromatography of iron, copper, manganese, and cobalt, A. R. Landgrebe, T. E. Gills, and J. R. DeVoe, *Anal. Chem.* **38,** *No. 9, 1265–1266 (Aug. 1966).*
A radioactive reagent was used for the quantitative determination of iron, copper, manganese, and cobalt after separating them by paper chromatography. The method has been applied to the analysis of a sample of nickel oxide (NBS Standard Reference Material No. 671). With this method which is operable at the μg/ml level, values of 0.37, 0.19, 0.14, and 0.32 percent for Fe, Cu, Mn, and Co respectively were found and the relative standard deviation of a single determination for Fe, Cu, Mn, and Co were 7.1, 6.8, 3.8, and 4.1 percent. Comparison of these results with those of other analytical techniques were made.

Key Words: Analysis, nickel oxide, paper chromatography, radiometric methods, NBS Standard Reference Material 671, Fe, Co, Cu, Mn.

A study of the heat of formation of oxygen difluoride, R. C. King and G. T. Armstrong, *Proc. Fifth Meeting ICRPG, Working Group on Thermochemistry* **1,** *CPIA Publ. 146, May 1967.*
The enthalpies of the reactions below ΔH°_{303}, were determined in a flow calorimeter operated at one atm. pressure, to be respectively, in kcal mol^{-1}, −227.52 (0.16), −153.38 (0.06), and −68.28 (0.03). The numbers in parentheses are the standard deviations of the means for 13, 5, and 6 experiments, respectively. The enthalpy of formation of $OF_2(g)$, ΔH°_{f298},

$$OF_2(g) + 2H_2(g) + 99H_2O(l) = 2[HF \cdot 5OH_2O](l)$$

$$F_2(g) + H_2(g) + 100H_2O(l) = 2[HF \cdot 50H_2O](l)$$

$$\tfrac{1}{2}\,O_2(g) + H_2(g) = H_2O(l)$$

$$F_2(g) + \tfrac{1}{2}\,O_2(g) = OF_2(g)$$

was calculated from the measured enthalpy changes to be +5.86 kcal mol^{-1}. The average bond energy E(O−F) in the gaseous molecule of OF_2 was calculated to be 45.72 kcal mol^{-1}. The results of the second reaction are compared with other recently derived data on HF(aq).

Key Words: Fluorine, reaction with hydrogen; oxygen, reaction with hydrogen; oxygen difluoride, reaction with hydrogen; oxygen difluoride, heat of formation; hydrofluoric acid, heat of formation; hydrogen, reactions with fluorine, oxygen difluoride and oxygen; calorimetry, fluorine flame.

Crystal nucleation in polyethylene: the droplet experiment, F. Gornick, G. S. Ross, and L. J. Frolen, *J. Polymer Sci.* **18,** *Part C, 79–91 (1967).*
The droplet technique was utilized to obtain estimates of the isothermal rate of homogeneous crystal nucleation in highly supercooled melts of unfractionated linear polyethylene. In a typical experiment a cell containing a suspension of several hundred micron-size spherical droplets of the polymer was placed on a microscope hot stage and quenched from a temperature well above the melting point of polyethylene to the desired crystallization temperature. When viewed between crossed polarizers, the droplets were initially invisible but, upon freezing, they appeared as visible birefringent spheres. The time dependence of the process was followed by time-lapse photography. Half times ($\tau^1/_2$) for the freezing of those droplets remaining unfrozen by the time the crystallization temperature was attained were thus obtained at a series of undercoolings and related to the desired nucleation rate constant

$$I(\text{nuclei-cm}^{-3} - \text{sec}^{-1})$$

by the equation $I = ln2/\tau^1/_2 v$, where v is the droplet volume.
The temperature dependence of I, as obtained by the above procedure, was analyzed in accord with current theories of homogeneous nucleation of chain-folded polymer crystals. From this analysis, an estimate, 14,960 $ergs^3$ cm^{-6} was made of the quantity $(\sigma^2\sigma_e)$, where σ and σ_e are respectively the lateral and end-surface free energies of the crystal.

Key Words: Crystallization, polyethylene, homogeneous nucleation, surface free energy, microscopy, kinetics.

Effects of temperature and of ultraviolet radiation on pyrene adsorbed on garden soil, A. J. Fatiadi, *Environ. Sci. Technol.* **1,** *No. 7, 570–572 (July 1967).*
The chemical and photochemical changes of pyrene adsorbed on soil have been studied. It was found that pyrene adsorbed on soil and subjected to either heat or ultraviolet radiation underwent self-coupling to 1,1′-bipyrene, apparently by free-radical mechanisms; this product was not found from pyrene adsorbed on a number of other particulates. Also formed in the pyrene−soil reaction were 1,6- and 1,8-pyrenediones, probably by a different reaction-path.

Key Words: Photochemical, reaction, photooxidation, particulates, polycyclic, aromatic, hydrocarbons, pyrene, 1,6- and 1,8-pyrenediones, 1,1′-bipyrene.

Electrolysis of nonaqueous systems, A. Brenner, *Book, Advances in Electrochemistry and Electrochemical Engineering, Ed. C. W. Tobias, V, 205–248 (John Wiley & Sons, Inc., New York, N.Y. 1967).*
A survey is presented of the electrodeposition from organic solutions of lithium, sodium, potassium, beryllium, magnesium, and

aluminum. The attempts to electrodeposit the rare-earth metals are discussed. Also treated are the electrodeposition of metals from liquid ammonia and the electrolysis of essentially pure liquids, both organic and inorganic.

Key Words: Electrolysis, non-aqueous systems, electrolysis of, lithium, sodium, potassium, beryllium, magnesium, aluminum, liquid ammonia.

High purity powdered CsI as a high reflectance infrared diffuser, J. Geist, G. J. Kneissl, and V. R. Weidner, *Appl. Opt.* **6,** *No. 7, 1280–1281 (July 1967).*
The spectral reflectance of powdered CsI is compared with that of flowers of sulfur between 2.5μm and 20μm. The experimental procedure is described and room temperature data are presented. The reflectance of ultra pure powdered CsI was found to be appreciably higher than that of the flowers of sulfur beyond 7μm.

Key Words: Body scatterer, cesium iodide, diffuse reflector, powdered cesium iodide and sulfur.

Internal friction in rutile containing Ni or Cr, J. B. Wachtman, Jr., S. Spinner, W. S. Brower, T. Fridinger, and R. W. Dickson, *Phys. Rev.* **148,** *No. 2, 811–816 (Aug. 12, 1966).*
Rutile containing Ni gives an internal-friction peak centered near 50 °C at 2 kHz characterized by an activation energy $E=15.3\pm2.4$ kcal/mole and a characteristic relaxation time $\tau_0=3\times10^{-15\pm1.7}$ sec; this peak occurs for tensile stress along [100] or [110]. A peak centered near 200 °C with $E=21.4\pm2.1$ kcal/mole and

$$\tau_0=8\times10^{-15\pm1.0}$$

sec occurs for stress along [100] but not for stress along [110]. Rutile containing Cr gives similar peaks characterized by $E=13.5\pm2.4$ kcal/mole and $\tau_0=2\times10^{-14\pm1.6}$ sec and by $E=22.2\pm1.5$ kcal/mole and $\tau_0=4\times10^{-15\pm0.9}$ sec. Light reduction in vacuum decreases the amplitude of the low-temperature peak and enhances the high-temperature peak in both cases. Heavy reduction of rutile containing Cr removes both peaks but they reappear upon subsequent reoxidation. The evidence suggests that the motion of interstitial cations is involved and that reduction causes the formation of a compound defect. A tentative interpretation is given in terms of unpaired Ni^{3+} interstitials for the low-temperature peak and of interstitial pairs composed of Ni^{3+}–Ti^{3+} for the high-temperature peak in Ni-doped specimens; the corresponding peaks in Cr-doped rutile are tentatively interpreted in terms of Ti^{4+} interstitials and of interstitial pairs consisting of Ti^{4+}–Ti^{3+}. It is possible to have two charge-compensating Cr^{3+} on adjacent substitutional sites and preserve the last two models.

Key Words: Activation energy, internal friction, point defect, reduction, rutile, symmetry conditions.

Electron probe microanalysis, K. F. J. Heinrich, *Book, Experimental Methods of Materials Research. Advances in Materials Research* **1,** *145–162, (John Wiley & Sons, Inc., New York, N.Y. 1967).*
This paper introduces the reader to the principles and techniques of electron probe microanalysis. After a brief description of the instrument, the characteristics of probe analysis, such as range of elements, spatial resolution, sensitivity, and conditions necessary for the specimen, are discussed. The corrections to be applied in quantitative analysis are enumerated and explained. Several signal evaluation systems, particularly for scanning microprobe analysis, are described, including the use of signals other than x-rays. The fields of application are briefly indicated.

Key Words: Characteristics of probe analysis, electron microanalysis, electron probe microanalysis, microanalysis, electron probe, probe.

Extraction-spectrophotometric determination of antimony as a ternary complex, R. W. Burke and O. Menis, *Anal. Chem.* **38,** *p. 1719 (Nov. 1966).*
A critical examination is presented of the many parameters associated with the extraction-spectrophotometric determination of Sb^{+5} as the ternary chloro complex of brilliant green, a triphenylmethane dye. The basic problem of dissolving the sample without residue problems and without volatilization of antimony is also discussed. A sealed tube dissolution procedure yields only Sb^{+3}, the requisite form. The step-wise reactions that may preclude the formation of the colored complex are discussed in terms of the interaction of the following variables: Oxidation and hydrolysis mechanism, spectral dependency on final choice of oxidant, role of H^+ and Cl^- in the oxidation-extraction steps, the side reaction due to impurities in the dye, and the extraction characteristics of the ternary complex. The method has been applied to the analysis of both ferrous and non-ferrous standard reference materials with good success. The coefficient of variation is 2 percent.

Key Words: Extraction-spectrophotometric, antimony, brilliant green, sealed tube dissolution, mechanism, dye impurity, ferrous and non-ferrous alloys.

Gas phase photolysis and radiolysis of methane. Formation of hydrogen and ethylene, R. Gorden, Jr. and P. Ausloos, *J. Chem. Phys.* **46,** *No. 12, 4823–4833 (June 15, 1967).*
The photolysis of CH_4 and of CH_4-CD_4 mixtures has been investigated at 1236 Å (10.0 eV) and at 1048–67 Å (11.5–11.8 eV). The excited methane molecule dissociates to form H_2, H, CH_3, CH_2, CH and probably also C. The CH and CH_2 radicals insert into methane to form internally excited $C_2H_5^*$ and $C_2H_6^*$ species, respectively. Below one atmosphere all C_2H_5 radicals decompose to form C_2H_4, while the ethane molecules are partially stabilized. The relative quantum yield of CH increases about three-fold when the wavelength is reduced from 1236 Å to 1048–67 Å. On the basis of an isotopic analysis of the hydrogen produced in the photolysis of CD_4-H_2S mixtures, it is concluded that at 1236 Å, D-atoms constitute at least 65 percent of the "molecular" deuterium yield.
In the radiolysis, ethylene is largely, although not exclusively formed by the insertion of CH into methane. It is demonstrated that addition of small concentrations of an unsaturated hydrocarbon to methane profoundly affects the ion-molecule reaction mechanism and, therefore, does not lead to a dependable value of the "initial" ethylene yield as suggested in earlier studies. Upon application of an electrical field, the production of CH and CH_2 is augmented in the saturation current region. The importance of the latter two radicals in the direct and rare gas sensitized radiolysis is examined briefly. The formation of hydrogen in the radiolysis will be discussed on the basis of new information derived from CD_4-H_2S experiments.

Key Words: Photolysis, radiolysis, free radical reactions, ion-molecule reactions.

Laser probe excitation in spectrochemical analysis. I. Characteristics of the source, S. D. Rasberry, B. F. Scribner, and M. Margoshes, *Appl. Opt.* **6,** *No. 1, 81–86 (Jan. 1967).*
A laser probe for spectrochemical anslysis is described. A high energy laser beam is focused onto a specimen to vaporize a sample from a small area, and the vapor thus formed is further excited by a spark discharge. The characteristics of emission spectra with and without auxiliary spark excitation are compared. Spectrograph illuminating-systems for qualitative and quantitative analysis were investigated. Some difficulties were encountered with the laser probe, and modifications were made to the instrument to alleviate some of these problems. Some typical analytical applications are discussed.

Key Words: Laser probe, qualitative, laser vaporization, Q-switched ruby laser, spectrochemical, high energy, spark excitation, illuminating system, analysis, high power, emission, emission spectra.

Laser probe excitation in spectrochemical analysis. II. Investigation of quantitative aspects, S. D. Rasberry, B. F. Scribner, and M. Margoshes, *Appl. Opt.* **6,** *No. 1, 87–93 (Jan. 1967).*
A study has been made of quantitative analysis by a laser probe with spark excitation of the sample vapor. Random errors come largely from variations in laser energy and from photometric errors. The parameters of the spark circuit affect the line intensities; however, these factors are well controlled. Correlations have been established between the energy of the laser beam, the size of the pit formed, and spectral intensities. Single-spike laser operation has been found to be preferable for most purposes to multiple-spike operation. At present, the coefficients of variation for analysis are 15 to 40%.

Key Words: Laser probe, spectrochemical analysis, quantitative, laser vaporization, spark excitation, high energy, high power, pit

volume, spectral intensity, spark, photographic emulsion, Q-switched ruby laser.

pH determination, R. G. Bates, *Encyclopedia of Industrial Chemical Analysis* **3,** *146–161 (John Wiley & Sons, Inc., New York, N.Y. 1966).*
Procedures for the determination of *p*H by both electrometric and indicator methods are set forth. The NBS reference standard solutions are described. Other topics discussed include the limitations of measured *p*H values, glass electrodes and reference electrodes, *p*H instrumentation, temperature effects, and the special requirements of industrial *p*H control.

Key Words: Glass electrodes, industrial analysis, *p*H determination, *p*H instrumentation, reference electrodes, temperature effect.

Surface studies of natural and synthetic bone mineral teeth, W. V. Loebenstein, *(Proc. 2nd Workshop, Adhesive Restorative Dental Materials, University of Virginia, Charlottesville, Va., Dec. 8–9, 1965), Book, Adhesive Restorative Dental Materials, ch. IV. Surface Measurements-Synthesis and Evaluation of Dental Adhesives, pp. 213–223 (Dept. of Health, Education, and Welfare, Washington, D.C. 1966).*
Low temperature nitrogen adsorption measurements have been performed using dentin and bone as well as synthetic calcium phosphate preparations. Surface areas ranging from about 1½ to nearly 150 $m^2.g^{-1}$ have been found. Pore size distribution calculated from the isotherm data shows promise of being a valuable and sensitive tool for aiding in the comparison of crystallographic forms and for detection of subtle changes in structure not measurable by other means presently in use. The pore structure of bone mineral in the range 20–300 Å appears to be entirely independent of the collagen matrix.

Key Words: Adsorption, surface chemistry, pore size dsitribution, surface area, teeth, bone, hydroxyapatite, calcium phosphate, octacalcium phosphate, pore volume, anorganic bone mineral and dentin.

Testing scouring powder abrasion, W. C. Wolfe, *Detergent Age* **2,** *No. 10, p. 22 (Mar. 1966).*
Five leading brands of household scouring powders were examined in order to establish a formulation for testing the abrasion or wear resistance of sanitary plumbing fixtures. A test abrasive of known composition and representative of commercial products was desired. The products examined all contained sodium dodecylbenzenesulfonate as the detergent, usually chlorine bleach, sometimes bactericide, and about 90 percent by weight of abrasive. The abrasive, in each case, was fine quartz powder, mostly less than 44 microns particle size, but containing some particles between 149 and 250 microns in diameter, which might scratch porcelain enamel or plastic.

Key Words: Abrasives, bathtubs, cleansers, detergents, particle, plumbing, plastic, porcelain, sieve, silica, sinks.

The estimation of molecular weights of vinyl acetate copolymers in latex paints, H. W. Berger, *J. Paint Technol.* **39,** *No. 508, 310–315 (May 1967).*
A viscometric technique has been used for the estimation of the molecular weights of vinyl acetate copolymers used in manufacturing latex paints. The whole paint is diluted with boiling acetone and the dissolved polymer is separated from pigments by centrifuging. The intrinsic viscosity, $[\eta]$, of the polymer in acetone at 25 °C is obtained and used to calculate a quantity related to the molecular weight. The various values for a and K, the constants in the Mark-Houwink Equation, that have been reported in the literature for PVA in acetone are used empirically to derive the equation, $\log \bar{M} = 1.45 \log [\eta] + 5.521$. This equation is used as the basis for the estimation of the molecular weights of PVA copolymers in experimental latex emulsions, experimental paints formulated with those latexes, and proprietary paints.

Key Words: Copolymer, intrinsic viscosity, latex, Mark-Houwink, molecular weight, polymer, polyvinyl acetate.

The National Standard Reference Data System program in atomic and molecular properties, S. A. Rossmassler, *(Proc. Symp. Compilations of Data on Chemical and Physical Properties of Substances, 152nd National Meeting, Am. Chem. Soc., New York, N.Y., Sept. 12, 1966) J. Chem. Doc.* **7,** *No. 1, 15–18 (Feb. 1967).*
In general, atomic and molecular properties are taken to mean properties primarily characteristic of the individual atoms or molecules rather than of any system or state of aggregation. For operational convenience, the area includes also certain general and fundamental physical constants.
An Advisory Panel listed sixty-three specific properties and gave high priority to twenty-eight of these. The Office of Standard Reference Data is supporting or monitoring sixteen projects which are concerned with fourteen of these high priority topics. Most of the projects are continuing ones. Five of the activities perform data center or information center functions.
In several cases, joint support or cooperative programs have been developed, and we are seeking to extend this type of activity.
To provide reasonable current coverage of the general area, the number of projects should be doubled (high priority topics only) or trebled, (high priority plus related moderate priority topics) as rapidly as possible. Projects being initiated in other countries (cf. next paper by R.M.S. Hall) are already assuming some of this burden. Ten compilations of data and a similar number of bibliographies and secondary publications will have appeared by the end of calendar year 1966.

Key Words: Atomic, molecular, properties, data, compilation, data center.

The radiation-induced copolymerization of tetrafluoroethylene and 3,3,3-trifluoropropene at high pressure, D. W. Brown and L. A. Wall, *(Proc. Symp. Compilations of Data on Chemical and Physical Properties of Substances, 152nd National Meeting, Polymer Preprint* **7,** *No. 2, 1116–1132, (Sept. 1966).*
A study was made of the gamma-ray induced copolymerization of tetrafluoroethylene (TFE) and 3,3,3-trifluoropropene (TFP). Copolymerizations were carried out at 100 °C and 5000 atm pressure and at 21 °C and various pressures up to 8000 atm. The reactivity ratios calculated from the composition data indicate that the propagation rate constants favor addition of TFP by a factor of three to seven; individual values depended little on the polymerization pressure and temperature. Polymerization rates changed little with monomer composition between zero and 75% TFE; between 75 and 95% TFE they increased by a factor of ten. As many as 850,000 (molecules) were polymerized per 100 electron volts absorbed.
The copolymers are soluble in hexafluorobenzene at 29.6 °C if they contain less than 70% TFE. Intrinsic viscosities range from 0.1 to about 10 dal/g. From various considerations it appears likely that the degree of polymerization is about equal to the kinetic chain length in high pressure polymerizations at 21 °C; at autogenous pressure or at 5000 atm and 100 °C monomer transfer reduces the value considerably.

Key Words: Tetrafluoroethylene, trifluoropropene, copolymerization, pressure, radiation, reactivity ratios.

A dual frequency VLF timing system, L. Fey and C. H. Looney, *IEEE Trans. Instr. Meas.* **IM-15,** *No. 4, 190–195 (Dec. 1966).*
The use of high precision portable clocks and radio signals is discussed in relation to synchronization of remotely located clocks. The demonstrated inherent phase stability, approximately two μs rms, of very-low frequency (VLF) propagation and its low attenuation rate with distance, have led to various approaches to exploit these virtues in timing applications. The system considered here employs two carrier frequencies with timing information contained in their difference frequency to permit identification of a specific cycle of one of the carrier frequencies. Such a system makes stringent demands on phase stabilities of the transmitted signals and of the receiving system as well as that of the propagation medium itself. The present system, whose development has been supported jointly by NBS and NASA, makes use of NBS radio station WWVL at Fort Collins, Colorado. Receivers are of the standard VLF phase tracking servo type. A special signal generator is used in conjunction with the local clock to simulate the transmitted signal in order to relate the local time scale to that at the transmitter.
One of the carrier frequencies is maintained at 20 kHz. With a second frequency (500 Hz removed from this frequency), carrier cycle identification was achieved on about 90 percent of the days for over a month on the path from Fort Collins, Colorado, to Greenbelt, Maryland. Since January 4, 1966, the difference frequency has

been 100 Hz, with somewhat more fluctuation in results. However, lower precision is required for the initial synchronization. The results of averaging to improve this performance will be discussed.

Key Words: Worldwide clock synchronization; VLF propagation; portable clock; multiple VLF transmissions; standard time broadcasts.

An analysis of low information rate time control unit, L. Fey, J. A. Barnes, and D. W. Allan, *Proc. 20th Annual Symp. Frequency Control, Atlantic City, N.J., Apr. 19–21, 1966 pp. 629–635 (1966).*
Computer simulation has been used to study the feasibility of producing a synchronized time station requiring minimum attention to operate.
The device simulated consists of a multiloop servo system to correct the output phase of a quartz crystal oscillator and to simultaneously compensate for the linear frequency drift common to these oscillators. Upon the occurrence of an occasional phase comparison, such as propagated from VLF transmission during the time of day when propagation conditions are most stable, the servo incorporates a resulting phase correction and establishes a new linear frequency drift compensation rate based on the past history of the oscillator—allowing extrapolation of the phase of the reference signal until the next phase comparison occurs. This in effect results in a remote, phase locked system operating automatically with an intermittant reference.
The effect on such a system of flicker noise modulation, the characteristic type of noise associated with quartz crystal oscillators in the domain of interest, is treated, along with servo system time constant considerations.
The use of such a system is discussed in relation to applications such as unmanned standard time and frequency stations, meteor burst synchronization, and the operation of atomic time scales with intermittant frequency calibrations. From available data, one anticipates a synchronization precision of 1 microsecond at stations as remote as 1,500 kilometers using the meteor burst technique. The system would be both low in initial cost and in operation.

Key Words: Time synchronization, flicker noise, multi-loop servo, VLF propagation, meteor burst, oscillator correction.

An equation for the local thermal emissivity at the vertex of a diffuse conical or V-groove cavity, F. J. Kelly, *Appl. Opt.* **5,** *925–927 (June 1966).*
An exact, closed-form expression is derived for the apparent local emissivity at the vertex of a diffuse conical or V-groove cavity. This expression is obtained by a substitution into an approximate equation for the apparent local emissivity of a point within a cavity of any shape. The exact expression depends only on the emissivity of the cavity wall material and the angle factor between the point at the cavity vertex and the cavity opening. Agreement is very good between the values predicted by the expression and those obtained from a numerical solution of the integral equation characteristic of a diffuse conical cavity.

Key Words: Diffuse conical or V-groove cavity, emissivity, vertex of a diffused conical or V-groove cavity, equation, apparent local emissivity, V-groove cavity, vertex of a diffused conical or V-groove cavity.

A precision current comparator, C. M. Allred and R. A. Lawton (*Proc. Annual ISA Conf., New York, N.Y., Oct. 1966), ISA Preprint No. 12. 8–2–66 (Oct. 1966).*
A technique capable of precise comparison of currents in different parts of a network or between currents in different networks is discussed. With proper conditions, this comparison can be done with negligible perturbation of the networks under measurement.
Experiments on a coaxial system at 30 MHz are discussed.

Key Words: Antenna, attenuation, comparator, current, phase, precision.

Impedance measurements in coaxial waveguide systems, R. L. Jesch and R. M. Jickling, *Proc. IEEE* **55,** *No. 6, 912–923 (June 1967).*
This article is a tutorial review of impedance measurements and standards in coaxial waveguide systems propagating a TEM wave. It describes the development of coaxial air lines as impedance standards, reviews representative measurement methods, and discusses the errors and measurement techniques of the slotted line in detail. A list of selected references to pertinent literature is included.

Key Words: Impedance, waveguide, transmission line, standards, coaxial, measurements, air lines.

International comparison of high frequency electromagnetic quantities, M. C. Selby, *Proc. IEEE* **55,** *No. 6, 745–747 (June 1967).*
Activities to establish international agreement on measurements of high frequency electrical quantities have been in progress since 1957 at the initiative of the URSI (International Radio Scientific Union) and the International Committee of Weights and Measures (CIPM). Results accomplished and the overall up-to-date status are presented.

Key Words: Electrical quantities at high frequencies, measurement of high frequency electrical measurements, international agreement on electromagnetic measurements.

Field strength above 1 GHz: Measurement procedures for standard antennas, R. R. Bowman, *Proc. IEEE* **55,** *No. 6, 981–990 (June 1967).*
To calibrate antennas for state-of-art field strength measurements, standard horns are needed with gain uncertainties well within ± 0.1 dB. To attain this degree of accuracy for absolute gain measurements, the two-antenna method is recommended. This method is considered to be essentially an insertion loss measurement (with many additional problems and sources of error), and a working formula is derived that is suitable for gain measurements of high accuracy. The problems that appear to be most limiting in gain measurements, insufficient antenna separation and multi-path interference, are chosen for detailed discussion. (The discussion concerning multi-path interference has application to anechoic chamber evaluations and radar cross-section measurements as well as to gain measurements). It is concluded that error estimates of less than ± 0.1 dB for horm gain measurements have been somewhat optimistic. Several ambiguities and sources of error have been overlooked or inadequately discussed, and additional discussion is presented to provide a more complete basis for horn gain measurements of high accuracy.

Key Words: Field strength, high accuracy gain measurements, horn antennas, two-antenna method, gain corrections, multi-path interference, antenna range design.

Impedance measurements and standards for uniconductor waveguide, R. W. Beatty, *Proc. IEEE* **55,** *No. 6, 933–941 (June 1967).*
A tutorial review is presented of the measurement of impedance and reflection coefficient in uniconductor waveguide. Impedance in a waveguide operating in a particular mode is defined and related to measured quantities such as the reflection coefficient and the VSWR.
Emphasis is given to the rectangular waveguide operating in its dominant mode and to the tuned reflectometer as an instrument for achieving the most accurate results. The evolution of the tuned reflectometer at NBS is outlined and recent techniques are discussed. Different types of standards of reflection coefficient are described and the advantages and limitations of each are mentioned.

Key Words: Impedance standard, reflection coefficient, reflectometers, standing-wave ratio, waveguide impedance.

Conference on burns and flame retardant fabrics, December 1966, New York, N.Y., A. F. Robertson, *Fire Res. Abst. Rev.* **9,** *No. 2, 119–122 (1967).*
A summary is presented of subject meeting which was held on 2 and 3 December 1966.

Key Words: Fire-retardant clothing, retardant treated fabrics, flame resistance, clothing, fire, accidents, clothing fires, burn injuries.

Doors as barriers to fire and smoke, H. Shoub and D. Gross, *Proc. Symp. Fire Testing, Lancaster, Pa., June 24–25, 1965, pp. I-1–I-10 (Armstrong Cork Co., Lancaster, Pa., 1965).*

A study was made of means for improving dwelling unit entrance doors as fire and smoke barriers. Existing combustible doors and frames could be modified to enhance their fire resistance, but it did not appear practical to raise them to the level of rated commercial fire door assemblies. Fire retardant paints, except those consisting of heavy, reinforced, intumescent-type coatings, provided little or no increase in fire resistance.
Several modifications of existing doors were not effective in preventing the transmission of smoke. However, controlling the pressure levels on both sides of a door, as by suitable venting, appeared to offer a means of reducing smoke penetration into an area.
It is recommended that current methods of fire tests of doors, and criteria relating to their fire and smoke transmission be improved.

Key Words: Doors, dwelling, dwelling unit entrance doors, fire and smoke barriers.

Calorimetric measurement of pulsed laser output energy, D. A. Jennings, *IEEE Trans. Instr. Meas.* **IM-15,** *No. 4, 161–164 (Dec. 1966).*
One of the important parameters of pulsed laser systems is their output energy. The application of pulsed lasers requires knowing this output energy with varying degrees of accuracy depending on the application. There are several methods by which one may measure the energy output of the laser. However, the technique which seems to be promising as far as accuracy and precision are concerned is the calorimetric method. We have designed, built, and calibrated calorimeters for measuring the output energy of the pulsed ruby laser (6943 Å). The heart of the calorimeter is a small absorption cell containing an aqueous solution of $CuSO_4$. The temperature of the absorption cell, as measured by a thermocouple, indicates the energy absorbed by the calorimeter. The calorimeter was calibrated in two different ways: (1) The known heat capacity of the absorption cell and the thermocouple sensitivity calibration gives a calorimeter calibration which agrees within 0.3 percent or (2) an electrical energy substitution calibration which is obtained via a heater wire contained in the absorption cell solution. A method has been devised by which two calorimeters may be intercompared. Calorimeters which we have built and calibrated agree with each other to about 0.7 percent. This specific calorimeter has been designed to measure energies up to 30 "Joules" and will take peak powers of up to 200 MW/cm^2.

Key Words: Laser, calorimeter, energy, measurement.

Long-time effects of humidity change on the dielectric properties of certain polymers, A. H. Scott and W. P. Harris, *(Proc. 1962 Annual Report Conf. Electrical Insulation, Hershey, Pa., Oct. 15–17, 1962), Natl. Acad. Sci.-Natl. Res. Council Publ. 1080, pp. 41–44 (1963).*
The results of a study of the long-time effects of humidity change on the dielectric properties are given for three materials, polyethylene, polystyrene, and polycarbonate. The polyethylene and polystyrene specimens were disks about 4 cm. in diameter with gold electrodes. Measurements on polycarbonate specimens were made using the air-gap method without contact electrodes. The electrical properties of some specimens were still changing at the end of three years. The results are given in the form of graphs.

Key Words: Dielectric properties of certain polymers, humidity change, polycarbonate, polyethylene, polystyrene, properties of certain polymers, polymers.

Lumped parameter impedance measurements, L. E. Huntley and R. N. Jones, *Proc. IEEE* **55,** *No. 6, 900–911 (June 1967).*
This paper is a tutorial presentation dealing with two and three terminal lumped parameter impedance measurements at radio frequencies. Included is a very brief historical discussion with particular emphasis upon more important recent developments such as precision coaxial connectors and coaxial air line standards. The relationship of impedance standards to standards of length and time is shown together with a discussion of instruments and measurement techniques in current use. Special attention is given to particular areas of measurement difficulty. Also included is a presentation of the state-of-the-art wherein commercial instrumentation is compared with best practices from the standpoint of accuracy. The paper concludes with comments and recommendations for improving measurement and measurement agreement.

Key Words: Capacitance, inductance, impedance and admittance, measurement, radio frequency, resistance, standards, state-of-the-art.

Measurement of RF peak pulse power, P. A. Hudson, *Proc. IEEE* **55,** *No. 6, 851–855 (June 1967).*
Methods for radio and microwave measurements of dielectric and magnetic properties of materials are categorized, referenced, and placed in perspective. The reference period extends to mid-1966. Measurement errors are analyzed for appropriate cases where possible.

Key Words: Review of radio materials, radio materials measurement, dielectric constant, dielectric loss, ferromagnetic resonance, permeability.

Micrometer U-tube manometers for medium vacuum measurements, A. M. Thomas and J. L. Cross, *J. Vacuum Sci. Technol.* **4,** *No. 1, 1–5 (Jan.–Feb. 1967).*
A family of U-tube manometers, suitable for use as standard instruments, has been designed and constructed at the National Bureau of Standards to cover the range of pressures from 100 torr to 1×10^{-2} torr. In these instruments the levels of the two liquid surfaces are measured by adjusting micrometers with conical points ground on the ends of the spindles. Four inch and two inch range mercury manometers, with spindles approaching the liquid surface from above, are used for differential or absolute pressure measurements up to 100 torr. Pressures less than 3.5 torr are measured with oil manometers, in which the micrometer spindles approach the surfaces from below. Measurements made with the mercury manometer have an uncertainty of about 4×10^{-3} torr plus eight parts in one hundred thousand of the reading. Measurements made with the oil manometer have an uncertainty of about 4×10^{-4} torr plus two parts in ten thousand of the reading.

Key Words: Vacuum measurement, manometers, U-tube, micrometer, oil, mercury, water.

NBS Field-strength standards and measurements (30 Hz to 1000 MHz), F. M. Greene, *Proc. IEEE* **55,** *No. 6, 970–981 (June 1967).*
A description is given of the various CW field-strength standards and associated measurement instrumentation and techniques developed over the past twenty-five or thirty years at the National Bureau of Standards. These are used for the calibration of both commercial and military field-strength meters in various frequency bands of the overall range from 30 Hz to 1000 MHz. The techniques used are applicable only for evaluating the strength of steady-state, ac fields varying sinusoidally in time, and are not intended for use in broadband applications of any kind.
Two principal types of field-strength standards and a prototype near-zone field-strength meter are described. These are as follows:
(a) *Magnetic-Field-Strength Standards* used over the frequency range 30 Hz to 30 MHz for the calibration of CW field-strength meters employing small-loop receiving antennas;
(b) *Electric-Field-Strength Standards* used over the frequency range 30 to 1000 MHz for the calibration of CW field-strength meters employing half-wavelength self-resonant dipole receiving antennas; and
(c) *Near-Zone Electric-Field-Strength Meter and Interim Field-Strength Standards* used over the frequency range 150 kHz to 30 MHz for the evaluation of hazards of high-level electromagnetic radiation to ordnance devices and other uses.

Key Words: Magnetic-field-strength standards, electric-field-strength standards, near-zone electric-field-strength standards, calibration of field-strength meters, standard-field calibration method, standard-antenna calibration method.

Peak pulse voltage measurement (baseband pulses), A. R. Ondrejka, *Proc. IEEE* **55,** *No. 6, 882–885 (June 1967).*
Several methods are presently being used for the measurement of pulse voltage. Oscilloscopes are particularly useful because they provide information concerning the shape of the pulse, besides a measure of the peak voltage. Besides the oscilloscope, several peak voltmeter circuits are mentioned. These include pulse stretching, sampling, and the slideback method. A standard pulse generator

is described which provides a calibrated pulse voltage suitable for voltmeter calibration and other uses.

Key Words: Oscilloscope, peak voltage, pulse, sampling, slideback, standard.

Physical and performance properties of leather, J. R. Kanagy, *Book, The Chemistry and Technology of Leather,* **4,** *ch. 64, 369–416 (Reinhold Publ. Corp., New York, N.Y., 1965).*
This chapter gives an outline of the properties of leather including both strength and mechanical properties such as compressibility and flexing. In addition its value as an insulator and its stability to temperature and atmospheric conditions are discussed. The nature of the hide is described with regard to fiber structure and chemical composition in order to give a better understanding of its properties and indicate how it might be modified. The information should be useful in developing further uses for leather and to stimulate further research in the study of its properties.

Key Words: Physical properties, mechanical properties, fiber structure, stability, insulator leather, hide.

Precision coaxial connectors in lumped parameter immittance measurements, R. N. Jones and L. E. Huntley, *IEEE Trans. Instr. Meas.* **IM-15,** *No. 4, 375–380 (Dec. 1966).*
Amid the concern surrounding the design and application of precision coaxial connectors for use in precise electrical measurements there is one area which has received very little attention. This has to do with the application of such connectors to measurements in the lumped-parameter region. This paper points out significant sources of error in lumped-parameter measurements which are attributable to connector uncertainties and shows how they can be greatly reduced through the application of precision coaxial connectors. Where these connectors are utilized in lumped-parameter immittance measurements, extensions of frequency, magnitude and accuracy are realized. Specific examples are discussed.

Key Words: Immittance, precision, lumped-parameter, measurement, coaxial, connectors, radio frequency.

Progress in the development of a thermal-shock-resistance factor for bituminous built-up roofing, W. C. Cullen and T. H. Boone, *ASTM Spec. Tech. Publ.* **409,** *151–161 (Apr. 1967).*
The resistance of bituminous built-up roofing membranes to thermally induced forces is considered in terms of their strength properties such as breaking load in tension, modulus of elongation and apparent linear thermal expansion coefficient. The development of a thermal-shock resistance factor is described and values are given for three bituminous built-up membranes at temperatures of −30 °F (−34.4 °C), 0 °F (−17.8 °C), 30 °F (−1.1 °C) and 73 °F (22.8 °C). The apparent relation between the values obtained in the laboratory and the observed performance of roofing membranes in service is considered. The utilization of the thermal-shock resistance factor in the reduction of potential failures of bituminous built-up roofing membranes in service from thermally induced forces is also discussed.

Key Words: Development, roofing membrane, strength properties, thermally induced forces, thermal-shock resistance factor.

Radio frequency power measurements, A. Y. Rumfelt and L. B. Elwell, *Proc. IEEE* **55,** *No. 6, 837–850 (June 1967).*
The need for improved accuracy in and understanding of all kinds of measurements has come with the recent rapid advances in modern technology. RF power measurement, the subject of this paper, is no exception to this requirement. The basic principles of bolometric, calorimetric, and certain other types of power meters are reviewed. The methods for making accurate RF power measurements are discussed in detail. Emphasis is given to the techniques for eliminating or accounting for the errors due to mismatch, dc or LF substitution, and bolometer mount efficiency.

Key Words: Power meter, power measurement, mismatch error, substitution error, bolometer mount efficiency.

RF attenuation, D. H. Russell and W. Larson, *Proc. IEEE* **55,** *No. 6, 942–959 (June 1967).*
A tutorial review of r-f attenuation measurement methods and standards is presented.
Accepted and proposed definitions and attenuator models are discussed. Commonly used standards operating from d-c through most waveguide bands are compared with the "ideal" interlaboratory standard. Characteristics of fixed resistive, waveguide below-cutoff and rotary-vane standards are included.
Measurement methods are classified and described including comments concerning convenience and accuracy of various methods, and references are given which cover most of the basic and important research in the field.

Key Words: Attenuation, measurements, standards, coaxial, waveguide.

RF measurements of the speed of light, R. C. Baird, *Proc. IEEE* **55,** *No. 6, 1032–1039 (June 1967).*
Modern RF measurements of the velocity of light are reviewed, with emphasis on those methods capable of attaining an accuracy of 1.0 km/s or better. The geodimeter and microwave interferometer methods are discussed in some detail because of the significant role they have played in arriving at our present value for c. Serious limitations of the microwave resonant cavity method are pointed out and brief mention is made of the electrical units and band spectrum methods. A recent measurement by Karolus and Helmberger, who obtained the value 299 792.1 ± 0.2 km/s, is mentioned. Some experimental factors that should be considered in planning future velocity of light measurements are presented, and an experiment involving lasers, now in progress at NBS, is described briefly. The conclusion is that the presently accepted value of 299 792 ± 0.3 km/s is still valid. Only two or three measurements have been completed since its adoption nearly ten years ago and they are not of sufficient accuracy to warrant a reevaluation of c.

Key Words: Velocity of light, review, methods and limitations, recent results.

Sampling of leather for physical and chemical examination, J. Mandel and J. R. Kanagy, *Book, The Chemistry and Technology of Leather* **4,** *ch. 59, 223–242 (Reinhold Publ. Corp., New York, N.Y. 1965).*
A presentation of some general principles of sampling, with application to the sampling of leather.
The topics discussed in this chapter include:

1. General statistical principles of sampling: effect of sample size and of lot size;
2. formulas for the determination of sample size;
3. the selection of a sampling location on a leather side;
4. tables of the variability of physical and chemical tests between locations and between hides;
5. acceptance sampling; and
6. a survey of the literature.

Key Words: Sampling, Leather, quality control, statistics, test variability, acceptance sampling.

Standards for galvanomagnetic devices, S. Rubin (*Proc. Committee on Hall Effect Applications, Cambridge, Mass., Nov. 8–9, 1965), Book, Solid State Electronics* **9,** *No. 65, 559–566 (Pergamon Press, Inc., New York, N.Y., 1966).*
A summary is given of existing and "in-process" standards for galvanomagnetic devices. Controversial items in the IEC standard for Hall effect devices, 47(Secretariat)196, May 1965, are reviewed, and note is made of USA and Japanese comments on this document. Items in the USA document, 47(USA), September 1965, commenting on 47(Secretariat)196, are reviewed, and particular emphasis is given to items relating to linearity error, particularly as a percent of reading, to residual voltages, and to sensitivity indices.
A summary of items in an "in-process" document for "Standard Definitions and Terminology for Magnetoresistive Devices," is given. The concept of compatibility between definitions for flux and temperature sensitive resistors (i.e., magnetoresistors, thermistors, and photoresistors) is introduced. Some overlapping areas of application are noted. The linear input-output characteristics obtainable from a device which has a square law characteristic is noted and appropriate definitions for both characteristics are introduced. Copies of four documents dealing with standard terminology and definitions for Hall effect devices are included as appendices.

Key Words: Hall effect device, magnetoresistive device, magnetoresistor, Hall element, standard terminology, galvanomagnetic device.

Some accuracy limiting effects in an atomic beam frequency standard, R. J. Harrach, *Proc. 20th Annual Symp. Frequency Control, Atlantic City, N.J., Apr. 19–21, 1966, pp. 424–435 (1966).*
The accurate resonance frequency of the transition

$$(F, M_F) = (4, 0) \leftrightarrow (3, 0)$$

in the ground state of cesium-133 is expressed in the form of an operational equation for an atomic beam spectrometer. Emphasized are the terms in this equation which correct for the beam direction dependence and radiation field dependence of measured resonance frequencies: $\frac{1}{2}(\nu_{res_i}(P_1) + \nu_{res_j}(P_1)) - \frac{1}{2}(S_i + S_j)P_1$, where i and j refer to opposite beam directions through the apparatus, P_1 is the microwave power exciting the transition, and S_i and S_j are rates of linear frequency shift. The results of a detailed theoretical analysis are given which specify the contributions to these terms by various apparatus and fundamental shift-inducing effects.
This approach to accuracy specification is applied to the United States frequency standard, a National Bureau of Standards atomic beam machine designated NBS III, through a set of experiments using an atomic hydrogen maser as a highly stable reference frequency source. The corrections determined are -3.2×10^{-12} for beam direction dependence, -2.2×10^{-12} for power dependence and $+0.4 \times 10^{-12}$ for second-order Doppler shift. The uncertainties in these corrections and contributions from other sources give a present 1σ estimate of accuracy capability of $\pm 1.1 \times 10^{-12}$ for NBS III. This figure should be reducible by one order of magnitude through efforts to eliminate systematic errors in the measurements of ν_{res_i} and ν_{res_j}.

Key Words: Accuracy, cesium beam, frequency shifts, frequency standard.

Superconducting devices, T. M. Flynn and K. D. Timmerhaus (*Proc. Intern. Inst. Refrigeration Meeting of Comm. 1, Boulder, Colo., June 15–17, 1966*), *Book, Liquid Helium Technology, Bull. IIR Annexe 1966–5, pp. 459–490 (Paris, France, 1967).*
Superconductors may be treated as engineering materials having three unusual properties: (1) a transition occurs between two different states which depends upon external parameters, (2) zero resistivity is exhibited in one state, and (3) perfect diamagnetism is exhibited.
This paper views superconductors in this way, as engineering materials, and examines applications of these properties. Examples include applications of superconductors to thermometry, bolometery, level gauging, rectifiers, magnets (briefly), bearings, motors, electron microscope lenses, and a helium pump.

Key Words: Bearings, bolometer, electron microscope, helium, hydrogen, level gauging, liquid level, magnet, motor, pump, rectifier, solenoid, superconductivity, switch, temperature, thermometer.

The Measurement of baseband pulse risetimes of less than 10^{-9} seconds, N. S. Nahman, *Proc. IEEE* **55,** *No. 6, 855–864 (June 1967).*
This is a review paper dealing with the measurement of fractional nanosecond pulse rise time in which the following subjects are discussed: oscillographic systems, pulse comparison techniques, a basic instrumentation system, and the distortion of pulses by transmission lines. Extensive references are provided. Included in the discussion is a delineation of equivalent time oscillographic sampling systems and a classification into three sampling categories: sequential, random, and multiple. Also considered are single transient oscillographic systems employing either traveling wave deflection structure cathode ray tubes or multiple sampling methods. In order to clearly present the rise time limitations caused by TEM transmission lines, attention is given to the distortion incurred by pulses upon passing through such lines. Some suggestions and predictions relating to future work are presented.

Key Words: Baseband pulse rise-times, basic instrumentation system, fractional nanoseconds pulse rise-times, oscillographic systems, pulse comparison techniques, pulse rise-times.

The measurement of current at radio frequencies, W. W. Scott, Jr. and N. V. Frederick, *Proc. IEEE* **55,** *No. 6, 886–891 (June 1967).*
The state-of-the-art of radio-frequency current measurements is reviewed with emphasis on what the authors consider are the most useful current standards. In particular, thermocouple and electrodynamic ammeters are discussed in detail. Reference is made to photoammeters, air thermometer ammeters, and other types of current measuring apparatus, some of which deserve additional development. Extensive referencing is included for the convenience of investigators interested in an intensive review of radio-frequency current measurements.

Key Words: Ammeter, calibration, current, electrodynamic, measurement, radio-frequency, standards, thermocouple.

The role of the CCRL, J. R. Dise, *Construct. Specifier* **20,** *54–60 (June 1967).*
The history and methods of operation of the Cement and Concrete Reference Laboratory are described together with the benefits which can be derived from the inspection of cement and concrete testing laboratories.

Key Words: Cement and concrete testing laboratories, inspection of cement and concrete testing laboratories.

Transistorized UHF marginal oscillator and its application for the measurement of the magnetic flux density, S. Rubin, *Proc. IEEE Letter* **53,** *No. 9, 1249–1250 (Sept. 1965).*
A transistorized marginal oscillator operating in the UHF region has been used to measure magnetic flux density in a Helmholtz coil at 17.5 mT, with an accuracy of better than a part in 10^3. The instrument uses plug-in oscillator modules to simplify frequency changing. The results achieved indicate the feasibility of such a device for measurement of magnetic flux density in the 1 to 50 mT range in industrial environments and with accuracies approaching a part in 10^4.

Key Words: Density, magnetic flux, flux density, magnetic flux density, marginal oscillator, oscillator, marginal, UHF marginal oscillator.

UHF and microwave phase shift measurements, D. A. Ellerbruch, *Proc. IEEE* **55,** *No. 6, 960–969 (June 1967).*
A phase shift standard, a measurement system and the techniques for determining the corresponding limit of uncertainty are all required for obtaining the phase shift characteristics of UHF and microwave components. Differential phase shift standards, measurement techniques and measurement uncertainties are all discussed in a general sense and a comprehensive bibliography is included to supplement the general discussion.

Key Words: UHF, microwave, phase shift, measurements, standards, uncertainties.

Voltage measurement at high and microwave frequencies in coaxial systems, M. C. Selby, *Proc. IEEE* **55,** *No. 6, 877–882 (June 1967).*
The progress and up-to-date state of the art in measuring voltages at frequencies to 10 GHz and higher at three accuracy echelons is briefly described. The trend toward higher frequencies in voltmeter design is indicated. Justifications for this trend are listed. Advantages of voltage measurements and standards over computation of voltages from power and impedance measurements are briefly discussed. Some pending development problems are indicated and major steps are proposed to improve the application of voltmeters at frequencies above 30 MHz.

Key Words: Voltage measurement, high frequency voltages, microwave voltages, standards of rf voltage.

Computer languages and their use, S. N. Alexander, *Am. Mgmt. Assoc. Mgmt. Bull.* **79,** *8–12 (1966).*
Three levels of computer programming languages are discussed in terms of their effectiveness as tools for solving the man/machine interface problem. In this respect, the least effective of the three is the assembly level language which in general is used only when maximum system performance is required. At the next level of

effectiveness are the procedure-oriented languages such as FORTRAN, COBOL and ALGOL. In general, these are at a level of abstraction considerably above that of machine commands, but are still not at the working level of the average application analyst. The third level, problem oriented languages, are generally much closer to the specific mode of expression used by the analyst in describing the solution to a given problem. Several examples of this type of language are given including some that make use of ordered or graphical arrangements of inputs to facilitate the external mode of expression. The paper concludes with brief discussions of software documentation and the economic aspects of software development and utilization.

Key Words: Problem-oriented languages, software usage, man/machine interface problems, economics of software, documentation of software.

Representations of discrete groups, J. Lehner, *Proc. Symp. Pure Mathematics, California Institute of Technology, Pasadena, Calif., Nov. 21–22, 1963, ch. VIII, Theory of Numbers, pp. 203–208 (American Mathematical Society, Providence, R.I., 1965).*
It is shown that certain properties of a class of finitely generated abstract groups known as F-groups are preserved when the F-group is imbedded in SL(2, reals) as a discrete matrix subgroup. Thus the abstract structure of the F-group determines to a certain extent the topological properties of the matrix group.

Key Words: Abstract groups, discrete groups, F-groups, matrix groups.

The mathematical representation of physical entities, C. H. Page, *IEEE Trans. Educ.* **E–10,** *No. 2, 70–74 (June 1967).*
Mathematics comprises abstract operations upon abstract elements. For the application of mathematics to the sciences, we must not only know the rules for manipulating symbols, but must also define the correspondences between the mathematical abstractions and the concepts to which application is made.
Certain basic postulates about physical observables yield the structure of their mathematical representation. An understanding of this structure yields an inderstanding of measure equations, quantity equations, measurements units, abstract units, and the mathematical nature of domensional analysis. Writing equations in a dimensionally homogeneous form is often convenient, but not necessary; sometimes an inhomogeneous formulation is more useful.

Key Words: Abstract unit, angle, dimensional analysis, measurement unit, numeric, quantity calculus, quantity equation.

Noise standards, measurements, and receiver noise definitions, C. K. S. Miller, W. C. Daywitt, and M. G. Arthur, *Proc. IEEE* **55,** *No. 6, 865–877 (June 1967).*
This paper covers four topics: (1) basic principles of noise measurement, (2) the switching radiometer, (3) a survey of noise sources, and (4) concepts of noise factor and noise temperature. The first section presents basic formulas used in analyzing radiometers. The second discusses the switching radiometer briefly tracing its development and usage in the standards field. The third section surveys the development of hot and cold thermal noise sources, noise diodes, and gas-discharge noise generators. The last section presents and discusses the basic definitions of receiver noise performance.

Key Words: Radiometer, noise source, noise factor, noise temperature, error analysis.

On the problems of measuring transient temperature in cryogenic fluids, C. E. Miller and T. M. Flynn, *ISA Trans.* **6,** *No. 2, 133–138 (Apr.–June 1967).*
The complex and frequently unpredictable energy exchange mechanisms that govern the dynamic behavior of cryogenic sensors makes the measurement of transient temperatures extremely difficult. Without suitable models by which to predict and evaluate sensor performance, considerable measurement errors can and do occur. The intent of this paper is simply to delineate in detail those factors which give rise to this situation. The validity of using notions based on the performance of the "ideal" thermometer for characterizing the cryogenic case is also discussed.

Key Words: Cryogenic, instrumentation, measurement, metrology, response time, sensor, temperature, thermometer, time constant.

The use of semiconductors for the study of boiling heat transfer to low temperature liquids, G. G. Harman and L. H. Gordy, *Cryogenics* **7,** *89–92 (Apr. 1, 1967).*
It is shown that semiconductors, such as silicon and germanium, can be advantageously used to study boiling heat transfer from solids to low temperature liquids. Measurements can be made quickly and automatically. Widely different types of resistance versus temperature characteristics can be obtained from these materials and such characteristics can influence the nature of the nucleate to film-boiling transition. Because these materials have large positive temperature coefficients of resistance, the transitions are thermally self-regulating. All heat flux data obtained from such samples lie well within normal experimental values.

Key Words: Semiconductors, cryogenic heat transfer, measurements.

Diffusion and the Kirkendall shift in binary alloys, J. R. Manning, *Acta. Met.* **15,** *817–826 (May 1967).*
In alloys, the directions of successive vacancy jumps are correlated to one another. This tends to reduce the net vacancy flux in a Kirkendall shift experiment. The magnitude of the vacancy flux, including correlation effects, is calculated assuming that vacancies are not bound to any particular atoms and that fluctuations in average local composition can be ignored. New equations for the intrinsic diffusion coefficients, Kirkendall shift, and interdiffusion coefficient in binary alloys are obtained. The Kirkendall shift and interdiffusion coefficient given by these equations are larger than those predicted by Darken but smaller than those obtained when vacancy correlations are neglected. The appearance of cross terms and additional diagonal terms in the general thermodynamic equations is discussed.

Key Words: Diffusion, vacancies, Kirkendall shift, diffusion coefficients, binary alloys, thermodynamic equations for diffusion.

Digital computers, E. W. Cannon, *Book, Encyclopedia of Physics, Ed. R. M. Besancon, pp. 124–125 (Reinhold Publ. Corp., New York, N.Y., 1966).*
A general description of analog and digital computers is provided.

Key Words: Analog digital computers, computers-analog, digital computers.

Effect on chromatic aberration on the resolving power of photographic objectives, F. E. Washer, *J. Opt. Soc. Am.* **57,** *No. 5, 625–629 (May 1967).*
An empirical method for the estimation of the probable resolving power of a lens affected by longitudinal chromatic aberration is discussed. Values of the resolving power at a series of values of the f-number are calculated for selected values of longitudinal chromatic aberration, d_c. The variation of resolving power with f-number is presented graphically for selected values of longitudinal chromatic aberration and relative contrast. Indication is given of a critical aperture for which the resolving power is a maximum for a given set of values of chromatic aberration and relative contrast. The variation of relative contrast with resolving power is presented graphically for several values of the f-number for a lens having selected amounts of longitudinal chromatic aberration. A method for predicting the resolving power of a given lens-film combination is also indicated.

Key Words: Chromatic aberration, resolving power, critical aperture, relative contrast.

Hamilton's mixed and angle characteristic functions and diffraction aberration theory, A. B. Shafer, *J. Opt. Soc. Am.* **57,** *No. 5, 630–639 (May 1967).*
The use of Hamilton's mixed and angle characteristic functions in wave and diffraction aberration calculations is theoretically examined. The relation of Hamilton's mixed and angle characteristic functions to the wave aberration function is shown. From this relation a wave aberration function is derived. The mixed and angle characteristic functions as utilized in diffraction theory via the Luneberg-Debye integrals are examined. The mathematical and

physical approximations are discussed. The use of the Luneberg-Debye diffraction integrals for image evaluation is examined and some difficulties are pointed out. It is concluded that the above methods are poor approximations to more rigorous methods.

Key Words: Hamilton's characteristic functions, diffraction, aberration.

Lectures on critical phenomena, M. S. Green (*Proc. Summer School of Theoretical Physics, Cargese, Corsica, Summer 1964*), *Book, Cargese Lectures in Theoretical Physics-Statistical Mechanics, Ed. B. Jancovici, pp. 59–88 (Gordon and Breach Publ., New York, N.Y., 1964).*
Some speculative ideas on the theory of critical phenomena in liquid vapor systems are presented. As a background for these fundamental maximum principles of statistical mechanics, thermodynamics of phase changes in the activity temperature plane and sequence of Legendre transformations are discussed. It is suggested that critical phenomena will be simpler when expressed in term distribution functions rather than the potentials and that the critical points correspond to the existence of the zero eigenvalue of the derivative matrix of the transport from potentials of average force to potentials.

Key Words: Critical phenomena in liquid vapor systems, liquid vapor systems, statistical mechanics, thermodynamics of phase changes.

Light scattering from time-dependent molecular orientations at Raman frequencies in liquids, M. McClintock, D. A. Jennings, and M. Mizushima, *Bull. Am. Phys. Soc.* **12,** *Series II, No. 5, 711 (May 1967).*
The profiles of several Raman lines arising from nontotally symmetric molecular vibrations in liquid benzene and carbon tetrachloride have been measured using 4880 Å radiation from an argon ion laser as a source of illumination. These profiles have been analyzed on the assumption that scattering occurs from time-dependent molecular reorientations of small angle in the liquid, analagous to those producing depolarized scattering at the Rayleigh line. On this basis, the half width at half maximum of the 606 cm^{-1} Raman line in benzene was found to be 3.3 cm^{-1}, and the half width of the "orientation" line underlying this Raman line was found to 24.3 cm^{-1}. The rotational relaxation time calculated for the ν_{18} vibrationally excited molecule is therefore 1.38×10^{-12} seconds. This is short compared with a period of rotation and supports the assumption of rotational Brownian motion. It is also shorter than the rotational relaxation time for the molecule in the ground vibrational state, and indicates that there is weaker rotational coupling between molecules in the ground state than between vibrationally excited molecules and those in the ground state. The depolarization ratios of the Raman and the orientation components of the 606 cm^{-1} line for linearly polarized incident light were found to be 0.748 and 0.749, respectively, in agreement with the theoretically predicted 0.750.

Key Words: Benzene, carbon tetrachloride, Raman scattering.

Measurements in a turbulent boundary layer maintained in a nearly separating condition, W. G. Spangenberg, W. R. Rowland, and N. E. Mease (*Proc. Symp. Fluid Mechanics of Internal Flow, General Motors Research Labs., Warren, Mich., 1965*), *Book, Fluid Mechanics of Internal Flow, Ed. G. Sovarn, pp. 110–151 (Elsevier Publ. Co., Amsterdam, The Netherlands, 1967).*
A turbulent boundary layer on a smooth, flat wall was investigated where the pressure was increasing with increasing distance downstream such as to maintain the boundary layer in the condition of near separation. The investigation was conducted with air flowing in a channel having the boundary-layer wall as the bottom. The width was sufficient to permit realization of two-dimensional boundary-layer flow. Venting and sloping incorporated in the upper wall provided the control of pressure gradient by progressively decreasing the velocity within the duct with increasing distance downstream. The maximum free-stream velocity was always about 84 ft per sec. The depth was sufficient to realize a free stream above the boundary layer except at the farther downstream positions where the boundary-layer flow itself reached the upper wall and escaped through the vents. Measurements of turbulence as well as of mean flow are made in order to reveal more of the mechanics of such flows than hitherto known. Measurements of turbulence were made with hot-wire instrumentation, and these comprised turbulence intensity, transverse integral scale, and turbulent shearing stress. Mean velocities were measured both with the hot-wire anemometer and total-head tube. Skin friction was estimated from mean-velocity profiles. Results were obtained for two slightly different pressure distributions, one yielding a closer approach to separation and vanishing skin friction than the other.

Key Words: Boundary layer, adverse pressure, turbulence, near-separating flow, skin friction near-zero, turbulent boundary layer.

Neutron cross section evaluations—past, present, and future, K. Parker, D. T. Goldman, and L. Wallin (*Proc. Intern. Atomic Energy Agency Conf. Reactors, Vienna, Austria, 1966*), *Book, Nuclear Data for Reactors II, 292 (1967).*
A listing in computer output of all known neutron cross-section evaluations performed throughout the world is given.

Key Words: Neutron, cross section, evaluation, compilation, nuclear reactions.

NBSR converter tube, C. F. Kupiec and C. O. Muehlhause, *Trans. Am. Nucl. Soc.* **9,** *No. 2, 582–583 (Nov. 1966).*
There are plans to incorporate a high-power-density fast-neutron converter tube in the National Bureau of Standards 10-MW Research Reactor, the NBSR. The purpose of such a facility would be for radiation effects studies where the flux is free from a thermal-neutron component. A converter of this type would allow the experimenter to irradiate relatively large samples without allowing them to become excessively radioactive or appreciably perturb pile reactivity.

Key Words: Fast neutron, converter tube, research reactor, radiation effects, thermal neutron, radioactive, pile reactivity, NBSR.

Photographic standardization and research at the National Bureau of Standards, C. S. McCamy, *Appl. Opt.* **6,** *No. 1, 27–30 (Jan. 1967).*
The Photographic Research Section of NBS provides physical standards of measurement and calibration services, cooperates with national and international standardizing organizations, and conducts research related directly to the utilization of photographic materials and processes. Standardization and research in sensitometry, standard light sources, emulsion making, preservation of photographs, precise densitometry, and image evaluation have spanned a half century.

Key Words: Photography, standardization, densitometry, NBS.

Radiation-field-dependent frequency shifts of atomic beam resonances, R. J. Harrach, *J. Appl. Phys.* **38,** *No. 4, 1808–1819 (Mar. 15, 1967).*
Radiation field dependent frequency shifts arising in atomic beam spectroscopy are treated theoretically and experimentally. Shifts due to fundamental and unavoidable interactions between the radiation field and the atoms comprising the beam are distinguished from those due to various "apparatus effects." Precise measurements of frequency shifts are made for a cesium beam experiencing Ramsey-type excitation. For the magnetic field-sensitive transitions $(F, M_F) = (4, \pm 1) \leftrightarrow (3, \pm 1)$ the magnitude of the shifts is about 1 part in 10^{10} of the resonance frequency value, per milliwatt variation of input power to the radiation field. The shifts vary with input intensity in a non-monotonic fashion, and are shown to result from non-uniformity in the static magnetic c-field of the apparatus. Much smaller shifts of about 5 parts in 10^{13} per milliwatt are observed for the magnetic field-insensitive transition $(F, M_F) = (4, 0) \leftrightarrow (3, 0)$. The major features of these shifts are shown to arise from spectral impurities in the radiation exciting the transition and a small phase difference between the pair of separated radiation fields. The bearing these results have on evaluating the accuracy of an atomic beam frequency standard is discussed.

Key Words: Frequency shifts, atomic beam, radiation field, cesium beam, and frequency standard.

Report on International Conference on Crystal Growth (ICCG), R. L. Parker (*Proc. Intern. Conf. Crystal Growth, Boston, Mass., Dec. 1966*), *Phys. Today* **19,** *No. 12, 109–111 (Dec. 1966).*
An International Conference on Crystal Growth (ICCG) took place June 20–24, 1966 in Boston. The purpose of the Conference was to further the science and art of crystal growth by providing a forum for reporting and discussing recent original research in this field. The present report gives a brief summary of certain of the technical subjects dealt with at the Conference.

Key Words: Crystal, crystal growth, international conference, ICCG, report, 1966 ICCG.

Scaling-law equation of state for gases in the critical region, M. S. Green, M. Vincentini-Missoni, and J. M. H. L. Sengers, *Phys. Rev. Letters* **18,** *No. 25, 1113–1117 (June 19, 1967).*
The Widom-Kadanoff scaling-law equation of state has been confirmed for a variety of gases in a range of ±50% of the critical density and within a few percent above and below the critical temperature. Using a new procedure motivated by the scaling law the exponent δ describing the shape of the critical isotherm was found to be close to 5 while the compressibility exponents γ and γ' were found to be both equal to about 1.4.

Key Words: Scaling law, critical region, gases, critical exponents, critical isotherm, compressibility, density gradients, gravity effect, equation of state.

Shubnikov-de Haas effect in $SrTiO_3$, H. P. R. Frederiske, W. R. Hosler, and W. R. Thurber, *Phys. Rev.* **158,** *No. 3, 775–778 (June 15, 1967).*
The magnetoresistance of semiconducting $SrTiO_3$ has been investigated in high magnetic fields (up to 150 kOe). In the temperature range 1.4 to 2.1 °K, for fields of more than 50 kOe, well developed oscillations have been observed. The data support a conduction band consisting of spheroids along the $<100>$ crystalline axes, having 3 minima at the points X_3. The periods of oscillation as well as the temperature dependence of the amplitude and the magnetic field saturation lead to the following values for the transverse and longitudinal effective masses: $m_t = 1.5m_0 \pm 15\%$, $m_l = 6.0m_0 \pm 30\%$.

Key Words: Bandstructure, high magnetic field, oscillatory magnetoresistance, Shubnikov-de Haas effect, strontium titanate.

Some characteristic of commonly used time scales, G. E. Hudson, *Proc. IEEE* **55,** *No. 6, 815–821 (June 1967).*
The conception that time or duration is the ability of systems to experience events in a time sequence and to assign the same order to event sequences caused by other time sequences of events is examined. Time scales are defined ideally as the numerical measures which can be assigned to specific time sequences of events according to the theoretical analysis applicable to specific physical systems. Discussion of these ideas leads to the notions of phase and frequency and frequency standards, and to the theoretical and experimental basis for realizing a time scale. Examples of such realizations occur with the universal scales, the atomic scales, and the ephemeris scale, which are all defined ideally and then realized by the observations of specific physical systems and the use of the corresponding physical theories. There is a problem in the independent co-existence of gravitational and atomic scales which leads to the need for continued comparison, observation, and theoretical study.
Since 1958, several atomic clocks following various time scales have been maintained and are used in the control of standard frequency and time signal emissions from various radio stations. Several broadcast systems involving different time scales have evolved and are being studied. Two of these, designated as universal coordinated time (UTC) and stepped atomic time (SAT) are coordinated internationally and are useful in making the universal time information on the UT2 scale available to a certain approximation. Offsets in carrier frequencies and time pulse rates, and steps in pulse sequence epochs are used to derive the auxiliary approximating scales from a uniform atomic one. Statistical studies indicate some, but not much, difference in the choice of such systems. The CCIR is attempting to stimulate further investigations of the need and use of uniform scales of time on broadcasts, better ways to present universal scale information of use in navigation and in studying and knowing about earth rotation rates, the more efficient use of the electromagnetic spectrum for these broadcasts, and the international definition of a composite, uniform, reference scale of time.

Key Words: Time, time scales, broadcast time signals, time and frequency standards, standard frequency and time signals.

The calculation of nuclear cross-sections by the optical model, D. T. Goldman (*Proc. Intern. Atomic Energy Agency Conf. Nuclear Data for Reactors, Vienna, Austria, 1966*), *Book, Nuclear Data for Reactors I, 339–364 (1967).*
It is well recognized that there will always be limitations to the amount and certainty of microscopic nuclear cross-section data which are available for direct input into reactor design calculations. Therefore, scattering models for the interaction between incident nucleons and the target nucleus have been proposed and used to obtain appropriate values of necessary cross-sections, both where experimental data are lacking and to differentiate between conflicting data. The generic term for such computations is conveniently "optical model calculations" wherein the two-body internucleon potential is replaced by an effective nuclear potential.
This paper presents a systematic derivation of nuclear cross-sections beginning with the interaction between an incident particle and the target nucleons. The replacement of the exact potential by an effective potential results, to first order, in the ordinary time-independent Schrödinger equation. This equation, including a complex and spin-orbit potential is solved for the resultant wave function. By writing the wave function in its scattering solution form, it is possible to compute the shape elastic cross-section and the polarization directly in Lengendre moment expansions. The compound nucleus cross-section, as given originally by the statistical model of Hauser and Feshbach, arises naturally by examining the total wave function. By using the entire solution, including the complete interaction potential, it is possible to generalize these calculations to include the effect of non-spherical potentials and to derive the distorted wave Born approximation. The equations derived in this manner have been used in writing ABACUS-1 and OPTIC, two widely utilized optical model programmes developed by colleagues and the author at Knolls Atomic Power Laboratory. The results obtained from calculations with suitably adjusted potential parameters, have provided confidence for further use of these optical model techniques in providing cross-section information.

Key Words: Calculations, cross section, nuclear cross sections, nucleus, neutron, optical model, scattering.

The effect of other metallic ions on the electrocrystallization of silver from nitrate solutions, J. P. Young, *Plating, pp. 1–4 (Mar. 1967).*
Silver dendrites of various configuration and forms were grown electrolytically on small cathode surfaces in silver nitrate solutions to which small amounts of other metal ions had been added to alter the characteristics of the non-epitaxial silver formations.

Key Words: Dendrite, electrocrystallization, silver, crystal growth, electrodeposited crystals, electrodeposited dendrites.

The effects of rotor deceleration on equilibrium sedimentation experiments, I. H. Billick, M. Dishon, M. Schulz, G. H. Weiss, and D. A. Yphantis, *Proc. Natl. Acad. Sci.* **56,** *No. 2, 399 (Aug. 1966).*
It is the purpose of this note to present some results of a combined numerical and theoretical analysis of rotor deceleration, applicable to equilibrium sedimentation experiments. These results indicate the magnitude of errors in the data from sedimentation experiments where rotor slowing occurs. Of possibly greater interest is the conclusion that artificially induced rotor slowing can be used to substantially speed up equilibrium sedimentation experiments. We have developed the theory for the rectangular approximation to the Lamm equation, and concurrently solved the Lamm equation numerically by a method already described. Detailed accounts of both the theoretical analysis and the numerical results will be presented elsewhere.

Key Words: Centrifuge, sedimentation, rotor deceleration, equilibrium sedimentation, Lamm equation.

The momentum autocorrelation function in a Bernoulli chain, R. J. Rubin and P. Ullersma, *J. Math. Phys.* **7,** *No. 10, 1877–1885 (Oct. 1966).*
This paper is devoted to the study of the statistical dynamics of the small amplitude coplanar vibrations of a compound pendulum consisting of $N+1$ particles suspended in series by weightless strings in a gravitational field. All particles have the same mass m, except for the top particle whose mass is $n(1+\mathcal{Q})$: and all strings are of equal length. The behavior of this system in the limit in which $N\to\infty$ is of particular interest because the maximum normal mode frequency is proportional to $N^{1/2}$. In the limit $N\to\infty$, asymptotic formulas with error estimates are obtained for the time-dependence of the momentum autocorrelation function of: (1) the top particle when $\mathcal{Q}=0$; (2) the bottom particle when $\mathcal{Q}=0$; and (3) the top particle when $N\gg\mathcal{Q}\gg 1$.

Key Words: Statistical dynamics, coupled harmonic oscillators, momentum autocorrelation function, statistical mechanics.

The production and use of monoenergetic electron beams, J. A. Simpson, *Proc. 8th Annual Electron and Laser Beam Symp., University of Michigan, Ann Arbor, Mich., Apr. 6–8, 1966, pp. 437–447 (1966).*
The generation of dense electron beams of energy half-width below 0.1 eV presents special problems. Among these are generation of tightly collimated beams of very low energy space charge effects in deflectors and anomalous energy spreads. A discussion of one successful attack on these problems will be given together with examples of the uses of such beams in electron optics.

Key Words: Electrons, electron beams, electron energy distributions, space charge.

Two-mirror systems with spherical reflecting surfaces, O. N. Stavroudis, *J. Opt. Soc. Am.* **57,** *No. 6, 741–748 (June 1967).*
An analysis is made of two-mirror systems consisting of spherical refracting surfaces. Solutions are found for those systems having zero third order spherical aberration. It is shown that no practical solution exists for the configuration resembling the Gregorian telescope. For the configuration resembling the Cassegrainian telescope three one-parameter families of solutions obtain. These are given by

$$c_1=(q-1)/2t_0 \qquad t_1=(t_0-f)/q \qquad c_2=q/2f$$

$$t_0=\frac{27f}{32}\sec^2\theta \qquad q=-3[1+4\cos\frac{2}{3}(\theta+\pi r)]^{-1}$$

where c_1 and c_2 are the two curvatures; t_1, the axial separation of the two reflecting surfaces: t_0, the distance from a focus to the corresponding surface; and f, the focal length. The free parameter is θ and $r=0, 1, -1$.

Key Words: Optical design, reflecting systems, collimators, cubic equations, third order spherical aberration, Cassegrainian systems.

X-ray diffraction measurement of stacking faults in alpha silver-tin alloys, C. J. Newton and A. W. Ruff, Jr., *J. Appl. Phys.* **37,** *No. 10, 3860–3868 (Sept. 1966).*
Stacking fault probabilities and dislocation densities were studied by means of x-ray diffraction and transmission electron microscopy in both filed and compressed bulk specimens from a series of dilute silver alloys. In the filed samples the observed stacking fault probabilities increased smoothly from 3×10^{-3} for pure silver to 66×10^{-3} for 10.3 at.% tin. The compressed bulk specimens led to values of 6×10^{-3} and 95×10^{-3} respectively. Direct determinations of the dislocation densities were made in the bulk specimens (1 to 5×10^{11} cm^{-2}) leading to computed values for the stacking fault energy in the range 2 to 6 ergs/cm^{-2}, with a slight dip for pure silver. Values for the dislocation density in the filed samples were also calculated. The effect of directed residual stresses measured on the bulk specimens was shown to be negligible with respect to the low angle diffraction line shifts attributed to faulting.

Key Words: X-ray diffraction, electron microscopy, stacking faults, dislocations, silver-tin alloys.

Distribution of standard frequency and time signals, A. H. Morgan, *Proc. IEEE* **55,** *No. 6, 827–836 (June 1967).*
This paper reviews the present methods of distributing standard frequency and time signals (SFTS), which include the use of high frequency, low frequency, and very low frequency radio signals, portable clocks, satellites, and RF cables and lines. The range of accuracies attained with most of these systems are included along with an indication of the sources of error. Information is also included on the accuracy of signals generated by frequency dividers and multipliers.
Details regarding the techniques, the propagation media, and the equipment used in the distribution systems described are not included. Also, the generation of the signals is not discussed.

Key Words: Standard frequency, time signals, standard frequency broadcasts, portable clocks, satellite timing.

Measurement of RF properties of materials—A survey, H. E. Bussey, *Proc. IEEE* **55,** *No. 6, pp. 1046–1053 (June 1967).*
This paper is a survey of the principal methods developed during the past twenty years for the measurement of RF peak pulse power. The basic principles involved for each method are described together with accuracies attainable under normal operating conditions. General techniques for pulse power measurement and precautions to be observed are also given.

Key Words: Measurement, peak pulse power, pulse modulation, RF power.

Of time and frequency, D. H. Andrews, *Book, How to Listen to the World, pp. 3–7 (World Publ., Hellerup, Denmark, Jan. 1967).*
Following a short historical background of timekeeping, the author proceeds to describe Universal Time and how it is approximated by Atomic Time with corrections prescibed by the International Time Bureau. The use of radio broadcasts by various nations to disseminate time signals, standard radio frequencies and standard audio frequencies is described. Other services are also noted. The article includes an extensive listing of worldwide radio stations broadcasting standard frequencies and/or time signals. This tabulation is divided into two parts, Table I listing stations using frequencies above 1 megahertz, and, Table II listing stations using frequencies below 1 megahertz.

Key Words: Atomic time, frequency and time, international time bureau, standard audio frequencies, standard radio frequencies, time and frequency, worldwide radio stations.

Preliminary results of some new measurements of phase velocity at VLF, C. Kamas, A. H. Morgan, and J. L. Jespersen, *Radio Sci.* **1,** *No. 12, 1409–1410 (Dec. 1966).*
A new measurement of the phase velocity of VLF radio waves is described. The measured value of the phase velocity at 18.6 kc/s, for distances greater than 2400 kilometers from the transmitter, was -0.0021 ± 0.0006 in the form $v_p/c-1$. For both 18.6 and 20.0 kc/s, at distances less than 2400 kilometers, the phase velocity varied with distance from the transmitter.

Key Words: Phase velocity, VLF, ionosphere.

Other NBS Publications

J. Res. NBS 71A (Phys. and Chem.), No. 6 (Nov.–Dec. 1967), $1.00.

Guest Editor: Charles H. Corliss

William Frederick Meggers, A Tribute. K. G. Kessler.
The second spectrum of ytterbium (Yb II). W. F. Meggers. (Edited by C. E. Moore.)
An improved description of technetium spectra (Tc I and Tc II), 2000 to 9000 Å. W. R. Bozman, W. F. Meggers, and C. H. Corliss.
Lifetimes of energy levels in neutral iron. C. H. Corliss and J. L. Tech.
Transition probabilities in argon I. C. H. Corliss and J. B. Shumaker, Jr.
The fifth spectrum of praseodymium. V. Kaufman and J. Sugar.

Fundamental energy levels of neutral promethium (Pm I). J. Reader and S. P. Davis.

Analytical coordination chemistry; titrimetry, gravimetry, flame photometry, spectrophotometry, gas evolution and isotopic preparations, July 1965 to June 1966, Ed. O. Menis, Tech. Note 402 (July 21, 1967), 50 cents.

Bibliography of Liesegand rings (second edition), K. H. Stern, Misc. Publ. 292 (Sept. 1, 1967), 40 cents.

Directory of United States standardization activities, J. E. Hartman, Misc. Publ. 288 (Aug. 1, 1967), $2.00. (Supersedes Misc. Publ. 230).

Drawings of micrometer U-tube manometers for the ranges up to 100 mm of mercury, A. M. Thomas and J. L. Cross, Tech. Note 420 (Aug. 26, 1967), 15 cents.

Effects of finite lattice heat capacity on spin-lattice relaxation theory and numerical analysis, R. L. Peterson, Mono. 102 (Aug. 1, 1967), 25 cents.

Grading of abrasive grain on coated abrasive products, PS8–67 (Jan. 9, 1967), 15 cents. (Supersedes CS217–59.)

Hardboard, CS251–63, reprinted April 1967 with amendments (Nov. 15, 1966), 10 cents.

NBS standard frequency and time services, radio stations WWV, WWVH, WWVB, WWVL, Misc. Publ. 236, 1967 Edition (1967), 15 cents.

Nuclear science and technology for ceramists, Proceedings of the American Ceramic Society Symposium Washington, D.C., April 7–12, 1966, Misc. Publ. 285 (May 26, 1967), $1.75.

Proceedings of the 1966 Standards Laboratory Conference, Misc. Publ. 291 (July 13, 1967), $1.00.

Revision of the NBS tables of spectral-line intensities below 2450 Å, C. H. Corliss, Mono. 32 Supplement (July 7, 1967), 30 cents.

Standard Reference Materials: Mössbauer spectroscopy standard for the chemical shift of iron compounds, J. J. Spijkerman, D. K. Snediker, F. C. Ruegg, and J. R. DeVoe, Misc. Publ. 260–13 (July 28, 1967), 40 cents.

Standard Reference Materials: Recommended method of use of standard light-sensitive paper for calibrating carbon arcs used in testing textiles for colorfastness to light, E. Passaglia and P. J. Shouse, Misc. Publ. 260–15 (July 21, 1967), 20 cents.

Tables relating to Mathieu functions. Characteristic values, coefficients, and joining factors, AMS 59 (Aug. 1, 1967), $3.25. (A reissue, with additions, of Columbia University Press 13).

Thermal-shock resistance for built-up membranes, W. C. Cullen and T. H. Boone, Bldg. Sci. Series 9 (Aug. 21, 1967), 20 cents.

The single-engine Claude cycle as a 4.2 °K refrigerator, R. C. Muhlenhaupt and T. R. Strobridge, Tech. Note 354 (June 1, 1967), 45 cents.

Charge-transfer spectrum of the tetrachlorocuprate ion, M. Sharnoff and C. W. Reimann, J. Chem. Phys. **46,** No. 7, 2634–2640 (Apr. 1, 1967).

Correlation of some Precambrian rocks and metamorphic events in parts of Wyoming and Montana, E. J. Catazaro, Mt. Geol. **4,** No. 1, 9–21 (1967).

Erratum: Mass-spectrometric study of the reactions of O atoms with NO and NO_2, F. S. Klein and J. T. Herron, J. Chem. Phys. **44,** No. 9, 3645–3646 (May 1, 1966).

Magnetic and optical spectra of two dimeric copper-chloride pyridine-N-oxide complexes, G. F. Kokoszka, H. C. Allen, Jr., and G. Gordon, J. Chem. Phys. **46,** No. 8, 3020 (Apr. 1967).

Mass spectrometric study of the photoionization of small molecules, V. H. Dibeler, R. M. Reese, and M. Krauss (Proc. 3rd Intern. Conf. Mass Spectrometry, Paris, France, Sept. 1964), Book, Advances in Mass Spectrometry 3, 471–488 (Institute of Petroleum, London, England, 1966).

Measurement of the direct *l*-doublet transitions in carbonyl sulfide, A. G. Maki, J. Mol. Spectry. **23,** No. 1, 110–111 (May 1967).

Microwave spectrum of excited vibrational states of FCN, W. J. Lafferty and D. R. Lide, Jr., J. Mol. Spectry. **23,** No. 1, 94–96 (May 1967).

Microwave spectrum, structure, dipole moment, and barrier to internal rotation of phosphorus trifluoride-borane, R. L. Kuczkowski and D. R. Lide, Jr., J. Chem. Phys. **46,** No. 1, 357–365 (Jan. 1967).

Microwave studies of rotational isomerism, D. R. Lide, Jr., Trans. Am. Cryst. Assoc. **2,** 106–116 (1966).

Monomer-polymer equilibria of deuterated alpha-methylstyrenes, L. J. Fetters, W. J. Pummer, and L. A. Wall, J. Polymer Sci. **4,** Part A–1, 3003–3011 (1966).

Nuclear magnetic relaxation studies of $(CD_3O)_2^{11}BH$, N. Boden, H. S. Gutowsky, J. R. Hansen, and T. C. Farrar, J. Chem. Phys. **46,** No. 7, 2849 (Apr. 1, 1967).

Photolysis of cyclopentane at 1470, 1236, and 1048–67 A, R. D. Doepker, S. G. Lias, and P. Ausloos, J. Chem. Phys. **46,** No. 11, 4340–4346 (June 1, 1967).

Symposium on problems of small information groups. Introductory remarks, M. B. Henderson (Div. Chem. Lit. Symp. Problems of Small Information Groups, 151st Natl. Meeting Am. Chem. Soc., Pittsburgh, Pa., Mar. 25, 1966), J. Chem. Doc. **6,** 143 (Aug. 1966).

Systematic errors in "recovery" and "detection" efficiency as related to radiochemical analysis, L. A. Currie, Proc. 11th Annual Bio-Assay and Analytical Chemistry Meeting, Albuquerque, New Mexico, Oct. 7–8, 1965, AEC No. 651008, pp. 35 (Clearinghouse for Federal Scientific and Technical Information, Springfield, Va., 1967).

The chain decomposition of propane initiated by vacuum ultraviolet photolysis, A. H. Laufer and J. R. McNesby, J. Phys. Chem. **70,** 4094–4096 (1966).

The determination of bound styrene soluble high styrene-butadiene resins, M. A. Post, J. Paint Technol. **38,** No. 497, 336–342 (June 1966).

The microwave spectrum and dipole moment of pyrazole, W. H. Kirchhoff, J. Am. Chem. Soc. **89,** No. 6, 1312–1316 (Mar. 1967).

The microwave spectrum, structure, dipole moment, and quadrupole coupling constants of *trans*-nitrous acid, A. P. Cox and R. L. Kuczkowski, J. Am. Chem. Soc. **88,** No. 22, 5071–5074 (Nov. 1966).

Vacuum-ultraviolet photolysis of solid propane at 20° and 77 °K, R. E. Rebbert and P. Ausloos, J. Chem. Phys. **46,** No. 11, 4333–4339 (June 1967).

Vapor deposition of tungsten by hydrogen reduction hexafluoride process variables and properties of the deposit, J. F. Berkeley, A. Brenner, and W. E. Reid, Jr., J. Electrochem. Soc. **114,** No. 6, 561–568 (June 1967).

Anniversaries in 1966–67 of interest to statisticians. Part II: Tercentennials of Arbuthnot and De Moivre, C. Eisenhart and A. Birnbaum, Am. Stat. **21,** No. 3, 22–29 (June 1967).

Comparison of three spin algebras employed in SU(6) theories, R. C. Casella, Phys. Rev. **147,** No. 4, 962–964 (July 29, 1966).

Fundamental polygons for Fuchsian groups, L. Greenberg, J. Anal. Math. **18,** 99–105 (1967).

Fundamental polyhedra for kleinian groups, L. Greenberg, Ann. Math. **84,** No. 3, 433–441 (Nov. 1966).

Invariance of the homology of a lattice, J. Mather, Proc. Am. Math. Soc. **17,** No. 5, 1120–1124 (Oct. 1966).

On a theorem of Ahlfors and conjugate subgroups of kleinian groups, L. Greenberg, Am. J. Math. **LXXXIX,** No. 1, 56–68 (Jan. 1967).

Calibration of germanium thermometers from 2° to 20 °K, G. Cataland and H. H. Plumb (Proc. Intern. Inst. Refrigeration, Commission 1, Boulder, Colorado, 1966, Annexe 1966–5), Suppl. Bull. Inst. Intern. Froid. pp. 153–163 (Louvain, Belgium, 1966).

Cryogenic thermocouple thermometry, L. L. Sparks and R. L. Powell, Meas. Data **1,** No. 2, 82–90 (Mar.–Apr. 1967).

International standardization and expanded world trade, A. V. Astin, Mag. Std. **37,** No. 7, 191–194 (July 1966).

A simple and accurate method of calibration by photopeak efficiencies, J. M. R. Hutchinson and D. H. Walker, Intern. J. Appl. Radiation Isotopes **18,** No. 1, 86–89 (Jan. 1967).

Additional stopping power and range tables for protons, mesons and electrons, M. J. Berger and S. M. Seltzer, NASA–SP–3036 (1966).

Alpha gamma angular correlations in three heavy odd-A nuclides, J. M. R. Hutchinson, Phys. Rev. **157,** No. 4, 1093–1098 (May 1967).

Autoionizing D States in He below the $n=2$ level of He, J. W. Cooper, S. Ormonde, C. H. Humphrey, and P. G. Burke, Proc. Phys. Soc. **91,** 285–287 (1967).

Cold-neutron study of hindered rotations in solids and liquid methyl chloroform, neopentane and ethane, J. J. Rush, J. Chem. Phys. **46,** No. 6, 2285–2291 (Mar. 1967).

Conformation of adsorbed polystyrene measured by attenuated total reflection in the ultraviolet region, P. Peyser and R. R. Stromberg, J. Phys. Chem. **71,** No. 7, 2066–2074 (June 1967).

Correction of some erroneous calculations of the Einstein A coefficient for the 18 cm transition of OH. D. R. Lide, Jr., Nature **213,** No. 5077, 694–695 (Feb. 18, 1967).

Dependence of 50 and 100 keV bremsstrahlung on target thickness, atomic number, and geometric factors, R. C. Placious, J. Appl. Phys. **38,** No. 5, 2030–2038 (Apr. 1967).

Eigenchannel theory of nuclear reactions, M. Danos and W. Greiner, Phys. Rev. **146,** No. 3, 708–712 (June 1966).

Irradiation-induced color centers in magnesium fluoride, R. F. Blunt and M. I. Cohen, Phys. Rev. **153,** No. 3, 1031–1038 (Jan. 15, 1967).

Lineshapes due to anisotropic interactions in magnetic resonance experiments, R. A. Forman and A. H. Kahn, J. Chem. Phys. **45,** No. 12, 4586–4588 (Dec. 1966).

Mean lives of atomic levels excited by electron impulse, J. Z. Klose, Proc. Intern. Conf. Electronic Excitation of an Atomic Vapor—Application to Spectroscopy, Grenoble, France, May 23–26, 1966, pp. 191–192 (Centre Natl. de la Recherche Scientifique, Paris, France, 1967).

Microwave line shape and the inversion spectrum of ND_3 and ND_3-argon mixtures, A. A. Maryott and S. J. Kryder, J. Chem. Phys. **46,** No. 7, 2856–2857 (Apr. 1967).

Molecules in the sun, C. E. Moore-Sitterly, Proc. Symp. "Sun Spots" honoring Galileo, Florence, Italy, Sept. 9–12, 1964. Ed. G. Righini, pp. 181–185 (G. Barbera, Editore, Florence, Italy, 1966).

Multichannel photo-ionization of atomic systems, R. J. W. Henry and L. Lipsky, Phys. Rev. **153,** No. 1, 51–56 (Jan. 1967).

Multichannel resonances in the inelastic scattering of electrons by helium, G. E. Chamberlain, Phys. Rev. **155,** No. 1, 46–51 (Mar. 5, 1967).

Newly measured and calculated wavelengths in the vacuum ultraviolet spectrum of neutral nitrogen, V. Kaufman and J. F. Ward, Appl. Opt. **6,** No. 1, 43–46 (Jan. 1967).

Nuclear magnetic resonance of nitrogen-14 in potassium azide, R. A. Forman, J. Chem. Phys. **45,** No. 4, 1118–1123 (Aug. 13, 1966).

Nuclear magnetic resonance of ^{7}Li and ^{1}H in solid lithium imide, lithium amide, and lithium nitride, P. J. Haigh, R. A. Forman, and R. C. Frisch, J. Chem. Phys. **45,** No. 3, 812–816 (Aug. 1, 1966).

Nuclear-resonance spin-echo study of ^{61}Ni hyperfine fields in ferromagnetic Ni-Al, Ni-V, and Ni-Cr systems, R. L. Streever and G. A. Uriano, Phys. Rev. **149,** No. 1, 295–301 (Sept. 9, 1966).

Reflective scattering from substrates and evaporated films in the far ultraviolet, R. G. Johnston, L. R. Canfield, and R. P. Madden, Appl. Opt. **6,** 719 (Apr. 1967).

Resonances in the photo-ionization continuum of Ne I (20–150 eV), K. Codling, R. P. Madden, and D. L. Ederer, Phys. Rev. **155,** No. 1, 26–37 (Mar. 5, 1967).

Scattering of cold neutrons in ammonium carbonate, ammonium citrate, and ammonium acetate, V. Myers, J. Chem. Phys. **46,** No. 10, 4034–4035 (May 1967).

Spectral distribution of scattered light in a simple fluid, R. D. Mountain, Rev. Mod. Phys. **38,** No. 1, 205–214 (Jan. 1966).

Stretch scheme, a microscopic description of rotations in nuclei, M. Danos and V. Gillet, Phys. Rev. Letters **17,** No. 13, 703–705 (Sept. 26, 1966).

Structure of the alkali hydroxides. I. Microwave spectrum of gaseous CsOH. D. R. Lide and R. L. Kuczkowski, J. Chem. Phys. **46,** No. 12, 4768–4774 (June 1967).

SU(3) reaction inequalities at high energies, S. Meshkov and G. B. Yodh, Phys. Rev. Letters **18,** No. 12, 474–481 (Mar. 1967).

The photonuclear effect in heavy deformed nuclei, H. Arenhovel, W. Greiner and M. Danos, Phys. Rev. **157,** No. 4, 1109–1125 (May 1967).

The standardization of cobalt-57, S. B. Garfinkel and J. N. R. Hutchinson, Intern. J. Appl. Radiation Isotopes **17,** No. 10, 587–593 (Oct. 1966).

Transactions of the triple commission for spectroscopy, Subcommittee D-Atomic Spectra, C. E. Moore, J. Opt. Soc. Am. **55,** No. 6, 745 (1965).

Treatment of nuclear reactions above the two-particle threshold, M. Danos and W. Greiner, Z. Phys. **202,** 125 (1967).

Triple-filament method for solid-sample lead isotope analysis, E. J. Catanzaro, J. Geophys. Res. **72,** No. 4, 1325–1327 (Feb. 15, 1967).

Vacuum ultraviolet wavelength standards and improved energy levels in the first spectrum of silicon, L. J. Radziemski, Jr., K. L. Andrew, V. Kaufman, and U. Litzen, J. Opt. Soc. Am. **57,** No. 3, 336–340 (Mar. 1967).

W spin for any spin, H. Harari, D. Horn, M. Kugler, H. J. Lipkin, and S. Meshkov, Phys. Rev. **146,** No. 4, 1052–1057 (June 24, 1966).

Free rotation of methyl groups in dimethyltin difluoride, J. J. Rush and W. C. Hamilton, Inorg. Chem. **5,** No. 12, 2238–2239 (Dec. 1966).

Rate constants and the mechanism for the transfer of triplet excitation energy, R. A. Keller and L. J. Dolby, J. Am. Chem. Soc. **89,** 2768–2770 (May 1967).

Study of low-frequency motions in several ferroelectric salts by the inelastic scattering of cold neutrons, J. J. Rush and T. I. Taylor, Proc. 3rd Symp. Inelastic Scattering of Neutrons, Bombay, India, 1965, II, 333 (1965).

Volume change on formation of native collagen aggregate, J. Cassel and R. G. Christensen, Biopolymers **5,** 431–437 (1967).

Technological innovation: its environment and management, D. V. De Simone, U.S. Department of Commerce Cl.2:T22 (Supt. Docs., Govt. Printing Office, Washington, D.C., Jan. 1967).

The innovator, D. V. De Simone, Engineer **8,** No. 1, 8–9 (Jan.–Feb. 1967).

Progress report for O.S.A. committee on uniform color scales, D. B. Judd, Die Farbe **14,** 287–295 (1965).

Almost "head-on" collisions in the scattering of fast argon atoms by hydrogen isotopes, J. E. Jordan and I. Amdur, J. Chem. Phys. **46,** No. 10, 4145–4146 (May 1967).

Anomalous specific heat and viscosity of binary van der Waals mixtures. J. M. Deutch and R. Zwanzig, J. Chem. Phys. **46,** No. 5, 1612–1620 (Mar. 1, 1967).

Detachment of electrons from H^- by electron impact, G. C. Tisone and L. M. Branscomb, Phys. Rev. Letters **17,** No. 5, 236–238 (Aug. 1, 1966).

Electron impact dissociation of H_2^+, G. H. Dunn and B. Van Zyl, Phys. Rev. **154,** No. 1, 40–51 (Feb. 1967).

Exponential operators and parameter differentiation in quantum physics, R. M. Wilcox, J. Math. Phys. **8,** No. 4, 962–982 (Apr. 1967).

Energetic ions from N_2 produced by electron impact, L. J. Kieffer and R. J. Van Brunt, J. Chem. Phys. **46,** No. 7, 2728–2734 (Apr. 1967).

Experimental transition probabilities for the Ar I 4*s*-4*p* array, J. B. Shumaker, Jr. and C. H. Popenoe, J. Opt. Soc. Am. **57,** No. 1, 8–10 (Jan. 1967).

Formal theory of nonlinear response, R. L. Peterson, Rev. Mod. Phys. **39,** No. 1, 69–77 (Jan. 1967).

g_I/g_J ratios in Rb^{87} and Rb^{85}, L. C. Balling, Bull. Am. Phys. Soc. **12,** Series II, No. 4, 508 (Apr. 1967).

NBS to dedicate Gaithersburg facility, W. K. Wilson, J. Wash. Acad. Sci. **56,** No. 7, 165–167 (Oct. 1966).

Observation of two intrinsic nuclear relaxation rates in antiferromagnetic $KMnF_3$, R. J. Mahler, A. C. Daniel, and P. T. Parrish, Phys. Rev. Letters **19,** No. 2, 85–87 (July 10, 1967).

Short-range order in the Weiss molecular field approximation, R. L. Peterson, Bull. Am. Phys. Soc. **12,** Series II, No. 4, 502 (Apr. 1967).

CORRIGENDA FOR THE PAPER

Realistic Evaluation of the Precision and Accuracy of Instrument Calibration Systems, Churchill Eisenhart, Journal of Research of the National Bureau of Standards, Volume **67C**, No. 2, 161–187 (April–June 1963)

Page 177, Eq. (16). Should read

$$\sigma^2_{\bar{x}} = \frac{\sigma^2_{\bar{x}}}{n} = \frac{\sigma^2}{n}$$

Page 178, Eq. (18). Insert "$=$" between "$s^2_{\bar{w}}$" and the formula that follows it.

Page 179, Eq. (20). Should read

$$s^2_{\bar{x}} = \frac{\sum_{i=1}^{k} (\bar{x}_i - \bar{\bar{x}})^2}{k-1}$$

Page 184. Roy H. Wampler of the Statistical Engineering Laboratory, NBS, has recomputed the entries of Table 1 and has found a number of errors in the original, especially in the two "Binomial" columns, that necessitate changes in the second column of the text. A corrected Table 1, and revision of the affected text in column 2 follow.

TABLE 1. *Limits of error of a sum of n items indicated by various methods of evaluation*

n	Absolute ±	Binomial*		Uniform		Triangular		Normal. $2\sigma = 0.5$		Normal. $3\sigma = 0.5$	
		0.95 ±	0.99 ±	0.95 ±	0.99 ±	0.95 ±	0.99 ±	0.95 ±	0.99 ±	0.95 ±	0.99 ±
1	0.50	0.50	0.50	0.48	0.50	0.39	0.45	0.49	0.64	0.33	0.43
2	1.00	1.00	1.00	0.78	0.90	0.56	0.71	0.69	0.91	0.46	0.61
3	1.50	1.50	1.50	0.97	1.19	0.69	0.88	0.85	1.12	0.57	0.74
4	2.00	2.00	2.00	1.12	1.41	0.80	1.03	0.98	1.29	0.65	0.86
5	2.50	2.50	2.50	1.25	1.60	0.89	1.15	1.10	1.44	0.73	0.96
6	3.00	2.00	3.00	1.38	1.76	0.98	1.29	1.20	1.58	0.80	1.05
7	3.50	2.50	3.50	1.49	1.91	1.06	1.39	1.30	1.70	0.86	1.14
8	4.00	3.00	3.00	1.59	2.05	1.13	1.49	1.39	1.82	0.92	1.21
9	4.50	2.50	3.50	1.69	2.18	1.20	1.58	1.47	1.93	0.98	1.29
10	5.00	3.00	4.00	1.78	2.31	1.27	1.66	1.55	2.04	1.03	1.36
15	7.50	3.50	4.50	2.19	2.88	1.55	2.04	1.90	2.49	1.27	1.66
20	10.00	4.00	6.00	2.53	3.33	1.79	2.35	2.19	2.88	1.46	1.92
25	12.50	4.50	6.50	2.83	3.72	2.00	2.63	2.45	3.22	1.63	2.15
30	15.00	5.00	7.00	3.10	4.07	2.19	2.88	2.68	3.53	1.79	2.35
40	20.00	6.00	8.00	3.58	4.70	2.53	3.33	3.10	4.07	2.07	2.72
50	25.00	7.00	9.00	4.00	5.26	2.83	3.72	3.46	4.55	2.31	3.04
60	30.00	8.00	10.00	4.38	5.76	3.10	4.07	3.80	4.99	2.53	3.33

*The results are not monotonic due to the discreteness of the distribution.

might "allow" a maximum error of ±50 cents per check, but consider it reasonable to regard their signs as being equally likely to be plus or minus. In this way one would be led to conclude "with probability 0.95" that the total error lies between ±$4.00; or "with probability 0.99," between ±$6.00, as shown in the column headed "binomial" in table 1, for $n = 20$.

U.S. GOVERNMENT PRINTING OFFICE : 1968 OL—283-576

UNITED STATES
GOVERNMENT PRINTING OFFICE
DIVISION OF PUBLIC DOCUMENTS
WASHINGTON, D.C. 20402

OFFICIAL BUSINESS

POSTAGE AND FEES PAID
U.S. GOVERNMENT PRINTING OFFICE

JOURNAL OF RESEARCH of the National Bureau of Standards Vol. 72C, No. 1 January–March 1968
C. Engineering and Instrumentation

Contents

	Page
Acceleration due to gravity at the National Bureau of Standards. D. R. Tate.	1
Deflection of thin circular elastic plates under symmetrically distributed loading. A. F. Kirstein and R. M. Woolley.	21
A dynamic method for determining the vapor pressure of carbon dioxide at 0 °C. J. L. Edwards and D. P. Johnson.	27
An adiabatic saturation psychrometer. Lewis Greenspan and Arnold Wexler.	33
An injection method for self-calibration of inductive voltage dividers. Wilbur C. Sze.	49
Bolometric voltage and current (Bolovac) standard for high and microwave frequencies. M. C. Selby.	61
An admittance meter technique to measure the complex permeability at VHF. A. L. Rasmussen and C. M. Allred.	81
Publications of the National Bureau of Standards.	91

Library of Congress Catalog Card Number: 62-3900

For sale by the Superintendent of Documents, U.S. Government Printing Office, Washington, D.C. 20402. Price 75¢ (single copy). Subscription price: $2.75 a year; 75¢ additional for foreign mailing.
UNITED STATES GOVERNMENT PRINTING OFFICE, WASHINGTON : 1968